Final Report for BSEE Project E13PG00053:

Use of ROV Video for Rapid Estimates of Discharge Rates from Submerged Oil Leaks

by

Frank Shaffer, USDOE National Energy Technology Laboratory

Ömer Savaş, U.C. Berkeley, Department of Mechanical Engineering

funded by

United States Department of Energy, National Energy Technology Laboratory

and

United States Department of Interior, Bureau of Safety and Environmental Enforcement
BSEE Project E13PG00053, BSEE-NETL WFO Project 2810143

Contents

ABSTRACT

This report describes how to use video of a submerged oil leak jet to quickly estimate the discharge rate. Video is usually available from Remotely Operated Vehicles (ROV). This approach was first developed by the Flow Rate Technical Group (FRTG) Plume Analysis Team to estimate the discharge rate from the Deepwater Horizon oil leak. The authors were members of the FRTG Plume Analysis Team.

The approach uses ROV video to measure the velocity of visible features that propagate along the boundary of an opaque oil leak jet. The visible features include turbulent eddies, vortices, and particles entrained in the jet fluid. The velocity of visible features at the jet boundary can be used to estimate the internal velocity profiles of the leak jet. Once the internal velocity profiles are estimated, the jet discharge rate can be calculated.

Two approaches are described to measure the velocity of visible features: a manual tracking approach and an approach using automated software. The manual approach can be applied quickly (an hour or less) and can use video from ROV cameras at standard frame rates (in the range of 30 to 60 frames per second). The automated approach can also be applied quickly (hours), but may require higher frame rates.

BACKGROUND

During the Deepwater Horizon (DWH) oil leak, in May of 2010, the Flow Rate Technical Group (FRTG) was charged with generating official government estimates of the oil leak rate [McNutt et al.]. The Plume Team of the FRTG was given ROV video of the oil leak jets and asked to quickly produce the first official estimates of the leak rate. The basic approach developed by the Plume Team was to measure the velocity of visible features (turbulent eddies, vortices, entrained particles of hydrates and waxes) at the boundary of the opaque oil jets. The boundary velocity was then used to estimate the internal velocity profiles of the oil jets.

Figure 1 shows large visible features propagating at the boundary of the DWH oil leak jet through consecutive video frames from an ROV camera. Due to the low frame rate of PAL cameras (25 per second) used on ROVs for the DWH, only large features persist over the time between camera frames. Smaller features deform quickly and may not persist over the frame interval time. Features that persist from camera frame to camera frame, are referred to as "coherent" features.

Boundary velocities can be used to estimate internal velocity profiles. With the internal velocity profiles -- and with assumptions for the amount of entrained water, amount of gas dissolved in the oil, and the jet diameter -- an estimate of the total discharge rate can be calculated (as explained below). Before continuing the discussion of this approach, a brief discussion of the theory of turbulent jets is helpful.

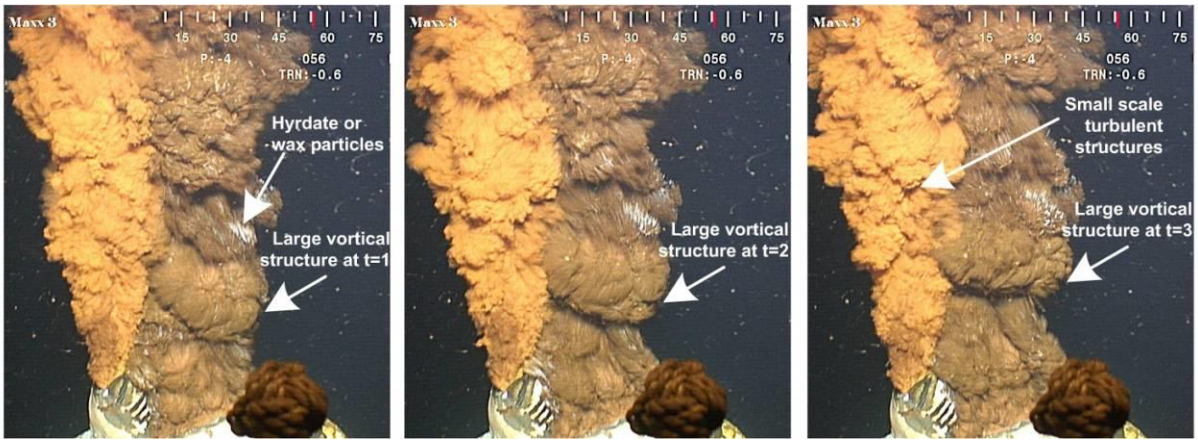

Figure 1. Consecutive video frames showing examples of visible features propagating in the flow direction on the Deepwater Horizon oil leak jet. The jet diameter was approximately 50 cm and the video frame rate was 25 per second.

Theory of Submerged Turbulent Jets

The theory of submerged turbulent jets is well established. Prandtl (1925) and others developed the theoretical foundation in the 1910's and 1920's. Abramovich (1963), Schlichting (2004) and others made advances in both experiments and theory from the 1930's through the 1950's. With recent advances in computational fluid dynamics (CFD), the time-averaged behavior of submerged turbulent jets can be accurately simulated (Eggers, 2007; Guo, 2000; Trujillo, 2007).

Figure 2 illustrates the velocity profiles of a fully developed turbulent pipe flow emitting into an infinite body of fluid at rest. Because the mean streamwise velocity (velocity in the direction of the jet) of a submerged turbulent jet is orders of magnitude higher than the mean radial velocity (velocity normal to the direction of the jet), the radial velocity can be ignored in many practical applications and will be ignored in this application. For

the remainder of this report, “velocity” will be defined as streamwise velocity in the x-direction of the jet centerline.

When a submerged turbulent jet discharges into an infinite body of fluid at rest, the edges of the jet shear against the surrounding fluid causing the formation of a "mixing layer." The mixing layer causes entrainment of the surrounding fluid into the jet, thereby causing the jet diameter to expand. As illustrated in Figure 2, the radial profile of velocity begins as nearly flat at the jet exit, then the shearing action causes the radial profile of velocity to transform into a Gaussian profile. All submerged turbulent jets have a divergence angle around 24 degrees (half angle of 12 degrees) [Lee, 2003; Albertson, 1950; Miller & Comings, 1957; and Bradbury, 1965]. The "statistical jet boundary" lines converge at a focal point at a distance of $2.5D_{jet}$ upstream of the jet exit, which is referred to as the virtual origin.

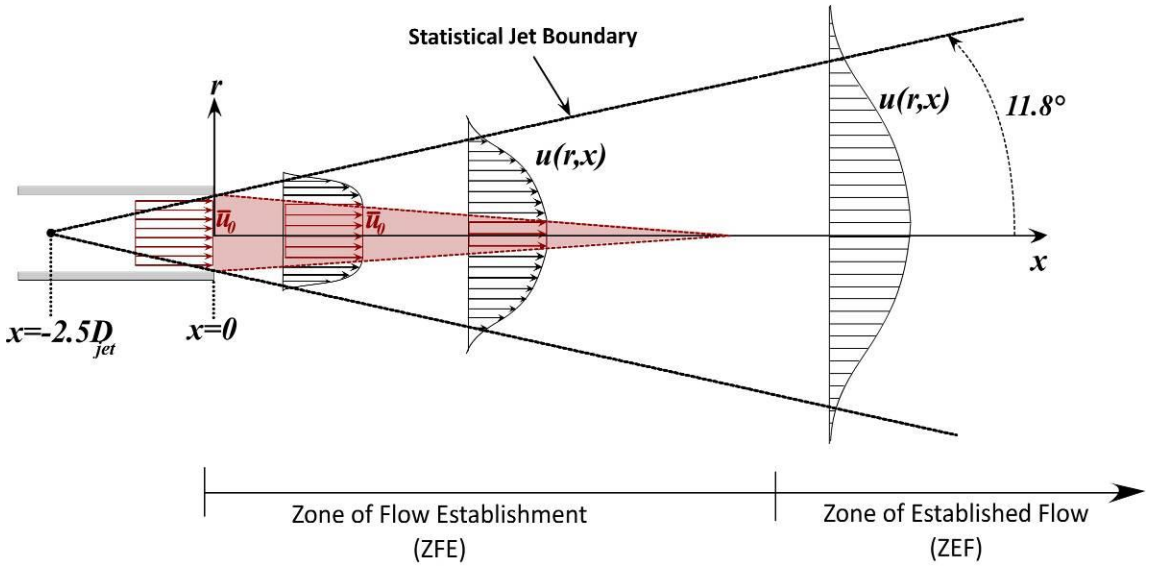

Figure 2. Velocity profiles and regions of a submerged turbulent jet.

The distance from the jet exit to the point where velocity drops below the mean exit velocity, $\bar{u}_0$ is called the Zone of Flow Establishment (ZFE). The ZFE has a constant velocity core, which in Figure 2 is shown as the red shaded area. For a submerged jet exiting from a fully developed pipe flow, the ZFE about six exit diameters long (Lee & Chu, 2003). The boundaries of the constant velocity core are formed by points where the velocity decreases infinitesimally below $\bar{u}_0$.

Downstream of the ZFE is the Established Flow Zone (EFZ). In the EFZ, radial profiles of mean streamwise velocity are Gaussian and self-similar. Self-similar means that at any distance, *x*, all data for mean velocity fall onto the same radial profile when plotted in the non-dimensional form of $u(r)/u_c$ and r/R_{jet}, where u_c is the centerline velocity at *x,* and R_{jet} is the radius of the jet at *x*.

Lee and Chu (2003) derive equations for the radial profiles of velocity and concentration in a submerged turbulent jet. In the ZFE, inside the constant velocity core, for $r < R_{core}(x)$, where $R_{core}(x)$ is the half width of the constant velocity core, the velocity and concentration (fraction of fluid at any point that is jet fluid) are given by

$$u(x,r) = u_0 \qquad c(x,r) = c_0 \tag{1}$$

In the ZFE, outside of the constant velocity core, where r > R_{core}, the velocity and concentration are given by

$$u = u_0 \exp\left[-\frac{(r - R_{core}(x))^2}{b(x)^2}\right] \qquad c = c_0 \exp\left[-\frac{(r - R_{core}(x))^2}{\lambda^2 b(x)^2}\right] \tag{2}$$

where *b* is the half width of the jet from the centerline to the statistical jet boundary, and λ is a turbulent diffusion coefficient. In the EFZ, the velocity profile is given by:

$$u = u(x,0) \exp\left[-\frac{r^2}{b(x)^2}\right] \qquad c = c(x,0) \exp\left[-\frac{r^2}{\lambda^2 b(x)^2}\right] \tag{3}$$

The half width of the jet is given by $b = \beta x$, where β is the slope of the statistical jet boundary. The experimental work of Albertson (1950) and Wygnanski and Fiedler (1969) found that $\beta = 0.114$ for a submerged turbulent jet emitting from a round orifice. The diffusion coefficient, λ, is equal to the ratio of the divergence angle of the statistical concentration boundary to the divergence angle of the statistical jet boundary. Experimental work of Papanicolaou and List (1988) found that $\lambda = 1.2$ for a submerged turbulent jet, indicating that the concentration half width is larger than the velocity half width.

Calculation of the Discharge Rate from a Submerged Turbulent Jet.

The following expression can be used to calculate discharge rates:

$$\dot{Q}_{oil} = \bar{u}(x) A_{jet}(x) [1 - X_{GOR}] E(x) \tag{4}$$

where

$\bar{u}(x)$ is the average jet velocity at a distance, x, from the jet exit

$A_{jet}(x)$ is the cross sectional area of the jet at a distance, x, from the jet exit

X_{GOR} is the volume fraction of methane gas dissolved in the oil. The DWH leaks had significant amounts of supercritical methane in the oil.

$E(x)$ is the ratio of the volume of oil to the total jet volume (oil plus entrained surrounding fluid)

The jet cross sectional area, $A_{jet}(x)$, can be found from the ROV video.

The gas-to-oil ratio, X_{GOR}, can be estimated, or measured by sampling the jet fluid with ROV probes and bringing it to the surface for analysis (Schlumberger, 2010).

The entrainment parameter, $E(x)$, can be found by measuring the expansion of the jet, or by using theory such as that of Lee & Chu (2003) as described above in Equations 1-3.

The main challenge is to determine the relationship between the velocity of visible features, u_{vf}, and the mean velocity of the jet, $\bar{u}(x)$. The Plume Team overcame this challenge by making measurements of the velocity of

visible features close to the jet exit, within, x/D <2, in the ZFE. An assumption was made that coherent structures this close to the jet exit are sampling the constant velocity core (moving at the velocity of the core). Entrainment was assumed to be negligible at x/D<2.

Manual Measurement of the Velocity of Visible Features

Manual feature tracking is simply using a mouse cursor (or other pointing device) to track visible, features from frame-to-frame through an ROV video. Figure 3 shows an example of manual tracking a large vortical feature through three consecutive video frames of the DWH post riser cut leak. The results are shown in the table below.

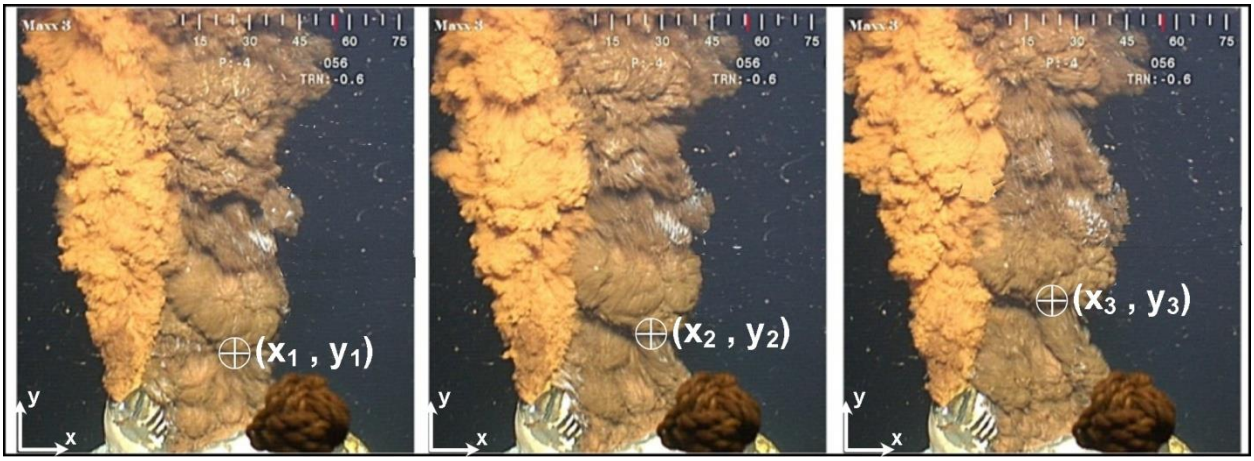

Figure 3. Manual tracking of a large eddy in the DWH post-riser cut jet.

Frame	x	y	DX	DY	DS
1	340	152			
2	350	197	10	45	46
3	360	245	10	48	49

Table 1. Positions of large visible feature through three video frames. Units in pixels.

The distances are in reference to an origin at the lower left corner of the video. The scale of the video is taken from measurement of a known distance; in this case, the diameter of the riser exit, 0.51 m. The scale is 1.91 mm/pixel. The frame rate of the PAL video camerasu used on DWH ROV's is 25 frames/sec, or 0.04 seconds between frames. The velocity from frame 1 to frame 2, and from frame 2 to 3, is found to be 2.3 m/s.

In this case, the MTrackJ plugin [Meijering] for the ImageJ image analysis suite from the National Institutes of Health (NIH) [Schneider] is used to track visible features. Both have advanced image analysis and tracking tools, and are available for free.

Manual Tracking Examples: The Deepwater Horizon Oil Leak Jets

There were three types of leaks from the DWH Macando Well: Riser Kink Jets, Riser End Jet, and Post Riser-cut Jet. The sections below are examples of manual tracking of these jets by Shaffer et al [FRTG].

Riser Kink Jet

The Riser Kink had several leak jets, but only one had a clear, unobstructed view. Figure 4 shows manual feature tracking for this jet. An average velocity of 1.7 m/s was measured at a distance of 0.6 meters downstream from the jet exit.

Figure 4: Manual feature tracing in the main jet of the Riser Kink Jets. (Trajectories were pseudocolored randomly to make them easier to see. The colors do not represent velocity magnitude).

Velocities measured for Riser End Jet

For the Riser End Jet, velocities were measured at two locations along the bottom edge of the jet (Figures 5). One location was 0.8 meters downstream from the jet exit and the other location was further downstream at 1.5 meters from the jet exit. Jet velocity was measured only when the jet was dark in color and assumed to be all oil[1].

[1] Oil and gas separated in the long distance to the riser end jet, producing an alternating slug flow of oil and gas.

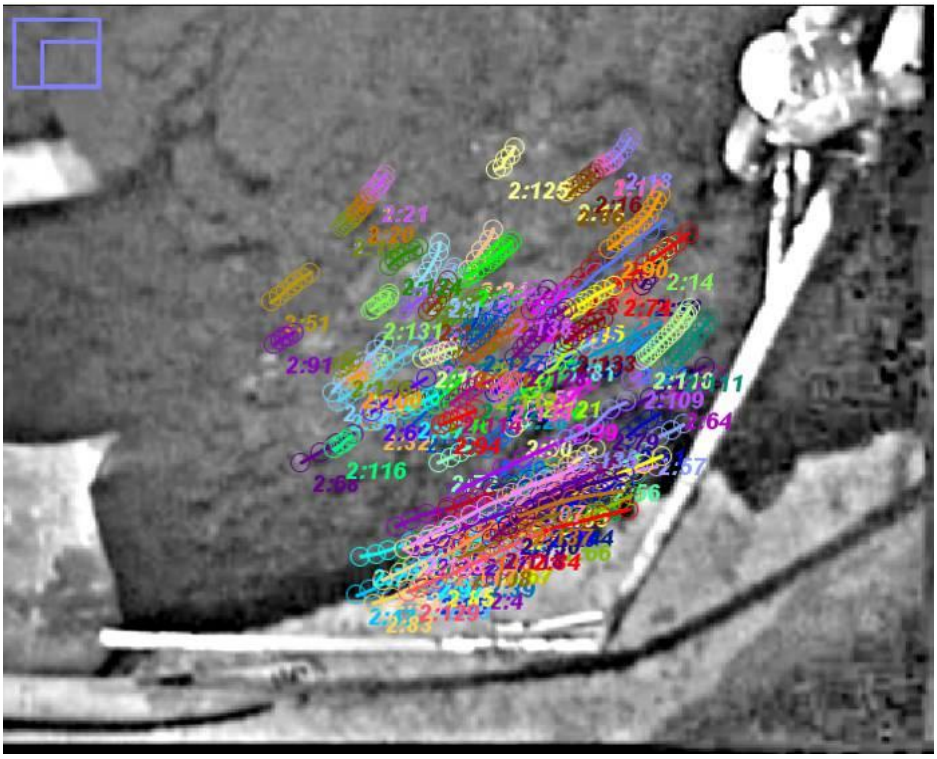

Figure 5: Manual feature tracking in the Riser End Jet.

Velocities measured in Post Riser-Cut Jet

For the Post Riser-Cut Jet, the features were tracked on frames 2810 to 3125 of the video "TOPHAT_06-03-10_14-29-22.avi." More than 500 features were tracked. The average distance downstream of the riser was 0.6 meters (about 1 jet diameter downstream). The average velocity measured was 1.5 meters per second. The plot below shows a histogram of the velocity measurements.

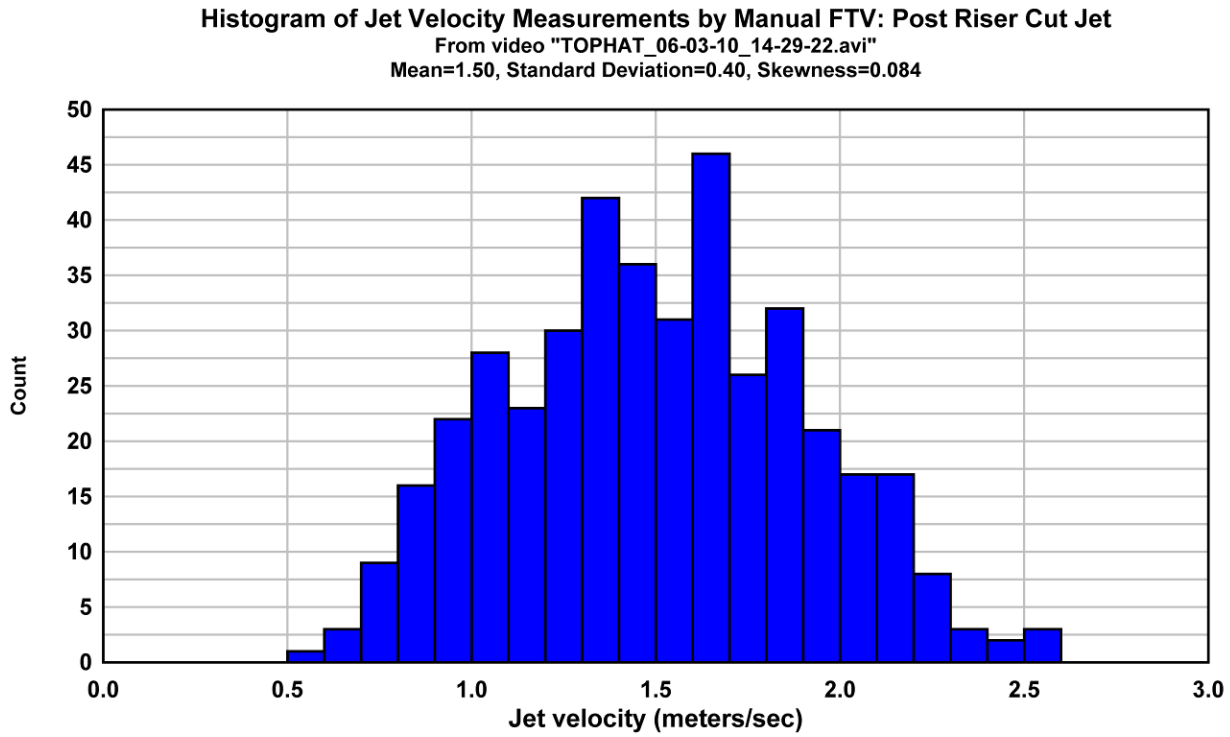

Figure 6. Histogram of velocity measurements by manual tracking in the post riser-cut jet. Mean velocity = 1.50 m/s; standard deviation = 0.40 m/s; skewness = 0.084 m/s.

Calculation of Discharge Rate for the Post Riser-Cut Jet:

The average discharge rate, $\dot{Q}_{oil}$, was calculated using Equation 4

$$\dot{Q}_{oil} = \bar{u}(x)A_{jet}(x)[1 - X_{GOR}]E(x)$$

The average velocity of visible features that propagated from frame-to-frame in the Post Riser-Cut Jet, $\bar{u}(x)$, was 1.5 m/s at an average location of 1.0 meters downstream of the jet exit. The average diameter of the jet at this location, $A_{jet}(x)$, was measured from ROV video to be 0.49 m, giving a cross sectional area of 0.19 m^2. The fluid mixture flowing out of the Post Riser Cut Jet is assumed to be a homogeneous mixture of oil and supercritical methane. The volume fraction of oil in this mixture was measured to be 0.29 at the sea floor and 0.4 at the sea surface [FRTG]. The discharge rate is measured in units of barrels of oil at the sea surface. The equation for oil discharge rate becomes

$$\dot{Q}_{oil} = 1.5 * 0.19 * 0.4 = 0.083 \, {}^{m^3}\!/_{s}$$

To convert this volumetric flow rate to barrels per day at the sea surface, conversion factors of 264.2 US liquid gallons per m^3/s and 42 US liquid gallons per barrel of crude oil are applied. Therefore, the total average oil leak rate from Post Riser-Cut Jet is calculated to be 61,000 barrels per day.

Automated Measurement of the Velocity of Visible Features

A type of object tracking called Image Correlation Velocimetry (ICV) can also be used to automatically measure the velocity of visible features. The use of automated software allows large amounts of video -- far too much for manual tracking -- to be analyzed quickly. A subcategory of ICV is called Particle Image Velocimetry (PIV) can be used for tracking visible features of turbulent jets [Shaffer et al.]. Traditionally, PIV is used to measure velocity fields in a transparent gas or liquid by seeding the flow with small (low Stokes number) particles that follow the fluid flow. Two consecutive video frames are selected and the second frame is divided into interrogation regions as shown in Figure 7. A smaller "template" region from the first frame is cross-correlated over the interrogation region of the second frame. The template cross-correlation can be described as

$$\Phi_{fg}(m,n) = \sum_{m}\sum_{n} f_1(i+m,\, j+n) g_2(i,\, j)$$

where $f_1(i, j)$ is the grey level array of template region in frame 1 and $g_2(i, j)$ is the grey level array of the interrogation region in frame 2. The subscripts m and n are the center position of the template over the interrogation region when a cross-correlation is calculated. The result is a correlation peak that measures the average displacement of the template region from frame 1 to frame 2. The correlation peak measures the average distance a visible feature moved from the first video frame to the second. With the time between video frames, Δt, a velocity vector can be calculated for each interrogation region. A threshold for the correlation peak can be set to reject poor correlations.

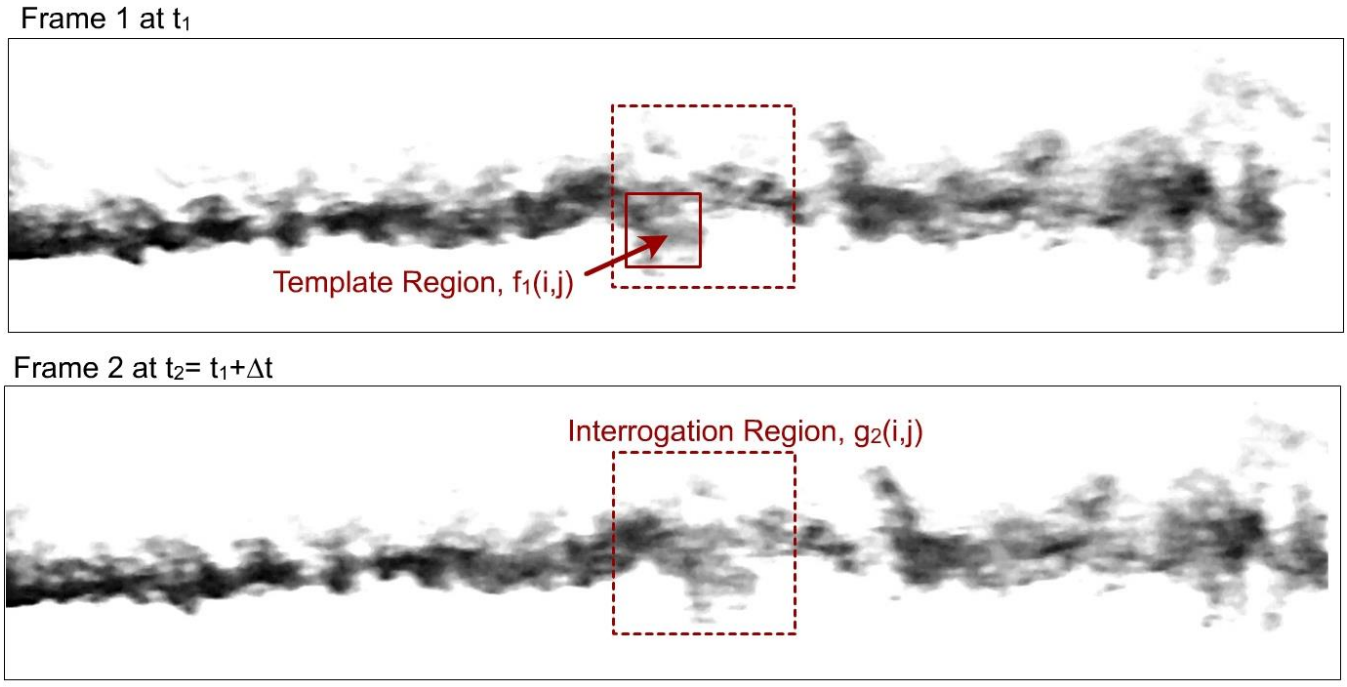

Figure 7. Illustration of template and interrogation regions in two consecutive video frames of dye colored features in water jet experiments at the UC Berkeley Tow Tank.

Verification of Automated PIV Measurement with UC Berkeley Water Tunnel Tests

To test and verify automated PIV software for tracking visible features of a submerged jet, experiments were conducted in the U.C. Berkeley Tow Tank. A dye colored water jet was used to simulate the visible features of the DWH jets. The flow circuit is shown in Figure 8. Jet exit diameters were 10.2 cm and 20.3 cm with flow rates up to 11 gallons/sec, producing Reynolds numbers in the range of the DWH oil leak jets (up to 500,000). The dye-colored water jets were recorded with high speed video and radial profiles of velocity were mapped with Laser Doppler Anemometry (LDA). Particle Image Velocimetry (PIV) software was applied to measure the velocity of visible features. The experiments and results are summarized below. For a thorough discussion see [Shaffer et al]. The velocities measured with PIV software were in good agreement with the LDA measurements.

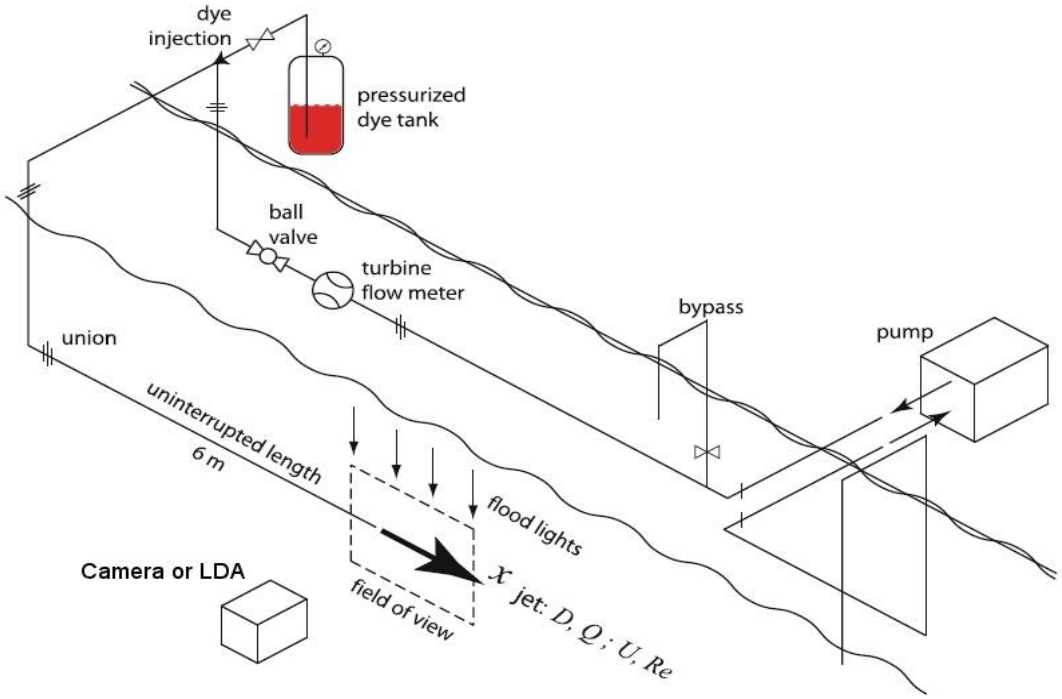

The dye-colored jets were recorded with a high definition, high speed video camera (Vision Research Model v341) at frame rates up to 1500 per second at resolutions up to 2560x1100 pixels. Two types of dye coloring of the water jet were used. The entire jet was dyed or “point” injection of dye was used.

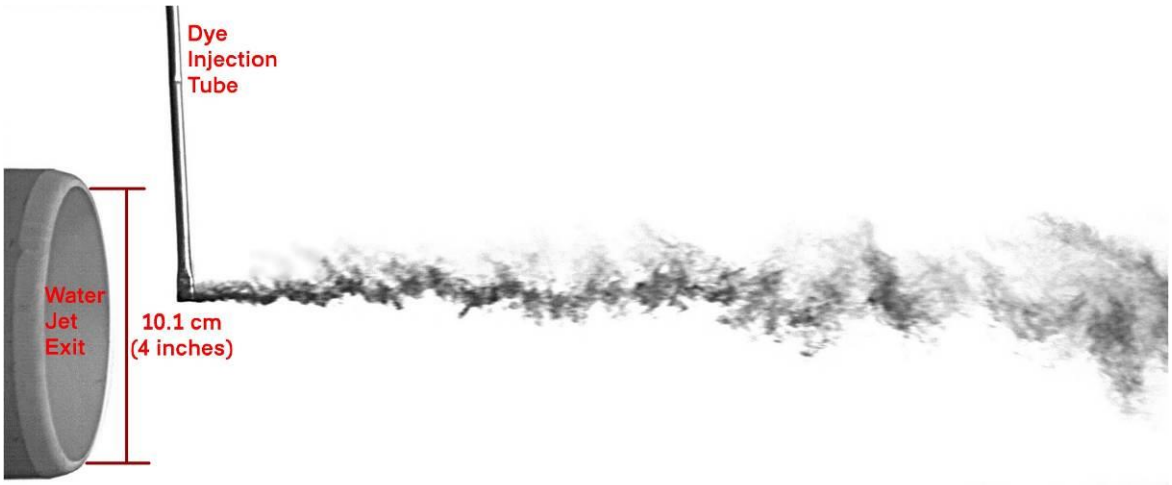

Figure 8. Flow visualization with dye point injection. Water flow rate was 41.7 liters/sec (11 gallons/sec) producing a Reynolds number of 500,000. The camera frame rate was 1500/second and the exposure time was 0.75 ms.

To measure the velocity of dyed flow features, the high speed video was analyzed with a PIV code developed by Q. Tseng (Tseng, 2011; Tseng, 2013). The code is implemented as a plugin for ImageJ, an image analysis tool developed by the National Institutes of Health (NIH) (Schneider, 2012). The PIV tool by Tseng is based on a template matching approach.

The radial profiles of streamwise velocity of the jet were also mapped with a Dantec FlowExplorer Laser Doppler Anemometer (LDA) (Dantec, 2013) at downstream distances of x/D_{jet} = 0.25, 2.0 and 4.0. A 300 mm focal length lens was used. The LDA was operated in non-coincidence mode. The jet flow was seeded with 50 micron diameter silver coated ceramic spheres of density 0.8-1.2 g/cm^3.

Laser Doppler Anemometry

Since submerged turbulent jets are self-similar, when normalized velocity is plotted against normalized radius, all data fall onto the same profile. Figure 9 shows normalized LDA data for a 10.2 cm diameter pipe jet measured at a distance of two jet diameters downstream of the exit.

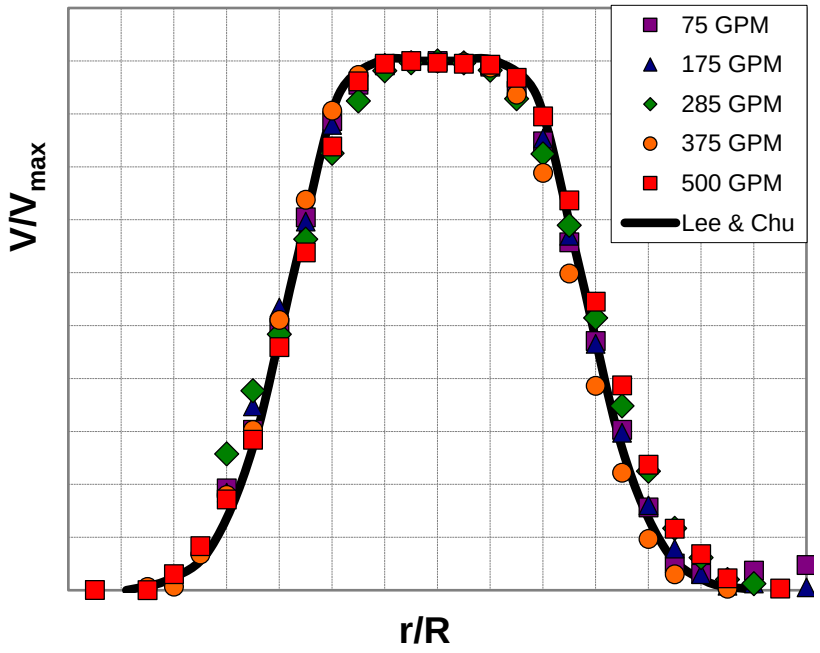

Figure 9. Normalized LDA data for a submerged water jet exiting from a 10.2 cm diameter pipe at various jet discharge rates. From the UC Berkeley Tow Tank.

Image Correlation Velocimetry of Dyed Flow Features

For the flow condition of 660 gallons/minute, a total of 44,867 video frames were recorded at 1150 frames/sec for a total sample period of 39.0 seconds. ICV was applied with as interrogation window of 200x200 pixels and a subregion template of 125 x 125 pixels. The center of the interrogation region was moved in steps of 50 pixels. The mean velocity at the jet centerline was 4.31 m/s. Figures 10 and 11 show good agreement between LDA and PIV measurements.

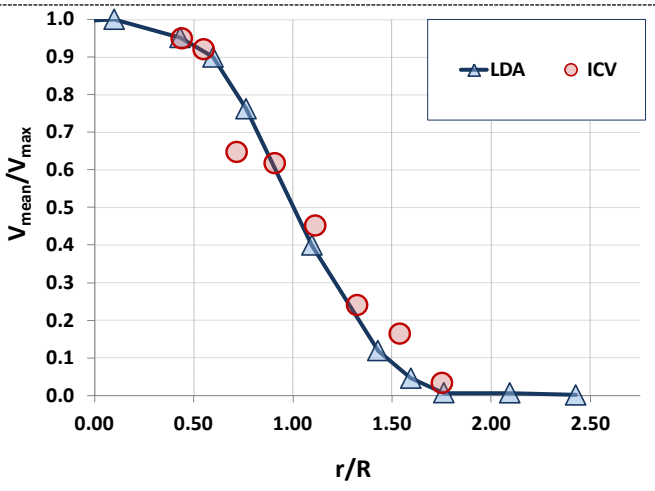

Figure 10. Radial profiles of mean velocity at x/D = 2; 4 in pipe jet; 660 GPM. Reynolds number ~500,000.

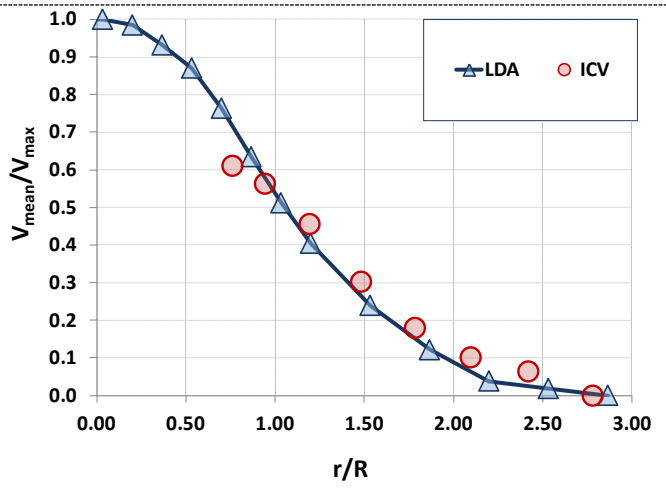

Figure 11. Radial profiles of mean velocity at x/D = 4; 4 in pipe jet; 660 GPM. Reynolds number ~500,000.

Camera Selection and Operation

For operation in an ROV, the quality of camera images may be limited by the data transfer link. The camera resolution and frame rate should be set as high as memory capacity and data transfer rates allow. Frame exposure time should be as short as necessary to freeze the motion of the fastest visible features.

When memory or data transfer capabilities limit the frame rate, suitable frame rates can be estimated using turbulence theory. This is discussed below.

Turbulent eddies, such as those visible at the boundary of a submerged oil jet, have and range of sizes and lifetimes. The lifetime of a turbulent eddy is proportional to its size, with smaller eddies having shorter lifetimes. The key parameter in describing the sizes and persistence of turbulent eddies is the turbulent dissipation rate, ε, [Hinze] which is on the order of

$$\varepsilon \sim u^3/l \sim (4/\pi)^3 (Q^3/D^7)$$

where u and l are the velocity and length scales of the largest eddies, Q is the discharge rate, and D is the jet diameter. Energy from turbulent eddies is dissipated through viscous interaction by the smallest eddies. The size of the smallest eddies, called the viscous scales or Kolmogorov scales, is represented by η, where

$$\eta = 1 / k_d \sim (\nu^3 / \varepsilon)^{1/4}$$

where ν is the kinematic viscosity and k_d the wavenumber. The size of the largest eddies is on the order of the jet diameter. The ratio of the Kolmogorov scales to the size of the largest eddies is

$$\eta / l = Re^{3/4}$$

where Re is the Reynolds number

$$Re = UD/\nu \sim Q/\nu D.$$

In the intermediate range of eddy sizes, (l, η), also called the universal equilibrium range or the inertial subrange, the eddies of a given wave number have eddy lifetimes of t_k and eddy turnover velocity u_k scales that are independent of viscosity,

$$t_k \sim (\varepsilon k^2)^{-1/3} \sim u^{-1}(k^2/l)^{-1/3}$$

$$u_k \sim (\varepsilon /k)^{1/3}$$

The camera framing rate should be sufficiently high so that the eddy does not *rotate* significantly between successive frames, i.e.,

$$f >> (\varepsilon k^2)^{1/3}$$

where k is the desired eddy wavenumber for tracking visible features. For automated analysis, the marker wavenumber, k, is selected based on the interrogation window size, $w \times w$, in units of pixels, and $1/k$ should be much smaller than the window size

$$k >> 1/w$$

Finally, we have

$$f >> >> (\varepsilon/w^2)^{1/3}$$

n lieu of the double >> signs, we suggest a factor of 10

$$f \sim 10\,(\varepsilon/w^2)^{1/3}$$

Using the ostensible parameters, an equation is derived for estimating required camera frame rates

$$f \sim 10(Q/D^{7/3})\,w^{-2/3}$$

Using the DWH post riser-cut jet as an example, let's assume a pixel covers an area of 10^{-3} x 10^{-3} m (1000x1000 pixels camera looking at a 1m x 1m area), so $w = 10^{-3}$ m, $Q = 0.1$ m^3/s (53,000 bbl/day), $D = 0.5$ m, and an interrogation area of 32 x 32 pixels is used. A suitable frame rate is estimated to be

$$f \sim 10(Q/D^{7/3})w^{-2/3} \sim 50\ frames/sec$$

For dyed jet water tank experiments done at UC Berkeley for this project, a typical pixel size was 10^{-4} m (1000x1000 pixels camera looking at a 0.1m x 0.1m area), Q=1x10^{-4} m^3/s, D=0.013 m, and w=64 pixel. So the required frame rate is estimated to be

$$f \sim 10\,(Q/D^{7/3})w^{-2/3} \sim 1000\ \mathrm{Hz}$$

UC Berkeley PIXTif Software

UC Berkeley has developed and tested a field deployable video analysis software package which is able to provide in the field sufficiently accurate flow rate estimates for initial responders in accidental oil discharges in submarine operations. The tool is called "UCB Plume." The essence of the approach is based on tracking coherent features at the interface in the near field of immiscible turbulent jets.

The software package is ready to be used by the first responders for field implementation. We have tested the tool on submerged water and oil jets which are made visible using fluorescent dyes. We have been able to estimate the discharge rate within 20% accuracy.

A high end WINDOWS laptop computer is suggested as the operating platform and a USB connected high speed, high resolution monochrome camera as the imaging device are sufficient for acquiring flow images under continuous unidirectional illumination and running the software in the field. Results are obtained over a matter of minutes.

References

Abdel-Rahman, A. A., Chakroun, W., and Al-Fahed, S. F., 1997. "LDA measurements in the turbulent round jet," *Mechanics Research Communications*, **24**:277-288.

FRTG Plume Analysis Team, 2010, "Deepwater Horizon Release Estimate of Rate by PIV," www.doi.gov/deepwaterhorizon

Gore, J. P., and Jian, C. Q., 1993. "Analytical solution to the flame trajectory based on the analysis of "Scaling of buoyant turbulent jet diffusion flames" by N. Peters and J. Gottgens," *Combust. Flame*, **93**:336-337.

Hill, B. J., 1972. "Measurement of local entrainment rate in the initial region of axisymmetric turbulent air jets," *J. Fluid Mech.*, 51:773-779.

Hinze, O.J., "Turbulence," 1975.

Kim, J. S., Yang, W, Kim, Y., and Won, S. H., 2009. "Behavior of buoyancy and momentum controlled hydrogen jets and flames emitted into the quiescent atmosphere," *Journal of Loss Prevention in the Process Industries*, **22**:943-949.

Meijering, E., et al., "Methods for Cell and Particle Tracking," Methods in Enzymology, vol. 504, February 2012, pp. 183-200

Meijering, E. et al., "MTrackJ: A motion analysis and tracking plugin for ImageJ," http://www.imagescience.org/meijering/software/mtrackj/

McNutt, M. K., Camilli, R., Crone, T. J., Guthrie, G. D., Hsieh, P. A., Ryerson, T. B., Savaş, Ö.& Shaffer, F., 2011, Review of flow rate estimates of the Deepwater Horizon oil spill. *PNAS: Proceedings of the National Academy of Sciences of the United States of America.* Published online on December 20, 2011. DOI: 10.1073/pnas.111213910

Mi, J., Kalt, P., Nathan, G. J., and Wong, C. Y., 2007. "PIV measurements of a turbulent jet issuing from round sharp-edged plate," *Exp. Fluids*, **42**:625-637.

Mi, J., Nathan, G. J., and Nobes, D. S., 2001. "Mixing characteristics of axisymmetric free jets from a contoured nozzle, and orifice plate and a pipe," *J. Fluids Eng.*, **123**:878-883.

Nathan, G. J., Mi., J., Alwahabi, Z. T., Newbold, G. J. R., and Nobes, D. S., 2006. "Impacts of a jet's exit flow pattern on mixing and combustion performance," *Prog. Energy Combust. Sci.*, **32**:496-538.

Peters, N., and Gottgens, J., 1991. "Scaling of buoyant turbulent jet diffusion flames," *Combust. Flame*, **85**:206-214.

Quinn, W. R., 2006. "Upstream nozzle shaping effects on near field flow in round turbulent free jets," *European Journal of Mechanics B/Fluids*, **25**:279-301.

Richards, C. D., and Pitts, W. M., 1993. "Global density effects on the self-preservation behavior of turbulent free jets," *J. Fluid Mech.*, **254**:417-435.

Ricou, F. P., and Spalding, D. B., 1961. "Measurements of entrainment by axisymmetrical turbulent jets," *J. Fluid Mech.*, 11:21-32.

Schneider, C.A., Rasband, W.S., Eliceiri, K.W. "NIH Image to ImageJ: 25 years of image analysis," Nature Methods 9, 671-675, 2012.

Shaffer, F. Savas, Ö., Lee, K., de Vega, G., "Determining the Discharge Rate from a Submerged Oil Leak Jet using ROV Video," Flow Measurement & Instrumentation, v. 43, 2015.

Tseng, Q. et al., 2000, Spatial Organization of the Extracellular Matrix Regulates Cell–cell Junction Positioning. PNAS (2012).doi:10.1073/pnas.1106377109

Tseng, Qingzong. 2011. "Study of multicellular architecture with controlled microenvironment". Ph.D. dissertation, Université de Grenoble. http://tel.archives-ouvertes.fr/tel-00622264.

Tseng, Q., 2013, "Template Matching and Slice Alignment--- ImageJ Plugins,"https://sites.google.com/site/qingzongtseng/piv

APPENDIX 1: Journal of Fluid Measurements & Instrumentation Paper: Determining the Discharge Rate from a Submerged Oil Leak Jet using ROV Video

Flow Measurement and Instrumentation 43 (2015) 34–46

Contents lists available at ScienceDirect

Flow Measurement and Instrumentation

journal homepage: www.elsevier.com/locate/flowmeasinst

Determining the discharge rate from a submerged oil leak jet using ROV video

Frank Shaffer [a,*], Ömer Savaş [b], Kenneth Lee [b], Giorgio de Vera [b]

[a] USDOE National Energy Technology Laboratory, United States
[b] U.C. Berkeley, Department of Mechanical Engineering, United States

ARTICLE INFO

Article history:
Received 4 February 2014
Received in revised form
15 December 2014
Accepted 27 December 2014
Available online 9 January 2015

Keywords:
Flow rate
Leak rate
Oil leak
Particle Image Velocimetry (PIV)
Deepwater horizon

ABSTRACT

With expanded deep sea drilling in the Gulf of Mexico, and possibly the Arctic, it is imperative to have a technology available to quickly and accurately measure the discharge rate from a submerged oil leak jet. This paper describes an approach to measure the discharge rate using video from a Remotely Operated Vehicle (ROV). ROV video can be used to measure the velocity of visible features (turbulent eddies, vortices, entrained particles) on the boundary of an oil leak jet, from which the discharge rate can be estimated. This approach was first developed by the Flow Rate Technical Group (FRTG) Plume Team, of which the authors Savaş and Shaffer were members, during the response to the Deepwater Horizon (DWH) oil leak. Manual tracking of visible features produced the first accurate government estimates of the oil discharge rate from the DWH. However, for this approach to be practical as a routine response tool, software is required that automatically measures the velocity of visible features. To further develop this approach, experiments were conducted to simulate a submerged oil leak jet using a dye-colored water jet in the U.C. Berkeley Tow Tank facility. Jet exit diameters were 10.2 cm and 20.3 cm. With flow rates up to 11 gal/s, Reynolds numbers in the range of the DWH oil leak jets (up to 500,000) were achieved. The dye-colored water jets were recorded with high speed video and radial profiles of velocity were mapped with Laser Doppler Anemometry (LDA). Particle Image Velocimetry (PIV) software was applied to measure the velocity of visible features. The velocities measured with PIV software were in good agreement with the LDA measurements. Finally, the PIV software was applied to ROV video of the DWH oil leak jet. The measured velocities were 10–50% lower than manual measurements of velocity. More research is required to determine the reasons why PIV software produced much lower velocities than manual tracking for the DWH oil leak jet.

Published by Elsevier Ltd.

1. Introduction

On April 21, 2010, the Deepwater Horizon (DWH) failed catastrophically and produced oil leaks in the form of submerged turbulent jets located 1500 m below the sea surface. To determine the type and level of response required, an accurate estimate of the oil leak rate was needed. However, at that time, a proven technology to measure the leak rate from a deep sea oil leak jet was not available. The National Commission on the DWH Oil Spill [18] concluded the oil leak rate was grossly underestimated during the first two months and that the underestimates resulted in an inadequate response and caused attempts to cap the well to fail. As the use of deep sea drilling expands and the depths increase, it is of paramount importance to develop an approach to quickly and accurately measure the leak rate from a deep sea oil or gas leak.

During the DWH oil leak, in mid May of 2010, the Flow Rate Technical Group (FRTG) was formed and charged with generating official government estimates of the oil leak rate. The Plume Team of the FRTG was given ROV video of the oil leak jets and asked to quickly produce estimates of the leak rate. The basic approach developed by the Plume Team was to measure the velocity of visible features (turbulent eddies, vortices, particles of hydrates and waxes), then use the boundary velocity to predict the mean velocity over the cross section of the opaque oil jets. Fig. 1 shows consecutive video frames with large visible features propagating at the boundary of the DWH oil leak jet. Due to the low frame rate of 25 per second, only large features persist over the frame interval time. Smaller features with faster deformation rates do not persist over the frame interval time. With the mean velocity, and with assumptions for the amount of entrained water, amount of gas dissolved in the oil, and the jet diameter, an estimate of the total leak rate could be calculated. Before continuing this discussion of this approach to measuring an oil/gas leak rate from a submerged leak jet, a brief description of classical submerged turbulent jets is necessary.

* Corresponding author.

http://dx.doi.org/10.1016/j.flowmeasinst.2014.12.006
0955-5986/Published by Elsevier Ltd.

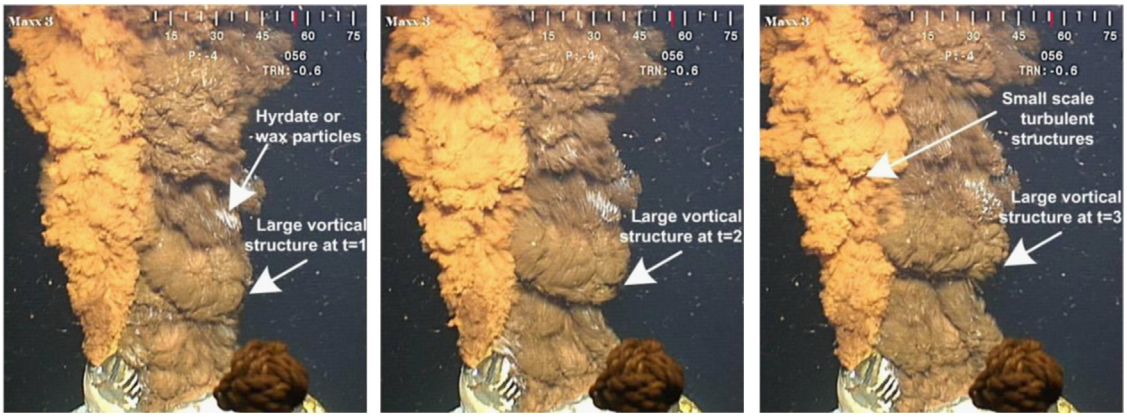

Fig. 1. Consecutive video frames showing examples of visible features propagating in the flow direction on the Deepwater Horizon oil leak jet. The jet diameter was approximately 50 cm and the video frame rate was 25 per second.

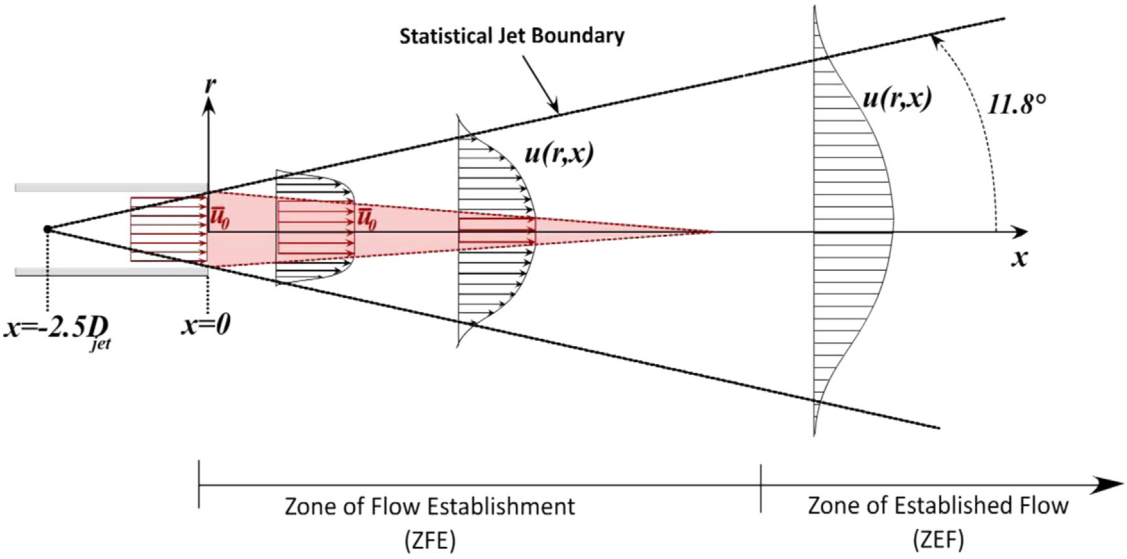

Fig. 2. Velocity profiles and regions of a submerged turbulent jet.

1.1. Submerged turbulent jets

The theory of submerged turbulent jets, both from an Eulerian and Langrangian approach, is well established. Prandtl [20–22] and others developed the theoretical foundation in the 1910s and 1920s. Abramovich [1–4] and others made advances in both experiments and theory between 1930 and 1950. With recent advances in computational fluid dynamics (CFD), the time-averaged behavior of submerged turbulent jets can be accurately simulated, assuming the properties of the jet fluid are known [11,12,27].

Fig. 2 illustrates the zones and velocity profiles of a turbulent pipe flow emitting into an infinite body of fluid at rest. Because the mean streamwise velocity (velocity in the x-direction of the jet centerline) of a submerged turbulent jet is orders of magnitude higher than the mean radial velocity (velocity in the r-direction orthogonal to the jet centerline), the radial velocity can be ignored in many practical applications, except when entrainment is central to the discussion, and will be ignored in this study. For the remainder of this paper, "velocity" will be defined as streamwise velocity.

The centerline velocity at the pipe exit is u_0. For purposes of this discussion, since the radial profile of velocity in a fully developed turbulent pipe flow is nearly flat (of uniform velocity), the radial profile of velocity at the jet exit is assumed to be flat with a value of $\overline{u}_0$ [24], where the overbar denotes average values.

When a submerged axisymmetric turbulent jet discharges into an infinite body of fluid at rest, the edges of the jet shear against the surrounding fluid causing the formation of a mixing layer. The dynamics of the shear layer causes the entrainment of the surrounding fluid into the jet, which causes the jet to expand. The radial profile of streamwise velocity begins as flat at the jet exit, then the shearing action causes the radial profile to transform into a nearly Gaussian profile. All submerged turbulent jets have a divergence angle around 24° (half angle of 12°), depending on how the statistical boundary is defined [13]. The statistical jet boundary is a point on the radial profile of mean streamwise velocity where the value decreases below a predefined level. Albertson [2], Miller and Comings [17] and Bradbury [3] define the statistical boundary velocity as equal to $1/e$ of the centerline. The statistical jet boundary lines converge at a focal point at a distance of $2.5D_{jet}$ upstream of the jet exit, commonly referred to as the virtual origin.

It is important to note that the velocity at the statistical boundary, u_{sb}, is not the same as the mean velocity of visible features, u_{vf}, i.e., $u_{vf} \neq u_{sb}$.

The distance from the jet exit in which the jet has a constant velocity core of $\overline{u}_0$ (the diverging area shaded in red) is called the Zone of Flow Establishment (ZFE). For a submerged jet exiting from a round exit, the ZFE is 6.2 exit diameters ($6.2D_{jet}$) long [13]. The boundaries of the constant velocity core (called the potential core when the discharge flow profile is irrotational) are formed by points where the velocity decreases infinitesimally below $\overline{u}_0$.

Downstream of the ZFE is the Established Flow Zone (EFZ). In the EFZ, radial profiles of mean streamwise velocity are Gaussian

and self-similar. Self-similar means that at any distance, x, all data for mean velocity fall onto the same radial profile when plotted in the non-dimensional form of $u(r)/u_c$ and r/R_{jet}, where u_c is the centerline velocity at x and R_{jet} is the radius of the jet at x.

Lee and Chu [13] derive equations for the radial profiles of velocity and concentration in a submerged turbulent jet. In the ZFE, inside the constant velocity core, for $r < R_{core}(x)$, where $R_{core}(x)$ is the half width of the constant velocity core, the velocity and concentration (fraction of fluid at any point that is jet fluid) are given by

$$u(x,r) = u_0, \quad c(x,r) = c_0 \tag{1}$$

In the ZFE, outside of the constant velocity core, where $r > R_{core}$, the velocity and concentration are given by

$$u = u_0 \exp\left[-\frac{(r-R_{core}(x))^2}{b(x)^2}\right], \quad c = c_0 \exp\left[-\frac{(r-R_{core}(x))^2}{\lambda^2 b(x)^2}\right] \tag{2}$$

where b is the half width of the jet from the centerline to the statistical jet boundary and λ is a turbulent diffusion coefficient. In the EFZ, the velocity profile is given by

$$u = u(x,0) \exp\left[-\frac{r^2}{b(x)^2}\right], \quad c = c(x,0) \exp\left[-\frac{r^2}{\lambda^2 b(x)^2}\right] \tag{3}$$

The half width of the jet is given by $b = \beta x$, where β is the slope of the statistical jet boundary. The experimental work of Albertson [2] and Wygnanski and Fiedler [31] found that $\beta = 0.114$ for a submerged turbulent jet emitting from a round orifice. The diffusion coefficient, λ, is equal to the ratio of the divergence angle of the statistical concentration boundary to the divergence angle of the statistical jet boundary. Experimental work of Papanicolaou and List [19] found that $\lambda = 1.2$ for a submerged turbulent jet, indicating that the concentration half width is larger than the velocity half width.

1.2. Measurement of the flow/leak rate from a submerged turbulent jet

The following expression was used by members of the Plume Team in 2010 to calculate oil leak rates:

$$\dot{Q}_{oil} = \overline{u}(x) A_{jet}(x)[1 - X_{GOR}]E(x) \tag{4}$$

where $\overline{u}(x)$ is the average jet velocity at a downstream distance, x, from the jet exit, $A_{jet}(x)$ is the cross sectional area of the jet at a distance downstream from the jet exit, X_{GOR} is the volume fraction of methane gas dissolved in the oil. Near the jet exit, methane was dissolved in the oil. Downstream the methane was liberated from the oil and $E(x)$ is the ratio of the volume of oil minus sea water entrained into the jet to the total jet volume at any distance x.

The jet cross sectional area, $A_{jet}(x)$, can be found by measuring the jet diameter from the ROV video at the distance x where visible jet boundary velocity was measured. The gas-to-oil ratio, X_{GOR}, was found by sampling the oil with ROV probes and bringing it to the surface for analysis [25]. The gas-to-oil ratio was assumed to be constant. The entrainment parameter, $E(x)$, can be found by measuring the expansion of the jet, or by using theory such as that of Lee and Chu [13] as described above in Eqs. (1)–(3).

Several challenges were encountered in applying this approach. The first challenge was how to measure the velocity of visible features on the boundary of the immiscible oil leak jets. Six members of the Plume Team began by using Particle Image Velocimetry (PIV) software to automatically measure the velocity of visible features. Three of the members (Leifer, Savaş and Shaffer) who began using PIV software concluded that it was producing erroneously low values of velocity [10]. They resorted to manual tracking of larger, faster visible features by hand. It was later determined that PIV software led to erroneously low estimates of the oil leak rate [16,23].

The next challenge was to determine the relationship between the velocity of visible features, u_{vf}, and the mean velocity of the jet, $\overline{u}(x)$. During the work of the Plume Team and during this study,

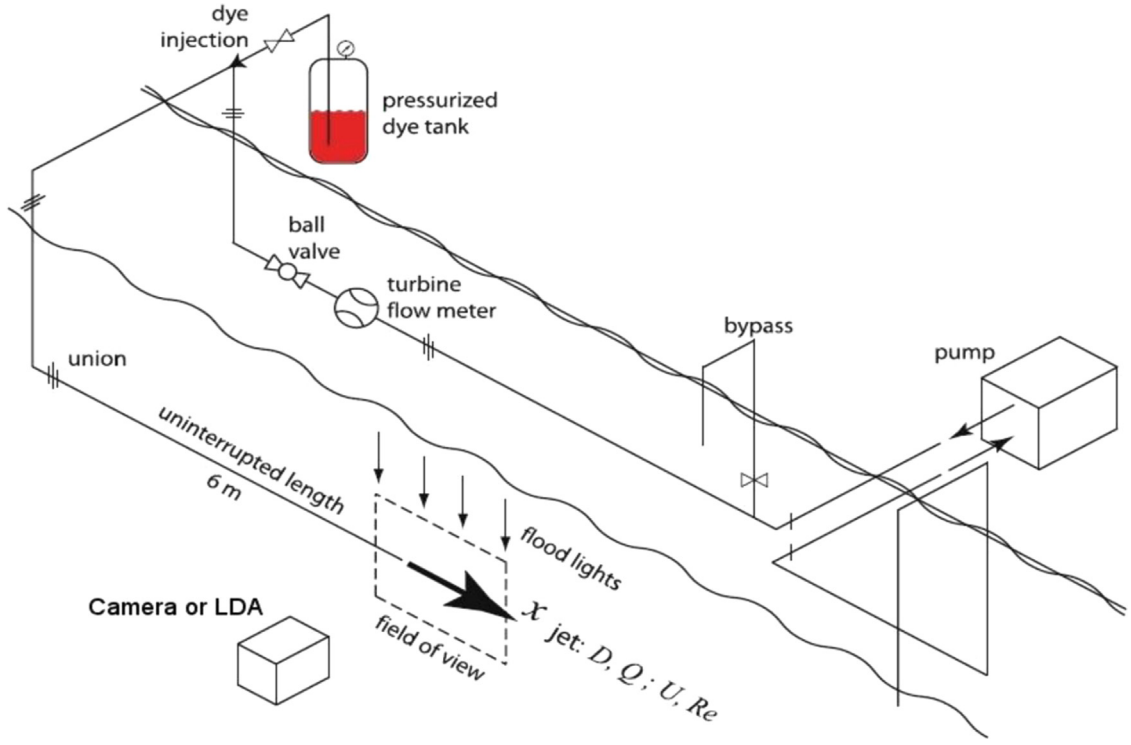

Fig. 3. Experimental setup for flow visualization at Berkeley Tow Tank.

literature searches found no experimental data to relate u_{vf} to $\overline{u}(x)$. Therefore, each member of the Plume Team had to make an educated guess for the relationship between u_{vf} and $\overline{u}(x)$. It is important to note that u_{vf} is not the same as the velocity at the statistical jet boundary, u_{sb}. The statistical jet boundary velocity, u_{sb}, is a statistical point on the radial profile of mean jet velocity, $\overline{u}_{jet}$.

The final challenge was to estimate the amount of water entrained into the oil jet, $E(x)$. The amount of entrainment can be calculated using the expansion of the jet, however, because the instantaneous boundary is constantly changing, an accurate measurement of the time-averaged jet expansion can be difficult.

The Plume Team overcame the challenges of the radial velocity profile and entrainment by making measurements of the velocity of visible features close to the jet exit, within, $x/D < 2$, in the ZFE. An assumption was made that coherent structures this close to the jet exit are sampling the constant velocity core, and therefore moving at the velocity of the core. Because entrainment is negligible at $x/D < 2$, and because the cross sectional area of the jet exit was used, the need for an estimate of entrainment was eliminated.

2. Description of UC Berkeley tow tank experiments

The authors of this paper have continued to develop this ROV video based approach since the DWH crisis. In October of 2010, Savaş [23] conducted experiments to simulate a large, submerged oil leak using a submerged, 10.1 cm diameter, dye-colored water jet in the U.C. Berkeley Tow Tank facility. The Tow Tank is 1.8 m deep, 2.4 m wide, and 67 m long. Submerged turbulent jets of dye-colored water were created at the midpoint of the Tow Tank, thereby avoiding wall effects. As will be explained later, LDA measurements confirmed that recirculation caused by wall effects were negligible.

The flow circuit used to create the submerged turbulent jet is shown in Fig. 3. Water is supplied to the submerged jet though Schedule 40, white PCV pipe of 10.1 cm inner diameter (4 in.) and a total length of approximately 20 m. Water is drawn from the tow tank through 10.1 cm diameter PVC pipe with a length of about 5 m. Before the jet exit, a straight, uninterrupted length of about 6.1 m ($L/D=60$) allows for a fully developed turbulent pipe flow at the jet exit [14,15]. The internal surfaces of the pipes have a measured relative roughness of about 0.001. The effect of the roughness was not considered in this study.

For Savaş's experiments in late 2010, water flow was supplied to the jet with a 9 HP gasoline centrifugal impeller pump (Duromax – XP904WP – 427 GPM). The impeller has three vanes and was run at 60 revolutions per sec (RPS). Thus, it can be expected that the pump will produce slight pressure/flow variations in the range of 180 Hz. To damp pressure fluctuations from the impeller pump, the pump is connected to the PVC pipe with 2.2 m length sections of flexible tubing on both the suction and discharge sides. As will be explained later, a frequency analysis of LDA data taken at the jet exit did not show dominant frequencies in the ranges expected from the pump impellers, indicating that the pump frequencies had been damped by the jet exit. The flexible tubing connecting the pump, the flow control valves, the turbine meter and 20 m of PVC pipe between the pump and the jet exit was sufficient to damp flow fluctuations caused by the pump.

The Duromax pump supplied flow rates of up to 4.8 gal/s to produce Reynolds numbers up to 220,000 with the 10.1 cm diameter jet exit. The Reynolds numbers of the DWH oil leak were in the range of 5×10^5–10^6. The flow rate was measured with a turbine flow meter (GPI Model TM400N) with a listed accuracy of $\pm 2\%$. The dye-colored jet was recorded with a high definition video camera with pixel resolution of 1920×1080 and a frame rate of 60 per second. The exposure time was set at 10 ms.

Fig. 4. Flow visualization with dye point injection. Water flow rate was 41.7 l/s (11 gal/s) producing a Reynolds number of 500,000. The camera frame rate was 1500/s and the exposure time was 0.75 ms.

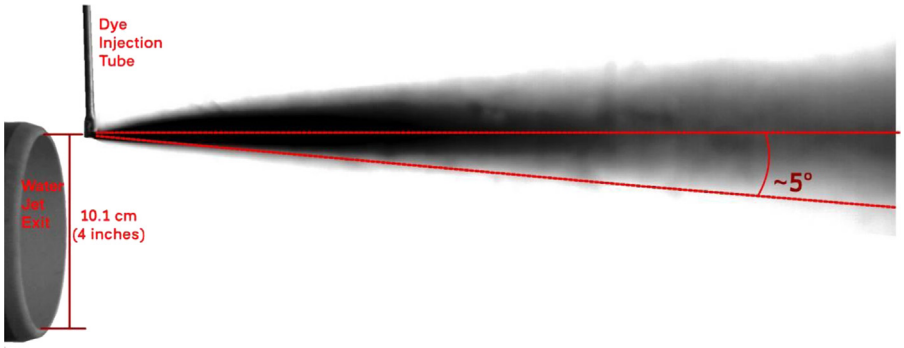

Fig. 5. Gray levels averaged over 2000 video frames with dye injector at $r/R=0.95$ and $x/D=0.20$.

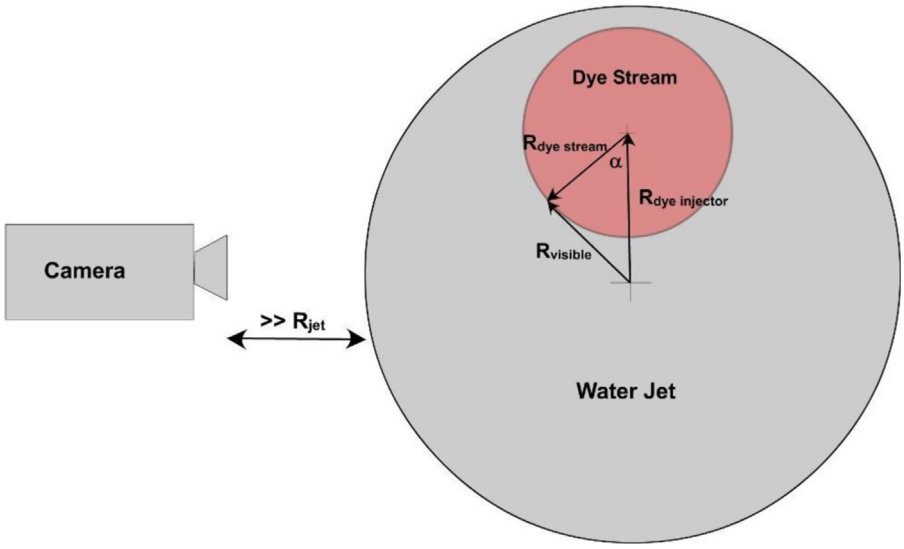

Fig. 6. Slice through the water jet tangential to jet centerline illustrating the expansion of dye stream.

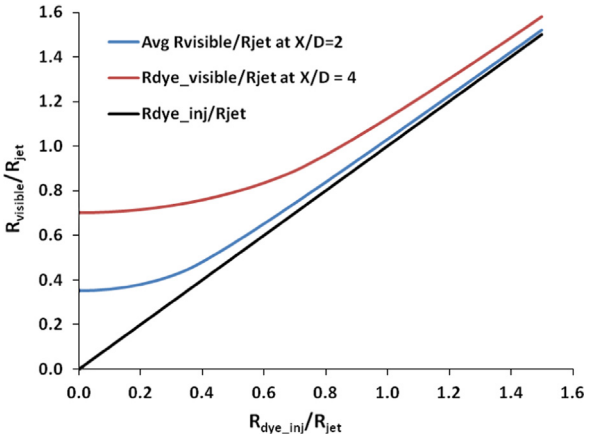

Fig. 7. Comparison of the average $R_{visible}$ and $R_{dye\_injection}$ at downstream distances of $x/D=2$ and 4.

In July of 2012, the authors of this paper conducted additional testing in the Berkeley Tow Tank with higher flow rates and better instrumentation. A diesel centrifugal pump (Power Prime Pumps, Model DV-100) was used to create flow rates up to 41.7 l/s (11 gal/s), thereby producing Reynolds numbers up to 5×10^5, within the range of the DWH oil leak jets. The DV-100 pump has a three-vane impeller that runs at 1400–2200 rpm. Thus, slight pressure/flow fluctuations with frequencies in the range of 70–110 Hz would be expected from the pump. A frequency analysis of LDA data at the jet exit did not show dominant frequencies at 70–110 Hz or harmonics of these frequencies, indicating that fluctuations from the impeller pump were damped by the jet exit.

The water jets were emitting from either a 10.1 cm diameter pipe or a 10.1 cm orifice at the end of a 20.2 cm diameter pipe. The edges of the orifice were smoothed and rounded.

The dye-colored jets were recorded with a high definition, high speed video camera (Vision Research Model v341) at frame rates up to 1500 per second at resolutions up to 2560 × 1100 pixels. The exposure time was 1.0 ms or less. Thus, frame rates were an order of magnitude higher and exposure times an order of magnitude lower than the October 2010 experiments [23]. This provided better temporal resolution of the rapidly changing flow features.

Two types of dye coloring of the water jet were used. The entire jet was dyed or "point" injection of dye was used. With point injection, dye is injected at a low velocity through a tube with an inner diameter of 3.175 mm (1/8 in.). To reduce flow disturbance, the end of the tube was tapered in the form of an air foil with the longest dimension aligned with the jet. Visual observations indicated minimal turbulence or vortex shedding caused by the dye injector. Fig. 4 shows point injection of dye in a water jet with a 4 in. diameter exit.

Turbulent diffusion caused the dye stream to expand radially. Fig. 5 shows the average gray level of the dye stream over 2000 video frames with the injector at the same position. The half angle of the dye expansion is about 5°.

Because of the expansion of the dye stream, the camera is viewing the outer boundary of the dye stream. Fig. 6 illustrates a slice through the jet tangential to the centerline. As will be explained below, PIV software was applied to the high speed video to measure the velocity of dyed flow features. Since the camera is viewing the outer boundary of the dye stream, the actual radial position of dyed features seen by the camera is at, $R_{visible}$, which is not the same as the radial position of the dye injector, $R_{dye\_injector}$.

To account for the effect of the expanding dye stream, an average radial position of the dye seen by the camera, $\overline{R}_{visible}$ was calculated. Using the Law of Cosines, $R_{visible}$, is calculated at points along the perimeter of the dye stream from $\alpha=0°$ to 180°, where $\alpha=0°$ is pointing vertically downward and $\alpha=180°$ is pointing vertically upward, then the values of $R_{visible}$ are averaged as

$$\overline{R}_{visible} = \sqrt{\frac{1}{n_\alpha}\sum_{\alpha=0°}^{\alpha=180°}\left[R_{dye\_inj}^2 + R_{dye\_stream}^2 - 2R_{dye\_inj}R_{dye\_stream}\cos\alpha\right]}$$

Substituting the radius of the dye stream, $R_{dye\_stream} = x \tan(\Phi_{dye\_stream})$, where Φ_{dye_stream} is the divergence half angle of the dye stream, gives

$$\overline{R}_{visible} = \sqrt{\frac{1}{n_\alpha}\sum_{\alpha=0°}^{\alpha=180°}\left[R_{dye\_inj}^2 + (R_{dye\_stream}\tan\Phi_{dye\_stream})^2 - 2R_{dye\_inj}R_{dye\_stream}\tan\Phi_{dye\_stream}\cos\alpha\right]}$$

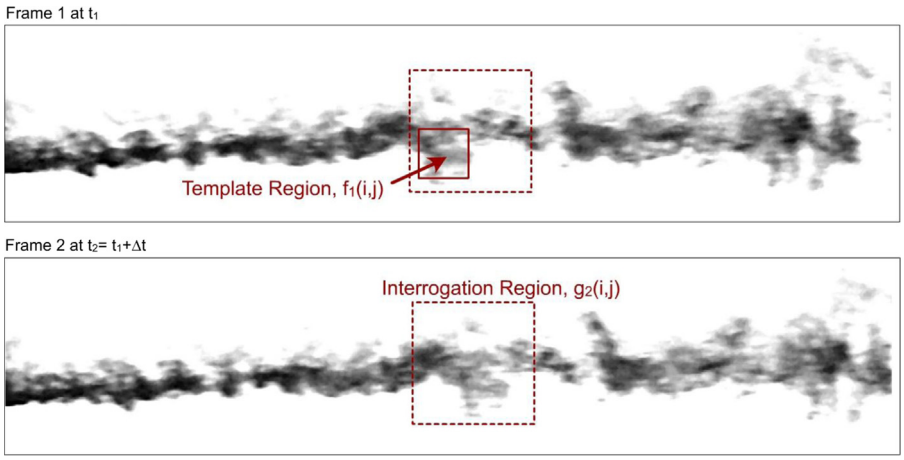

Fig. 8. Illustration of template and interrogation regions in two consecutive video frames.

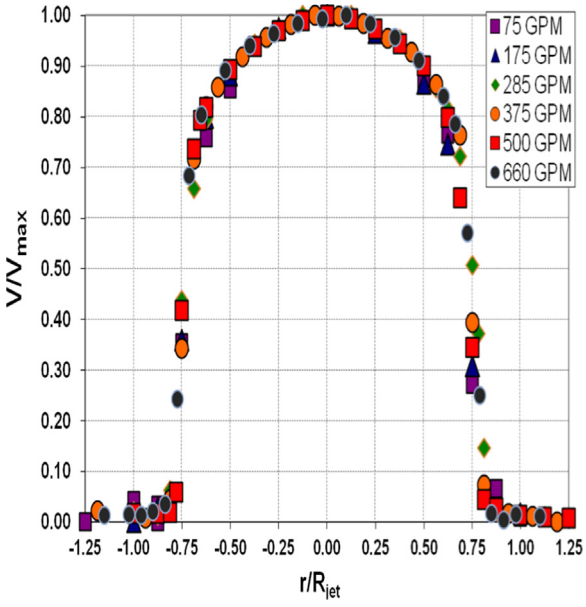

Fig. 9. Radial profiles of mean streamwise velocity measured with LDA for 10.1 cm diameter pipe jet at $x=0.25D$.

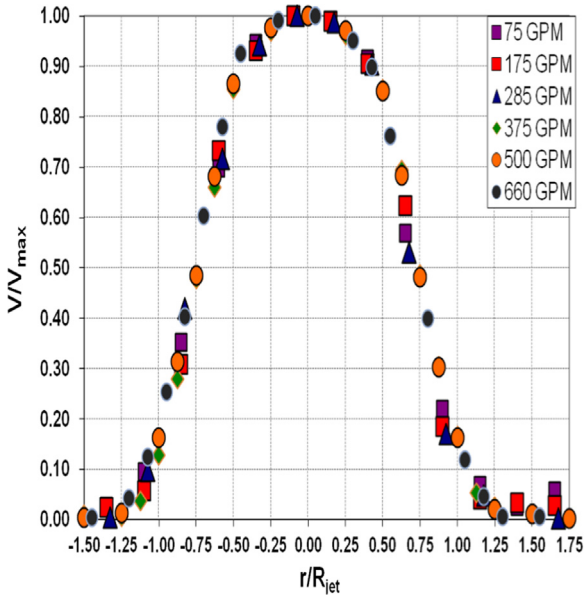

Fig. 10. Radial profiles of mean streamwise velocity measured with LDA for 10.1 cm diameter pipe jet at $x=2.0D$.

Fig. 7 shows the result of the calculation of $\overline{R}_{visible}$ at downstream distances where LDA data was taken, $x/D=2$ and 4. All radial profiles of streamwise velocity as measured with PIV software have the radial position corrected for expansion of the dye stream.

To measure the velocity of dyed flow features, the high speed video was analyzed with a PIV code developed by Tseng [28–30] The code is implemented as a plugin for ImageJ, an image analysis tool developed by the National Institutes of Health (NIH) [26].

The PIV tool by Tseng is based on a template matching approach. Two consecutive video frames are selected and the second frame is divided into interrogation regions as shown in Fig. 8. A smaller "template" region from the first frame is cross-correlated over the interrogation region of the second frame. The template cross-correlation can be described as

$$\Phi_{fg}(m,n)=\sum_{m}\sum_{n}f_1(i+m,j+n)g_2(i,j)$$

where $f_1(i, j)$ is the gray level array of template region in frame 1 and $g_2(i, j)$ is the gray level array of the interrogation region in frame 2. The subscripts m and n are the center position of the template over the interrogation region when a cross-correlation is calculated. The result is a correlation peak that measures the average displacement of the template region from frame 1 to frame 2. The correlation peak measures the average distance a dyed flow feature moved from the first video frame to the second. With the time between video frames, Δt, a velocity vector is calculated for each interrogation region. A threshold for the correlation peak can be set to reject poor correlations.

Large interrogation regions of around 200×200 pixels with a template region of around 100×100 pixels gave the best results, i.e., the best match with LDA data below. This is likely because larger flow features, with dimensions around 100×100 pixels for these experiments, tended to persist longer than smaller flow features. Additional research is being conducted to determine how to choose optimal sizes for interrogation regions [9].

At this point, it should be noted that the measurements being performed with PIV software are not traditional PIV measurements. PIV is actually a type of "Image Correlation Velocimetry (ICV)." ICV uses cross correlation of regions in consecutive video frames to measure the displacements of moving images. With PIV, the images are of seed particles which have been added to a transparent flow field that is being illuminated by a sheet of laser light. For this application, there are no seed particles in the flow field and it is not illuminated with a sheet of laser light. The images are of visible features at the

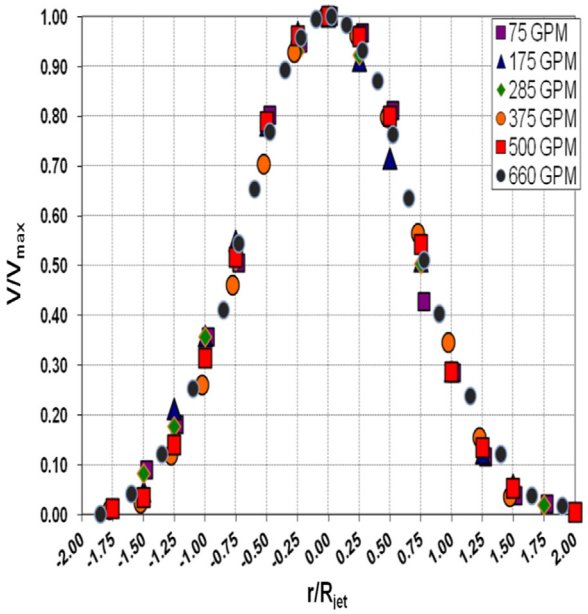

Fig. 11. Radial profiles of mean streamwise velocity measured with LDA for 10.1 cm diameter pipe jet at $x=4.0D$.

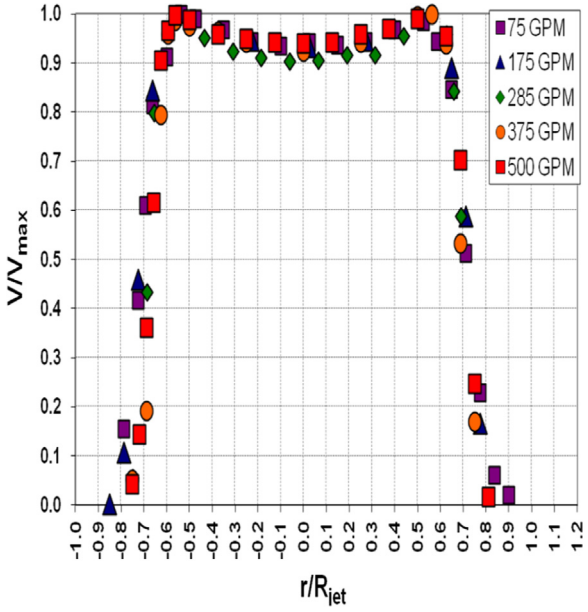

Fig. 12. Radial profiles of mean streamwise velocity measured with LDA for 10.1 cm diameter orifice at $x=0.25D$.

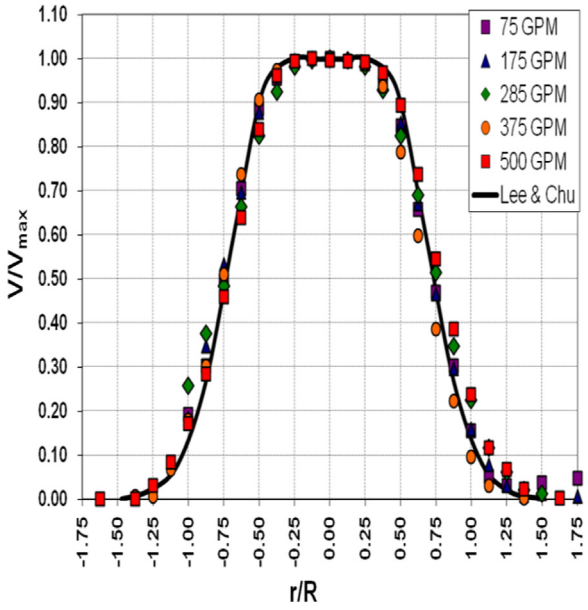

Fig. 13. Radial profiles of mean streamwise velocity measured with LDA for 10.1 cm diameter orifice at $x=2.0D$.

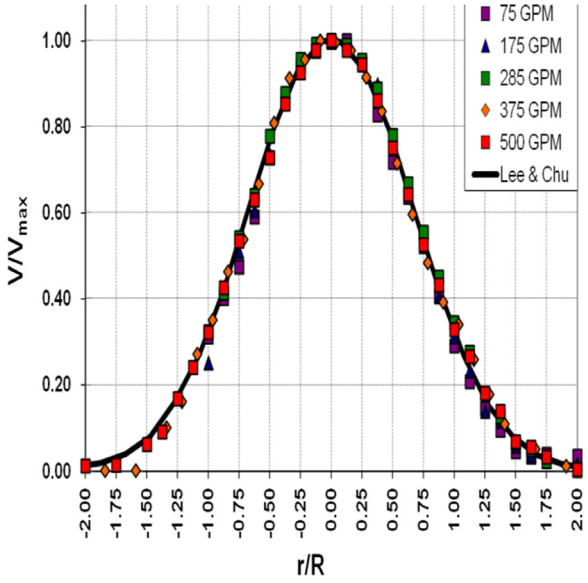

Fig. 14. Radial profiles of mean streamwise velocity measured with LDA for 10.1 cm diameter orifice at $x=4.0D$.

boundary of a submerged jet. This application is more appropriately called Image Correlation Velocimetry (ICV). For the remainder of this paper, the term ICV will be used. However, it should be understood that ICV means the application of software developed for PIV to measure the velocity of visible features at the boundary of a submerged jet.

Before the ICV analysis was performed, the high speed video was enhanced. To remove low frequency variations in gray levels caused by non-uniform illumination, a high pass Fast Fourier Transform (FFT) was performed to remove variations larger than $\frac{1}{4}$ of the maximum dimension of the video frame. The tubing producing the jet and the dye injection tube was removed from the video. The gray levels were inverted and contrast enhancement steps were applied to result in gray levels of zero outside of the dyed flow features. Some of the video was enhanced with an edge detection Sobel filter to increase the signal-to-noise ratio of visible features, but a systematic study of the effect of the Sobel filter was not performed. Choice of optimal enhancement filters is being studied in the ongoing DOI-BSEE project [9].

The radial profiles of streamwise velocity of the jet were also mapped with a Dantec FlowExplorer Laser Doppler Anemometer (LDA) [8] at downstream distances of $x/D_{jet}=0.25$, 2.0 and 4.0. A 300 mm focal length lens was used. The LDA was operated in non-coincidence mode. The jet flow was seeded with 50 μm diameter silver coated ceramic spheres of density 0.8–1.2 g/cm^3.

3. Results

3.1. Laser Doppler anemometry

Figs. 9–14 show LDA measurements of the radial profile of mean streamwise velocity for all flow rates for pipe and orifice

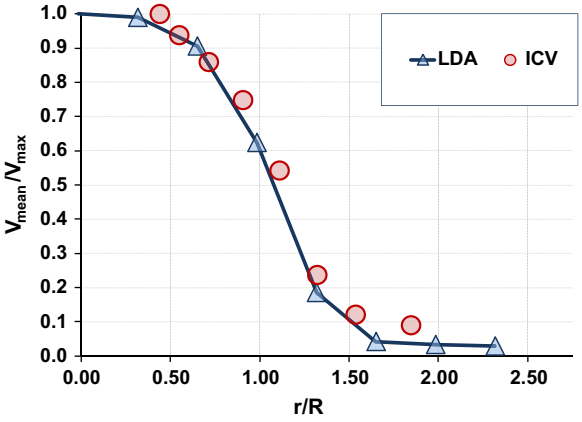

Fig. 15. Radial profiles of streamwise mean velocity at $x/D=2$.

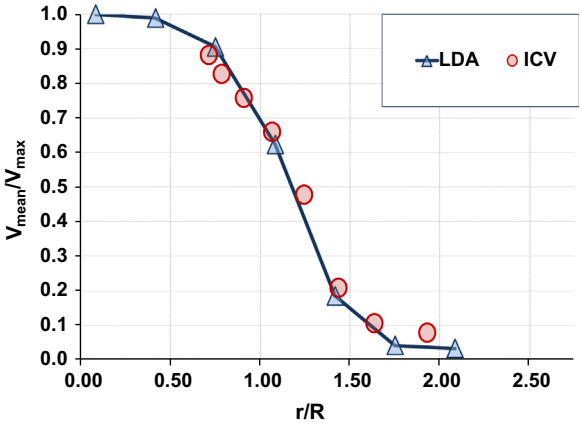

Fig. 16. Radial profiles of streamwise mean velocity at $x/D=4$.

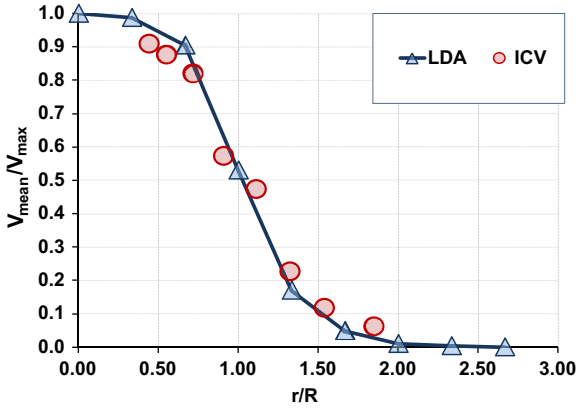

Fig. 17. Radial profiles of streamwise mean velocity at $x/D=2$.

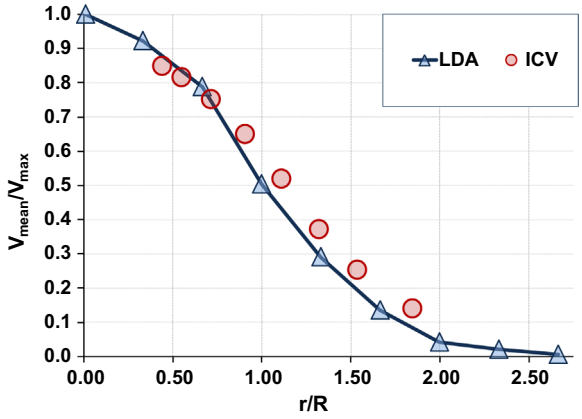

Fig. 18. Radial profiles of streamwise mean velocity at $x/D=4$.

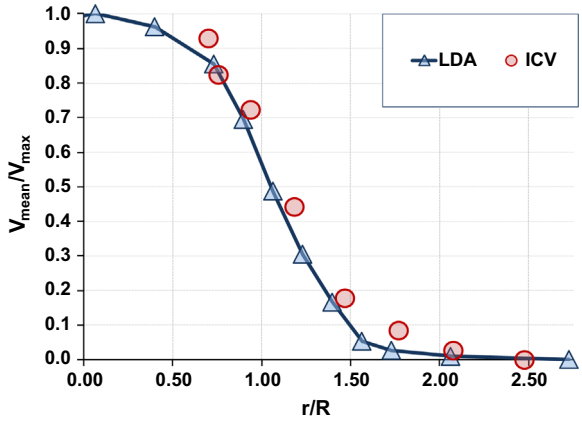

Fig. 19. Radial profiles of streamwise mean velocity at $x/D=2$.

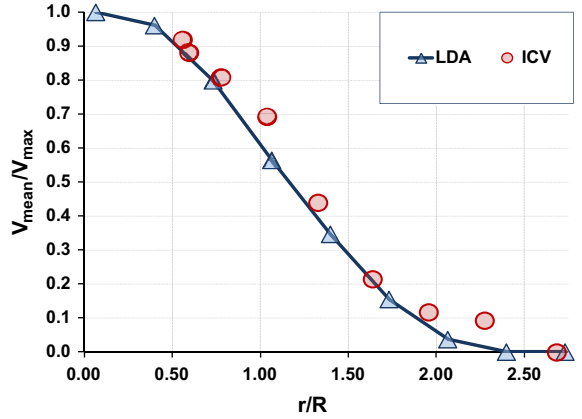

Fig. 20. Radial profiles of streamwise mean velocity at $x/D=4$.

discharges. The plots show mean streamwise velocity normalized with the mean centerline velocity on the ordinate axis and radial distance from the centerline normalized with the jet exit radius on the abscissa axis. Regardless of flow rate, all data fall onto the same profile at each measurement station. LDA measurements were extended outside the jet to ensure that the flow was still outside the jet, indicating negligible wall effects or recirculation currents. The profile for the 10.1 cm diameter orifice shows some "pinching effect" at $x=0.25D$, i.e., the radial profile of velocity shows maxima near the edge of the jet. This was likely caused by the rounded edges of the orifice. The pinching effect dissipates before $x=2.0D$.

Figs. 13 and 14 also show the theoretical predictions from Eqs. (1)–(3) of Lee and Chu. Good agreement with the theory of Lee and Chu further indicates that a classical submerged turbulent jet was created from a fully developed turbulent pipe flow.

3.2. *Image correlation velocimetry of dyed flow features*

Figs. 15–30 show the mean streamwise velocity normalized with the mean centerline velocity and radial distance from the centerline

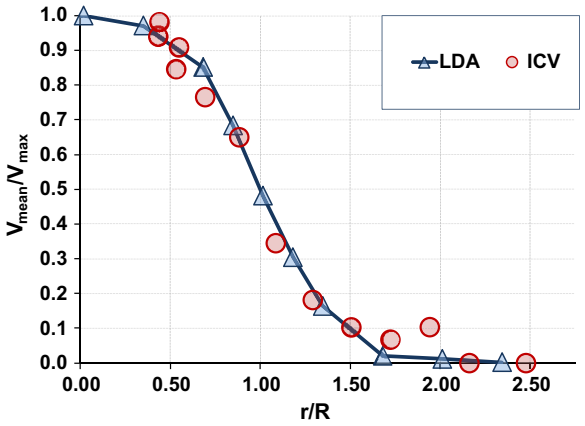

Fig. 21. Radial profiles of streamwise mean velocity at $x/D=2$.

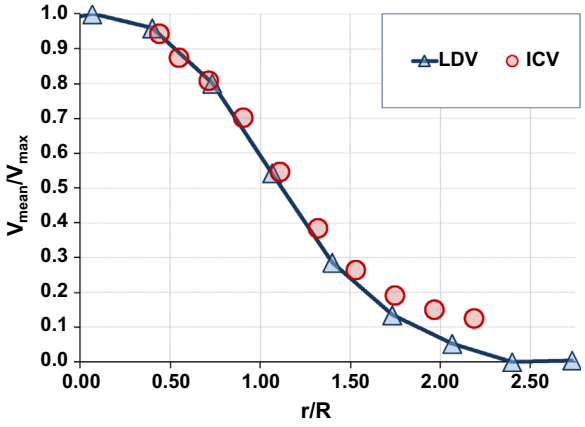

Fig. 22. Radial profiles of streamwise mean velocity at $x/D=4$.

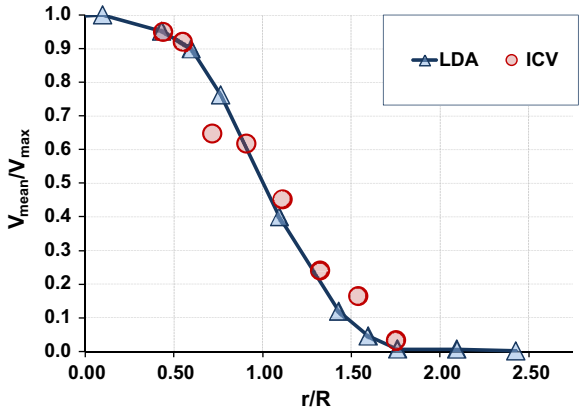

Fig. 23. Radial profiles of streamwise mean velocity at $x/D=2$; 4 in pipe jet; 660 GPM.

normalized with the jet exit radius as measured with ICV. Figs. 15–24 are for pipe discharge and Figs. 25–30 for orifice discharge.

3.2.1. *Pipe jet at 175 GPM (Re=133,000)*

A total of 16,837 video frames were recorded (10,000 video frames were recorded at 700 frames/s and 6837 frames at 1000 frames/s) for a total sample period of 16.6 s. ICV was applied with an interrogation window of 175 × 175 pixels and a subregion template of 125 × 125 pixels. The center of the interrogation region was moved in steps of 50 pixels. The mean velocity at the jet centerline was 1.61 m/s.

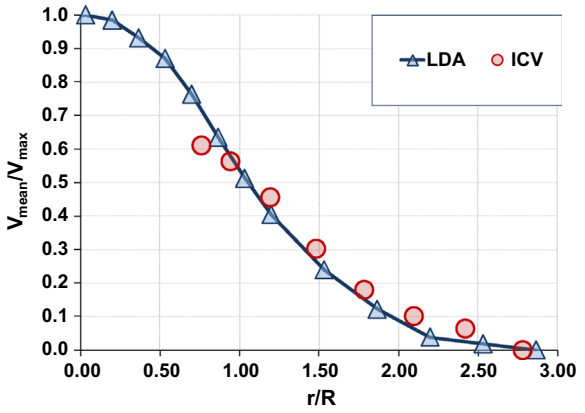

Fig. 24. Radial profiles of streamwise mean velocity at $x/D=4$; 4 in pipe jet; 660 GPM.

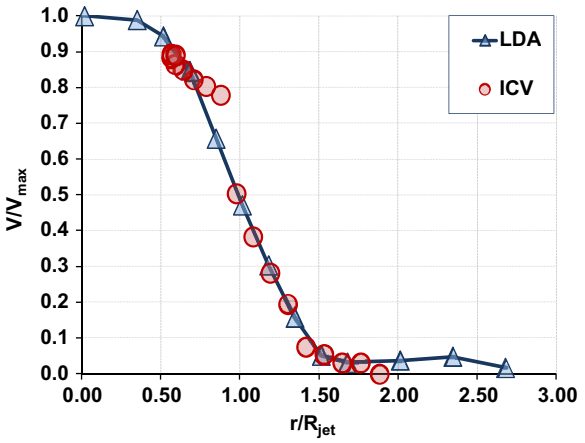

Fig. 25. Radial profiles of streamwise mean velocity at $x/D=2$; 4 in orifice jet; 75 GPM.

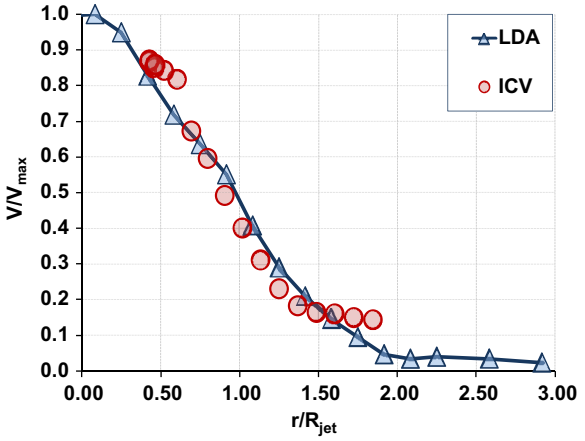

Fig. 26. Radial profiles of streamwise mean velocity at $x/D=4$; 4 in orifice jet; 75 GPM.

3.2.2. *Pipe jet at 285 GPM (Re=217,000)*

A total of 33,933 video frames were recorded at 1000 frames for a sample period of 33.9 s. ICV was applied with an interrogation window of 175 × 175 pixels and a subregion template of 125 × 125 pixels. The center of the interrogation region was moved in steps of 50 pixels. The mean velocity at the jet centerline was 2.55 m/s.

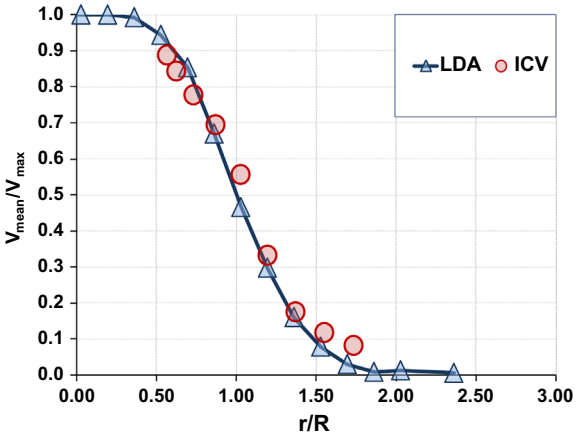

Fig. 27. Radial profiles of streamwise mean velocity at $x/D=2$; 4 in oriice jet; 175 GPM.

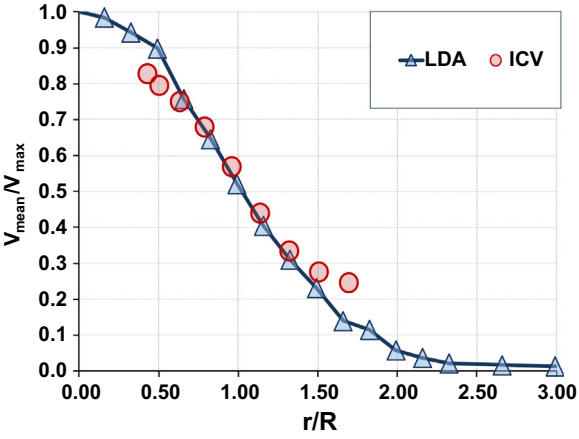

Fig. 28. Radial profiles of streamwise mean velocity at $x/D=4$; 4 in orifice jet; 75 GPM.

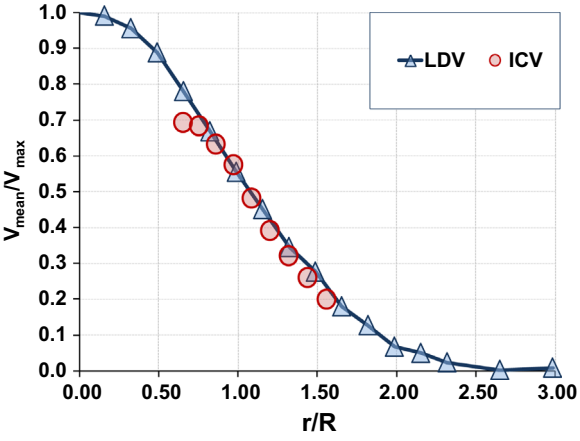

Fig. 29. Radial profiles of streamwise mean velocity at $x/D=2$; 4 in orifice jet; 285 GPM.

3.2.3. Pipe jet at 375 GPM (Re=280,000)

For this case, 34.3 s of high speed video were recorded with dye point injection. A total of 31,265 video frames were recorded (19,100 frames at 1000 frames/s and 12,165 frames at 800 frps) for a total sample period of 34.3 s. ICV was applied with an interrogation window of 175 × 175 pixels and a subregion template of 125 × 125 pixels. The center of the interrogation region was moved in steps of 50 pixels. The mean velocity at the jet centerline was 3.27 m/s.

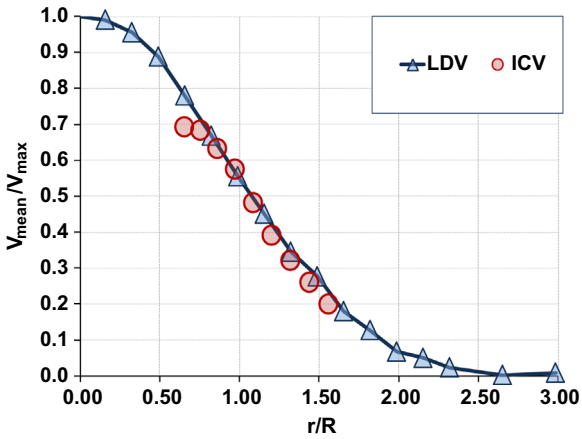

Fig. 30. Radial profiles of streamwise mean velocity at $x/D=4$; 4 in orifice jet; 285 GPM.

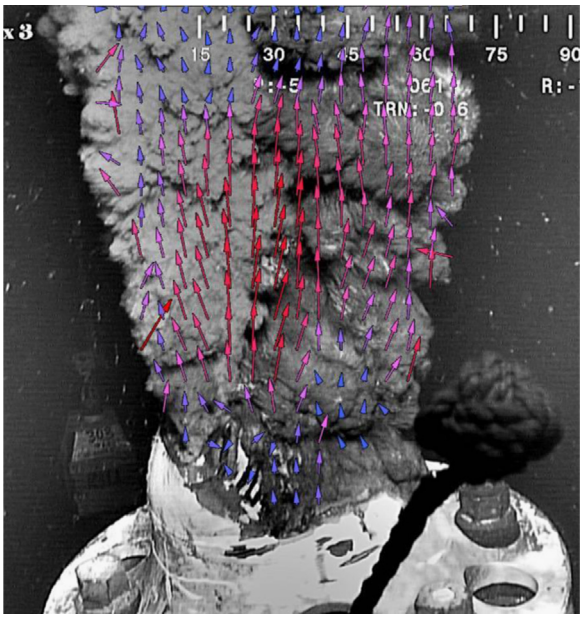

Fig. 31. Overlay of velocity vectors measured with ICV onto one video frame of the DWH oil leak jet taken on June 3, 2010. Pseudocoloring of velocity vectors ranges from blue at 0.1 m/s to red at 0.7 m/s. (For interpretation of the references to color in this figure legend, the reader is referred to the web version of this article.)

3.2.4. Pipe jet at 500 GPM (Re=379,000)

A total of 44,867 video frames were recorded for this case at 1150 frames/s for a total sample period of 39.0 s. To account for larger displacements at this higher jet velocity, ICV was applied with a larger interrogation window of 200 × 200 pixels and a subregion template of 125 × 125 pixels. The center of the interrogation region was moved in steps of 50 pixels. The mean velocity at the jet centerline was 4.31 m/s.

3.2.5. Pipe jet at 660 GPM (Re=500,000)

A total of 44,867 video frames were recorded for this case at 1150 frames/s for a total sample period of 39.0 s. To account for larger displacements at this higher jet velocity, ICV was applied with a larger interrogation window of 200 × 200 pixels and a subregion template of 125 × 125 pixels. The center of the interrogation region was moved in steps of 50 pixels. The mean velocity at the jet centerline was 4.31 m/s.

3.2.6. Orifice jet at 75 GPM (Re=57,000)

For this case, 45.4 s of high speed video of the dye injection stream were recorded: 22,700 video frames were recorded at 500 frames/s. The exposure time was 750 μs. ICV was applied with an interrogation window of 200 × 200 pixels and a subregion template of 100 × 100 pixels. A velocity vector was calculated at increments of 75 pixels. The mean velocity at the jet centerline was 0.74 m/s. The figures below shows the ICV and LDA measurements of mean velocity.

3.2.7. Orifice at 175 GPM (Re=133,000)

For this case, 23.6 s of high speed video of the dye injection stream were recorded: 11,800 video frames at 500 frames/s. The exposure time was 750 μs. ICV was applied with an interrogation window of 150 × 150 pixels and a subregion template of 90 × 90 pixels. A velocity vector was calculated at increments of 50 pixels. The mean velocity at the jet centerline was 1.72 m/s.

3.2.8. Orifice jet at 285 GPM (Re=216,000)

For this case, 43.8 s of high speed video of the dye injection stream were recorded: 21,900 video frames at 500 frames/s. The exposure time was 750 μs. ICV was applied with an interrogation window of 150 × 150 pixels and a subregion template of 90 × 90 pixels. A velocity vector was calculated at increments of 75 pixels. The mean velocity at the jet centerline was 2.62 m/s.

3.3. ICV applied to ROV video of the Deepwater Horizon leak jet

The ICV template matching tool of [29,30] was applied to a 10-s video clip of the Deepwater Horizon leak jet. Fig. 31 shows one frame of the video with velocity vectors measured with PIV software overlain. The video clip was recorded on June 3, 2010, after the riser pipe had been severed just about the Blow Off Preventor. The frame rate was 25 frames per second and the resolution of the field-of-view shown in Fig. 31 is 815 × 890 pixels. An interrogation region of 200 pixels and a template region of 100 pixels was applied at increments of 50 pixels. The radial profile of mean streamwise velocity at $x/D=1$ is shown in Fig. 32.

The direction of the velocity vectors in Fig. 31 appears to be qualitatively correct for most of the jet. The mean velocity measured at $x=1D$ was 0.44 m/s and the mean velocity for the entire jet was 0.35 m/s.

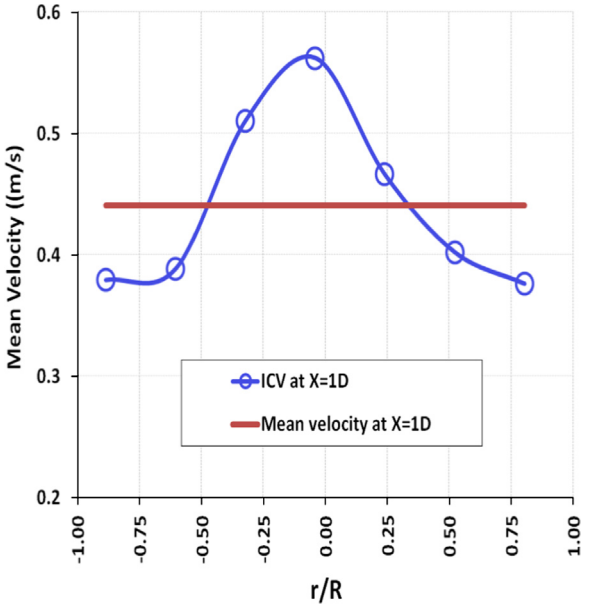

Fig. 32. Radial profile of mean streamwise velocity at $x=1D$ measured with ICV applied to ROV video taken on June 3, 2010.

4. Discussion

Given that our measurements of the dye-colored water jet using PIV software are in good agreement with the LDA measurements, it can be assumed that PIV is a relatively accurate tool for the experimental conditions of the dye-colored jet. The measurements of the DWH oil leak jet by three members of the Plume Team, each using a different PIV software and ROV video taken on June 3, 2010, produced consistent results of mean velocities in the range of 0.4–0.6 m/s. The measurements of this study of the DWH oil leak jet using ICV produced mean velocities of 0.44 m/s, which is in agreement with the results from the Plume Team. However, the velocities produced by manual feature tracking velocimetry (manual FTV) for the same ROV video were much higher, in the range of 1.1–1.5 m/s, and resulted in accurate estimates of the DWH oil leak rate. The leak rate was calculated by the Plume Team with Eq. (4).

Table 1 shows the calculations of the oil leak rate by members of the Plume Team. For the post riser-cut ROV video of June 3, 2010, all members of the Plume Team made their measurements close to the jet exit in the ZFE. The gas-to-oil ratio, X_{GOR}, was measured to be 0.41 by sampling the oil/gas mixture and taking it to the surface for analysis. All members used the cross-sectional area of the jet exit for their calculations. Entrainment was assumed to be negligible close to the jet exit, so the entrainment factor was 1.0.

The members using ICV (PIV software) made an assumption that the mean velocity of the jet near the jet exit was 1.6 times the velocity of visible features as measured with ICV (PIV software). The rationale for a value of 1.6 was based on two assumptions. First, it was assumed that the velocity of coherent structures at the boundary of the jet in the ZFE is equal to the mean streamwise velocity in the ZFE. The second assumption was stated as "*The level of intermittency in the shear layer, γ, is used as a fiduciary indicator of the presence of turbulent coherent structures, so that the average of the mean streamwise velocity weighted with γ provides an estimate of the convection velocity of the jet turbulent structures, which yields a ratio of 1/0.62 ≈ 1.6 between the velocity of the jet coherent structures measured by PIV and the bulk flow velocity at the potential cone of the jet*" [10].

The members using manual FTV also assumed that the velocity of coherent structures at the boundary of the jet in the ZFE is equal to the mean streamwise velocity in the ZFE. However, with manual FTV, only coherent structures were selected and measured, therefore assumptions about the intermittency of coherent structures or the effect of non-coherent structures were not necessary. The resulting estimates of oil leak rate with manual FTV were 38–84% higher than the estimates with PIV.

Table 1
Estimates of oil discharge rate from Deepwater Horizon by members of the FRTG Plume Team.

	Technique	u_{vf}	Intermittency factor	A_{jet}(m^2)	χ_{GOR}	$E(x)$	$\dot{Q}_{oil}$ (barrels/day)
Member A	ICV with PIV software	0.49	1.6	0.19	0.4	1	34,000
Member B	ICV with PIV software	0.50	1.6	0.19	0.4	1	34,000
Member C	ICV with PIV software	0.51	1.6	0.19	0.4	1	35,000
Leifer	Manual FTV	1.4	1.0	0.19	0.4	1	62,500
Savaş	Manual FTV	1.1	1.0	0.19	0.4	1	47,000
Shaffer	Manual FTV	1.4	1.0	0.19	0.4	1	61,000

The Plume Team developed their estimates of the oil leak rate in June and early July of 2010. The oil leak rate was later measured in the final well capping system with an improvised orifice system in late July 2010 and on August 2, 2010, the government announced its official estimate of the oil leak rate to be 53,000 bpd at the time of well capping and 62,000 bpd in April 2010 when the oil leak started [16]. The uncertainty was estimated to be $\pm$10%. The oil leak was also estimated to be in the range of 53,000–62,000 bpd by several other technologies, including sonar measurements, modeling of the well reservoir, and satellite imaging of the oil slick [16].

Since the velocity of the DWH oil leak jet could not be accurately measured with another technique, as the dye-colored jet could be measured with LDA, it is not possible to say how accurate ICV with PIV software was for the DWH oil leak jet. However, the fact that PIV software produced lower velocities that resulted in underestimates of the oil leak rate, suggest that either the PIV software was producing erroneously low velocities, or different assumptions are required for the relationship between the velocity of visible structures and the mean jet velocity.

Crone et al. [6,5] have measured the velocity of visible features on a dye-colored water jet, but at lower Reynolds numbers than in this study. The Reynolds numbers were in the range of 1000–10,000 to simulate hydrothermal ocean vents. They measured velocities of visible features with a custom pixel cross-correlation technique and with PIV software. The pixel correlation technique cross-correlates the gray level signal from two pixels, one downstream of the other. Crone et al. found that velocities measured with PIV software were 50% too low and led to underestimates of the jet flow rate. Crone et al. also applied their cross-correlation technique to ROV video of the DWH oil leak jets and estimated the leak rate to be 56,000 bpd [7].

There are numerous factors that could have influenced the PIV results for the DWH. The frame rate of the ROV cameras was 25 frames/s which was too slow to detect the rapid growth, deformation and decay of smaller scale coherent structures. The frame rate used to record the dye-colored water jet in the Berkeley Tow Tank was in the range of 500–1500 frames/s. This provided good temporal resolution of the smaller coherent structures. Choice of optimal frame rates is being studied in the DOI-BSEE project [9].

Use of PIV software also requires an estimate of the intermittency of coherent structures. Members of the FRTG Plume Team using PIV software estimated the intermittency to be 62%, i.e., coherent structures were present 62% of the time. However, it has not been verified that PIV software is indeed measuring coherent structures 62% of the time.

In this study it was found that PIV results are sensitive to the choice of the sizes of the interrogation and template regions. Using region sizes that are too small tends to produce erroneously low values of velocity near the center of the dye-colored jet. Because of the computation time required for a PIV analysis of high resolution, high speed video, a systematic study of the effect of the sizes of interrogation and template regions was not completed. For each flow condition, 20–50 GBytes of video were analyzed with PIV software. This required 1–2 days of CPU time on an HP Z800 computer with two Intel Xenon liquid cooled CPU's with 6 cores at a clock speed of 3.46 GHz, 96 GBytes of RAM, and a RAID0 array of eight 300 GByte SSD drives. With nine flow conditions, a systematic study of the size of the interrogation region and the template region, using just five size increments for each region, would require 225–450 days of CPU time.

Yet another factor influencing PIV results are the image processing steps used to enhance video images prior to PIV. In this study, a high pass FFT was applied to remove variations in brightness caused by variations in illumination. The high pass FFT was set about 1/4th the width of the field-of-view. Several contrast enhancement steps were applied to enhance the brightness of the dyed features and reduce the areas without dye to a gray level of zero. A median filter with a kernel size of 3×3 was applied to reduce high frequency pixel-to-pixel noise. A Sobel edge detection filter as applied to some of the high speed video prior to PIV software, however, a systematic study was not done, so conclusions cannot be drawn at this time regarding whether or not edge detection improves PIV software results.

5. Conclusions

Application of PIV software to the high speed video of dye-colored jets in the Berkeley Tow Tank produces velocities that are in good agreement with velocities measured with LDA. Application of PIV software to the DWH oil leak jets by several different members of the Plume Team and in this study produced consistent velocities in the range of 0.4–0.6 m/s using ROV video from June 3, 2010 applied close to the jet exit ($x/D < 2$). However, the velocities from PIV software are 2–3 times lower than velocities measured with manual feature tracking by hand. The fact that the estimates of the DWH oil leak rate using velocities from manual tracking were in good agreement with the actual leak rate suggests that the velocities from PIV software are erroneously low, or that different assumptions are required for the intermittency of coherent structures and the relationship between the velocity measured with PIV software and the mean velocity. The studies by Crone et al. support this conclusion. Because the DWH oil leak jet was not well controlled and velocities were not measured with an alternative technique, it is not possible at this time to definitively know why PIV software produced lower velocities. It is recommended that studies be conducted with a well characterized, submerged oil jet. The submerged oil jet should be recorded at very high frame rates to resolve the deformation of smaller scale features. It is also suggested that a systematic study of effect of sizes of interrogation regions be conducted.

References

[1] Abramovich GN. The theory of turbulent jets. MIT Press; 2003.
[2] Albertson ML, Dai YeB, Jensen RA, Rouse H. Diffusion of submerged jets. Trans ASCE 1950;115:629–44.
[3] Bradbury LJS. The structure of a self-preserving turbulent plane jet. J Fluid Mech 1965;23:31–64.
[4] Chen CJ, Rodi W. Vertical turbulent buoyant jets: a review of experimental data. Science and applications of heat and mass transfer, vol. 4. Pergamon Press; 1980.
[5] Crone TJ, Wilcock WSD, McDuff REF. Flow rate perturbations in a black smoker hydrothermal vent in response to a mid-ocean ridge earthquake swarm. Geochemistry Geophysics Geosystems 23 March 2010;11(3):1–3.
[6] Crone TJ, McDuff RE, Wilcock WSD. Optical plume velocimetry: a new flow measurement technique for use in seafloor hydrothermal systems. Experiments in Fluids, Volume 45, Issue 5, p.899-915.
[7] Crone TJ, Tolstoy M. Magnitude of the 2010 Gulf of Mexico oil leak. Science 2010;330(6004):634.
[8] Dantec. 2013. ⟨www.dantecdynamics.com⟩.
[9] DOI-BSEE Project E13PS00032. Development of a ROV deployed video analysis tool for rapid measurement of submerged oil/gas leaks. Department of the Interior, Bureau of Safety and Environmental Enforcement funded project with NETL and UC Berkeley; 2013.
[10] FRTG Plume Analysis Team. Deepwater Horizon Release Estimate of Rate by PIV, ⟨www.doi.gov/deepwaterhorizon⟩; 2010.
[11] Eggers J, Villermaux E. Physics of liquid jets. Reports on Progress in Physics 2008;71:1–79.
[12] Guo B, Langrish TAG, Flecther DF. An Assessment of Turbulence Models applied to the Simulation of a Two Dimensional Submerged Jet. Applied Mathematical Modeling 2001;25(8):635–53.
[13] Lee and Chu, 2003, "Turbulent Jets and Plumes: A Lagrangian Approach," Authors. Joseph Hun-wei Lee and Vincent Chu, Kluwe Academic Publishers ISBN numbers are ISBN-13: 978-1402075209 ISBN-10: 159693350X.
[14] Nikuradse, J. Gesetzmasigkeiten der turbulenten Stromung in glaten Rohren. Translated as 'Laws of turbulent flow in smooth pipes'. NASA TT F-10 359 (1966); 1932.
[15] Nikuradse, J. Stromungsgesetze in rauhen Rohren VDI-Forschungsheft no. 356. Translated as 'Laws of Flow in Rough Pipes',NACA-TM 1292 (1950); 1933.

[16] McNutt MK, Camilli R, Crone TJ, Guthrie GD, Hsieh PA, Ryerson TB, Savaş Ö, Shaffer F. Review of flow rate estimates of the Deepwater Horizon oil spill. (Published online on December 20, 2011). Proc Natl Acad Sci USA 2011. http://dx.doi.org/10.1073/pnas.1112139108.
[17] Miller D, Coming E. Static pressure distribution in the free turbulent jet. J Fluid Mech 1957;3:1–16.
[18] National Commission on the Deepwater Horizon Oil Spill and Offshore Drilling, December 2010. Deepwater: The Gulf Disaster and the Future of Offshore Drilling. Report to the President, available at: www.oilspillcommission.gov.
[19] Papanicolaou P, List EJ. Investigations of round vertical turbulent buoyant jets. J Fluid Mech 1988;209:151–90.
[20] Pope SB. Turbulent flows. Cambridge University Press; 2000 (ISBN: 9780521598866).
[21] Prandtl L. Bericht über Untersuchungen zu ausgebildeten Turbulenz. ZAMM 1925;5:136.
[22] Rajaratnam N. Turbulent jets; developments in water science. Elsevier; 1976 (ISBN 0444413723, 9780444413727).
[23] Savaş Ö. A visual study in the near field of turbulent jets and implications for estimating accidental discharges. (Published online on September 4, 2012). Exp Fluids 2012;53(5):1501–14. http://dx.doi.org/10.1007/s00348-012-1372-7.
[24] Schlichting H, Gersten K. Boundary layer theory. 8th ed. Springer-Verlag; 2004 ISBN:81-8128-121-7.
[25] Schlumberger Report. Fluid analysis on Macondo samples, BP field, Mississippi Canyon 252, well: OCS-G, 32306#1, reservoir sample analysis report. Schlumberger Report 201000053; 2010.
[26] Schneider CA, Rasband WS, Eliceiri KW. NIH Image to ImageJ: 25 years of image analysis. Nat Methods 2012;9:671–5.
[27] Trujillo MF, Hsiao CT, Choi JK, Paterson EG, Chahine GL, Peltier LJ. Numerical and experimental study of a horizontal jet below a free surface. In: Proceedings of the 9th international conference on numerical ship hydrodynamics, Ann Arbor, MI; 2007.
[28] Tseng Q, et al. Spatial organization of the extracellular matrix regulates cell–cell junction positioning. Proc Natl. Acad Sci 2000(2012):. http://dx.doi.org/10.1073/pnas.1106377109.
[29] Tseng Qingzong. Study of multicellular architecture with controlled microenvironment. (Ph.D. dissertation). Université de Grenoble; 2011.
[30] Tseng Q. Template matching and slice alignment—ImageJ plugins 2013.
[31] Wygnanski IJ, Fiedler H. Some measurement in the self-preserving jet. J Fluid Mech 1969;38(3):577–612.

APPENDIX 2: UC Berkeley Final Report to NETL

Development of a ROV Deployed Video Analysis Tool for Rapid Measurement of Submerged Oil/Gas Leaks

Final Report

Reporting Period
May 4, 2014 – March 31, 2016

Ömer Savaş

Submission Date
March 21, 2017

Award No: DE-FE0014314

Submitting Organization
The Regents of the University of California
c/o Sponsored Projects Office,
2150 Shattuck Avenue, Suite 300,
Berkeley, CA 94704-5940

Abstract

Expanded deep sea drilling around the globe makes it necessary to have readily available tools to quickly and accurately measure discharge rates from accidental submerged oil/gas leak jets for the first responders to deploy adequate resources for containment.

We have developed and tested a field deployable video analysis software package which is able to provide in the field sufficiently accurate flow rate estimates for initial responders in accidental oil discharges in submarine operations. The essence of our approach is based on tracking coherent features at the interface in the near field of immiscible turbulent jets.

The software package, **`UCB_Plume`**, is ready to be used by the first responders for field implementation. We have tested the tool on submerged water and oil jets which are made visible using fluorescent dyes. We have been able to estimate the discharge rate within 20% accuracy.

A high end WINDOWS laptop computer is suggested as the operating platform and a USB connected high speed, high resolution monochrome camera as the imaging device are sufficient for acquiring flow images under continuous unidirectional illumination and running the software in the field. Results are obtained over a matter of minutes.

Table of contents

Introduction

Expanded deep sea drilling around the globe makes it necessary to have readily available tools to quickly and accurately estimate discharge rates from accidental submerged oil/gas leak jets (Figure 1). We had proposed developing a field deployable video analysis software package which is able to provide in the field sufficiently accurate flow rate estimates for initial responders in accidental oil discharges in submarine operations. The essence of our approach is based on tracking in the near field flow features at the interface of immiscible turbulent jets. Then, the flow velocities at the edge are intrapolated to the center of the jet after which the flux is estimated.

The task assumed by Berkeley is to develop the software and to test it in small scale experiments designed to obtain detailed, high-resolution PIV velocity maps of coherent visible features and inside a transparent oil jet under very closely controlled conditions. The small-scale water and oil jet experiments allows for viewing and measuring the velocity of visible features and relate the velocity of visible features to the internal velocity profiles.

We have developed a software package, **`UCB_Plume`**, that is ready to be used by the first responders for field implementation. We have tested the tool on submerged water and oil jets which are made visible using fluorescent dyes. We are able to estimate the discharge rate within 20% accuracy.

A high end WINDOWS laptop computer is suggested as the operating platform and a high speed, high resolution monochrome camera as imaging device are sufficient for acquiring flow images under continuous unidirectional illumination and running the software in the field over a matter of minutes.

Berkeley experiments

A series of small-scale water and oil jet experiments are designed for viewing and measuring the velocity of visible features and relate the velocity of these features to the internal velocity profiles. The data are used to fine tune the parameters of the image correlation velocimetry algorithm and flow rate estimation strategy.

Experimental setup

The experiments are setup in a 4'×4'×8' glass tank located in 140 Hesse Hall of UC Berkeley Campus. The first set of experiments conducted in August 2014 employed horizontal discharge tubes. While this is of no concern when discharging water into water, it was obviously a severe restriction when oil (of lower density than water) was injected into water. Therefore, the setup is reconfigured for vertical discharge. Figure 2 shows the overall view of the setup. Figure 3 is a mosaic of various views and components. The schematic of the vertical discharge flow setup is shown in Figure 4 along with the specifications of its major components. The flow fields are recorded using simultaneous schlieren, PIV, and FV cameras at high speed; IDT X3 and Y3 cameras. A 10W (CW) Argon Ion laser is employed for both flow visualization (FV) and PIV. The laser light sheet illuminates the flow from the side of the tank. The PIV and FV cameras are positioned normal to the plane of the laser sheet. The schlieren system is wrapped around the tank by folding the classical Z-configuration using flat mirrors and set at 12 degrees off the normal the laser sheet in order to allow clear 90-degree access for the PIV and FV cameras. The flow is driven by a pump and the flow rate is monitored using an industrial grade 1% accurate turbine flow meter.

In order to minimize the use of oil, the gear pump was driven by a micro-stepper motor under computer control for 10-20 seconds at a time. For simultaneous vertical- and horizontal- knife edge schlieren images, the optics is reconfigured temporarily where the uninterrupted light bean was split by a cubic beam splitter for the two schlieren imaging schemes. For fluorescent-dyed water and oil jet visualization experiments, the *shell* of the jets were visualized under oblique LED illumination at about 35 degrees.

The discharge tube was fixed as 1/2" nominal diameter smooth copper tube with 16-inch length. The flow at the inlet to the tube is tripped with a mesh screen. Therefore, the length of the tube is sufficient for fully developed turbulent flow to establish at sufficiently high Reynolds numbers.

Sample images

Figures 5 and 6 show horizontal discharge oil experiments, sample shadowgraph and PIV runs. Due to the buoyancy of the jet, the flows bend upward quickly. Even though these are reasonable experiments in their own right, they are not amenable to verification of code development. Hence the horizontal discharge experiments are quickly abandoned in favor of vertical discharge runs.

- Figures 7 shows a sample schlieren image of a vertically discharging water jet and Figure 8 a sample PIV image.
- Figure 9 is mosaic of simultaneous shadowgraph and visible images of vertical oil jets of 5cs silicone oil at 45 cm^3/s (Re=900); and of oil jet of 1cs silicone oil at 360 cm^3/s (Re=35,000).
- Figure 10 shows sample flow images at Q=1.0 gallon/min (63 cm^3/s): schlieren with vertical knife edge and horizontal knife edge. The images are not simultaneous.
- Figure 11 shows simultaneous schlieren and cross-sectional fluorescent dye images at Q=1.0 gallon/min (63 cm^3/s), vertical knife edge.
- Figure 12 shows simultaneous schlieren and PIV images at Q=1.0 gallon/min (63 cm^3/s), vertical knife edge.
- Figure 13 shows simultaneous schlieren and PIV images at Q=1.0 gallon/min (63 cm^3/s), horizontal knife edge.

Completed experimental work

We completed the data acquisition phase of the project by the end of January 2015. These final experiments included fluorescent-opaque water discharge experiments, where the shadows of the edge features of the flows are recorded simultaneously with schlieren images. We also recorded *simultaneous* vertical and horizontal knife edge schlieren visualizations of water jets. Lastly, we carried out opaque oil discharge runs using 1cs and 5sc silicone oils which were made fluorescent-opaque using an oil soluble fluorescent dye. These data are cataloged for algorithm development.

Rudimentary data processing

Figures 14 and 15 show the results of rudimentary image correlation velocimetry results corresponding to images in figure 11 and 12, respectively. We have used our inhouse software called WALPT for processing. All image pairs are processed using identical processing parameters, such as interrogation window size, using our in-house code. No preprocessing is done. The results in these figures are not normalized. They are presented for qualitative discussion only. Clearly, results based on the schlieren images and flow visualization images do not even identify the jet. At this stage, it is not immediately clear what the reason for this behavior is. For example, that the flow seems reversed in the right frame of figure 14 may be an artifact of the decreasing dye concentration hence, decreasing image intensity as the jet gets diluted through entrainment. On the other hand, the particle image (Figure 15, right frame) very clearly identifies the jet. Obviously, if an autonomous processing algorithm is desired, much innovation has to be done.

Algorithm development

We have developed of a novel image processing technique for analyzing video decks.. The impetus for this development is the necessity of separating features that are moving at different speeds in a video stream. In the context of flow discharge, eddies of different size move or seem to move at different speeds in video streams. A similar case is observed when looking into discharges via schlieren videography. Our eyes can easily distinguish such features by comparing *successive* images. The approach we devised attempts to mimic human perception. The process is illustrated in figure 16. To identify a feature moving at given speed, we look at successive images. We extract from the video stream, the time history of image intensity at a given pixel $I_{ij}(t)$. A slow moving feature will have a slowly varying signature in $I_{ij}(t)$ and a fast moving, a fast varying signature. Therefore, filtering (or, equivalently, convolution) of $I_{ij}(t)$ allows us selectively extract features for their propagation speeds. We name this process PIXelwise TIme Filtering or PIXTIF for short. The process preserves spatial gradients. Once a video stream is processed for PIXTIF, the images can be further process to extract tractable features, such as Canny filtering to detect edges for image correlation velocimetry. The implementation of PIXTIF using Fourier transforms is straight forward: The Fourier transform of $I_{ij}(t)$ is multiplied by a suitably chosen filter kernel $G(\omega)$ in frequency domain. The resultant spectrum is inverted to construct the PIXTIFed image $\sim I_{ij}(t)$:

$$\sim I_{ij}(t) = F^{-1} \{ F [I_{ij}(t)] * G(\omega) \}. \qquad (1)$$

The process requires large computational resources, especially, computer memory. The whole video stream must be loaded at once into the computer memory for rapid access. The construction of the filter kernel $G(\omega)$ requires delicate attention. In particular, the filter shape (band-pass, low/high-pass) and cut-off parameter as well as the cut of rate are critical to obtaining useful results. For example, when employing a Gaussian filter,

$$G(\omega) = \exp[-(\omega - \omega_o)^2 / \Delta] \qquad (2)$$

the center frequency ω_o and the filter width Δ must be carefully chosen. These parameters are linked to the inertial range of the turbulence spectrum of the flow and must be adjusted for the Reynolds number. We have chosen an iterative approach to settle on the final choices for flow rate estimation. This strategy is built into the software package and is not discussed here further.

In parallel, we have developed methods to process uncompressed AVI files and subroutines to analyze image sequences. Figure 17 shows a PIXTIF example. In this exercise, a schlieren video sequence is PIXTIF'ed as illustrated in figure 16 using a Gaussian bandpass filter in frequency domain. The left image in figure 17 shows the PIXTIF'ed version of the schlieren image on the left in figure 16. The corresponding image pair is processed through the correlation velocimetry algorithm using the very same parameter used earlier. The resulting velocity vector field is shown on the right in figure 17. Clearly, the discharge jet is now well captured.

Discharge rate estimation

We assume that, in the region of interest of a developed or nearly developed turbulent jet, the average velocity profile u(r), averaged over both radial and axial directions, can be adequately described as a Gaussian bell curve (Figure 18)

$$u(r)/U_c = \exp[-r^2/\sigma^2] \quad (3)$$

where U_c is the average centerline velocity and σ a width parameter. At the mean visible outer shell of the boundary r_c, the velocity of the eddies, the celerity C, is, from Equation (3),

$$C/U_c = \exp[-r_c^2/\sigma^2]. \quad (4)$$

Similar to the classical shear layer, if we assume that we can relate to U_c to C to as

$$U_c = (1+\varphi^{-1/2})\, C \quad (5)$$

where φ is the density ratio, we can extract from Equation (4) the width parameter σ as

$$\sigma^2 = r_c^2 / ln(1+\varphi^{-1/2}). \quad (6)$$

The flow rate Q is now deduced, by integration the Gaussian profile (3) over the interval $[0, r_c]$ as

$$Q = \pi r_c^2 C / [\varphi^{1/2}\, ln\, (1+\varphi^{-1/2})] \quad (7)$$

where r_c is the radius of the visible discharge radius, C the average celerity of the eddies at r_c and φ is now the specific gravity (sg) of the fluid discharging into water. Note that $Q=1.44\pi r_c^2 C$ when $\varphi = 1$, which corresponds to the case where the ambient fluid and the discharging fluid are the same, such as water jet in water.

The key assumption in proceeding approach is that, if the jet and ambient fluids are immiscible, as the case is in an oil spill, flow images show the fluid interface, hence, the velocity information based on those images is the celerity $C(r_c)$ at the interface. The implication is that, one would obtain nearly uniform celerity around during the data analysis. Figure 20 shows a water jet made visible with fluorescent dye at Q=1 gpm, Re=4500. The intricacy of the jet-ambient fluid interface is clearly delineated due to low molecular diffusivity of water. The velocity of the interface features are expected to be uniform around the *interface shell*. Figure 21 shows the velocity profile at the *interface shell* of the jet fluid which is nearly uniform over the width of the jet.

In proposing the flow rate calculation in the above equation (7), we neglected entrainment of the ambient fluid into the jet. Since we focus our attention on the near field of the jet, the fraction of the entrained fluid is still small, hence the error incurred is well within the uncertainty inherent in the calculation of Q. Further, the incurred error will tend to make Q an overestimate of the actual discharged species flow rate, which is

less undesirable than an underestimated value. Instead of the Gaussian profile in Eq. (3), on could propose the algebraic profile deduced from the assumption of constant eddy viscosity across the jet. The final results, however, show little difference.

Image Processing

Video stream are processed at multiple steps for flow rate estimation. The flow chart in Chart 1 highlights the procedure. Figure 22 shows a snapshot from the video stream, the average flow field, and its rms field. The details in Figure 22a highlight the flow scales that have to be considered. These scales depend of the jet Reynolds number. An a priori estimate of these scales is later be used in setting the processing parameters for the video image deck. The average picture in (b) is used to establish the jet geometry in autonomous operation. The rms picture in (c) is used to determine the average edge of the jet fluid r_c over the region of interest, ROI.

Figure 23 shows highlights of the image processing prior to correlation velocimetry. Figure 23a shows the PIXTIF'ed result of image in Figure 22a. PIXTIF'ed video deck is used to determine the velocity field via cross correlation of deformed fluid parcels in WALPT. The picture in Figure 23(b) shows the Canny edge-detection result corresponding to the PIXTIF'ed image in 23(a). We are currently continuing with PIXTIF'ed image deck. The highlighted strip in Figure 23(c) marks the region of interest which is used to determine the edge of the jet fluid r_c. The strip, which is determined from the rms picture in Figure 22(c) is also used to mask the results of WALPT to determine the average celerity C at the interface over ROI. Note that ROI is deliberately chosen to be in the near field of the jet, where it may not have fully developed yet. The advantage of this choice is that the flow feature can be clearly identified.

Implementation

The implementation of the flow rate calculation in equation (7) is done by the batch script **plume.bat,** which is outlined in Chart 2. After some minimal interaction from the operator, the software produces its final results on the screen and archives them permanently. Chart 3 shows the screen flow during the execution of the batch process, which simply requires a double click on the **plume** icon to start.

Sample results

Table 1 shows the results from **`UCB_Plume`** processing for the flow rate. Two oil jets are shown: 5cs and 1 cs. Figure 24 shows the salient steps during data processing for three selected flows. Depending of the choice of numerous parameters specified, the estimated flow rate from the video stream can either closely match that determined from the flow meter in the flow loop or deviate substantially.

Accomplishments

Implementation

The script for discharge rate calculation is outlined in Chart 2. After some minimal interaction from the operator, the software proceeds autonomously, and produces its final results on the screen and archives them permanently. The User's Manual of the software package is presented in Appendix 1. The listing of the script may be found in Appendix 2.

Algorithm development

Video stream or image sequences are processed at multiple steps for discharge rate estimation. The flow chart in Chart 1 highlights the procedure. Chart 2 shows the operation block diagram of the software. Chart 3 shows the screen shot of the process from start to end, showing the final output of the software; an estimate of the flow rate in various units. After some minimal interaction from the operator, the software proceeds autonomously, and produces its final results on the screen and archives them permanently. The User's Manual of the software package is presented in Appendix 1. The listing of the script may be found in Appendix 2.

Table 1 shows our most recent runs of the software on our experiments, and Table 2 on OMSETT experiments at the highest flow rate. As can be seen from the end results in the last columns, the software is able to estimate the flow rates within 20% accuracy which is deemed sufficient for the first-response purposes in the field.

Presentation at BSEE

We made a presentation at BSEE in Sterling, Virginia, on March 24, 2016. Franklin Shaffer of NETL and Ömer Savaş of UCB made presentations to the cognizant officers of the program at BSEE. It was well received. Slides of this presentation may be found in Appendix 3.

Hardware requirements for field implementation

A high end WINDOWS laptop computer as the operating platform and a high speed, high resolution monochrome camera as imaging device are sufficient for acquiring flow images and running the software in the field over a matter of minutes. Suggested resources are:

- A high end laptop computer (32GB RAM, Intel i7 core), Windows/DOS operating system
- A high speed, high resolution monochrome camera (3000+ fps, 2Mpix+, e.g. MotionPro Y3). Framing rate must be high enough to record the life span of the inertial eddies at the edge of the jet. Imaging through polarizing filter may be useful to remove reflections at interfaces
- Continuous unidirectional polarized illumination along the jet axis, we suggest self-contained LED lighting which is now ubiquitous. Alternatively, a collimates halogen light source may be used
- Optional third party software for visualization (Adobe CS Professional, IDL, MATLAB, VLC …)

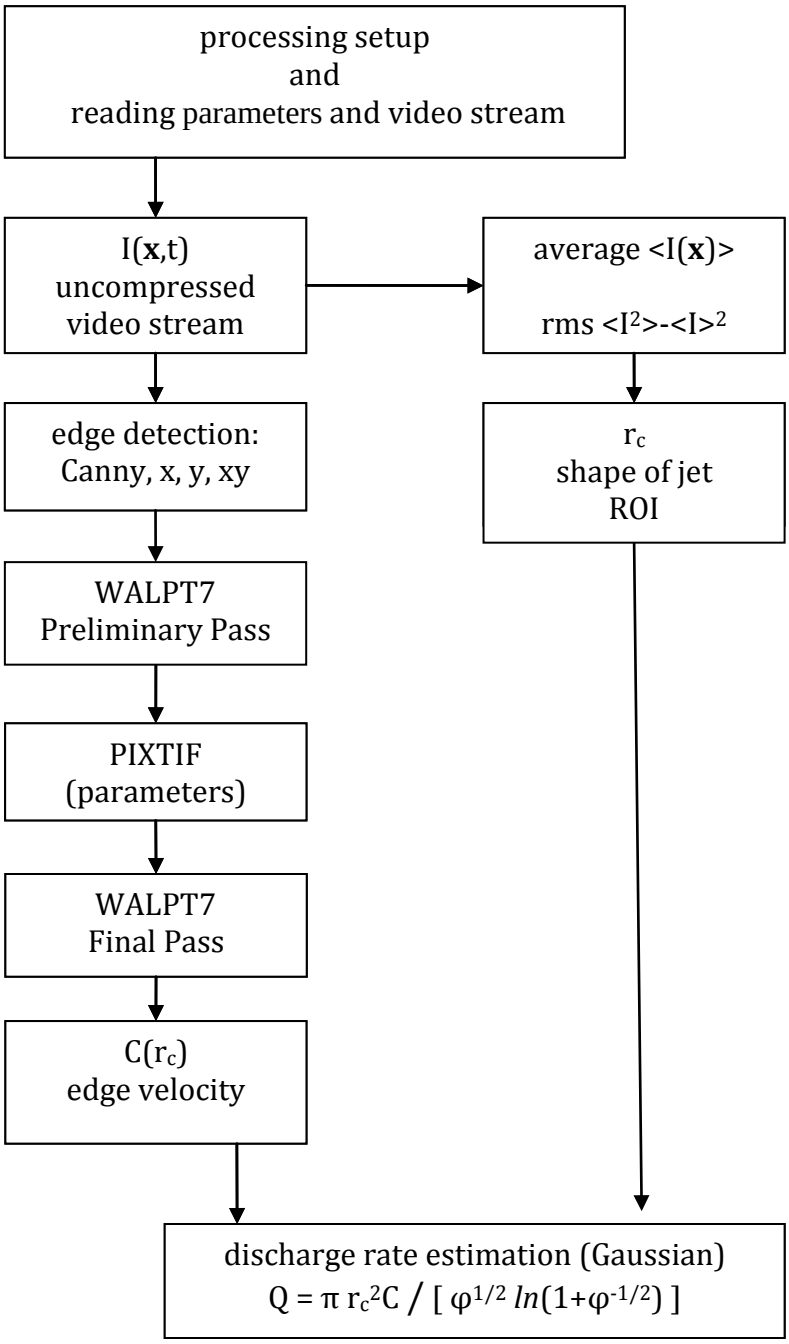

Chart 1. **`UCB_Plume`** flow chart.

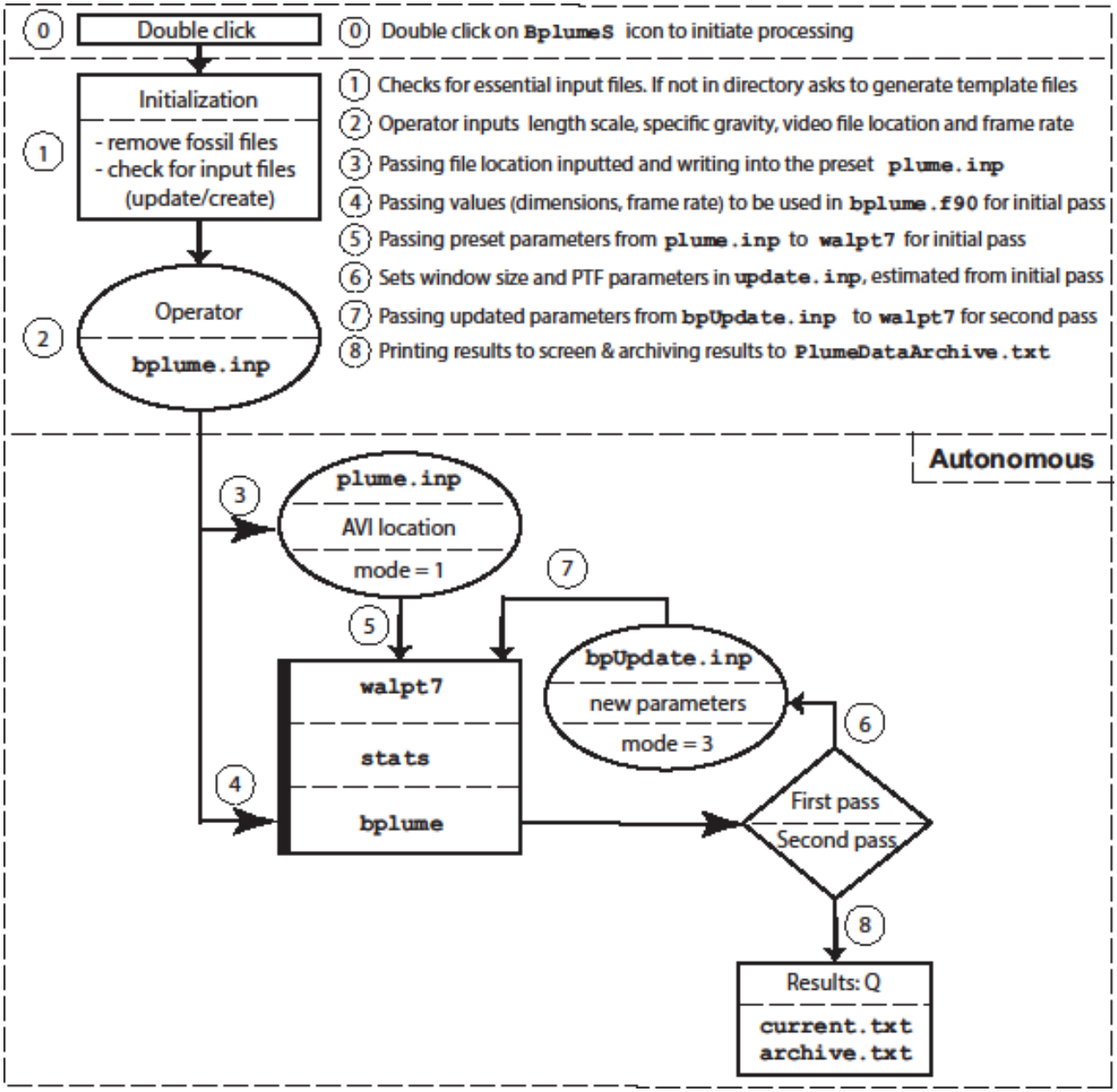

Chart 2. Operation of software package: **UCB_Plume**.

```
  bplums: berkeley plume software
  Semptember 18, 2015
  UCB-ME Fluid Mechanics Laboratory

Press any key to continue . . .
    confirm the contents of the input file [ bplume.inp ]
    edit the video parameters as needed

    S A V E  and  C L O S E [ bplume.inp ] when finished

    hit any key to continue, CTRL-C to abort

Press any key to continue . . .

    processing... may take   S E V E R A L   M I N U T E S

    CTRL-C to abort

    First pass


    Second Pass

    finished processing

-------------------------------------------------------
    current results in  [PlumeData.txt]
-------------------------------------------------------
 =======================================================
                          10 Feb 2016,  11:25 hours
 -------------------------------------------------------
  AVI file :
    c:\avi\AVIReadTestFile19.avi

 -------------------------------------------------------
  Field of View [ m x m ]              0.123 x   0.049
         W [ pix ] x H [ pix ]         01280 x 00512
  Framing rate [ frames/sec ]           1000
  Specific Gravity                     0.900
 -------------------------------------------------------
  PixTifed images:  1024
  PixTif Filter Type, Center, Width: High-Pass Filter   2    4
 -------------------------------------------------------
  Edge detection: None
 -------------------------------------------------------
  Average  (u,v, |U|)[pix/int]:   3.929   0.183   4.263
 -------------------------------------------------------
 Discharge Rate [ liter/sec ]              0.312
 Discharge Rate [ cubic meter/sec ]        0.000312
 Discharge Rate [ cubic meter/day ]       26.9
 Discharge Rate [ gallons/min ]            4.94
 Discharge Rate [ gallons/day ]         7113
 Discharge Rate [ USbbls/day ]           169
 =======================================================
-------------------------------------------------------
    accumulated results in  [PlumeDataArchive.txt]
-------------------------------------------------------
Press any key to continue . . .

    C L O S E [PlumeDataArchive.txt] when finished
```

Chart 3. Screen shot **`UCB_Plume`**.

Fluid	Frame rate	Flow rate	Re	error
	(fps)	(gpm)	x 10^4	%
water	500	1.02	0.45	-3
water	500	4.10	2.67	-23
water(*)	500	7.40	4.83	-18
1cs oil	1000	4.14	2.70	-9
1cs oil(*)	1000	5.52	3.60	-7
5cs oil(*)	1000	3.45	0.45	-11
5cs oil	1000	5.80	0.76	-2
5cs oil	1000	6.90	0.90	-15

Table1. Summary of Berkeley experiments. WALP& mode (3.2), PIXTIF filter parameters set at (1, 2, 8). (*)- See figure 23 for images.

WALP Mode,Passes	PIXTIF Filter Parameters	u	v	Calculated Flow Rate	error
				(gpm)	
3.2	1.3.6	0.91	0.047	595	-30%
3.2	1.4.8	0.998	0.072	653	-23%
3.2	1.5.10	1.058	0.058	692	-19%
3.2	1.6.12	1.069	0.059	700	-18%
3.2	1.7.14	1.065	0.059	697	-18%
3.2	1.8.16	1.057	0.056	691	-19%
3.2	1.9.18	1.044	0.048	683	-20%
3.2	1.10.20	1.032	0.869	675	-21%

Table 2. PIXTIF exercise on the OHMSETT Test 18: 850 gallons per minute, video frame rate 500 frames per second.

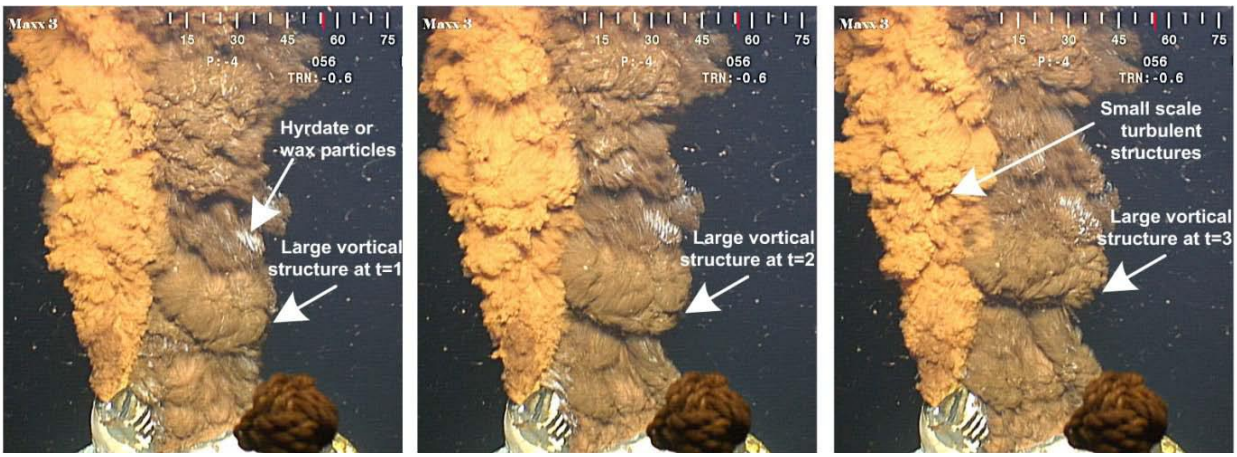

Figure 1. Examples of visible features tractable in the flow direction on the Deepwater Horizon oil leak jet.

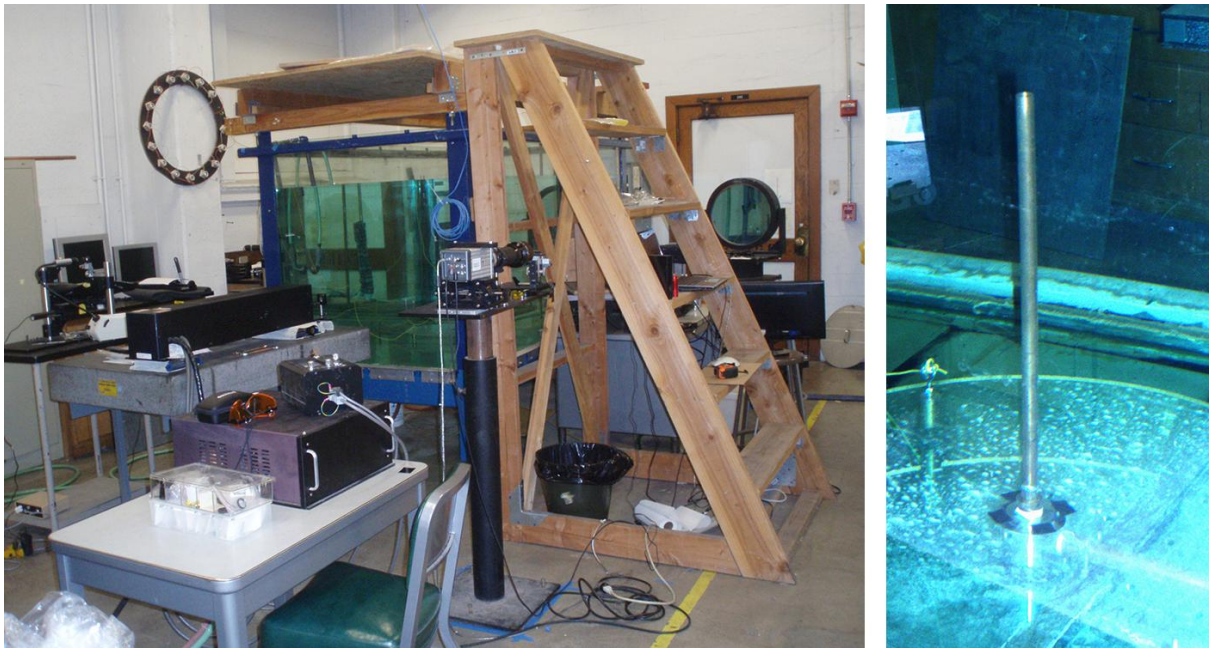

Figure 2. Overall view of the final setup (left) and the ½ inch diameter, 16 inches long discharge tube (right).

Figure 3. A mosaic of the components of the final setup. Top row: three general views showing the water tank, optical layout and its major components. Middle row: schlieren camera, shclieren light source and optics, and PIV/FV camera, Bottom row: turbine flow meter, pressurized dye tank, heater, and discharge tube.

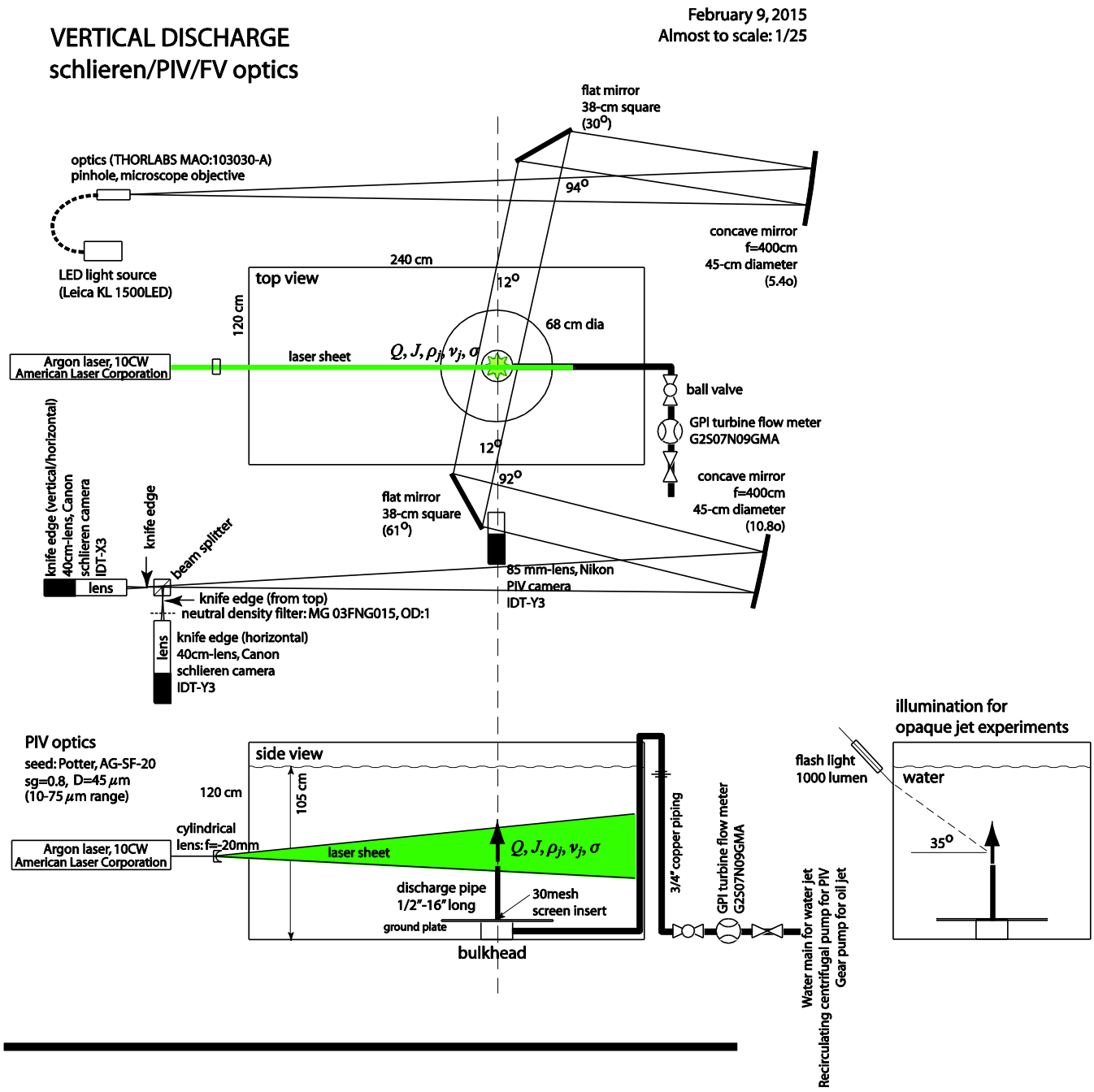

Figure 4. The final configuration of the experimental setup showing the schlieren/shadowgraph optical layout (top), PIV, and FV optical layout for vertical jet discharge experiments. The schlieren/shadowgraph light beam path is skewed 12 degrees to allow for normal clear access for PIV and FV cameras. . Simultaneous horizontal/vertical knife edge schlieren layout is at the left-center of the layout. Illumination scheme for fluorescent-opaque jet experiments is on the lower-right.

Figure 5. Schlieren/shadow photographs of 5 cs, 0.92 g/cm^3 n=1.49 oil discharging horizontally into water tank.

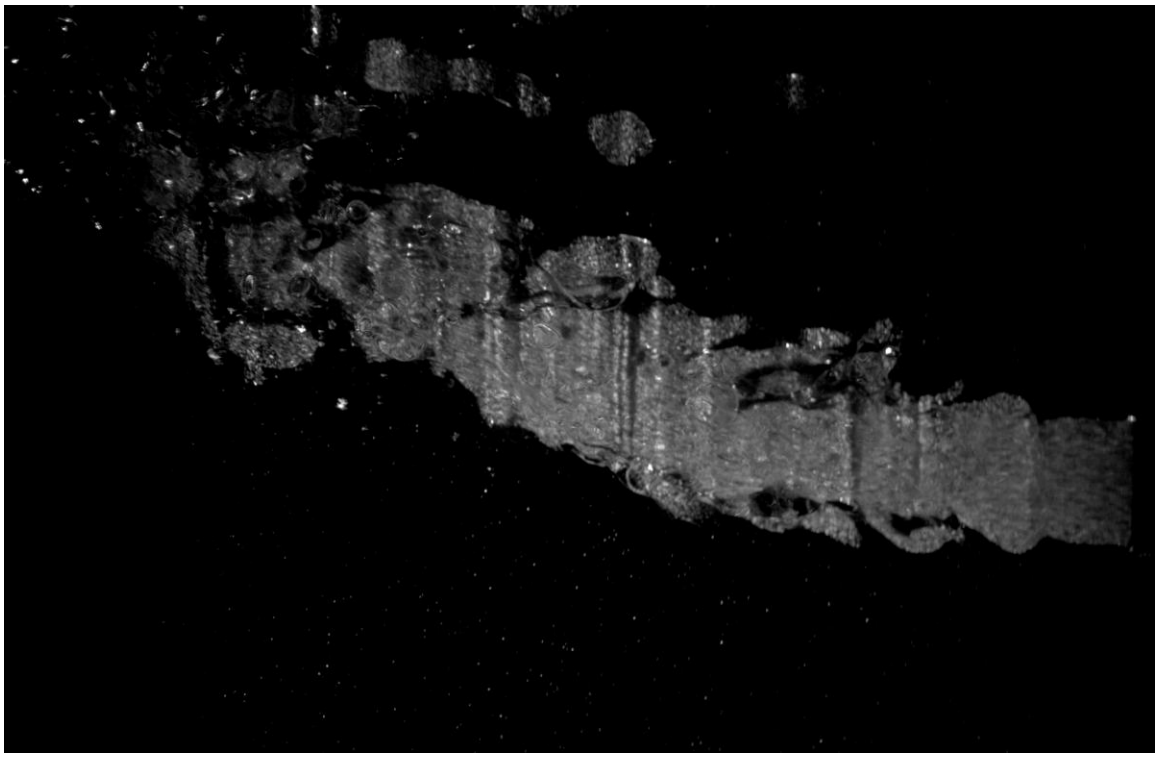

Figure 6. PIV image of 5 cs, 0.92 g/cm^3 n=1.49 oil discharging horizontally into water tank. The flow is made visible by seeding the oil and water with silver coated hallow ceramic spheres,

Figure 7. Schlieren photograph of water discharging vertically up into tank. The flow is made visible by slightly heating the discharge pipe exterior to the tank.

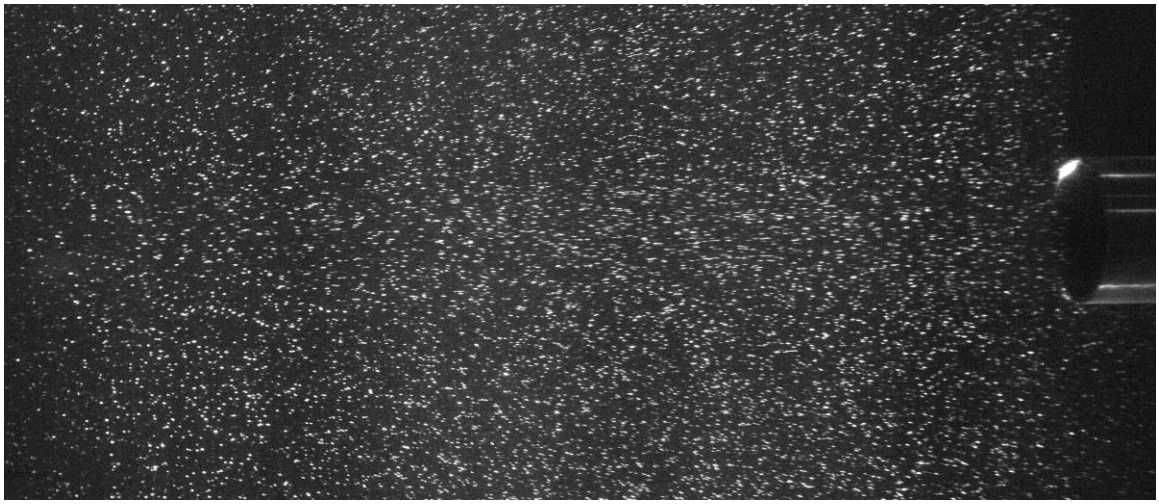

Figure 8. PIV image of water discharging vertically up into tank. The flow is made visible by seeding the water with silver coated hallow ceramic spheres.

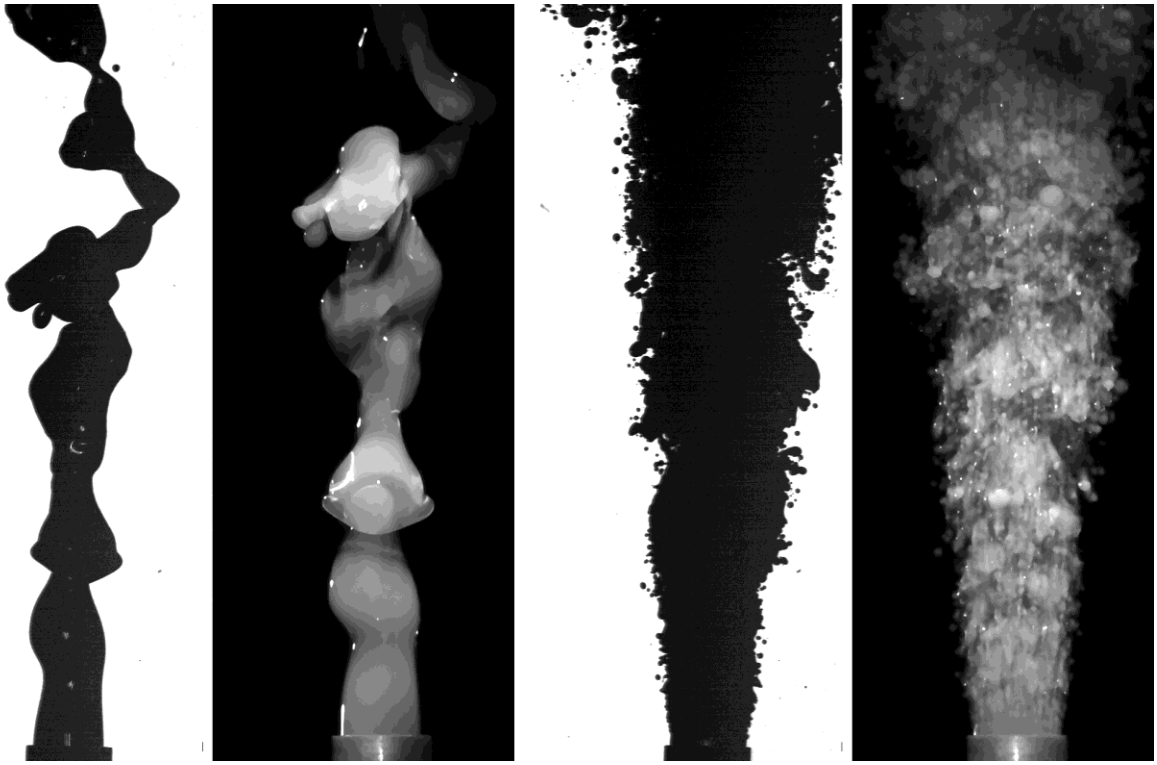

Figure 9. A mosaic of images of vertical oil jets. Left pair: 5cs silicone oil at 45cc/s (Re=900); Right pair: 1 cs silicone oil at 360 cc/s (Re=35,000). In each pair, the left image (white background) is a shadowgraph and the right one (dark background) a direct image of the exterior of the oil jets which is marked with oil soluble fluorescent dye. The image pairs are simultaneous, even though the magnifications are slightly larges for the direct images (1 versus 1.16).

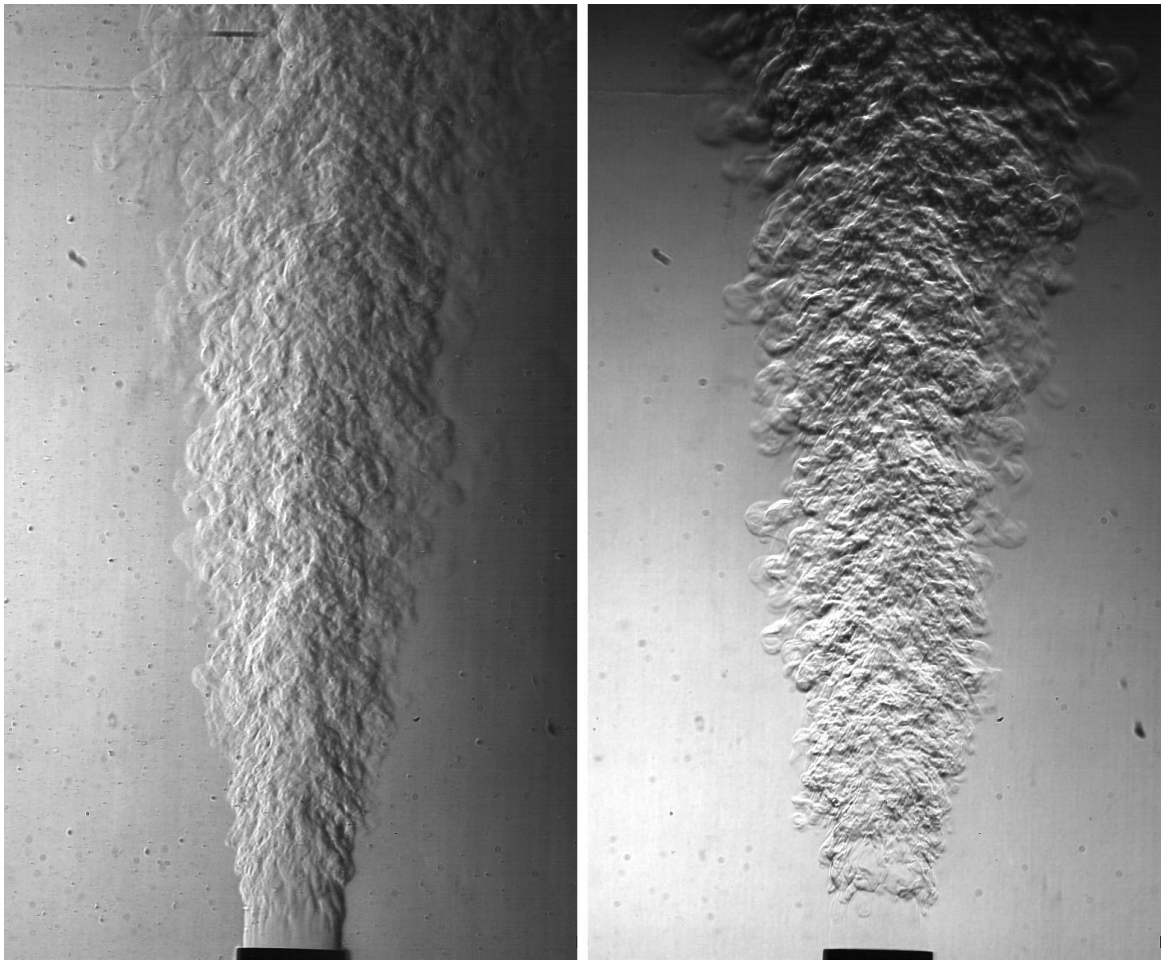

Figure 10. Sample flow images at Q=1.0 gallon/min (63 cm^3/s): schlieren with vertical knife edge and horizontal knife edge. Images 2048/4096 of the video streams are shown. The images are not simultaneous. Both images are 85 mm x137 mm (768x1280 pixels).

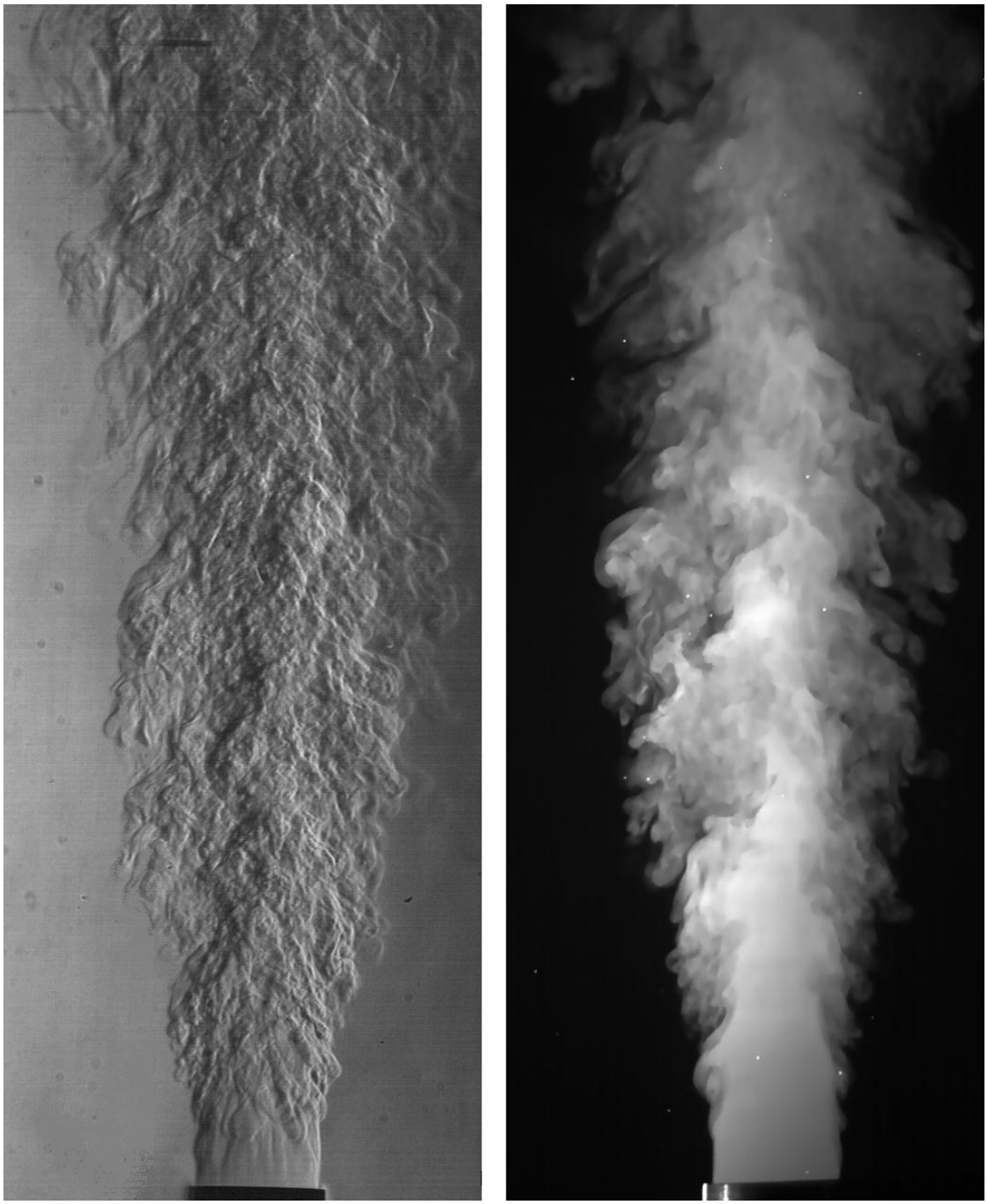

Figure 11. Sample flow images at Q=1.0 gallon/min (63 cm^3/s): simultaneous schlieren and cross-sectional fluorescent dye images. Images 2048/4096 of the video streams are shown. Left image: 56.5mmx137mm, Right image: 52mmx132mm. Both images 512x1280 pixels.

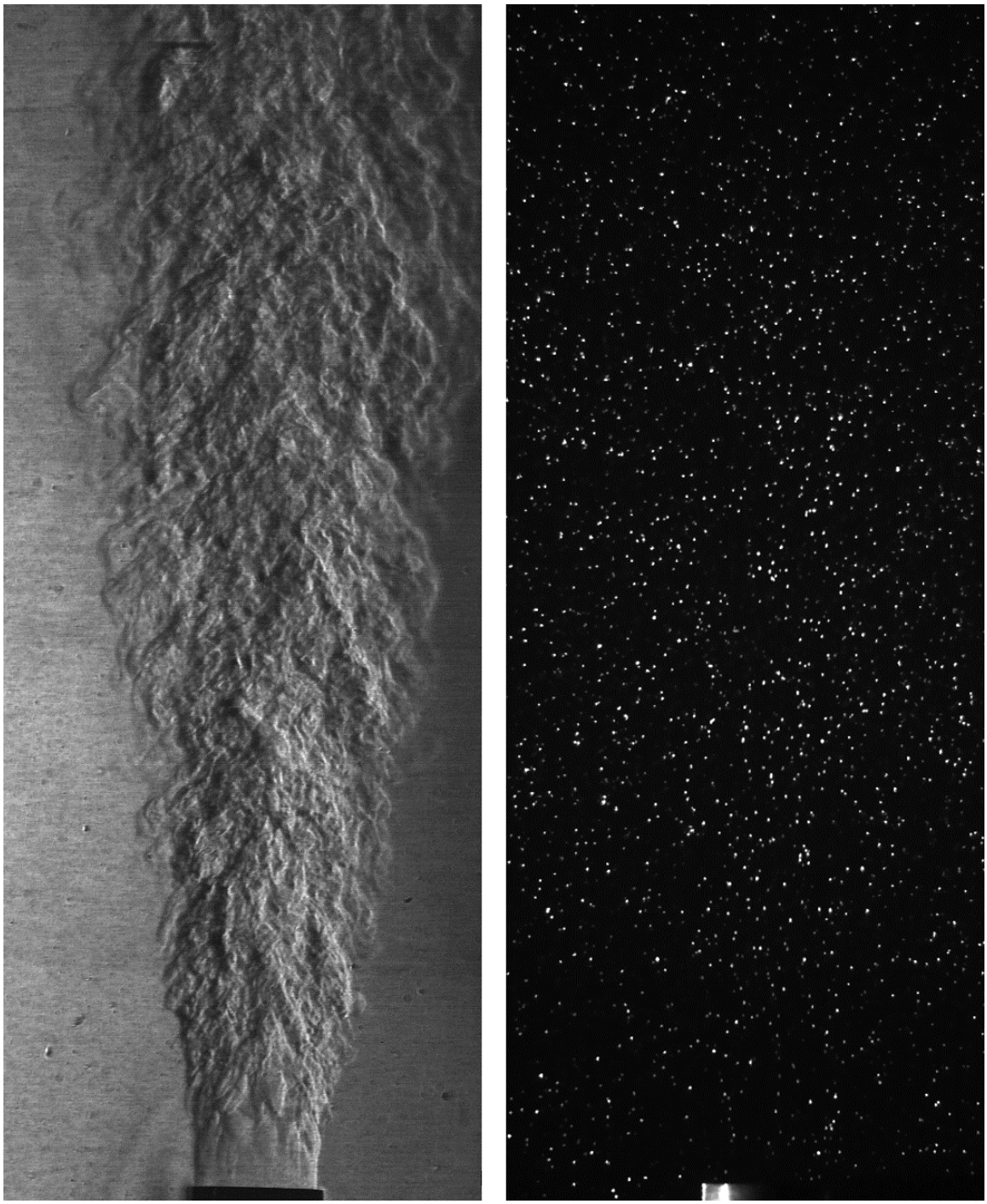

Figure 12. Sample flow images at Q=1.0 gallon/min (63 cm^3/s): simultaneous schlieren and PIV images, vertical knife edge. Images 2048/4096 of the video streams are shown. . Left image: 56.5mmx137mm, Right image: 52mmx132mm. Both images 512x1280 pixels.

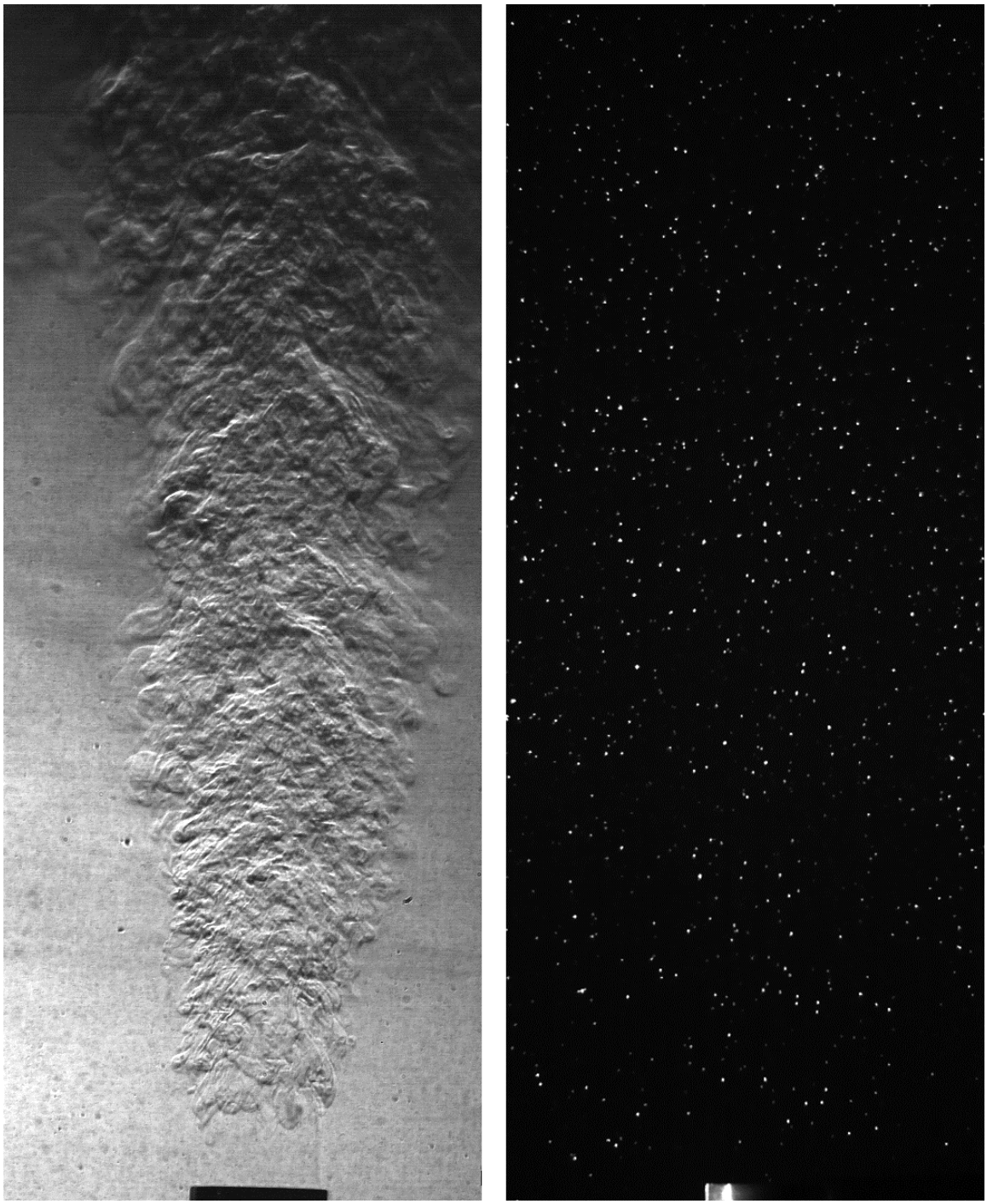

Figure 13. Sample flow images at Q=1.0 gallon/min (63 cm^3/s): simultaneous schlieren and PIV images horizontal knife edge. Images 2048/4096 of the video streams are shown. . Left image: 56.5mmx137mm, Right image: 52mmx132mm.

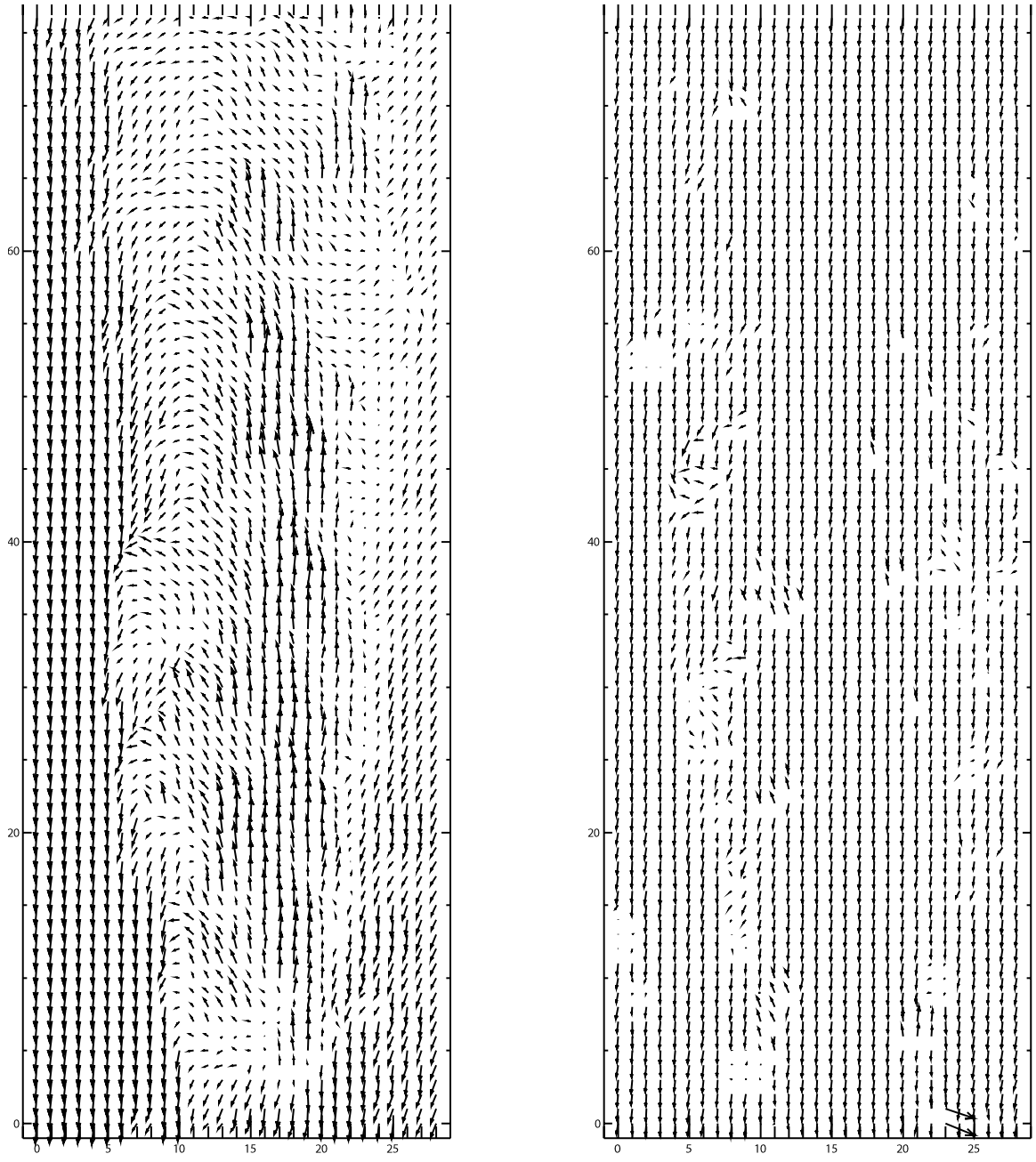

Figure 14. Rudimentary processing for velocity vector field of image pairs corresponding to those in figure 11. Right: schlieren images, Left: cross-sectional dye images. Vectors indicate only their relative magnitudes in each frame.

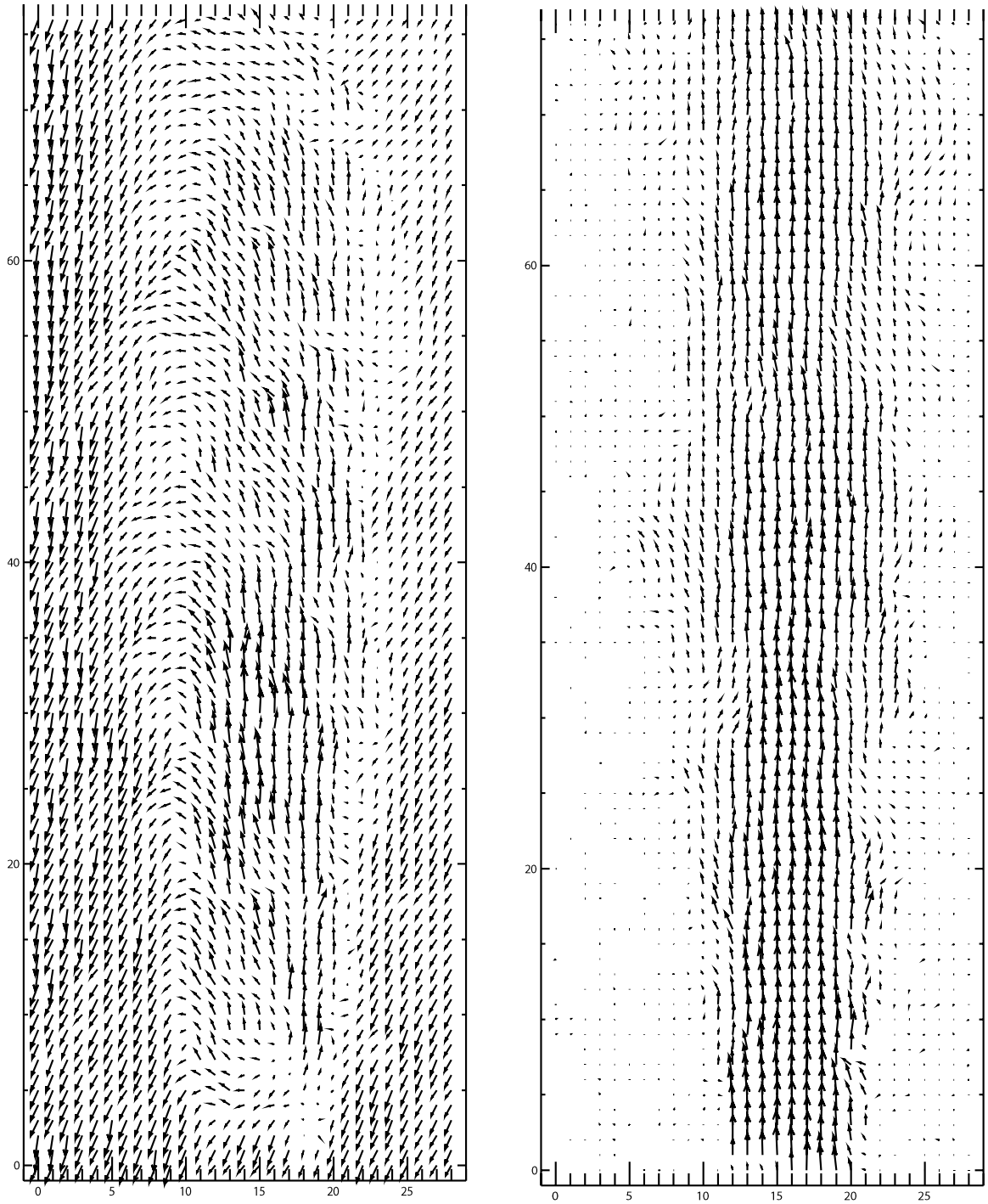

Figure 15. Rudimentary processing for velocity vector field of image pairs corresponding to those in figure 13. Right: schlieren images, Left: cross-sectional particle images. Vectors indicate only their relative magnitudes in each frame.

PIXTIF: Pixelwise Time Filtering

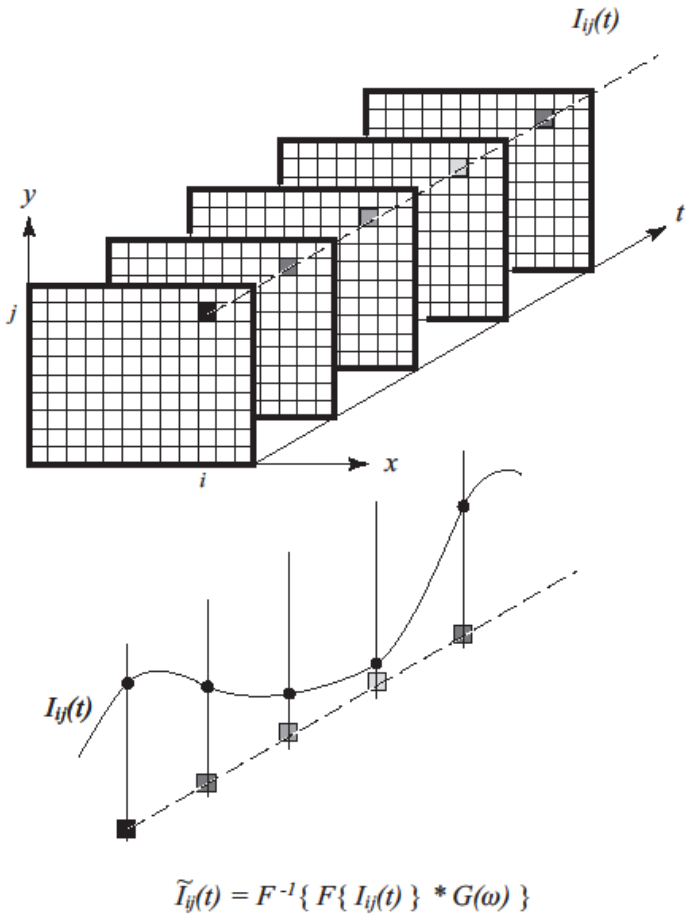

Figure 16. Pixelwise time filtering, PIXTIF, sketched.

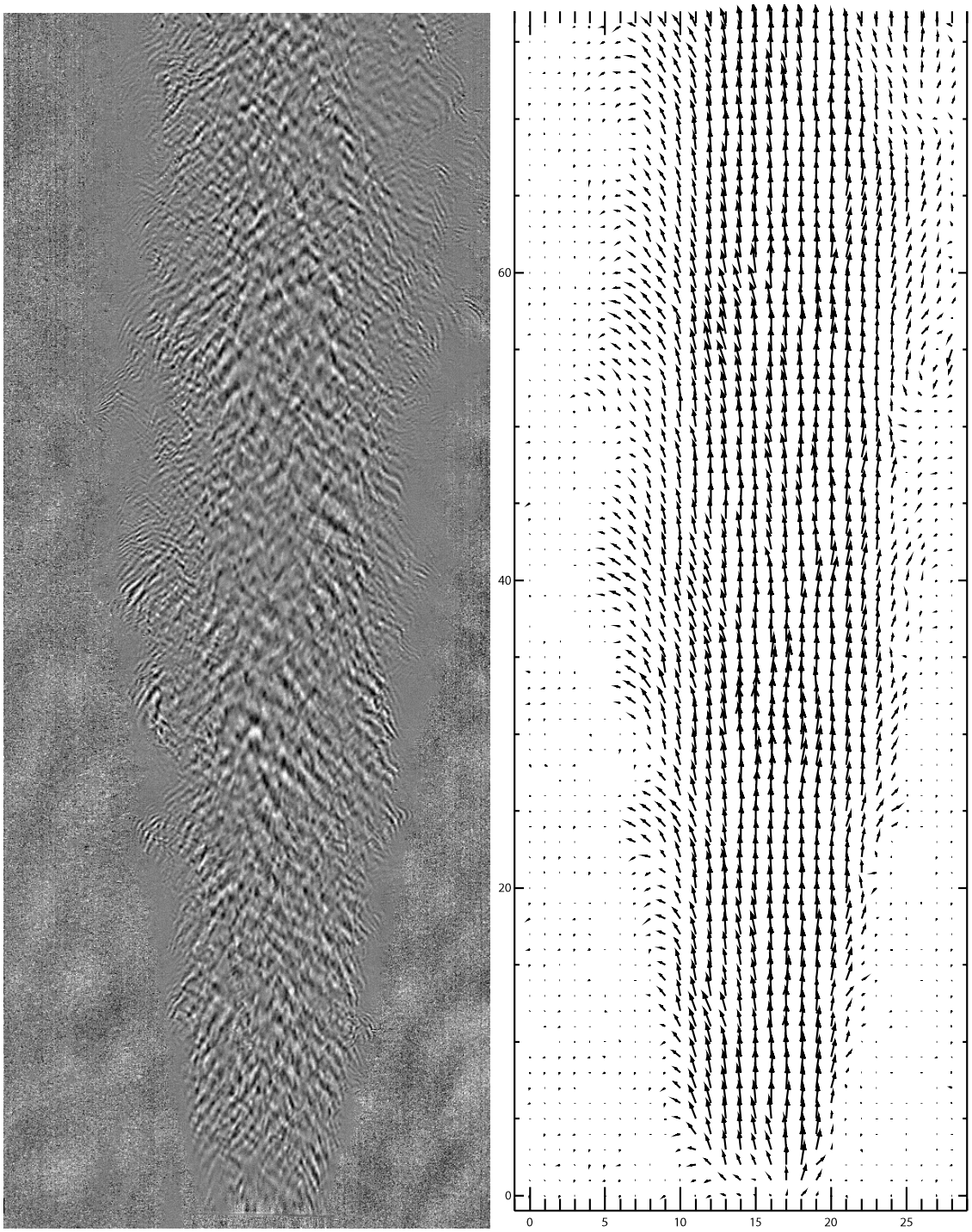

Figure 17. PIXTIF'ed image corresponding to the schlieren image in figure 13, and the velocity vector field determined from the corresponding image pair. Vectors indicate only their relative magnitudes. Image on the left is 56.5mmx137mm.

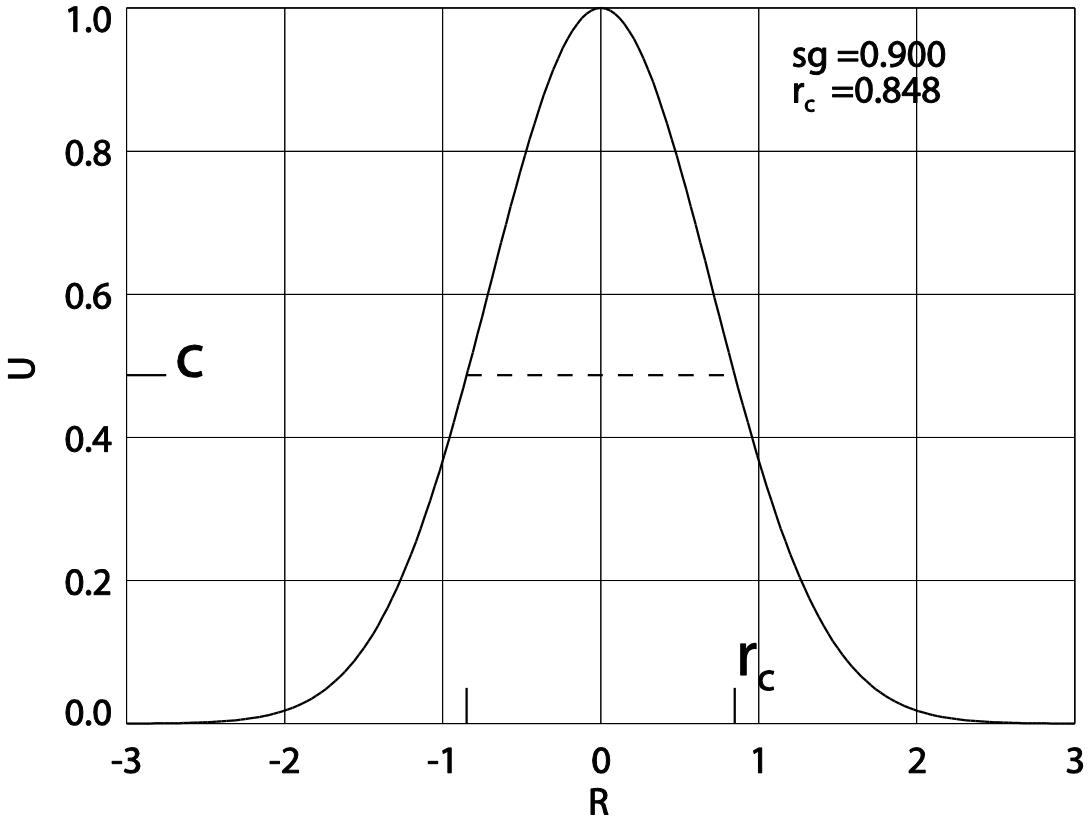

Figure 18. Schematic of a jet and symbol definitions. . Gaussian mean velocity profile, interface r_c, and velocity at the interface C, celerity.

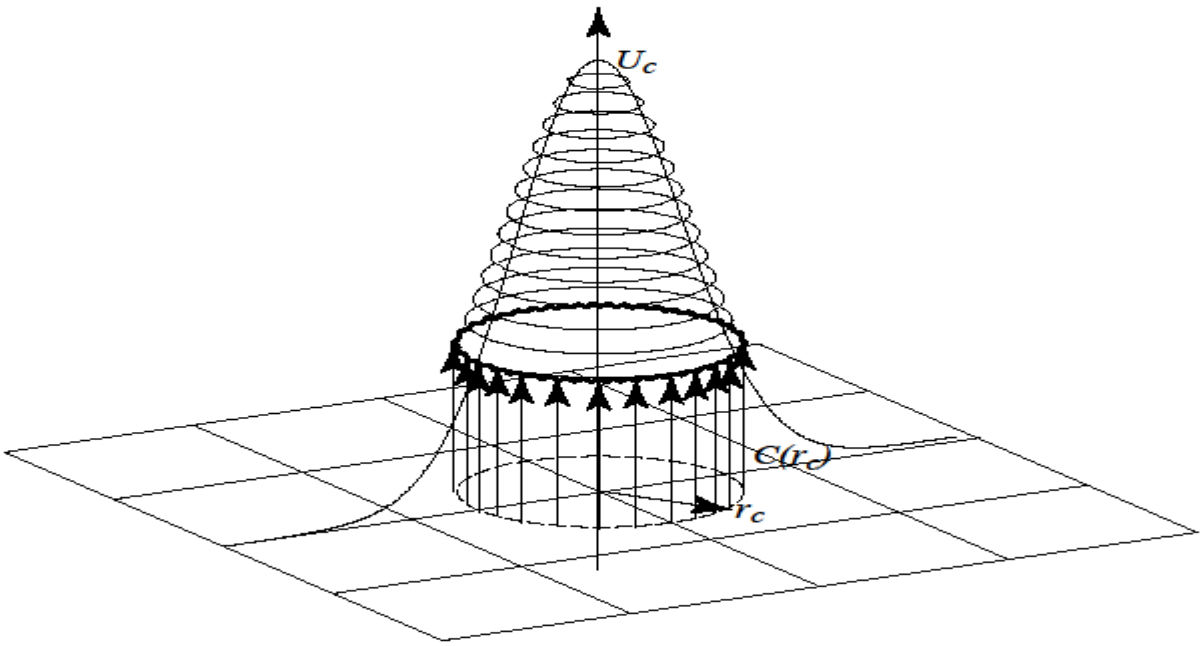

Figure 19. Jet edge velocity illustration.

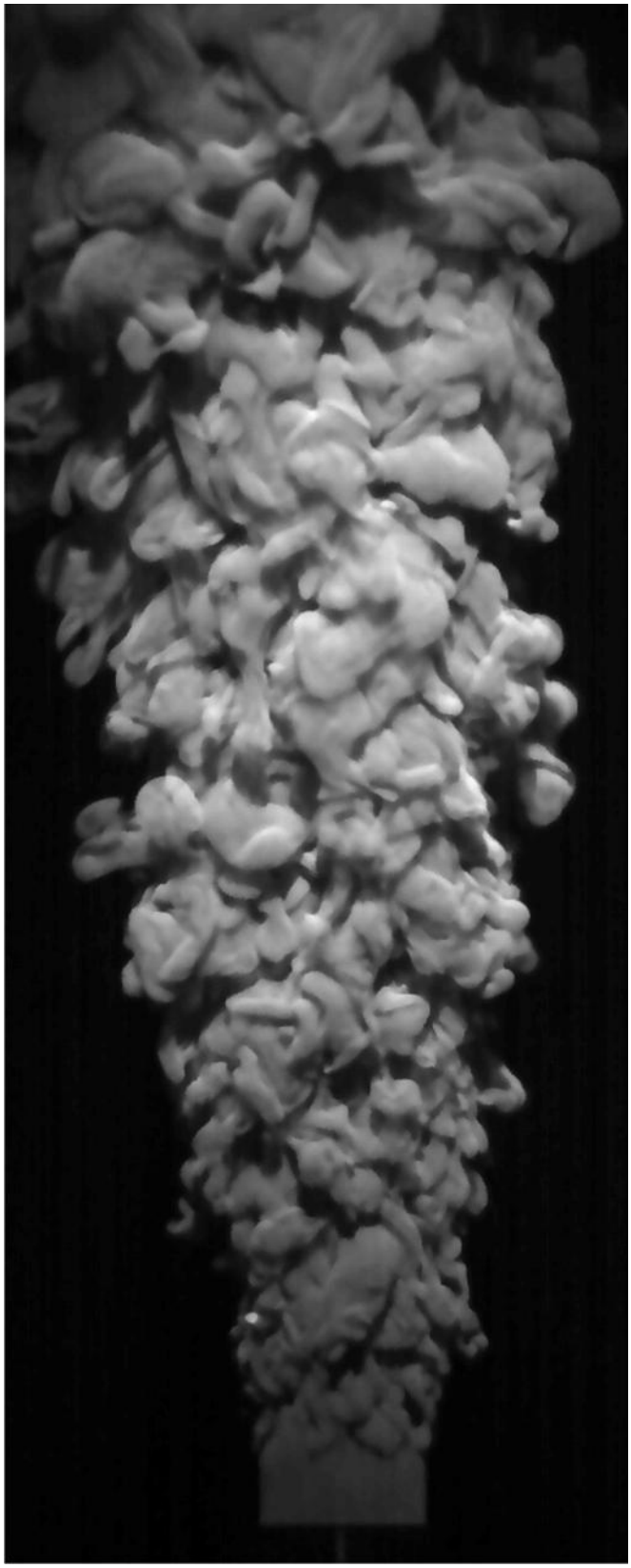

Figure 20. Water jet made visible with fluorescent dye. The intricacy of the jet-ambient fluid interface is clearly delineated. Q=1 gpm, Re=4500.

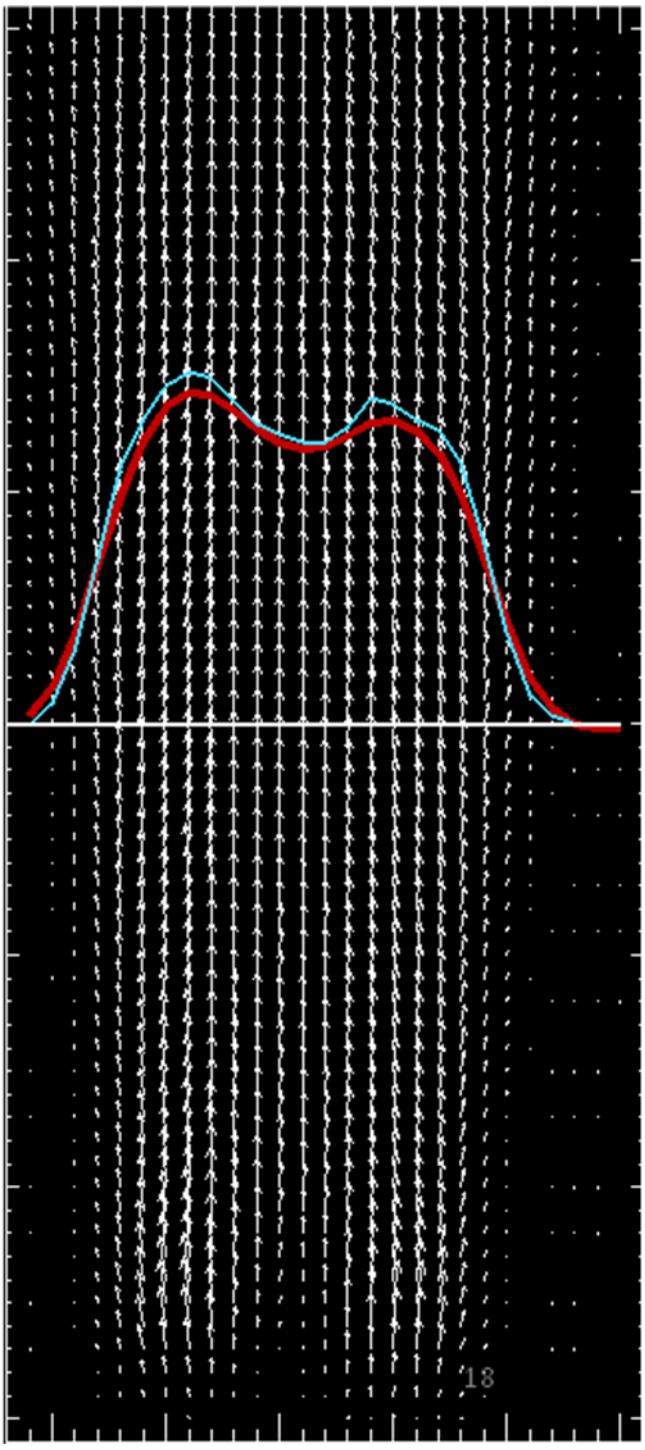

Figure 21. Typical jet edge velocity measurements.

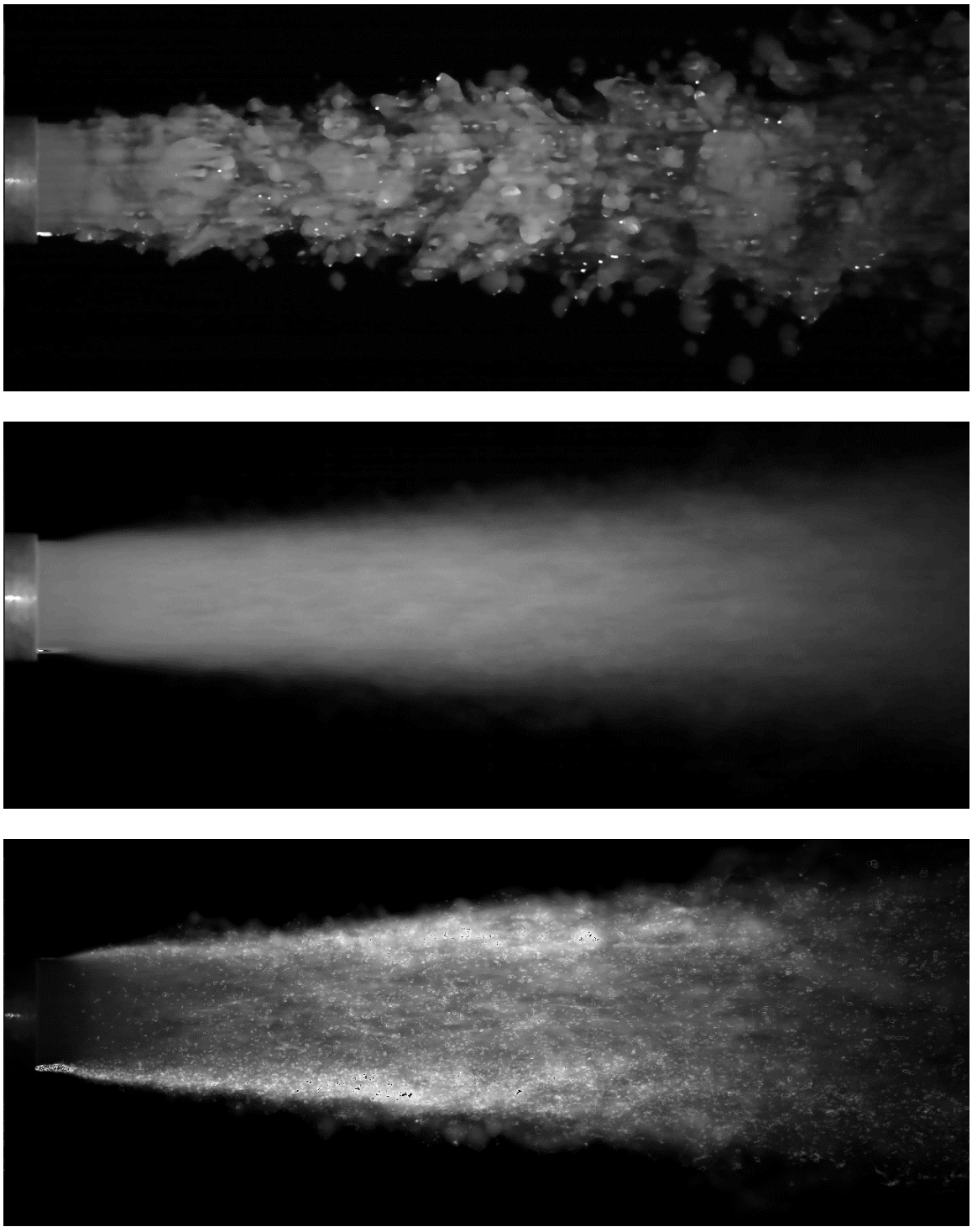

Figure 22. Images at the salient stages of **UCB_Plume** processing: 1cs silicone oil, 4.14 gpm, 1000 fps. (a) a raw image, (b) average image, and (c) rms image. (images (a) and (b) are enhanced for clarity)

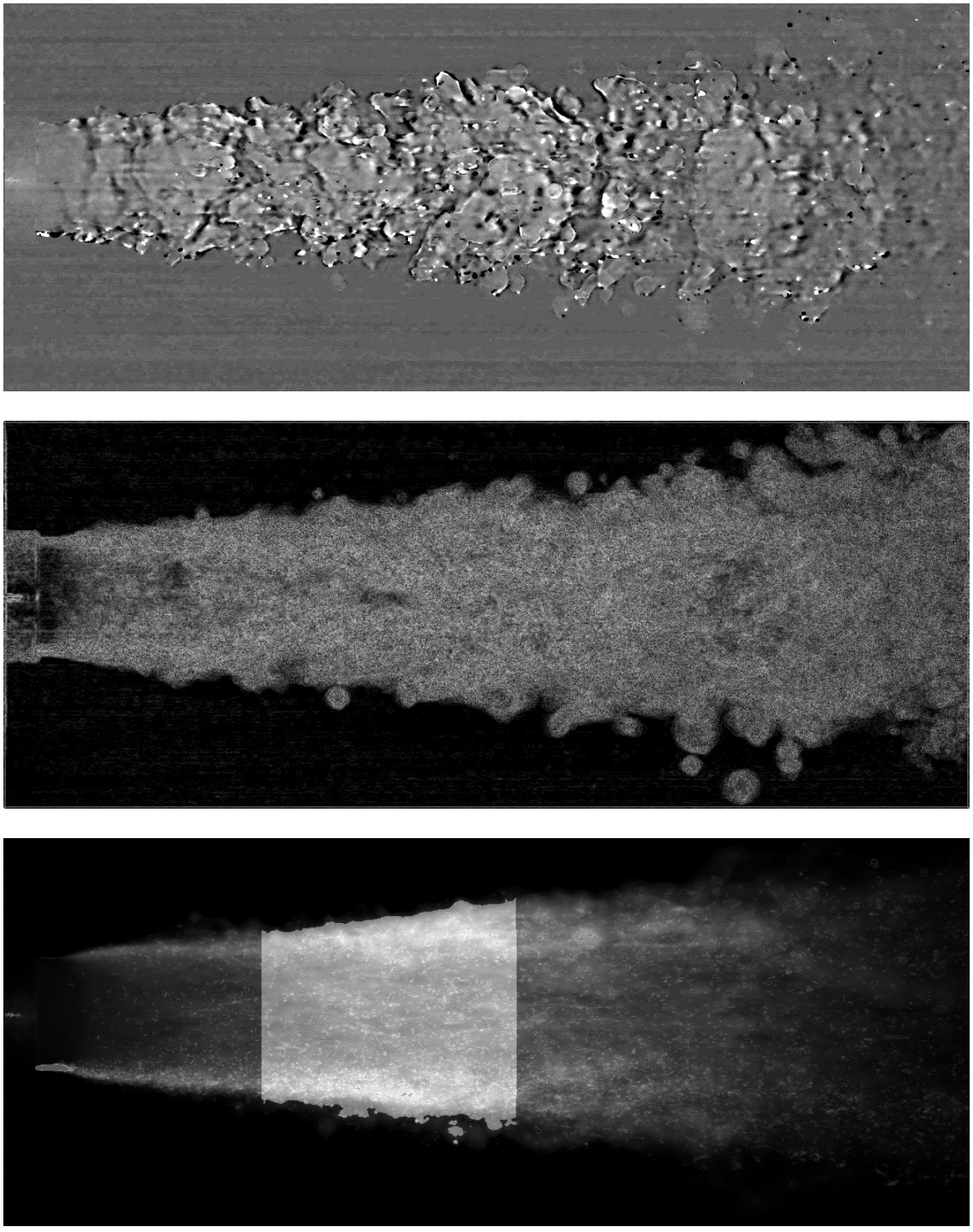

Figure 23. Images at the salient stages of image processing **`UCB_Plume`** processing: 1cs silicone oil, 4.14 gpm, 1000 fps. (a) PIXTIF'ed image (b) Canny Edged PIXTIF image, and (c) striped image, ROI. (images (a) and (b) are enhanced for clarity)

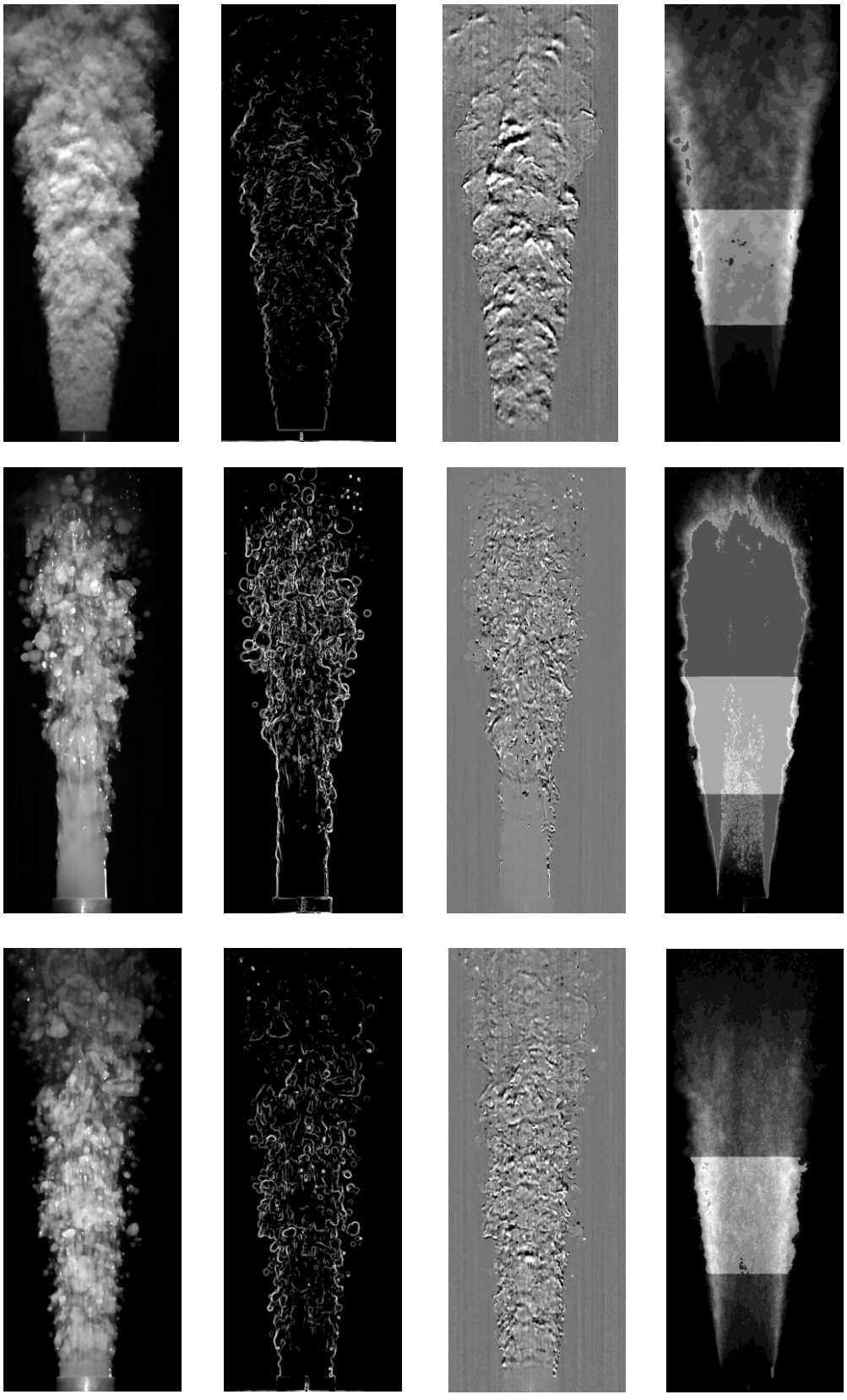

Figure 24.Top: Water jet Re=48,000, Middle: 1cs oil, Re=36,000, and Bottom : 5cs oil, Re=4,500 (see Table 1 for summary).

APPENDIX-1

UCB_Plume

USER'S MANUAL

UCB Plume

UCB Plume Analysis Tool
USER'S MANUAL

Version 1.01

June 2016

Fluid Mechanics Laboratory
140 Hesse Hall
Department of Mechanical Engineering
University of California, Berkeley, California, 94720-1740

Scope of Manual

This manual will describe the steps to use **UCB Plume** to estimate the flow rate of jet discharges. This involves both outlining the limitations of the software and describing its ideal application conditions. Methods for interpreting additional data that is calculated, as well as the visualization of results, will also be outlined. A list of common error messages and their solutions will be detailed as well. The name **UCB Plume,** UCB Plume Analysis Tool, and **UCB_Plume.exe** will be used interchangeably to refer to the software.

Point of Contact

UCB Plume was developed at UC Berkeley with support from National Energy and Technology Laboratories and Bureau of Safety and Environmental Enforcement.
Please contact with field use questions.

Contact:	Savaş, Ömer
Email:	savas@berkeley.edu
Phone:	(510) 642 - 5272

Contact:	Ibarra, Eric
Email:	ibarraeric89@gmail.com
Phone:	(323) 327 - 5868

Project References

This software was tested on laboratory experiments whose Reynolds number ranged from 4,500-550,000. These tested experiments were conducted at UC Berkeley and OHMSETT. On average, the flow rate estimation tends to be conservative by ~30%.

Glossary

The following terms are used as operator inputs and calculated results described in the manual.

ROI length/width:

The physical dimension in meters corresponding to the length/width of the image

Specific gravity (φ):

Density of the fluid comprising the Jet/Plume (ρ_{jet}) over the density of the quiescent fluid ($\rho_{ambient}$).

(i.e. Density of Crude oil / Density of Sea Water)

Frame Rate:

The rate at which the video was recorded by the camera, different from the playback rate that will be listed in the details of the AVI file.

Celerity (C):

The velocity of the trackable features. The mean center velocity of the trackable eddies along the visible surface of the opaque jet/plume.

Centerline Velocity (U_C):

The maximum velocity to be found at the center axis of the discharging fluid jet.

Algorithm Development

Cross Correlation: A measure of the similarity between two signals as a function of the delay between the two images. In our correlation, the signal is the intensity value in the image and the lag is the time interval elapsed between successive images.

Particle Image Velocity (PIV): A flow visualization technique that provides the instantaneous velocity measurements to be taken. For PIV, density neutral particles are seeded into a flow. The motion of the particles are used to calculate the velocity field of the flow.

Image Correlation Velocimetry (ICV): ICV performs a cross correlation of interrogation regions in consecutive images to measure the displacements of moving images. Using the delay between the images, a velocity is measured.

PixTif: A pixel-wise filtering done on time. Features in the flow move at a certain speed. At a given pixel, these features leave a distinct signature in the pixel's intensity history. By taking the intensity signal into the Fourier domain, features moving with a certain speed can be filtered with a convolution. We then apply a high-pass filter, and we define the filter center and width using the celerity and radius calculated during the first pass using a Stouhal number.

Parameter generation: During a run of `UCB_Plume.exe`, `WALPT7.exe` is called for two passes over the images. An initial pass is run with preset processing parameters and the user's flow parameters. This initial pass gives a first approximation of the velocities, length scales, and flow rates that are being considered. Based on the results, `WALPT7.exe` will output an updated input file with processing parameters adjusted. The updated input file will be used to run `WALPT7.exe` for the final pass, the results of which will be outputted.

Radius estimation: The root mean square (RMS) of the all the images processed is used to estimate the radius. The RMS of the image deck removes constant features in the ROI, while outlining the location of fluctuating intensity values, such as where moving features in the jet occur.

Celerity: The velocity of the surface features measured and is used as the celerity for the calculation. By using image correlation velocimetry, a velocity field of the jet is calculated, and an average of this field is taken about the region of calculation.

Discharge Rate estimation

Assumptions:

In the integration of the estimated jet profile these assumptions are made.

A *Gaussian velocity profile* of the jet that is axisymmetric is assumed. This is used to relate the observable feature's velocity to what is inside for flow rate calculations.

The velocity profile is evaluated at a distance of 3 pipe diameters downstream from the discharging orifice, which is in the *near field*. In this range the inertial terms are the same order of magnitude as the buoyant terms, allowing them to be neglected in the flow rate calculations.

It is assumed in the *near field* that the velocity of the surrounding fluid, U_2, is small in comparison to the celerity of the jet/plume, allowing $U_2 \approx 0$. The limit of this software is to where jets are not being affected by currents in the same order of magnitude as the jet/plume.

A derivation of the flow rate (Q) is as follows:

$$u(r)\ /U_c\ =\ \exp(\ -r^2/\sigma^2)$$

$$C\ /U_c\ =\ \exp(\ -r_c^2/\sigma^2)$$

$$U_c =\ (1+\varphi^{-1/2})\ C$$

$$\varphi\ =\ \frac{\rho_{jet}}{\rho_{ambient}}$$

$$\sigma^2 = \frac{r_c^2}{\ln(1+\varphi^{-1/2})}$$

$$Q = 2\pi \int_0^{r_c} u(r)\ r\ dr = \frac{\pi\ r_c^2\ C}{\varphi^{1/2}\ln(1+\varphi^{-1/2})}$$

Hardware Requirements

A high end Windows laptop computer as the operating platform and a high speed, high resolution monochrome camera for uncompressed video recording are the hardware requirements.

Capable Camera:

A high speed, high resolution camera (2000+ fps, 2Mpix+). Successive images in a video stream must be recorded within the life span of flow structure at the edge of the jet. Camera should use a polarizing filter to remove reflection at jet/environment interfaces. The Y models and X models by Integrated Design Tools Inc. have been used in the laboratory setting for these higher speed flow experiment, and have performed well. An additional benefit, the capturing software provided by IDT Inc. can write AVI files using the Basic Windows bitmap format which is required by `UCB_Plume.exe`.

i7 processor/32 GB Ram or better:

The `UCB_Plume.exe` software has been tested on contemporary WINDOWS operating systems; here are their listings with the average times to processes 512 frames:

-Intel® Xeon® CPU E5607 @ 2.27 GHZ, 128 GB Ram
Running Windows 2008 R2
~60 minutes
-Intel® Core™ i7-4700 MQ CPU @ 2.40 GHZ, 24GB RAM
Running Windows 7
~25 minutes
-Intel® Core™ i7-4710 MQ CPU @ 2.50 GHZ, 16 GB RAM
Running Windows 8.1
~25 minutes
-Intel® Core™ i5-4430 MQ CPU @ 3.00 GHZ, 12 GB RAM
Running Windows 8.1
~35 minutes

Imaging requirements

Uncompressed AVI Gray level

-Compressed, lossless, or lossy video will result in the code aborting. Only uncompressed AVI using the Basic Windows bitmap format codec is supported for gray level.

Static recording position

-Have the ROV record the jet/plume in a fixed reference with respect to the orifice. The camera should be faced perpendicular to the jet's/plume's centerline axis

Lighting

-The flows must be illuminated by a continuous, directed, polarized light source. Continuous light is critical, and must be differentiated from certain light sources that only simulate continuous by pulsing on and off at a high frequency not discernible to the human eye. When recording pulsing light with a high speed camera, consecutive images can alternate from high to low intensity leading to poor results. The light source should originate from near the ROV/camera. Polarization of the light along with the use of a polarized lens will diminish the occurrences of bright reflections of light at the interfaces, these glares lead to less reliable results if not dealt with.

Image centered 3 orifice diameters along the jets axis

-Include the discharging orifice in the image and have the image centered at 3 orifice diameters lengths from the orifice itself.

Video image's length is aligned with axis of the jet

-The jet should discharge left to right in the video recording.

Sufficient Frame Rate to capture evolution of features

-The recording frame rate should be sufficient to continuously capture the motion of the visible features.

Execution

In the directory UCB_Plume, four files are essential to the operation of the software:

- **UCB_Plume.exe:** The main batch file that prompts and automates the invocation of the `WALPT7.exe` with the proper input file.

-**WALPT7.exe:** The computing heart of this software. **WALPT7** source code written in FORTRAN, allowing it to both efficiently and effectively run calculation.

-**bplume.inp**: This input file will be edited and verified by the user. It contains parameters pertaining to the AVI as well as the flow.

-**plume.inp**: This is a self-contained input file which houses parameters used in analyzing the video.

Running Program:

-Double-click **UCB_Plume.exe** and follow the command line instructions.

-The user will be required to input/verify the information in **bplume.inp**:

- **Camera view dimension along plume axis, in meters (Line 2)**
- **Camera view dimension across plume axis, in meters (Line 4)**
  -real world ("Physical") length scale of the captured video
- **Discharge orifice diameter in meters (Line 6)**
  -the diameter of the jet's/plume's orifice

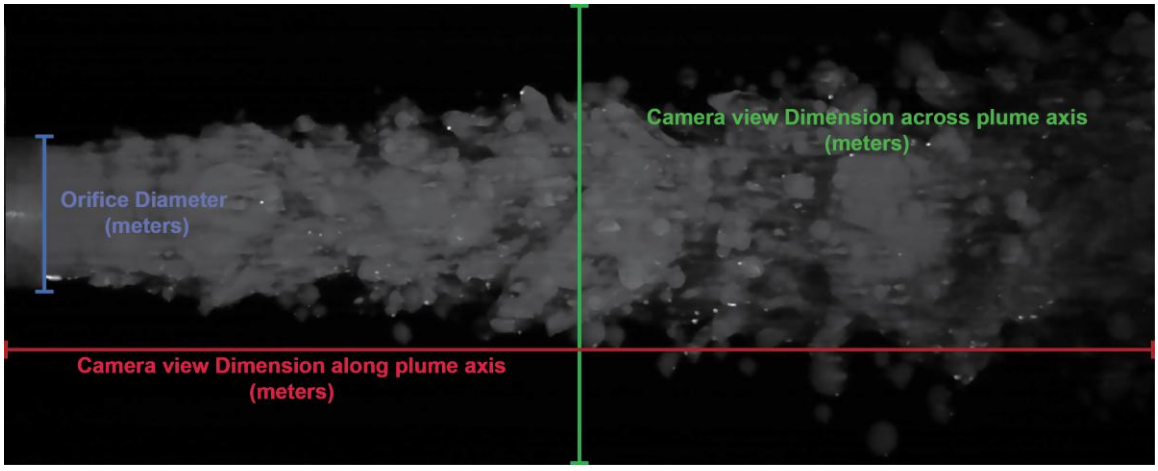

(Test image for reference)

Each of these length are related to field measurements and estimations

- Camera frame rate (Line 8)

-the capture frame rate of the video

- Discharge fluid specific gravity (Line 10)

-the specific gravity of the jet/plume being discharged

-AVI file location (Line 12)

-the path to the video file storage location

Note: There are many ways to copy the file path. Here is one for reference:

-Locate the AVI file

-Shift + Right-Click the file and select

Copy as path

-Paste the path in bplume.inp in the correct line (line 12)

(Remove the quotation marks from the front and end of the pasted file path)

After editing, verifying, saving, and closing the input file, follow the command line instructions.

NOTE: Assume that the calculation time will scale with the number of frames, $N_{frames,}$ by

$$Time \propto N_{frames} \cdot log(N_{frames})$$

2.5 GHz i7 processor with 24 GB ram

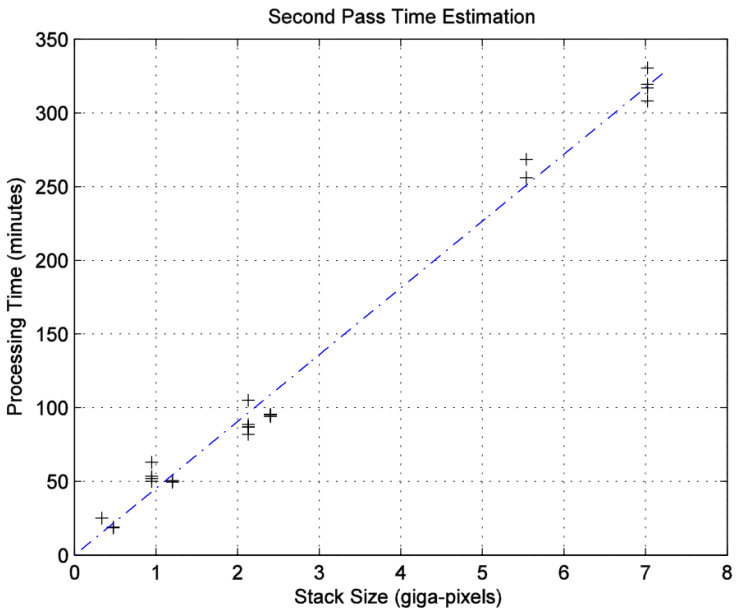

Results

Two **.txt** files are generated upon completion of the program.

PlumeData.txt:
Holds the printed information of the most recent run. This information lists parameters input by the user, such as:

- AVI file location
- Field of view dimensions
- Framing rate
- Specific gravity

Listed also are other processing parameters that were derived from information gained in the initial pass. These parameters are:

- Image resolution
- Number of images used in PixTif'ing
- PixTif filter type, center, and width

The listing of these parameters allows for a connection between a video and how it was processed to calculate the estimated flow rate, which is listed in a range of units.

PlumeDataArchive.txt:
An archive of the all **PlumeData.txt** from prior runs of **UCB_Plume.exe**. To start a new archive, move/rename the current **PlumeDataArchive.txt** prior to running **UCB_Plume.exe.**

Images: A range of images are saved for diagnostic and process visualization purposes. While other image handling programs can open these file, the process using ImageJ will be described due to its open source and robust use.

For all **`.raw, .edg, .pxt`**, begin by running ImageJ.

Click: File > Import > Raw…

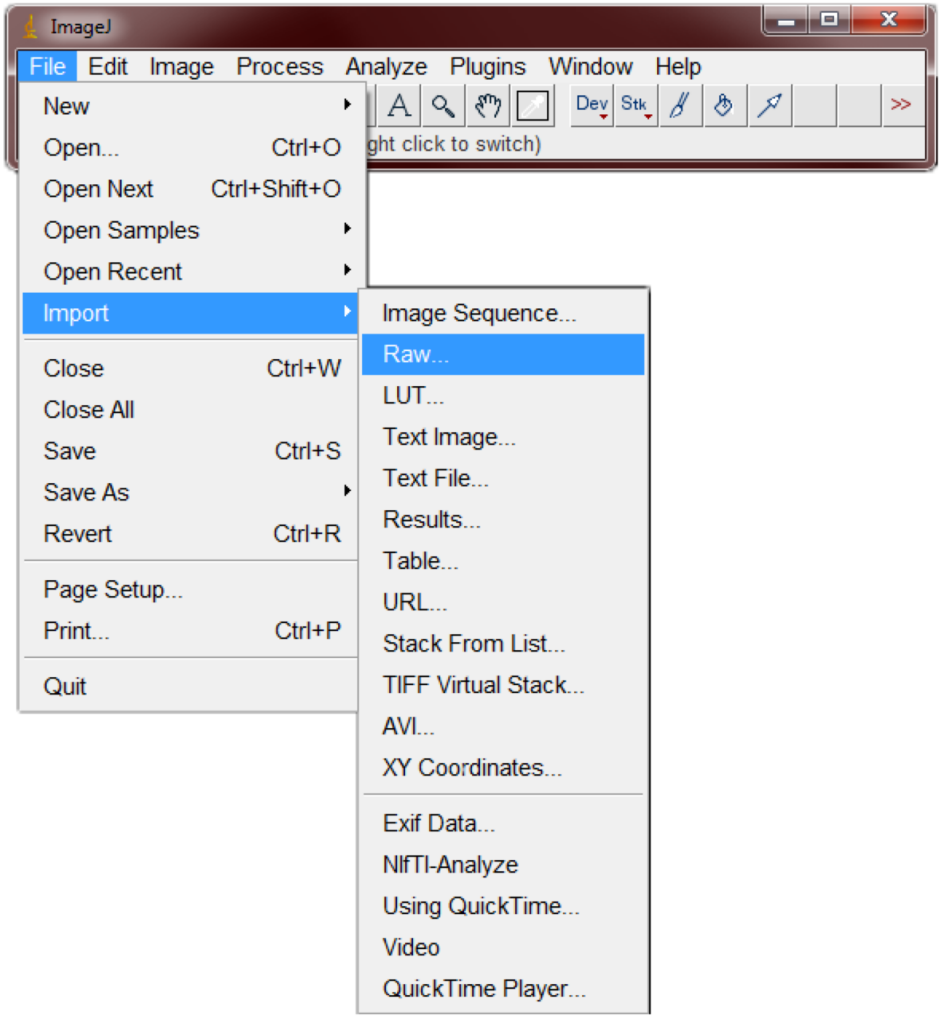

Select the file desired to be opened

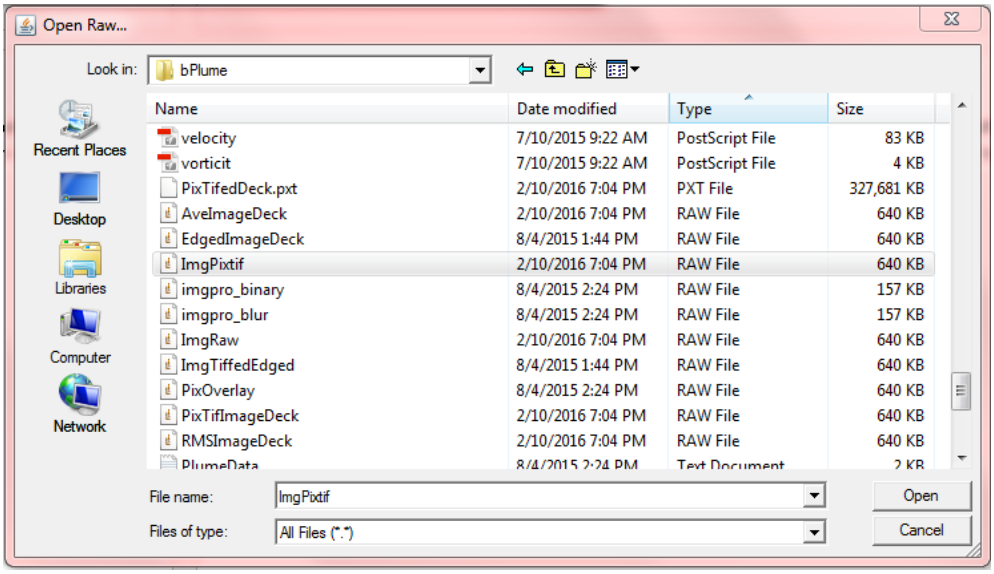

For **single image**, continue by inputting **NXC**, number of pixels along the width of the video image, and **NYC** ,number of pixels along the height of the video image, that correspond to the processed video.

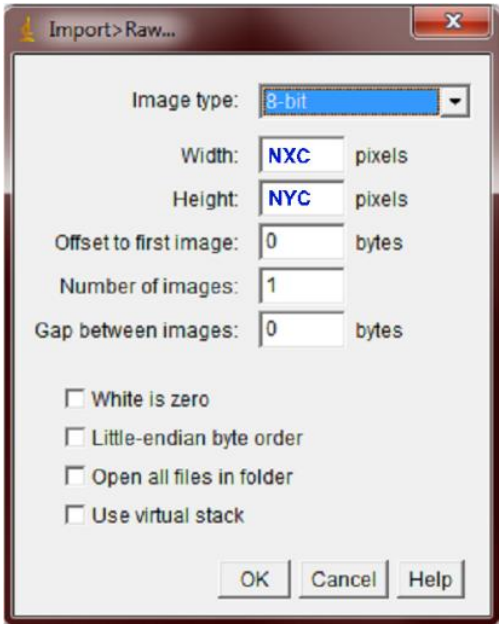

-ImgRaw.raw: An image frame taken from the middle of the image deck, unprocessed image for reference.

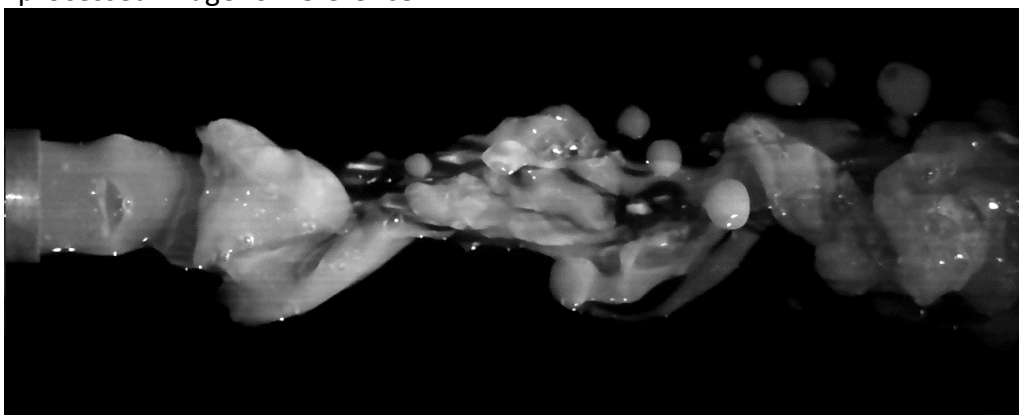

-ImgEdged.raw: A Canny edge detected version of image saved in **ImgRaw.raw**. This provides insight into which features are being tracked in the first pass.

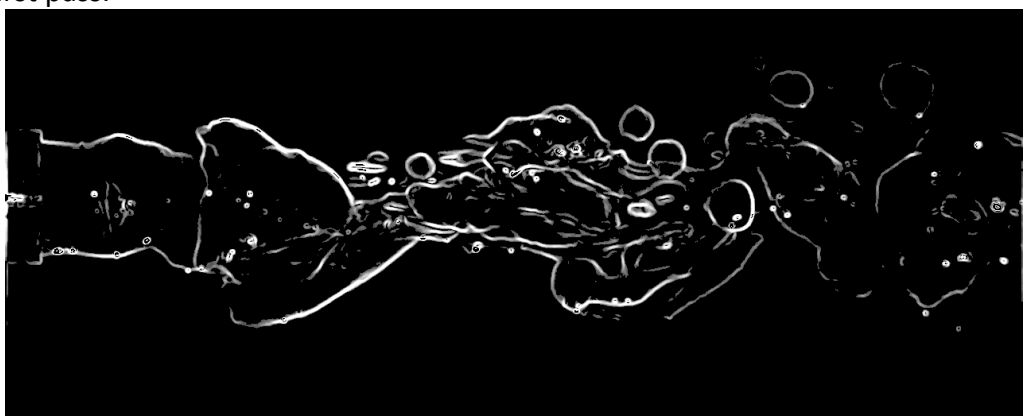

-ImgPixtif.raw: A Pixtif processed version of the image saved in **ImgRaw.raw**. This provides insight into which features are being pronounced in the flow to be tracked during the second pass.

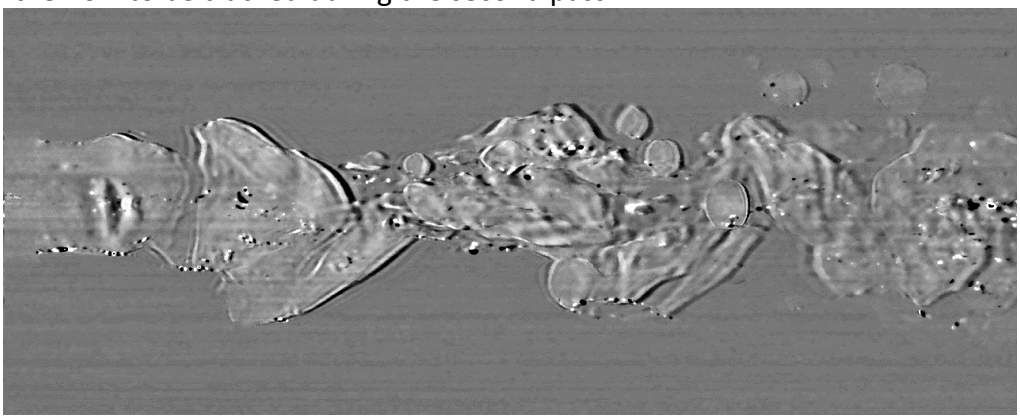

-RMSImage.raw: As stated earlier in assumptions, the RMS of the image deck removes constant features in the ROI, while outlining the location of fluctuating intensity values, such as where moving features in the jet occur.

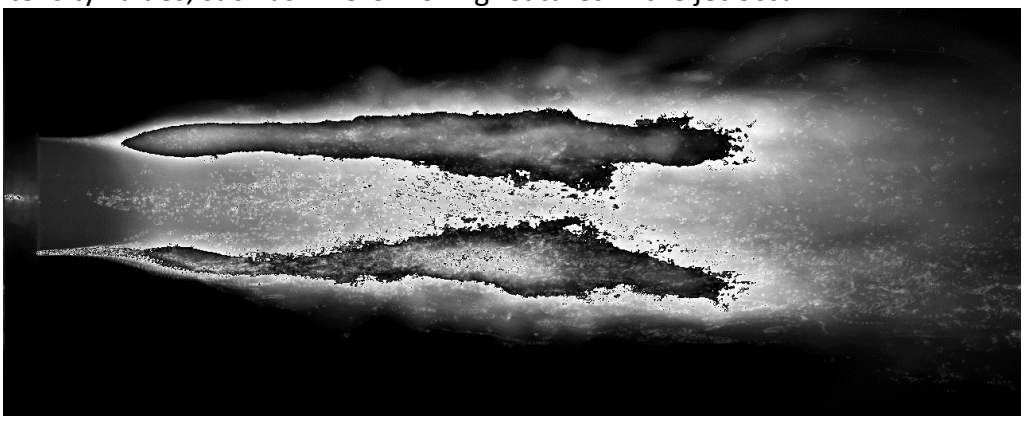

-PixOverlay.raw: The area of calculation is outlined as a whited region overlaid on the RMS of the entire image deck.

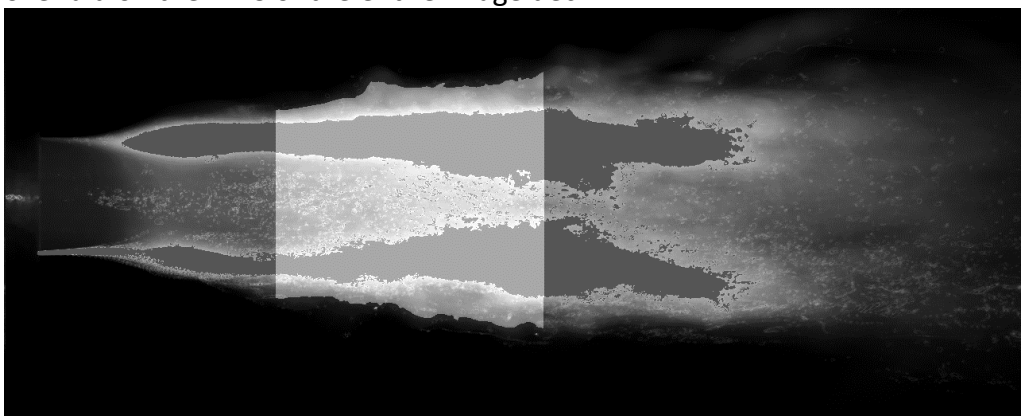

For **an image deck**, continue by inputting **NXC**, number of pixels along the width of the video image, and **NYC**, number of pixels along the height of the video image, and **NF** (this number is recorded in PlumeData.txt), number of frames processed, that correspond to the processed video. The "Offset to first image" should be set to 128 bytes to bypass the header information stored along with each image deck.

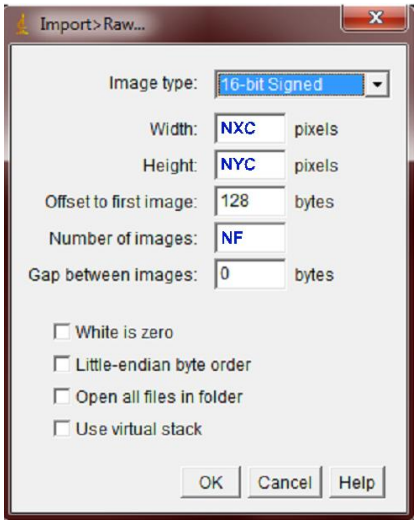

-EdgedDeck.edg: The raw image deck is ran through canny edge detection algorithm. The **EdgedDeck.edg** used for calculation during the first pass of **WALPT7.exe** in **UCB_Plume.exe**.

-PixTifedDeck.pxt: The raw image deck is ran through a pixel-wise filtering using parameters derived from the first pass. The **PixTifedDeck.pix** is used for calculation during the second pass of **WALPT7.exe** in **UCB_Plume.exe**.

Five **.out** files will be generated by **UCB_Plume.exe**. Third party software can be used to interpret the data stored in these files (Adobe CS, IDL, Matlab, VLC, ImageJ …).

The files are as follows:

The instantaneous information will be ordered as **AviTensor.####**. The **.####** will indicate which pair of images are being examined between. A correlation between Image1 and Image2 of the video deck will correspond to **AviTensor.0001**. In **AviTensor.####** information is stored as follows:

The output data file contains three arrays, **header, uvtensor, intwinxy,** all in binary. **header** contains processing and id information; **uvtensor** contains velocity data; and **intwinxy** consists of interrogation window dimensions in pixels when adaptive processing mode is used.

```
.
integer(2) header(64)
integer(1),allocatable :: intwinxy(:,:)
real(4),   allocatable :: uvtensor(:,:,:)
.
allocate(uvtensor(nxuv,nyuv,10))
allocate (intwinxy(nxuv,nyuv,2))
   intwinxy=0
.
open(1,file=utensor,form='binary')
write(1) header, uvtensor, intwinxy
close(1).
```

This output file contains a header which is **integer*2(64).**

Current contents are:

header(1)=version number (x100), used to determine compatibility	
header(2)=nxc	camera size-x
header(3)=nyc	camera size-y
header(4)=nxuv	output array size-x
header(5)=nyuv	output array size-y
header(6)=nxw	window size-x
header(7)=nyw	window size-y
header(8)=nxs	step size-x
header(9)=nys	step size-y
header(10)=nxf	flow region size-x
header(11)=nyf	flow region size-y
header(12)=xf	flow region offset-x
header(13)=yf	flow region offset-y
header(14)=nbits	pixel depth
header(15)=ipx_ctr	number of boundaries in ipx, 0=no ipx
header(16)=mode	processing mode
header(17)=FileType	input file type 0=raw,1=tiff,2=avi stream
header(18)=(nt-1) or (ntfft-1)	Tensordeck output depth, for AVIbatch or PixTif processing for .raw and .tifdecks

header(19:64) reserved for future use

The output data array **uvtensor** is a **binary** tensor containing the filtered velocity vector **u**=(u, v), velocity gradient tensor $\partial u_i/\partial x_j$, unfiltered velocity vector **u**=(u, v), and the correlation normalized coefficient in a (*,*,10) array. Horizontal pixel dimension [hpixel] is the length unit. Both u and v velocity components have units of [hpixel/δt]. For example, to calculate circulation, the arc length must be measured in horizontal pixel units. The unit of vorticity is [hpixel/δt] / [xstep].

The velocity data are in a 3D array of dimensions uvtensor(nxuv,nyuv,10) where

uvtensor(*,*, 1) = u	[hpixel/δt]
uvtensor(*,*, 2) = v	[hpixel/δt]
uvtensor(*,*, 3) = ∂u/∂x	[1/δt]
uvtensor(*,*, 4) = ∂v/∂x	[1/δt]
uvtensor(*,*, 5) = ∂u/∂y	[1/δt]
uvtensor(*,*, 6) = ∂v/∂y	[1/δt]
uvtensor(*,*, 7) = u_unfiltered	[hpixel/δt]
uvtensor(*,*, 8) = v_unfiltered	[hpixel/δt]
uvtensor(*,*, 9) = 0 reserved	
uvtensor(*,*,10) = correlation coefficient	[normalized]

1.1. `ImageDeck.out` : image deck consisting of the first image of each pair

`tensordeck.out` : tensor output file is stacked in a deck for each image pair

`tensorave.out` : average tensordeck.out, written by stats.f90

`statistics.out` : statistics of results in **`tensordeck.out`**, written by **`stats.f90`**

statistics(*,*, 1) = u_ave
statistics(*,*, 2) = v_ave
statistics(*,*, 3) = average vorticity
statistics(*,*, 4) = average speed
statistics(*,*, 5) = u^prime
statistics(*,*, 6) = v^prime
statistics(*,*, 7) = speed^prime
statistics(*,*, 8) = vorticity^prime
statistics(*,*, 9) = u_ave (unfiltered)
statistics(*,*,10) = v_ave (unfiltered)
statistics(*,*,11) = average unfiltered speed
statistics(*,*,12) = unused
statistics(*,*,13) = unused
statistics(*,*,14) = unused
statistics(*,*,15) = unused
statistics(*,*,16) = unused

Using IDL, **`statistics.out`** can be used to visualize:

Average Velocity

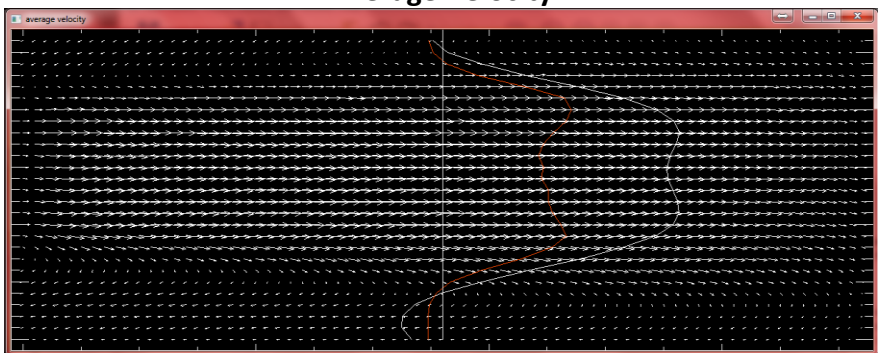

Average Vorticity

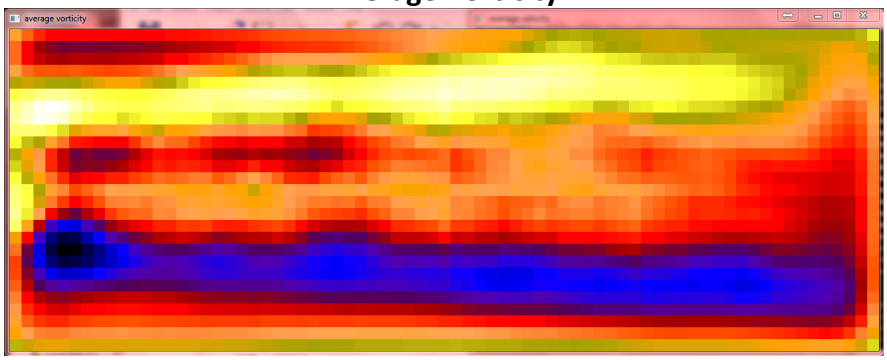

Filtered Average Speed

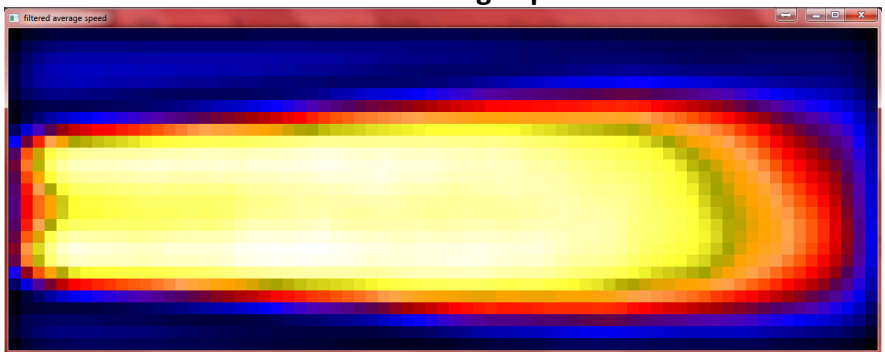

Raw Average Speed

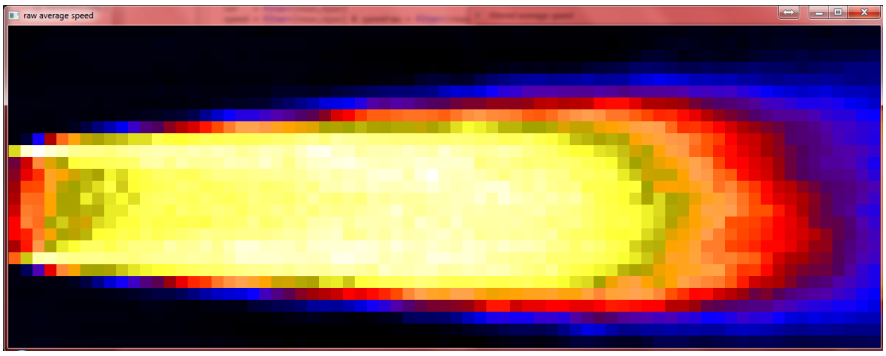

Common Errors

ERROR [`.inp`] does not exist
Do you want to generate a template [`.inp`]?

If **`bplume.inp`** or **`plume.inp`** does not exist in the same directory as **`UCB_Plume.exe`**, the user will be prompted for permission to generate respective template input files. The user input file, **`bplume.inp`**, will still be presented to operator to be modified to run desired video recording.

A B O R T I N G [`File.avi`] video stream file does not exist

This error is stating the code could not find the file in the specified directory. Verify the files existence and that correct file path was specified in **`bplume.inp`** in line 12.

Known Issues

Insufficient Virtual Memory: Range of tests have been completed using hardware:

Windows OS [2008R2 / 7 / 8.1 / 10]
Intel i7 processor
24GB Ram

Using this range of hardware, an error stating insufficient virtual memory has occurred while processing large video files. As currently tested on our hardware, a video file of 7GB is processable.

Noise sensitivity: Noise found in the video recording can be pronounced and lead to the generation of erroneous velocity fields. Noise can be introduced to the recording via substandard recording equipment, compression/decompression of recording, or certain video enhancement processes.

Nulled image: Removal of certain frequencies while using PixTif'ing has resulted in the zeroing of all pixels in the processed image decks. By adjusting the filter width and center this can be corrected.

References

The uses of coherent structure –Coles, Donald

- http://resolver.caltech.edu/CaltechAUTHORS:20141210-131347636

A Computational Approach to Edge Detection –Canny, John

- Canny, John. "A computational approach to edge detection." Pattern Analysis and Machine Intelligence, IEEE Transactions on6 (1986): 679-698.

Deepwater Horizon: A Preliminary Bibliography of Published Research and Expert Commentary

- http://www.lib.noaa.gov/researchtools/subjectguides/dwh.html

Appendix

Advanced Operation

UCB_Plume.exe is a program that runs almost autonomously, taking in few inputs from a user to describe the physical parameters of the recording. With this information UCB_Plume.exe generates plume.inp to run a preliminary pass with WALPT7.exe and then uses a generated update.inp to run the second pass with estimated filtering parameters. While this functionality is set to be available for quick use, advance use of WALPT7.exe directly is possible.

To use WALPT7.exe three files will be required to be in the same directory:

- **WALPT7.exe**
- **bplume.inp:** outlined in detail on page 8 under **Running Program** of this manual. It would be recommended to make a copy of the bplume.inp as generated by UCB_Plume.exe. The file name bplume.inp must remain unchanged, as WALPT7.exe will search the working directory for the exact file name.
- **test_00.inp:** The format of this file must be compatible with that of plume.inp as generated by UCB_Plume.exe. It would be recommended to make a copy of the plume.inp, rename as desired while preserving the .inp file extension, **test_00.inp** will be used to reference this duplicated file.

The directory housing these three files will be referred to as <TEST_DIR>, this can be named as desired. This directory will require an allotment of memory space to save to, roughly thrice the size of the images/.avi used.

From a command window, change the working directory to <TEST_DIR>.
Entering:

```
WALPT7.exe < test_00.inp
```

will use the parameters set in test_00.inp to process the images, computing a velocity field per image pair and, along with the information given in bplume.inp, the estimated flow rate.

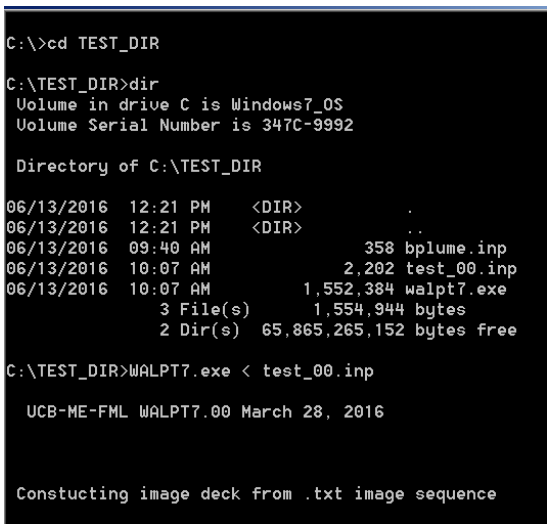
C:\>cd TEST_DIR
C:\TEST_DIR>dir
Volume in drive C is Windows7_OS
Volume Serial Number is 347C-9992
Directory of C:\TEST_DIR
06/13/2016 12:21 PM <DIR> .
06/13/2016 12:21 PM <DIR> ..
06/13/2016 09:40 AM 358 bplume.inp
06/13/2016 10:07 AM 2,202 test_00.inp
06/13/2016 10:07 AM 1,552,384 walpt7.exe
3 File(s) 1,554,944 bytes
2 Dir(s) 65,865,265,152 bytes free
C:\TEST_DIR>WALPT7.exe < test_00.inp
UCB-ME-FML WALPT7.00 March 28, 2016
Constucting image deck from .txt image sequence

Parameter Description: `plume.inp / test_00.inp`

mode npass silent batch edgeflag PTFlag PTCenter PTWidth
A) 1 1 0 1 0 0 0 0
file that contains the names of image files, prefix for outputfiles
B) D:\OHMSETT\OHM\Test_23_input\Test_23_input
C) TxtTensor
image size nxc, nyc, nbits, pixr
D) 1040 564 8 1.00
flow size, nxf, nyf
E) 1040 564
flow offset, xf, yf
F) 0 0
window size, nxw, nyw, 2n**
G) 64 64
amod, min, max windows dimensions 2n, correlation level corlvl**
H) 1 8 32 0.40
step size, nxs, nys
I) 16 16
window type, wtype 1-7, see source listing
J) 2
peak type, ptype 0=grid,1=parabolic,2=gaussian
K) 2
laundary type, ltype 0=no laundering,1=rejection
L) 0
extension parameter, 0= none, zero padding, 1= smooth
M) 0
filter widths fltrwx, fltrwy wavenlength in steps; exponent
N) 9 9 2
wall parameters: nwalls, parex, motion, intflag, outmask
O) 0 0 0 1 1
wall geometry file
P) Wall_Mask.raw
motion parameters: dxcg, dycg ,rot
Q) 0.00 0.00 0.00
0.00 0.00 0.00
9.00 0.00 0.00

A) Primary Processing Parameters

MODE: Sets which type of PIV algorithm will be implemented.

MODE=1 : Standard DPIV. In this mode, only one pass is done with the parameters specified. The code checks for questionable vectors and does some repairs; some ad-hoc, some rigorous. (relative time=1)

MODE=2 : Predictor corrector DPIV; moving from smaller windows to larger ones. It is quick at the cost of robustness. The code makes the first pass at the specified window size, and repairs suspect

vectors at twice or, if needed, at four times the window size to obtain an estimate for the final velocity pass. During the final pass, window pairs that are separated by the estimated velocity are used to determine the final velocity. Some repairs are done at the end. (relative time=2)

MODE=3: Lagrangian parcel tracking LPT with multiple passes. The velocity field calculated using MODE=2 is used as the first estimate in LPT. First, the domain is extended to $2^m x 2^n$. Then velocity gradient tensor and its derivative are calculated using Fourier methods after some filtering in frequency domain. Fluid parcels are deformed according to the local velocity field to determine the deformed correlation windows from which a new velocity field is determined. Each pass is done with a newly calculated velocity field. No repairs are done. (relative time=2+2*passes)

MODE=4: Adaptive Lagrangian parcel tracking aLPT with multiple passes. Chooses windows commensurate with the velocity vector, thus increases the spatial resolution of the instrument. The processing is the same as that in mode 3 except the dynamic adaptation of the window size and orientation. The velocity field calculated using MODE=3 with 2 passes is used as the first estimate in aLPT. No repairs are done. Since smaller windows are used most of the time, the incremental processing is faster than that in mode 3.

npass: is the number of passes for **walpt** processing when **MODE** = 3 or 4. Otherwise set to 1. The code expects a valid integer entry for **npass** even if the **mode** is other than 3 and 4.

silent: screen display mode,

silent = 0 : Verbose mode slows the CPU to crawl, probably due to poor operating system design (Windows)

silent = 1 : silent (minimal display of status). Set to 1 if processing a large number of files (say, larger that 20) when **batch** >0.

batch:. The contents of files **file_1** and **file_2** below are interpreted differently depending on the value of **batch**.

batch = 0 : Single image pair processing

batch = 1 : Multiple image pair processing

edgeflag: Parameter flag setting whether edge detection processing is ran on the images, and if so which type.

edgeflag = 0 for no filtering

edgeflag = 10 for Sobel, all around

edgeflag = 11 for Sobel, along x-axis

edgeflag = 12 for Sobel, along y-axis
edgeflag = 25 for 5x5 Laplace filtering.
edgeflag = 30 for Canny filtering, all around.
edgeflag = 31 for Canny filtering, along x-axis.
edgeflag = 32 for Canny filtering, along y-axis

PixTifFlag:
PTFlag = 0: no PxTif'in
PTFlag = 1: high-pass filter (tanh)
PTFlag = 2: low-pass filter (1-tanh)
PTFlag = 3: band-pass filter (exp(-t^2))
PTFlag = 4: band-reject filter (notch) (1-exp(-t^2))
PTFlag > 4: returns without filtering, 2^n image deck written out.
PTFlag = 9: special handling

PixTifCenter: PixTif center of filter.

PixTifWidth: PixTif filter width parameter.

B) file_1: File name that is processed differently based on content and batch flag

C) file_2: File name that is processed differently based on content and batch flag

batch =0 ; single pair of images are processed

file_1 and **file_2** are the names of the pair of images for processing, one line per file, include full path to avoid confusion. Both image files must be of the same type, i.e. **.raw** and **.tif** files may not be mixed. The output data are written in **'tensor.out'** in the current directory (described below). If ipx is invoked, the path data are written in **'ipxpaths.out'** in the current directory.

batch =n>0: multiple pairs of images are processed

file_1 is the name of the file containing the names of images for processing. The images are taken as pairs until all entries are processed. If there are odd number of entries, the last one is discarded. Include full path to avoid confusion. Image files must all be of the same type, i.e. **.raw** and **.tif** files may not be mixed.

file_2 is the prefix used to construct the output file names for each of the pairs processed. The output files are numbered consecutively starting with the value of **batch** **.0001** extension. For example if **batch =99** and

file_2=tensor, then the output files will start from **tensor.0099** in the specified folder. If no folder is specified, the output files will be in **TensorFolder** directory.

2. AVI image stream

file_1 is the name of the avi file to be processed. It must have .**avi** or .**AVI** or .**Avi** extension. Compressed avi files are rejected. Images are processed for every interval; that is, if there are N images in the avi file, there will be N-1 output files. If the images are equi-spaced, then, no special handling is needed. If, however, the images are recorded in 'double exposure' mode for PIV operations, then successive output files will have alternating time intervals, one corresponding to the laser pulse separation and the other corresponding to sampling interval for PIV image pairs. Therefore, the output files must be processed with the timing considerations in mind. Even and odd numbered files must be grouped together

file_2 is the prefix used to construct the output file names for each of the pairs as well as the consolidate output file for the whole stream

3. TXT image sequence

file_1 is the name of the folder storing all the .txt image file to be processed. It must have i**nput** or **Input** or **INPUT** as its ending characters. Numbering style should be consistent with that exported from ImageJ. If there are N .txt images in the input folder, there will be N-1 output files. If the images are equi-spaced, then, no special handling is needed. If, however, the images are recorded in 'double exposure' mode for PIV operations, then successive output files will have alternating time intervals, one corresponding to the laser pulse separation and the other corresponding to sampling interval for PIV image pairs. Therefore, the output files must be processed with the timing considerations in mind. Even and odd numbered files must be grouped together

file_2 is the prefix used to construct the output file names for each of the pairs as well as the consolidate output file for the whole stream

When **ipx** is invoked, the same prefix is used to generate the ipx'ed image and path files. This time, '**ipx1/2**' suffix is inserted in the file names for images and **ipxpaths** for path files. For example, the ipx'ed image file names corresponding to **tensor.0099** output are **tensoripx1.0099** and **tensoripx2.0099,** and the corresponding path file is **tensoripxpaths.0099**.

If the full path is included in **file_2,** e.g., **file_2 = d:\airfoil\tensor**, then, the appropriate directory must already exist.

D) Image Size: (figure 1a)

nxc: Number of pixels horizontally across the image
nyc: Number of pixels vertically across the image
nbit: Pix bit depth
pixr: camera pixel ratio, vertical/horizontal pixel dimensions

Camera	nxc x nyc	pxr	(µm x µm)	bits	*max frame rate*	
IDT-MP-X3	1280H x 1024V	1.00	(12x12)	8	1000 Hz	digital
Kodak ES1.0	1008H x 1018V	1.00	(9x9)	8	30 Hz	digital
Sony 7500	640H x 480V	1.00	(9.9x9.9)	8	30/60 Hz	analog/ non-interlaced

E) Flow Size: (figure 1a)

nxf, nyf: flow region of interest imbedded in **(nxc,nyc)** image array

F) Flow Offset window size: (figure 1a)

xf, yf: position of **(nxf,nyf)** region with respect to the image origin

G) Window size: (figure 1a)

nxw, nyw: correlation window size 2^m x 2^n. Consider using rectangular windows in nearly parallel flows

H) Adaptation Parameters

amod: Adaptation mode
amod = 0: square windows only, no directional adaptation
amod = 1: include rectangular windows aligned with axes

minw, maxw: are minimum and maximum window dimensions 2^m used in mode 4 LPT. The minimum value may be as low as 8 if image quality permits.

corlvl: is the minimum correlation coefficient level to double the window dimensions during LPT.

I) Step Size

nxs, nys: step size for scanning the flow region **(nxf,nyf)**

J) Window Type

wtype: window type for windowing data before correlating. If the images are periodic, you must use a window.

wtype = 1: square window (no windowing)
wtype = 2: Rosenfeld
wtype = 3: triangle(Parzen, Bartlett)
wtype = 4: parabolic (Welch)
wtype = 5: cosine (Hanning)
wtype = 6: Hamming
wtype = 7: Blackman-Harris

K) Peak Type

ptype: method of determining correlation maximum

ptype = 0: read off the array values (you might as well not use the program)

ptype = 1: paraboloid fitting

ptype = 2: gaussianoid fitting (logarithms are used, correlation data must be positive values).

L) Launder Type

ltype: bad vector rejection flag,

ltype = 0: no rejections

ltype = 1: rejections enabled

M) Extension Parameter

exten: domain extension flag

exten = 0: extend with zero padding (use when far field is quiescent),

exten = 1: smooth extension with matching 2nd order derivatives.

N) Filtering parameters

Filtering parameters used in wavenumber domain (Figure 5).

fltrwx, fltrwy are the wavelengths (in units of steps) at the 1/e cut-off point of the filter kernel. Note that the step sizes **(nxs,nys)** determine the actual cut-off wavelengths (in pixels) on PIV images. The larger the parameters are, the smoother the output is. Equivalently, features smaller

than the parameters are filtered out (blurred). If **fltrwx=0**, or **fltrwy=0**, then, no filtering is done in x or y, respectively.

Nfil: is the exponent in the filter kernel.

Higher values mean sharper cut-off in wavenumber domain.

The filter kernel is $[1-\exp(-1/k^n)]$ where k is the magnitude of the wave vector,

(k_x, k_y) : $k \sim \{ [k_x / (1 / \text{fltrwx})]^2 + [k_y / (1 / \text{fltrwy})]^2 \}^{1/2}$

Alternatively,

(k_x, k_y) : $k \sim \{ [\text{fltrwx} \cdot k_x]^2 + [\text{fltrwy} \cdot k_y]^2 \}^{1/2}$

O) Wall parameters (figure 2).

nwall: number of interfaces(s) in PIV images, to be dealt with.

- **nwall** = 0: no interfaces
- **nwall** = +n , n interfaces, **boundary** data file is needed (described below).
- **nwall** = -n , n interfaces, boundaries are determined from the first flow image. Requires high contrast data, to clearly delineate the flow region.

parex: image parity exchange at walls to extend velocity measurements to interfaces

- **parex** = 0: Off
- **parex** = 1: On

motion: interfaces to be dealt with

- **motion** = 0: no motion, fixed walls
- **motion** = 1: walls in rigid body motion (individually or in unison)
- **motion** = -1: compliant interfaces (every interface is treated independently)

intflag: used when **parex** =1

- **intflag** = 0: nearest pixel,
- **intflag** = 1: interpolation over 3x3 region (recommended)

outmask: used when **wall** =1 to deal with output data in extended regions.

- **outmask** = 0: output as is (for further processing at interfaces, e.g. shear at wall)
- **outmask** = 1:set wall regions to 1001.0 (suitable for display in IDL using **MISSING** keyword in **velovect** procedure)

P) Wall Geometry File

mpairs=0
file marking the interfaces(s) appearing the first image file **imagefile_1**. Must be supplied when **nwall > 0**. Has the same structure as the image files **imagefile_1/2** above. Byte elements are 255 (-1)(white) when in the metric flow domain and 0(black) when in the non-metric domain (figures 2,4). The interface outlines can be closed loops or open lines. There is no limit to the number of interfaces in the flow field. High curvatures should be avoided. Cusps are not allowed in autonomous processing.

mpairs=1
boundary is the name of the file containing the names of boundary files for batch processing. A boundary mask file matched to each image pair listed in **file_1**.

Q) Motion Parameters

rigid body motion parameters of wall outlines, needed when **motion=1.** One line for each boundary.

dxcg translation displacement of the centroid of wall outline in x-direction (pixels)
dycg translation displacement of the centroid of wall outline in y-direction (pixels)
rot rotation of wall outline in radians

CAUTION: If the number of line entries are fewer than the boundaries in **boundary**, then, the last entry is used for the remaining boundaries. If the walls are in pure translation, then the results are correct. If there is any rotation, the results will be wrong.

NOTE: If there are multiple walls which are moving as a solid body in unison, a single entry is sufficient provided that **nwall=1**.

See figure 4 for the ordering convention of the interfacess. **ipx** looks for interfaces in **boundary** starting on **edge_1**, going around the four edges counterclockwise. Interfaces starting on the edges are numbered sequentially until the open-ended interfaces are taken care of. Then, **ipx** starts scanning vertically the interior of the **boundary** file stating from x=0. The numbering of the closed interfaces then continues until all interior interfaces are accounted for. If all interfaces are rigid walls, then, **ipx** can automatically perform image parity exchange using the rigid-body-motion parameters prescribed above.

FIGURES

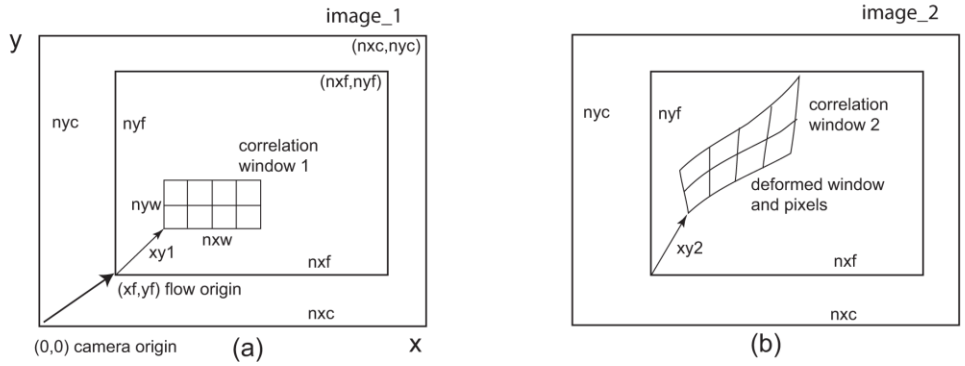

Figure 1. Lagrangian Parcel Tracking -- LPT.

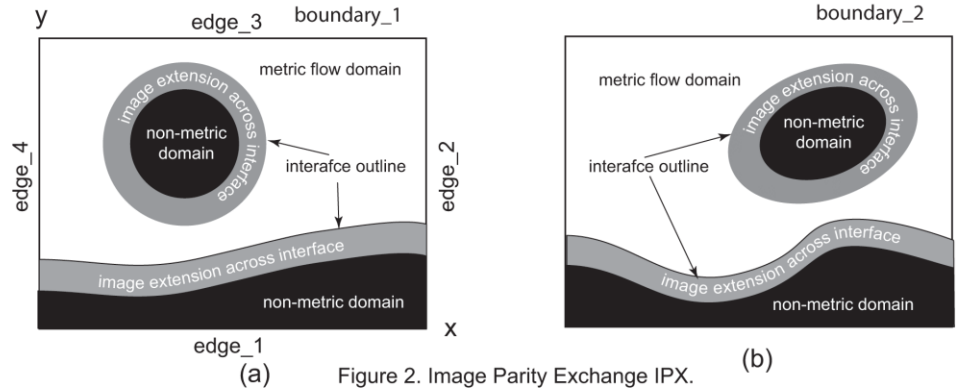

Figure 2. Image Parity Exchange IPX.

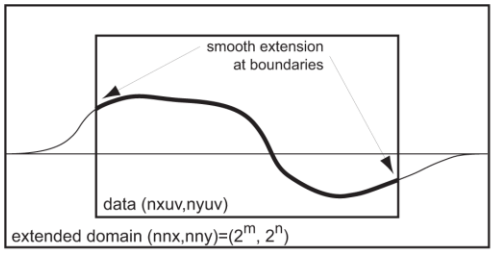

Figure 3. Extending data domain for FFT processing.

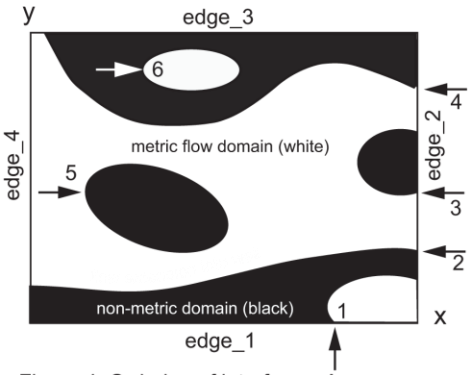

Figure 4. Ordering of interfaces. Arrows indicate starting points of interface outlines.

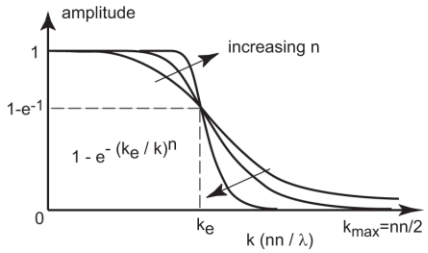

Figure 5. Wavenumber filter kernel.

APPENDIX-2

`Plume.bat` source listing

BplumeS.bat

```
rem executes plume software
rem June 13, 2016
rem Omer Savas, UCB-ME-FML-140HH
rem Eric Ibarra
echo off
title UCB_Plume: berkeley plume analysis tool
         cls
color 1f
setlocal enableextensions  enabledelayedexpansion


set InputFile=plume.inp
set UserInput=bplume.inp
set update=bpUpdate.inp

set tempfile=tmpy.tmp
copy /y nul %tempfile% > nul


set extract=12
set extract2=14
set replace=4
set replace2=7
set replace3=9

echo.
echo   UCB_Plume: berkeley plume analysis tool
echo   June 5, 2016
echo   UCB-ME Fluid Mechanics Laboratory


if     exist %update% (erase %update% > nul)



REM _____ CHECKING FOR bplume.inp _____
if     exist %UserInput% (goto :continue1)

echo.
echo ERROR [ %UserInput% ] does not exist
echo.
```

```
REM Template Generator for UserInput
echo      Do you want to generate a template [ %UserInput%
]?
     set /p INPUT= Type [ Y/N ]:
     SET INPUT_=%INPUT:~0,1%
     If "%INPUT_%"=="Y" goto yes1
     If "%INPUT_%"=="y" goto yes1

echo     A B O R T I N G [ %UserInput% ] does not exist
goto :eof

:yes1
REM iput file generated
echo.
copy /y nul %UserInput% > nul
echo. Camera view dimension along plume axis, in meters >>
%UserInput%
echo. 0.12 >> %UserInput%
echo. Camera view dimension across plume axis,  in meters
>> %UserInput%
echo. 0.049 >> %UserInput%
echo. Discharge orifice diameter in meters >> %UserInput%
echo. 0.013 >> %UserInput%
echo. Camera frame rate >> %UserInput%
echo. 500 >> %UserInput%
echo. Discharge fluid specific gravity >> %UserInput%
echo. 0.90 >> %UserInput%
echo. AVI file location >> %UserInput%
echo. c:\avi\AVIReadTestFile7.avi >> %UserInput%
echo. Recording pixel dimension (Required for .txt
processing) >> %UserInput%
echo. 1280 512 >> %UserInput%

echo Template [ %UserInput% ] successfully generated.
pause

:continue1
REM _____ CHECKING FOR plume.inp _____
if    exist %InputFile% (goto :continue2)

echo.
echo ERROR [ %InputFile% ] does not exist
echo.

REM Template Generator for InputFile
echo      Do you want to generate a template [ %InputFile%
]?
```

```
      set /p INPUT= Type [ Y/N ]:
      SET INPUT_=%INPUT:~0,1%
      If "%INPUT_%"=="Y" goto yes2
      If "%INPUT_%"=="y" goto yes2

echo     A B O R T I N G [ %InputFile% ] does not exist
goto :eof

:yes2
echo.
copy /y nul %InputFile% > nul
echo. mode npass silent batch edgeflag PTFlag PTCenter
PTWidth >> %InputFile%
echo. 1 1 0 1 30 5 4 8 >> %InputFile%
echo. file that contains the names of image files, prefix
for outputfiles >> %InputFile%
echo. c:\avi\AVIReadTestFile7.avi >> %InputFile%
echo. AviTensor >> %InputFile%
echo. image size nxc, nyc, pixr >> %InputFile%
echo. 1280 512 8 1.00 >> %InputFile%
echo. flow size, nxf, nyf >> %InputFile%
echo. 1280 512 >> %InputFile%
echo. flow offset, xf, yf >> %InputFile%
echo. 0 0 >> %InputFile%
echo. window size, nxw, nyw, 2**n >> %InputFile%
echo. 64 64 >> %InputFile%
echo. amod, min, max windows dimensions 2**n, correlation
level corlvl >> %InputFile%
echo. 1 8 32 0.40 >> %InputFile%
echo. step size, nxs, nys >> %InputFile%
echo. 16 16 >> %InputFile%
echo. window type, wtype 1-7, see source listing >>
%InputFile%
echo. 2 >> %InputFile%
echo. peak type, ptype 0=grid,1=parabolic,2=gaussian >>
%InputFile%
echo. 2 >> %InputFile%
echo. laundary type, ltype 0=no laundering,1=rejection >>
%InputFile%
echo. 0 >> %InputFile%
echo. extension parameter, 0= none, zero padding, 1= smooth
>> %InputFile%
echo. 0 >> %InputFile%
echo. filter widths fltrwx, fltrwy wavenlength in steps;
exponent >> %InputFile%
echo. 9 9 2 >> %InputFile%
```

```
echo. wall parameters: nwalls, parex, motion, intflag,
outmask >> %InputFile%
echo. 0 0 0 1 1 >> %InputFile%
echo. wall geometry file >> %InputFile%
echo. plane1.raw >> %InputFile%
echo. motion parameters: dxcg, dycg ,rot >> %InputFile%
echo. 0.00 0.00 0.00 >> %InputFile%
echo. 0.00 0.00 0.00 >> %InputFile%
echo. 9.00 0.00 0.00 >> %InputFile%

echo Template [ %InputFile% ] successfully generated.

:continue2

echo.
         pause

echo     confirm the contents of the input file [
%UserInput% ]
echo     edit the video parameters as needed
echo.
echo     S A V E  and  C L O S E [ %UserInput% ] when
finished
         notepad %UserInput%
echo.

rem ____________________________________________________

rem extracting video file location

set "var="
set /a extract-=1
for /f "skip=%extract% delims=" %%i in (%userinput%) do if
not defined var set "var=%%i"

rem extracting video file location

set "var2="
set /a extract2-=1
for /f "skip=%extract2% delims=" %%i in (%userinput%) do if
not defined var2 set "var2=%%i"

rem Editing input file %inputfile%
set line=0

for /f "delims=" %%j in (%inputfile%) do (
    set /a line+=1
```

```
    if !line!==%replace% (
        echo.%var%>>%tempfile%
     )    else if !line!==%replace2% (
        echo.%var2% 8 1.00>>%tempfile%
    )     else if !line!==%replace3% (
        echo.%var2%>>%tempfile%
    ) else (
        echo %%j>>%tempfile%
    )
)

erase %inputfile%
ren %tempfile% %inputfile%
rem type %inputfile%


rem ____________________________________________________

if  not  exist %var% (
echo.
echo     A B O R T I N G [ %var% ] video stream file does
not exist
     pause
goto :eof
)

echo     hit any key to continue, CTRL-C to abort
echo.
         pause
echo.
echo     processing... may take   S E V E R A L   M I N U T
E S
rem         if not exist TensorFolder (mkdir TensorFolder >
nul)
echo.
echo     CTRL-C to abort
echo.
echo     First pass
echo.
         walpt7<%InputFile% >nul  rem First pass
echo.
echo     Second Pass
           walpt7<%update% >nul  rem Second pass

echo     finished processing
rem echo.    >> PlumeData.txt
rem echo         %DATE:/=-%   %TIME::=-% >> PlumeData.txt
```

```
rem echo.    >> PlumeData.txt
echo.
echo ------------------------------------------------------
--
echo     current results in  [PlumeData.txt]
echo ------------------------------------------------------
--
         type PlumeData.txt
rem echo ------------------------------------------------
------
rem         if     exist Plume.txt (copy /y
Plume.txt+PlumeData.txt Plume.txt > nul)
rem         if not exist Plume.txt (copy /y PlumeData.txt
Plume.txt > nul)
echo ------------------------------------------------------
--
echo     accumulated results in  [PlumeDataArchive.txt]
echo ------------------------------------------------------
--
         pause
echo.
echo     C L O S E [PlumeDataArchive.txt] when finished
echo.
         notepad PlumeDataArchive.txt
         pause

 rem        start c:\rsi\idl63\bin\bin.x86\idlde.exe
c:\walpt6\stats.pro

 rem restore DOS color scheme

         color 0f
         title Command Line  Interface

         exit /b
 rem END
```

APPENDIX-3

BSEE Presentation

UCB Plume

UCB Plume Analysis Tool
USER'S MANUAL

Version 1.01

June 2016

Fluid Mechanics Laboratory
140 Hesse Hall
Department of Mechanical Engineering
University of California, Berkeley, California, 94720-1740

Scope of Manual

This manual will describe the steps to use **UCB Plume** to estimate the flow rate of jet discharges. This involves both outlining the limitations of the software and describing its ideal application conditions. Methods for interpreting additional data that is calculated, as well as the visualization of results, will also be outlined. A list of common error messages and their solutions will be detailed as well. The name **UCB Plume,** UCB Plume Analysis Tool, and **UCB_Plume.exe** will be used interchangeably to refer to the software.

Point of Contact

UCB Plume was developed at UC Berkeley with support from National Energy and Technology Laboratories and Bureau of Safety and Environmental Enforcement.
Please contact with field use questions.

Contact: Savaş, Ömer
Email: savas@berkeley.edu
Phone: (510) 642 - 5272

Contact: Ibarra, Eric
Email: ibarraeric89@gmail.com
Phone: (323) 327 - 5868

Project References

This software was tested on laboratory experiments whose Reynolds number ranged from 4,500-550,000. These tested experiments were conducted at UC Berkeley and OHMSETT. On average, the flow rate estimation tends to be conservative by ~30%.

Glossary

The following terms are used as operator inputs and calculated results described in the manual.

ROI length/width:

The physical dimension in meters corresponding to the length/width of the image

Specific gravity (φ):

Density of the fluid comprising the Jet/Plume (ρ_{jet}) over the density of the quiescent fluid ($\rho_{ambient}$).

(i.e. Density of Crude oil / Density of Sea Water)

Frame Rate:

The rate at which the video was recorded by the camera, different from the playback rate that will be listed in the details of the AVI file.

Celerity (C):

The velocity of the trackable features. The mean center velocity of the trackable eddies along the visible surface of the opaque jet/plume.

Centerline Velocity (U_C):

The maximum velocity to be found at the center axis of the discharging fluid jet.

Algorithm Development

Cross Correlation: A measure of the similarity between two signals as a function of the delay between the two images. In our correlation, the signal is the intensity value in the image and the lag is the time interval elapsed between successive images.

Particle Image Velocity (PIV): A flow visualization technique that provides the instantaneous velocity measurements to be taken. For PIV, density neutral particles are seeded into a flow. The motion of the particles are used to calculate the velocity field of the flow.

Image Correlation Velocimetry (ICV): ICV performs a cross correlation of interrogation regions in consecutive images to measure the displacements of moving images. Using the delay between the images, a velocity is measured.

PixTif: A pixel-wise filtering done on time. Features in the flow move at a certain speed. At a given pixel, these features leave a distinct signature in the pixel's intensity history. By taking the intensity signal into the Fourier domain, features moving with a certain speed can be filtered with a convolution. We then apply a high-pass filter, and we define the filter center and width using the celerity and radius calculated during the first pass using a Stouhal number.

Parameter generation: During a run of `UCB_Plume.exe`, `WALPT7.exe` is called for two passes over the images. An initial pass is run with preset processing parameters and the user's flow parameters. This initial pass gives a first approximation of the velocities, length scales, and flow rates that are being considered. Based on the results, `WALPT7.exe` will output an updated input file with processing parameters adjusted. The updated input file will be used to run `WALPT7.exe` for the final pass, the results of which will be outputted.

Radius estimation: The root mean square (RMS) of the all the images processed is used to estimate the radius. The RMS of the image deck removes constant features in the ROI, while outlining the location of fluctuating intensity values, such as where moving features in the jet occur.

Celerity: The velocity of the surface features measured and is used as the celerity for the calculation. By using image correlation velocimetry, a velocity field of the jet is calculated, and an average of this field is taken about the region of calculation.

Discharge Rate estimation

Assumptions:

In the integration of the estimated jet profile these assumptions are made.

A *Gaussian velocity profile* of the jet that is axisymmetric is assumed. This is used to relate the observable feature's velocity to what is inside for flow rate calculations.

The velocity profile is evaluated at a distance of 3 pipe diameters downstream from the discharging orifice, which is in the *near field*. In this range the inertial terms are the same order of magnitude as the buoyant terms, allowing them to be neglected in the flow rate calculations.

It is assumed in the *near field* that the velocity of the surrounding fluid, U_2, is small in comparison to the celerity of the jet/plume, allowing $U_2 \approx 0$. The limit of this software is to where jets are not being affected by currents in the same order of magnitude as the jet/plume.

A derivation of the flow rate (Q) is as follows:

$$u(r)\,/U_c = \exp(-r^2/\sigma^2)$$

$$C\,/U_c = \exp(-r_c^2/\sigma^2)$$

$$U_c = (1+\varphi^{-1/2})\,C$$

$$\varphi = \frac{\rho_{jet}}{\rho_{ambient}}$$

$$\sigma^2 = \frac{r_c^2}{\ln(1+\varphi^{-1/2})}$$

$$Q = 2\pi \int_0^{r_c} u(r)\, r\, dr = \frac{\pi\, r_c^2\, C}{\varphi^{1/2}\ln(1+\varphi^{-1/2})}$$

Hardware Requirements

A high end Windows laptop computer as the operating platform and a high speed, high resolution monochrome camera for uncompressed video recording are the hardware requirements.

Capable Camera:

A high speed, high resolution camera (2000+ fps, 2Mpix+). Successive images in a video stream must be recorded within the life span of flow structure at the edge of the jet. Camera should use a polarizing filter to remove reflection at jet/environment interfaces. The Y models and X models by Integrated Design Tools Inc. have been used in the laboratory setting for these higher speed flow experiment, and have performed well. An additional benefit, the capturing software provided by IDT Inc. can write AVI files using the Basic Windows bitmap format which is required by `UCB_Plume.exe`.

i7 processor/32 GB Ram or better:

The `UCB_Plume.exe` software has been tested on contemporary WINDOWS operating systems; here are their listings with the average times to processes 512 frames:

-Intel® Xeon® CPU E5607 @ 2.27 GHZ, 128 GB Ram
Running Windows 2008 R2
~60 minutes
-Intel® Core™ i7-4700 MQ CPU @ 2.40 GHZ, 24GB RAM
Running Windows 7
~25 minutes
-Intel® Core™ i7-4710 MQ CPU @ 2.50 GHZ, 16 GB RAM
Running Windows 8.1
~25 minutes
-Intel® Core™ i5-4430 MQ CPU @ 3.00 GHZ, 12 GB RAM
Running Windows 8.1
~35 minutes

Imaging requirements

Uncompressed AVI Gray level

-Compressed, lossless, or lossy video will result in the code aborting. Only uncompressed AVI using the Basic Windows bitmap format codec is supported for gray level.

Static recording position

-Have the ROV record the jet/plume in a fixed reference with respect to the orifice. The camera should be faced perpendicular to the jet's/plume's centerline axis

Lighting

-The flows must be illuminated by a continuous, directed, polarized light source. Continuous light is critical, and must be differentiated from certain light sources that only simulate continuous by pulsing on and off at a high frequency not discernible to the human eye. When recording pulsing light with a high speed camera, consecutive images can alternate from high to low intensity leading to poor results. The light source should originate from near the ROV/camera. Polarization of the light along with the use of a polarized lens will diminish the occurrences of bright reflections of light at the interfaces, these glares lead to less reliable results if not dealt with.

Image centered 3 orifice diameters along the jets axis

-Include the discharging orifice in the image and have the image centered at 3 orifice diameters lengths from the orifice itself.

Video image's length is aligned with axis of the jet

-The jet should discharge left to right in the video recording.

Sufficient Frame Rate to capture evolution of features

-The recording frame rate should be sufficient to continuously capture the motion of the visible features.

Execution

In the directory UCB_Plume, four files are essential to the operation of the software:

- **UCB_Plume.exe:** The main batch file that prompts and automates the invocation of the `WALPT7.exe` with the proper input file.

-**WALPT7.exe:** The computing heart of this software. **WALPT7** source code written in FORTRAN, allowing it to both efficiently and effectively run calculation.

-**bplume.inp**: This input file will be edited and verified by the user. It contains parameters pertaining to the AVI as well as the flow.

-**plume.inp**: This is a self-contained input file which houses parameters used in analyzing the video.

Running Program:

-Double-click **UCB_Plume.exe** and follow the command line instructions.

-The user will be required to input/verify the information in **bplume.inp**:

- **Camera view dimension along plume axis, in meters (Line 2)**
- **Camera view dimension across plume axis, in meters (Line 4)**
  -real world ("Physical") length scale of the captured video
- **Discharge orifice diameter in meters (Line 6)**
  -the diameter of the jet's/plume's orifice

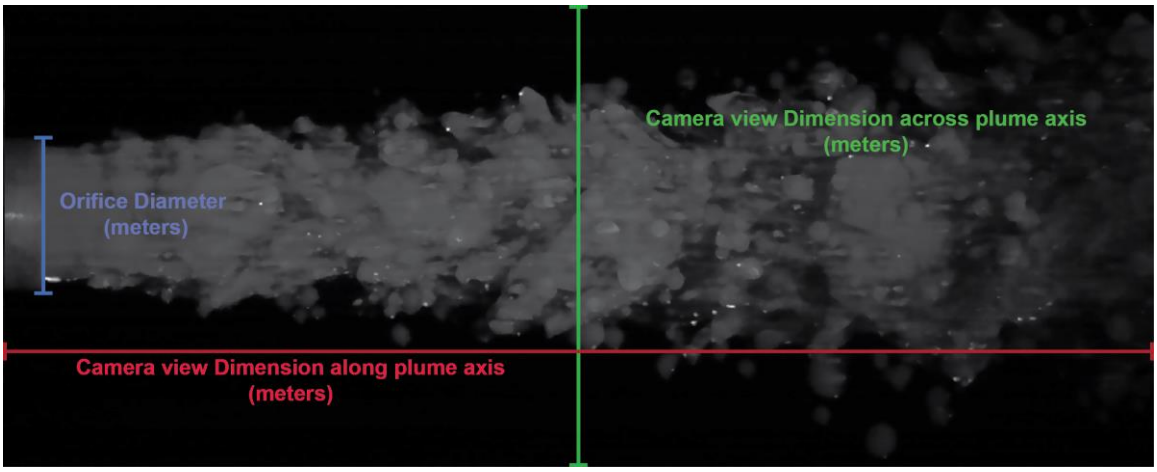

(Test image for reference)

Each of these length are related to field measurements and estimations

- Camera frame rate (Line 8)

-the capture frame rate of the video

- Discharge fluid specific gravity (Line 10)

-the specific gravity of the jet/plume being discharged

-AVI file location (Line 12)

-the path to the video file storage location

Note: There are many ways to copy the file path. Here is one for reference:

-Locate the AVI file

-Shift + Right-Click the file and select

Copy as path

-Paste the path in bplume.inp in the correct line (line 12)

(Remove the quotation marks from the front and end of the pasted file path)

After editing, verifying, saving, and closing the input file, follow the command line instructions.

NOTE: Assume that the calculation time will scale with the number of frames, N_{frames}, by

$$Time \propto N_{frames} \cdot log(N_{frames})$$

2.5 GHz i7 processor with 24 GB ram

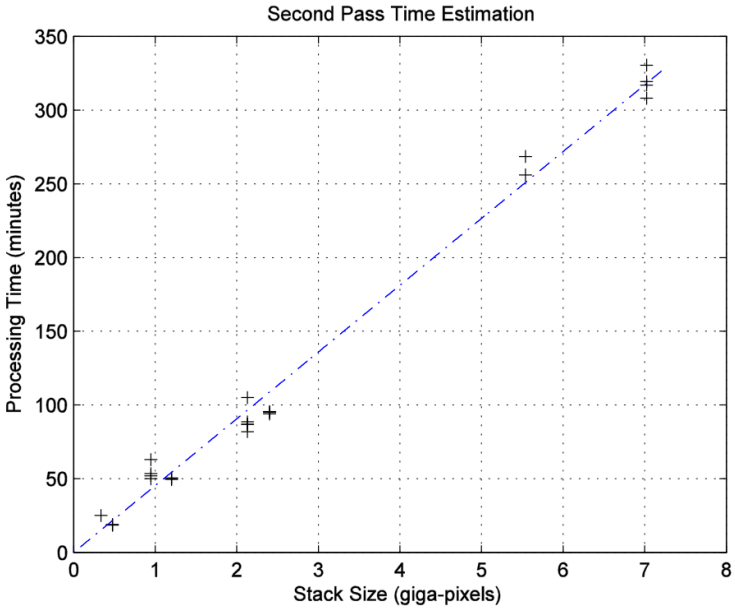

Results

Two **.txt** files are generated upon completion of the program.

PlumeData.txt:
Holds the printed information of the most recent run. This information lists parameters input by the user, such as:

- AVI file location
- Field of view dimensions
- Framing rate
- Specific gravity

Listed also are other processing parameters that were derived from information gained in the initial pass. These parameters are:

- Image resolution
- Number of images used in PixTif'ing
- PixTif filter type, center, and width

The listing of these parameters allows for a connection between a video and how it was processed to calculate the estimated flow rate, which is listed in a range of units.

PlumeDataArchive.txt:
An archive of the all **PlumeData.txt** from prior runs of **UCB_Plume.exe**. To start a new archive, move/rename the current **PlumeDataArchive.txt** prior to running **UCB_Plume.exe.**

Images: A range of images are saved for diagnostic and process visualization purposes. While other image handling programs can open these file, the process using ImageJ will be described due to its open source and robust use.

For all **`.raw, .edg, .pxt`**, begin by running ImageJ.

Click: File > Import > Raw…

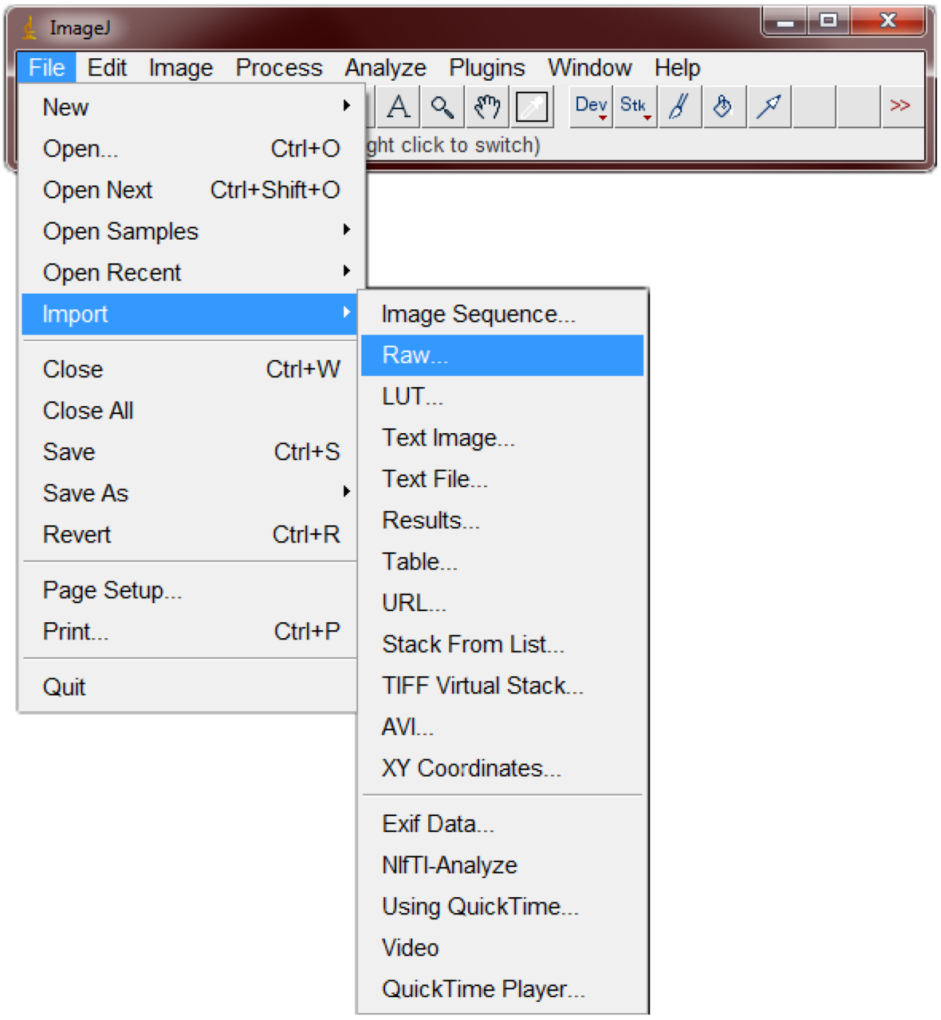

Select the file desired to be opened

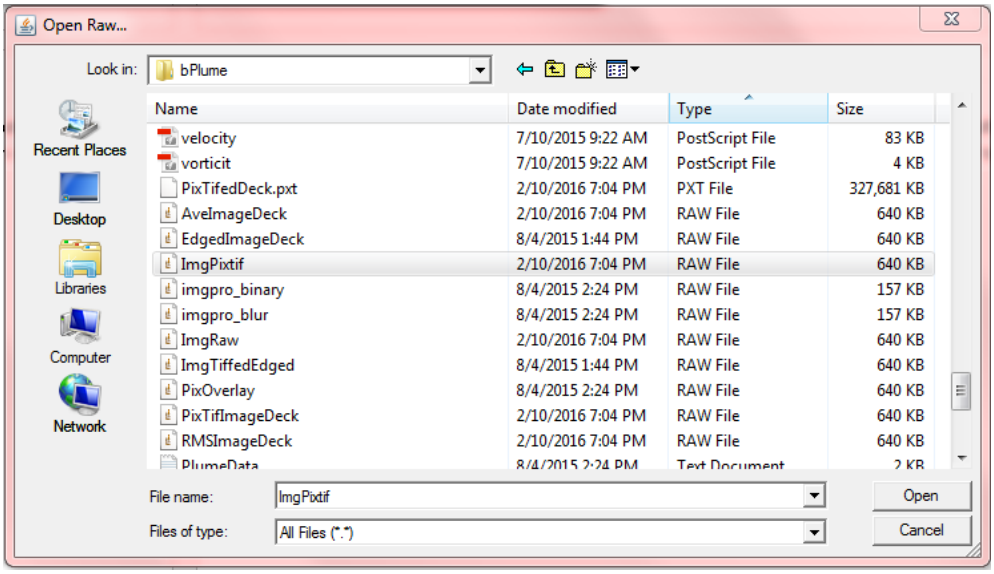

For **single image**, continue by inputting **NXC**, number of pixels along the width of the video image, and **NYC** ,number of pixels along the height of the video image, that correspond to the processed video.

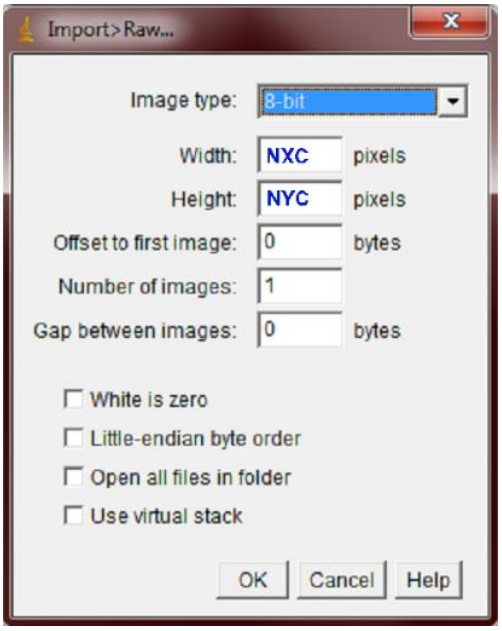

-ImgRaw.raw: An image frame taken from the middle of the image deck, unprocessed image for reference.

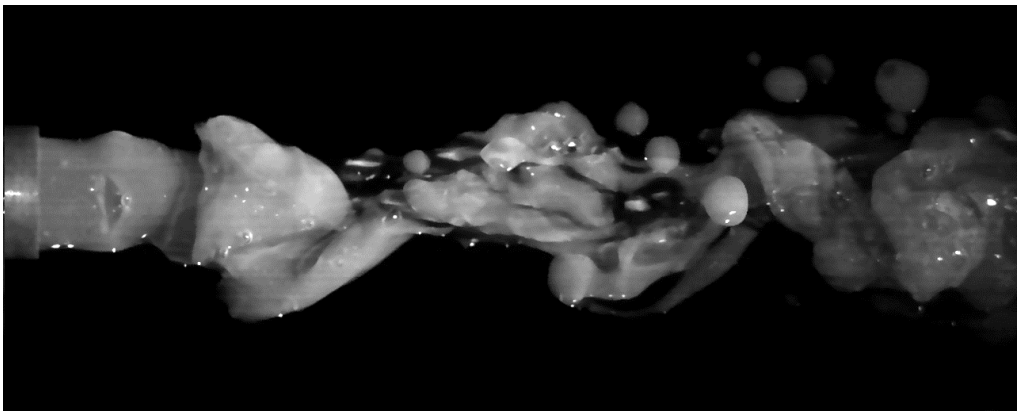

-ImgEdged.raw: A Canny edge detected version of image saved in **ImgRaw.raw**. This provides insight into which features are being tracked in the first pass.

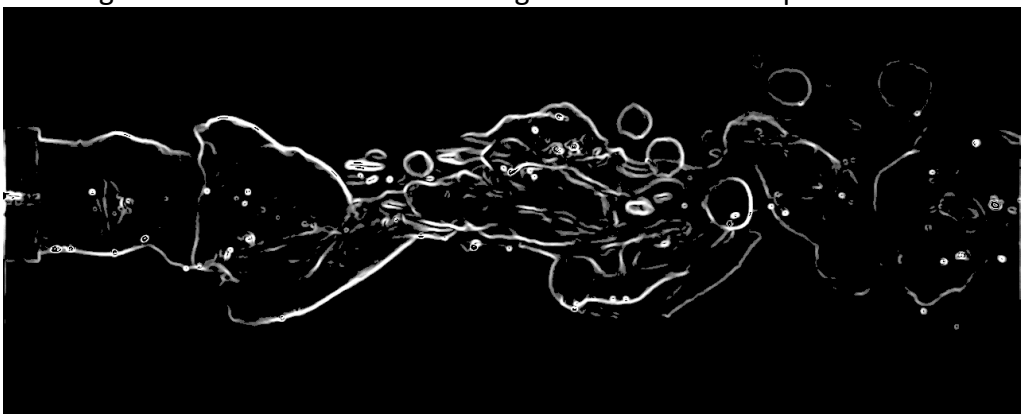

-ImgPixtif.raw: A Pixtif processed version of the image saved in **ImgRaw.raw**. This provides insight into which features are being pronounced in the flow to be tracked during the second pass.

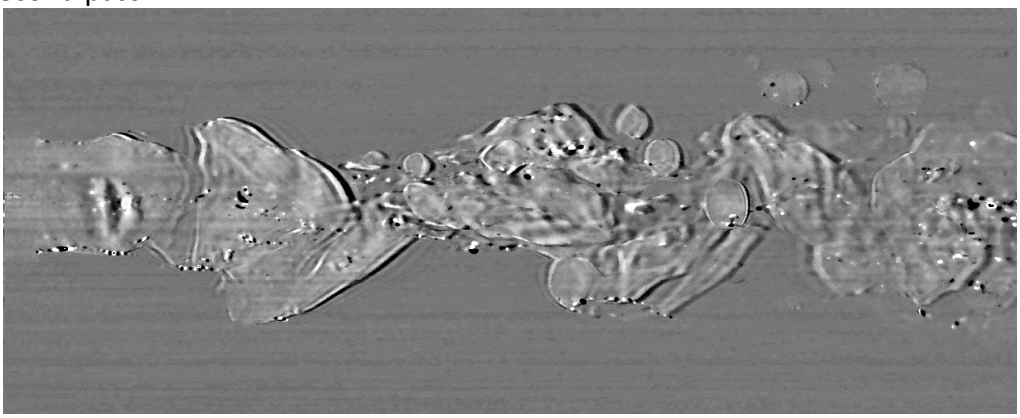

-RMSImage.raw: As stated earlier in assumptions, the RMS of the image deck removes constant features in the ROI, while outlining the location of fluctuating intensity values, such as where moving features in the jet occur.

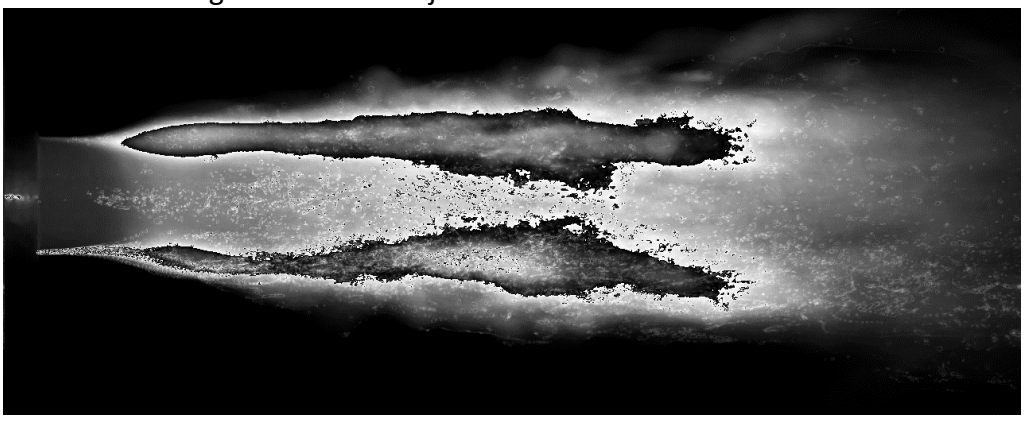

-PixOverlay.raw: The area of calculation is outlined as a whited region overlaid on the RMS of the entire image deck.

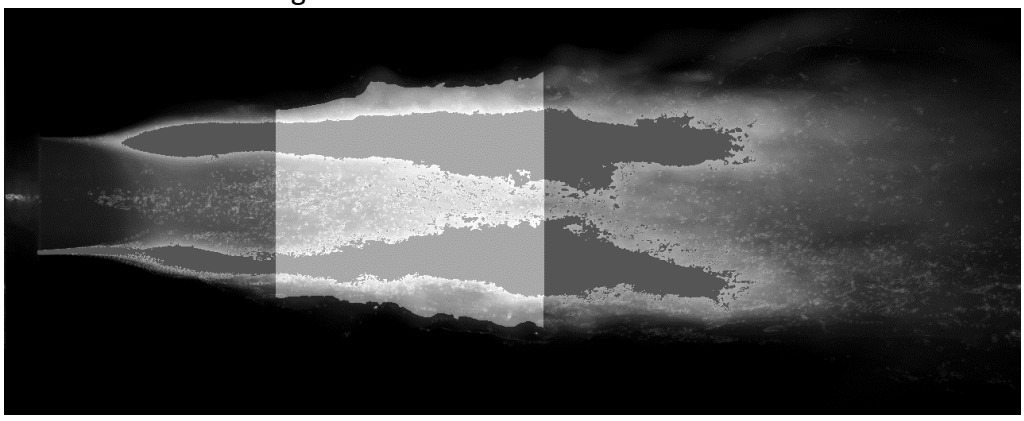

For **an image deck**, continue by inputting **NXC**, number of pixels along the width of the video image, and **NYC**, number of pixels along the height of the video image, and **NF** (this number is recorded in PlumeData.txt), number of frames processed, that correspond to the processed video. The "Offset to first image" should be set to 128 bytes to bypass the header information stored along with each image deck.

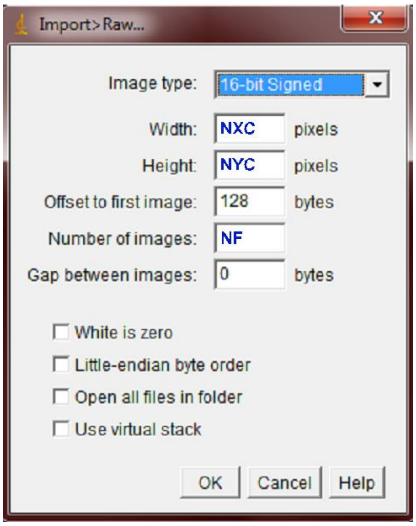

-`EdgedDeck.edg`: The raw image deck is ran through canny edge detection algorithm. The **`EdgedDeck.edg`** used for calculation during the first pass of **`WALPT7.exe`** in **`UCB_Plume.exe`**.

-`PixTifedDeck.pxt`: The raw image deck is ran through a pixel-wise filtering using parameters derived from the first pass. The **`PixTifedDeck.pix`** is used for calculation during the second pass of **`WALPT7.exe`** in **`UCB_Plume.exe`**.

Five **`.out`** files will be generated by **`UCB_Plume.exe`**. Third party software can be used to interpret the data stored in these files (Adobe CS, IDL, Matlab, VLC, ImageJ …).

The files are as follows:

The instantaneous information will be ordered as **`AviTensor.####`**. The **`.####`** will indicate which pair of images are being examined between. A correlation between Image1 and Image2 of the video deck will correspond to **`AviTensor.0001`**. In **`AviTensor.####`** information is stored as follows:

The output data file contains three arrays, **header, uvtensor, intwinxy,** all in binary. **header** contains processing and id information; **uvtensor** contains velocity data; and **intwinxy** consists of interrogation window dimensions in pixels when adaptive processing mode is used.

```
.
integer(2) header(64)
integer(1),allocatable :: intwinxy(:,:)
real(4),   allocatable :: uvtensor(:,:,:)
.
allocate(uvtensor(nxuv,nyuv,10))
allocate (intwinxy(nxuv,nyuv,2))
   intwinxy=0
.
open(1,file=utensor,form='binary')
write(1) header, uvtensor, intwinxy
close(1).
```

This output file contains a header which is **integer*2(64).**

Current contents are:

header(1)=version number (x100), used to determine compatibility	
header(2)=nxc	camera size-x
header(3)=nyc	camera size-y
header(4)=nxuv	output array size-x
header(5)=nyuv	output array size-y
header(6)=nxw	window size-x
header(7)=nyw	window size-y
header(8)=nxs	step size-x
header(9)=nys	step size-y
header(10)=nxf	flow region size-x
header(11)=nyf	flow region size-y
header(12)=xf	flow region offset-x
header(13)=yf	flow region offset-y
header(14)=nbits	pixel depth
header(15)=ipx_ctr	number of boundaries in ipx, 0=no ipx
header(16)=mode	processing mode
header(17)=FileType	input file type 0=raw,1=tiff,2=avi stream
header(18)=(nt-1) or (ntfft-1)	Tensordeck output depth, for AVIbatch or PixTif processing for .raw and .tifdecks
header(19:64)	reserved for future use

The output data array **uvtensor** is a **binary** tensor containing the filtered velocity vector **u**=(u, v), velocity gradient tensor $\partial u_i/\partial x_j$, unfiltered velocity vector **u**=(u, v), and the correlation normalized coefficient in a (*,*,10) array. Horizontal pixel dimension [hpixel] is the length unit. Both u and v velocity components have units of [hpixel/δt]. For example, to calculate circulation, the arc length must be measured in horizontal pixel units. The unit of vorticity is [hpixel/δt] / [hpixel] = [δt].

The velocity data are in a 3D array of dimensions uvtensor(nxuv,nyuv,10) where

uvtensor(*,*, 1) = u	[hpixel/δt]
uvtensor(*,*, 2) = v	[hpixel/δt]
uvtensor(*,*, 3) = ∂u/∂x	[1/δt]
uvtensor(*,*, 4) = ∂v/∂x	[1/δt]
uvtensor(*,*, 5) = ∂u/∂y	[1/δt]
uvtensor(*,*, 6) = ∂v/∂y	[1/δt]
uvtensor(*,*, 7) = u_unfiltered	[hpixel/δt]
uvtensor(*,*, 8) = v_unfiltered	[hpixel/δt]
uvtensor(*,*, 9) = 0 reserved	
uvtensor(*,*,10) = correlation coefficient	[normalized]

`ImageDeck.out`: image deck consisting of the first image of each pair

`tensordeck.out` : tensor output file is stacked in a deck for each image pair

`tensorave.out` : average tensordeck.out, written by stats.f90

`statistics.out` : statistics of results in **`tensordeck.out`**, written by **`stats.f90`**

statistics(*,*, 1) = u_ave
statistics(*,*, 2) = v_ave
statistics(*,*, 3) = average vorticity
statistics(*,*, 4) = average speed
statistics(*,*, 5) = u^prime
statistics(*,*, 6) = v^prime
statistics(*,*, 7) = speed^prime
statistics(*,*, 8) = vorticity^prime
statistics(*,*, 9) = u_ave (unfiltered)
statistics(*,*,10) = v_ave (unfiltered)
statistics(*,*,11) = average unfiltered speed
statistics(*,*,12) = unused
statistics(*,*,13) = unused
statistics(*,*,14) = unused
statistics(*,*,15) = unused
statistics(*,*,16) = unused

Using IDL, **`statistics.out`** can be used to visualize:

Average Velocity

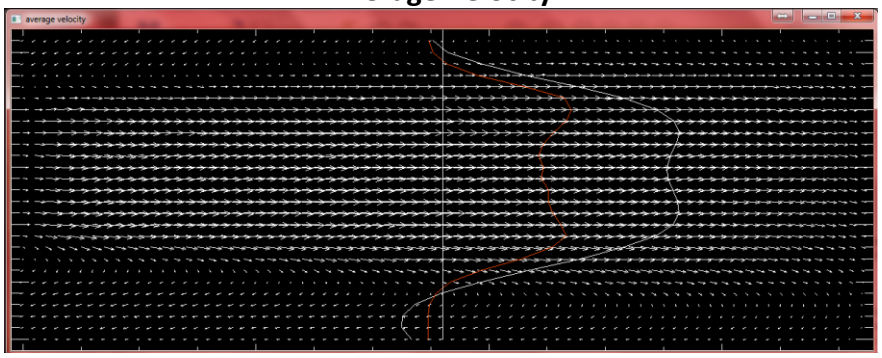

Average Vorticity

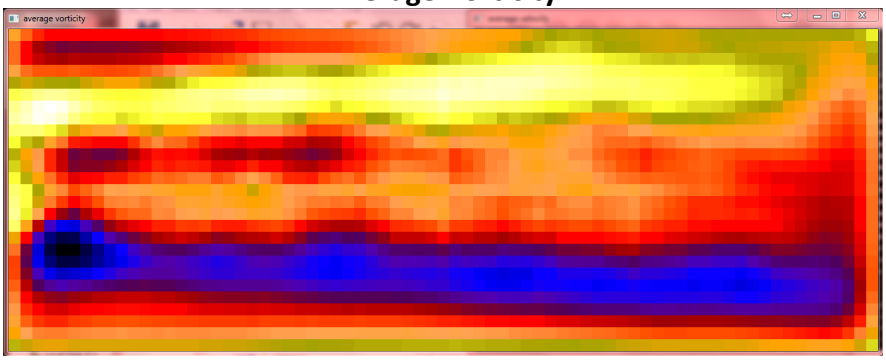

Filtered Average Speed

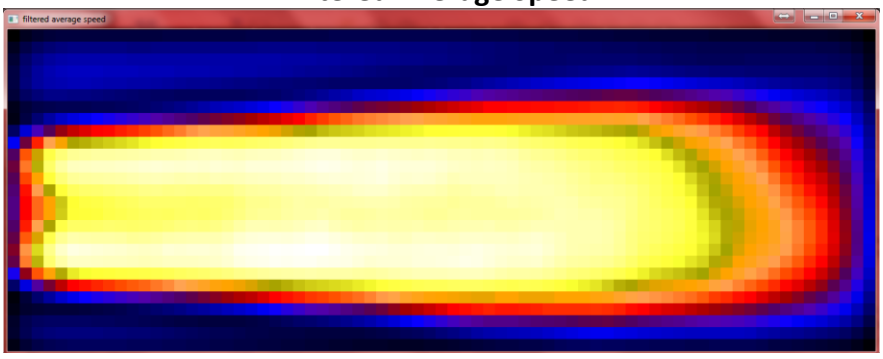

Raw Average Speed

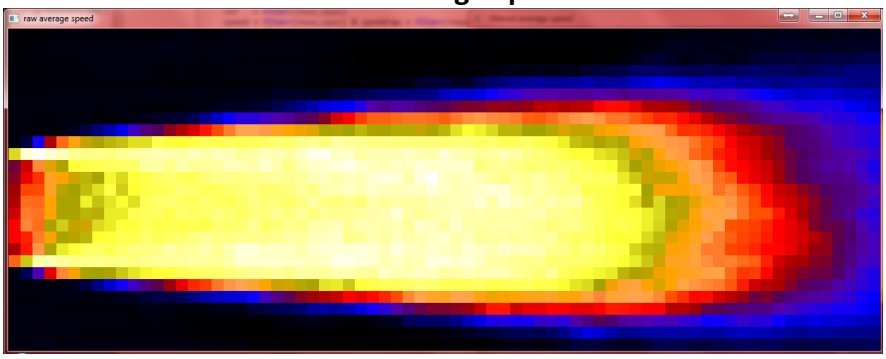

Common Errors

ERROR [`.inp`] does not exist
Do you want to generate a template [`.inp`]?

If **`bplume.inp`** or **`plume.inp`** does not exist in the same directory as **`UCB_Plume.exe`**, the user will be prompted for permission to generate respective template input files. The user input file, **`bplume.inp`**, will still be presented to operator to be modified to run desired video recording.

A B O R T I N G [`File.avi`] video stream file does not exist

This error is stating the code could not find the file in the specified directory. Verify the files existence and that correct file path was specified in **`bplume.inp`** in line 12.

Known Issues

Insufficient Virtual Memory: Range of tests have been completed using hardware:

Windows OS [2008R2 / 7 / 8.1 / 10]
Intel i7 processor
24GB Ram

Using this range of hardware, an error stating insufficient virtual memory has occurred while processing large video files. As currently tested on our hardware, a video file of 7GB is processable.

Noise sensitivity: Noise found in the video recording can be pronounced and lead to the generation of erroneous velocity fields. Noise can be introduced to the recording via substandard recording equipment, compression/decompression of recording, or certain video enhancement processes.

Nulled image: Removal of certain frequencies while using PixTif'ing has resulted in the zeroing of all pixels in the processed image decks. By adjusting the filter width and center this can be corrected.

References

The uses of coherent structure –Coles, Donald

- http://resolver.caltech.edu/CaltechAUTHORS:20141210-131347636

A Computational Approach to Edge Detection –Canny, John

- Canny, John. "A computational approach to edge detection." Pattern Analysis and Machine Intelligence, IEEE Transactions on6 (1986): 679-698.

Deepwater Horizon: A Preliminary Bibliography of Published Research and Expert Commentary

- http://www.lib.noaa.gov/researchtools/subjectguides/dwh.html

Appendix

Advanced Operation

UCB_Plume.exe is a program that runs almost autonomously, taking in few inputs from a user to describe the physical parameters of the recording. With this information UCB_Plume.exe generates plume.inp to run a preliminary pass with WALPT7.exe and then uses a generated update.inp to run the second pass with estimated filtering parameters. While this functionality is set to be available for quick use, advance use of WALPT7.exe directly is possible.

To use WALPT7.exe three files will be required to be in the same directory:

- **WALPT7.exe**
- **bplume.inp:** outlined in detail on page 8 under **Running Program** of this manual. It would be recommended to make a copy of the bplume.inp as generated by UCB_Plume.exe. The file name bplume.inp must remain unchanged, as WALPT7.exe will search the working directory for the exact file name.
- **test_00.inp:** The format of this file must be compatible with that of plume.inp as generated by UCB_Plume.exe. It would be recommended to make a copy of the plume.inp, rename as desired while preserving the .inp file extension, **test_00.inp** will be used to reference this duplicated file.

The directory housing these three files will be referred to as <TEST_DIR>, this can be named as desired. This directory will require an allotment of memory space to save to, roughly thrice the size of the images/.avi used.

From a command window, change the working directory to <TEST_DIR>.
Entering:

```
WALPT7.exe < test_00.inp
```

will use the parameters set in test_00.inp to process the images, computing a velocity field per image pair and, along with the information given in bplume.inp, the estimated flow rate.

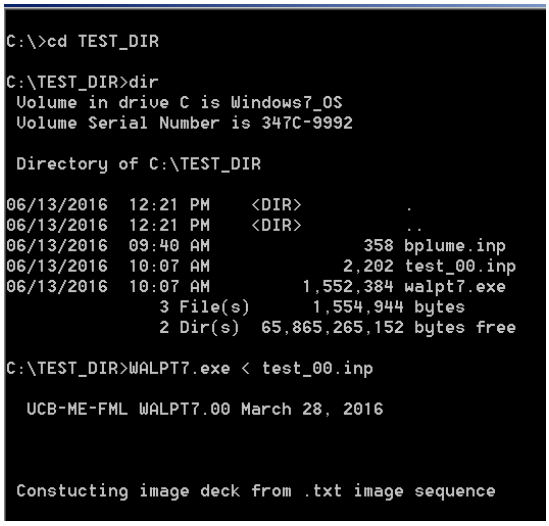

Parameter Description: `plume.inp / test_00.inp`

mode npass silent batch edgeflag PTFlag PTCenter PTWidth
A) 1 1 0 1 0 0 0 0
file that contains the names of image files, prefix for outputfiles
B) D:\OHMSETT\OHM\Test_23_input\Test_23_input
C) TxtTensor
image size nxc, nyc, nbits, pixr
D) 1040 564 8 1.00
flow size, nxf, nyf
E) 1040 564
flow offset, xf, yf
F) 0 0
window size, nxw, nyw, 2n**
G) 64 64
amod, min, max windows dimensions 2n, correlation level corlvl**
H) 1 8 32 0.40
step size, nxs, nys
I) 16 16
window type, wtype 1-7, see source listing
J) 2
peak type, ptype 0=grid,1=parabolic,2=gaussian
K) 2
laundary type, ltype 0=no laundering,1=rejection
L) 0
extension parameter, 0= none, zero padding, 1= smooth
M) 0
filter widths fltrwx, fltrwy wavenlength in steps; exponent
N) 9 9 2
wall parameters: nwalls, parex, motion, intflag, outmask
O) 0 0 0 1 1
wall geometry file
P) Wall_Mask.raw
motion parameters: dxcg, dycg ,rot
Q) 0.00 0.00 0.00
0.00 0.00 0.00
9.00 0.00 0.00

A) Primary Processing Parameters

MODE: Sets which type of PIV algorithm will be implemented.

`MODE=1:` Standard DPIV. In this mode, only one pass is done with the parameters specified. The code checks for questionable vectors and does some repairs; some ad-hoc, some rigorous. (relative time=1)

`MODE=2:` Predictor corrector DPIV; moving from smaller windows to larger ones. It is quick at the cost of robustness. The code makes the first pass at the specified window size, and repairs suspect vectors at twice or, if needed, at four times the window size to obtain an estimate for the final velocity pass. During the final pass, window pairs that are separated by

the estimated velocity are used to determine the final velocity. Some repairs are done at the end. (relative time=2)

MODE=3: Lagrangian parcel tracking LPT with multiple passes. The velocity field calculated using MODE=2 is used as the first estimate in LPT. First, the domain is extended to 2^mx2^n. Then velocity gradient tensor and its derivative are calculated using Fourier methods after some filtering in frequency domain. Fluid parcels are deformed according to the local velocity field to determine the deformed correlation windows from which a new velocity field is determined. Each pass is done with a newly calculated velocity field. No repairs are done. (relative time=2+2*passes)

MODE=4: Adaptive Lagrangian parcel tracking aLPT with multiple passes. Chooses windows commensurate with the velocity vector, thus increases the spatial resolution of the instrument. The processing is the same as that in mode 3 except the dynamic adaptation of the window size and orientation. The velocity field calculated using MODE=3 with 2 passes is used as the first estimate in aLPT. No repairs are done. Since smaller windows are used most of the time, the incremental processing is faster than that in mode 3.

npass: is the number of passes for **walpt** processing when **MODE** = 3 or 4. Otherwise set to 1. The code expects a valid integer entry for **npass** even if the **mode** is other than 3 and 4.

silent: screen display mode,

silent = 0 : Verbose mode slows the CPU to crawl, probably due to poor operating system design (Windows)

silent = 1 : silent (minimal display of status). Set to 1 if processing a large number of files (say, larger that 20) when **batch** >0.

batch:. The contents of files **file_1** and **file_2** below are interpreted differently depending on the value of **batch.**

batch = 0 : Single image pair processing

batch = 1 : Multiple image pair processing

edgeflag: Parameter flag setting whether edge detection processing is ran on the images, and if so which type.

edgeflag = 0 for no filtering
edgeflag = 10 for Sobel, all around
edgeflag = 11 for Sobel, along x-axis
edgeflag = 12 for Sobel, along y-axis
edgeflag = 25 for 5x5 Laplace filtering.
edgeflag = 30 for Canny filtering, all around.
edgeflag = 31 for Canny filtering, along x-axis.
edgeflag = 32 for Canny filtering, along y-axis

PixTifFlag:

PTFlag = 0: no PxTif'in
PTFlag = 1: high-pass filter (tanh)
PTFlag = 2: low-pass filter (1-tanh)
PTFlag = 3: band-pass filter (exp(-t^2))
PTFlag = 4: band-reject filter (notch) (1-exp(-t^2))
PTFlag > 4: returns without filtering, 2^n image deck written out.
PTFlag = 9: special handling

PixTifCenter: PixTif center of filter.

PixTifWidth: PixTif filter width parameter.

B) file_1: File name that is processed differently based on content and batch flag

C) file_2: File name that is processed differently based on content and batch flag

batch =0 ; single pair of images are processed

file_1 and **file_2** are the names of the pair of images for processing, one line per file, include full path to avoid confusion. Both image files must be of the same type, i.e. **.raw** and **.tif** files may not be mixed. The output data are written in **'tensor.out'** in the current directory (described below). If ipx is invoked, the path data are written in **'ipxpaths.out'** in the current directory.

batch =n>0: multiple pairs of images are processed

file_1 is the name of the file containing the names of images for processing. The images are taken as pairs until all entries are processed. If there are odd number of entries, the last one is discarded. Include full path to avoid confusion. Image files must all be of the same type, i.e. **.raw** and **.tif** files may not be mixed.

file_2 is the prefix used to construct the output file names for each of the pairs processed. The output files are numbered consecutively starting with the value of **batch .0001** extension. For example if **batch =99** and **file_2=tensor**, then the output files will start from **tensor.0099** in the specified folder. If no folder is specified, the output files will be in **TensorFolder** directory.

AVI image stream

file_1 is the name of the avi file to be processed. It must have .**avi** or .**AVI** or .**Avi** extension. Compressed avi files are rejected. Images are processed for every interval; that is, if

there are N images in the avi file, there will be N-1 output files. If the images are equi-spaced, then, no special handling is needed. If, however, the images are recorded in 'double exposure' mode for PIV operations, then successive output files will have alternating time intervals, one corresponding to the laser pulse separation and the other corresponding to sampling interval for PIV image pairs. Therefore, the output files must be processed with the timing considerations in mind. Even and odd numbered files must be grouped together

`file_2` is the prefix used to construct the output file names for each of the pairs as well as the consolidate output file for the whole stream

TXT image sequence

`file_1` is the name of the folder storing all the .txt image file to be processed. It must have i**nput** or **Input** or **INPUT** as its ending characters. Numbering style should be consistent with that exported from ImageJ. If there are N .txt images in the input folder, there will be N-1 output files. If the images are equi-spaced, then, no special handling is needed. If, however, the images are recorded in 'double exposure' mode for PIV operations, then successive output files will have alternating time intervals, one corresponding to the laser pulse separation and the other corresponding to sampling interval for PIV image pairs. Therefore, the output files must be processed with the timing considerations in mind. Even and odd numbered files must be grouped together

`file_2` is the prefix used to construct the output file names for each of the pairs as well as the consolidate output file for the whole stream

When `ipx` is invoked, the same prefix is used to generate the ipx'ed image and path files. This time, '`ipx1/2`' suffix is inserted in the file names for images and `ipxpaths` for path files. For example, the ipx'ed image file names corresponding to `tensor.0099` output are `tensoripx1.0099` and `tensoripx2.0099,` and the corresponding path file is **`tensoripxpaths.0099`**.

If the full path is included in `file_2,` e.g., `file_2 = d:\airfoil\tensor`, then, the appropriate directory must already exist.

D) <u>Image Size:</u> (figure 1a)

`nxc:` Number of pixels horizontally across the image

nyc: Number of pixels vertically across the image

nbit: Pix bit depth

pixr: camera pixel ratio, vertical/horizontal pixel dimensions

Camera	nxc x nyc	pxr	(µm x µm)	bits	*max frame rate*
IDT-MP-X3	1280H x 1024V	1.00	(12x12)	8	1000 Hz digital
Kodak ES1.0	1008H x 1018V	1.00	(9x9)	8	30 Hz digital
Sony 7500	640H x 480V	1.00	(9.9x9.9)	8	30/60 Hz analog/ non-interlaced

E) Flow Size: (figure 1a)

nxf, nyf: flow region of interest imbedded in **(nxc,nyc)** image array

F) Flow Offset window size: (figure 1a)

xf, yf: position of **(nxf,nyf)** region with respect to the image origin

G) Window size: (figure 1a)

nxw, nyw: correlation window size 2^m x 2^n. Consider using rectangular windows in nearly parallel flows

H) Adaptation Parameters

amod: Adaptation mode

amod = 0: square windows only, no directional adaptation

amod = 1: include rectangular windows aligned with axes

minw, maxw: are minimum and maximum window dimensions 2^m used in mode 4 LPT. The minimum value may be as low as 8 if image quality permits.

corlvl: is the minimum correlation coefficient level to double the window dimensions during LPT.

I) Step Size

nxs, nys: step size for scanning the flow region **(nxf,nyf)**

J) Window Type

wtype: window type for windowing data before correlating. If the images are periodic, you must use a window.

wtype = 1: square window (no windowing)

wtype = 2: Rosenfeld

wtype = 3: triangle(Parzen, Bartlett)

wtype = 4: parabolic (Welch)

wtype = 5: cosine (Hanning)

wtype = 6: Hamming

wtype = 7: Blackman-Harris

K) Peak Type

ptype: method of determining correlation maximum

ptype = 0: read off the array values (you might as well not use the program)

ptype = 1: paraboloid fitting

ptype = 2: gaussianoid fitting (logarithms are used, correlation data must be positive values).

L) Launder Type

ltype: bad vector rejection flag,

ltype = 0: no rejections

ltype = 1: rejections enabled

M) Extension Parameter

exten: domain extension flag

exten = 0: extend with zero padding (use when far field is quiescent),

exten = 1: smooth extension with matching 2nd order derivatives.

N) Filtering parameters

Filtering parameters used in wavenumber domain (Figure 5).

fltrwx, fltrwy are the wavelengths (in units of steps) at the 1/e cut-off point of the filter kernel. Note that the step sizes **(nxs,nys)** determine the actual cut-off wavelengths (in pixels) on PIV images. The larger the parameters are, the smoother the output is. Equivalently, features smaller than the parameters are filtered out (blurred). If **fltrwx=0**, or **fltrwy=0**, then, no filtering is done in x or y, respectively.

Nfil: is the exponent in the filter kernel.

Higher values mean sharper cut-off in wavenumber domain.

The filter kernel is $[1-\exp(-1/k^n)]$ where k is the magnitude of the wave vector,

(k_x, k_y) : $k \sim \{ [k_x / (1 / \text{fltrwx})]^2 + [k_y / (1 / \text{fltrwy})]^2 \}^{1/2}$

Alternatively,

(k_x, k_y) : $k \sim \{ [\text{fltrwx} \cdot k_x]^2 + [\text{fltrwy} \cdot k_y]^2 \}^{1/2}$

O) Wall parameters (figure 2).

nwall: number of interfaces(s) in PIV images, to be dealt with.

nwall = 0: no interfaces

nwall = +n , n interfaces, **boundary** data file is needed (described below).

nwall = -n , n interfaces, boundaries are determined from the first flow image. Requires high contrast data, to clearly delineate the flow region.

parex: image parity exchange at walls to extend velocity measurements to interfaces

parex = 0: Off

parex = 1: On

motion: interfaces to be dealt with

motion = 0: no motion, fixed walls

motion = 1: walls in rigid body motion (individually or in unison)

motion = -1: compliant interfaces (every interface is treated independently)

intflag: used when **parex** =1

intflag = 0: nearest pixel,

intflag = 1: interpolation over 3x3 region (recommended)

outmask: used when **wall** =1 to deal with output data in extended regions.

outmask = 0: output as is (for further processing at interfaces, e.g. shear at wall)

outmask = 1:set wall regions to 1001.0 (suitable for display in IDL using **MISSING** keyword in **velovect** procedure)

P) Wall Geometry File

mpairs=0
file marking the interfaces(s) appearing the first image file **imagefile_1**. Must be supplied when **nwall > 0**. Has the same structure as the image files **imagefile_1/2** above. Byte elements are 255 (-1)(white) when in the metric flow domain and 0(black) when in the non-metric domain (figures 2,4). The interface outlines can be closed loops or open lines. There is no limit to the number of interfaces in the flow field. High curvatures should be avoided. Cusps are not allowed in autonomous processing.

mpairs=1
boundary is the name of the file containing the names of boundary files for batch processing. A boundary mask file matched to each image pair listed in **file_1**.

Q) Motion Parameters

rigid body motion parameters of wall outlines, needed when **motion=1**. One line for each boundary.

dxcg translation displacement of the centroid of wall outline in x-direction (pixels)
dycg translation displacement of the centroid of wall outline in y-direction (pixels)
rot rotation of wall outline in radians

CAUTION: If the number of line entries are fewer than the boundaries in **boundary**, then, the last entry is used for the remaining boundaries. If the walls are in pure translation, then the results are correct. If there is any rotation, the results will be wrong.

NOTE: If there are multiple walls which are moving as a solid body in unison, a single entry is sufficient provided that **nwall=1**.

See figure 4 for the ordering convention of the interfacess. **ipx** looks for interfaces in **boundary** starting on **edge_1**, going around the four edges counterclockwise. Interfaces starting on the edges are numbered sequentially until the open-ended interfaces are taken care of. Then, **ipx** starts scanning vertically the interior of the **boundary** file stating from x=0. The numbering of the closed interfaces then continues until all interior interfaces are accounted for. If all interfaces are rigid walls, then, **ipx** can automatically perform image parity exchange using the rigid-body-motion parameters prescribed above.

FIGURES

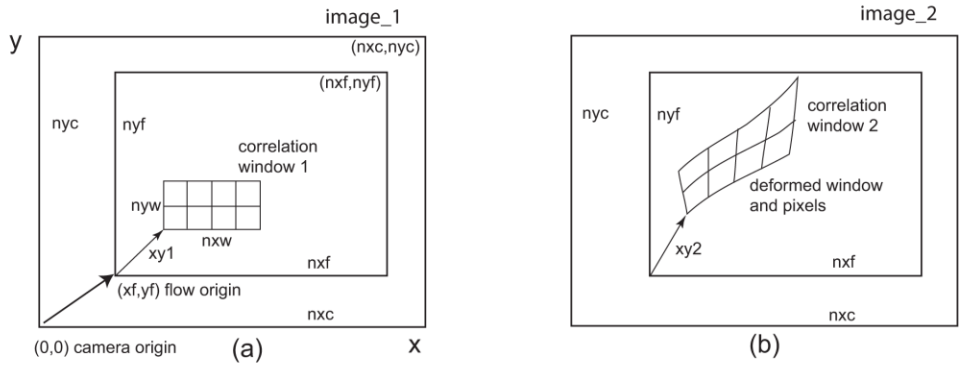

Figure 1. Lagrangian Parcel Tracking -- LPT.

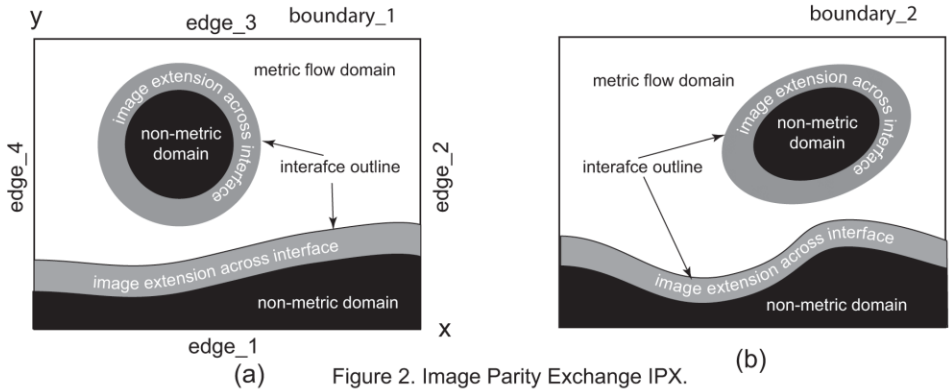

Figure 2. Image Parity Exchange IPX.

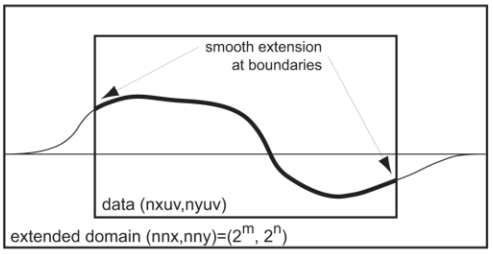

Figure 3. Extending data domain for FFT processing.

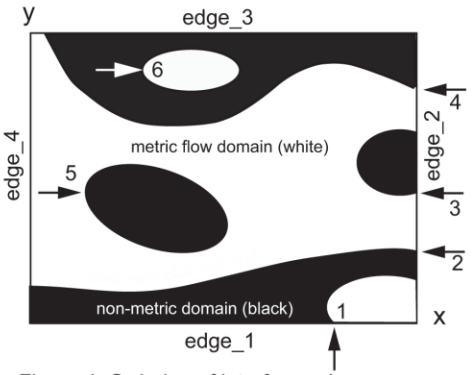

Figure 4. Ordering of interfaces. Arrows indicate starting points of interface outlines.

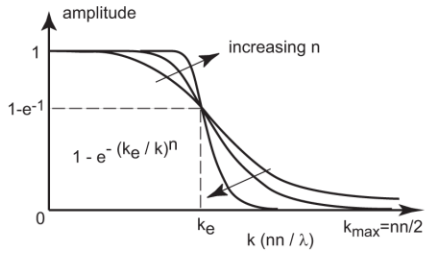

Figure 5. Wavenumber filter kernel.

APPENDIX 3: UCBPlumeAnalysisTool

Estimating Discharges from High Speed Videos

ÖmerSavaş & Frank Shaffer

September 2016

Objective Development of a field deployable tool with minimal operator input to obtain quickly and accurately a first order approximation of the flow rate of an accidental turbulent discharge for operational purposes

Achievement Developed such a tool which can estimate the flow rate within 20% uncertainty in laboratory

How I got into the oil business!

Subject: Re: Gulf Oil Leak Estimate Request from APS Division of Fluid Dynamics Chair
From: savas@newton.berkeley.edu
Date: Fri, May 14, 2010 2:07 pm
To: jlasheras@ucsd.edu
Bcc: savas@newton.berkeley.edu
Priority: Normal

I got a similar request earlier in the week but held off. Now, I could not resist the temptation any longer.

Using the celerite of the large eddies at the edge of the plume to estimate the mean discharge flow velocity (80 cm/s, underestimates), and assuming a fill factor of 1/3 for oil (from the video), I come up with oil discharge rate of 5100 m3/day or (43,000 barrels/day) for the 21-inch diameter pipe.

Ömer ,

Quoting dfd@aps.org:

>Message to members of the American Physical Society's
> Division of Fluid Dynamics - Authorized by
> Juan Lasheras, Chair of DFD

>**********

FRTG Report

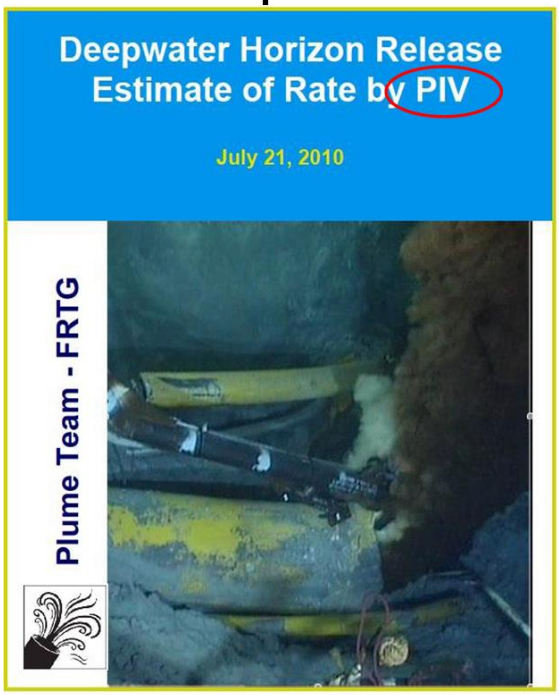

216 pages = 13 pages main body & 201 pages appendices

Report to
Dr. Marcia McNutt , USGS Director and Science Advisor to the Secretary of the Interior
Lead to the National Incident Command Flow Rate Technical Group

Prepared By
Plume Calculation Team

Aliseda, Alberto	Assistant Professor of Mechanical Engineering, University of Washington
Bommer, Paul	Senior Lecturer, Petroleum and Geosystems Engineering, University of Texas at Austin
Espina, Pedro	National Institute of Standards and Technology
Flores, Oscar	Department of Mechanical Engineering at University of Washington
Lasheras, Juan C.	Penner Distinguished Professor of Engineering and Applied Sciences, University of California at San Diego
Lehr , Bill (Lead)	Senior Scientist, National Oceanic and Atmospheric Administration Office of Response and Restoration
Leifer, Ira	Associate Researcher, Marine Science Institute and Institute for Crustal Studies, University of California, Santa Barbara.
Possolo, Antonio	National Institute of Standards and Technology
Riley, James	PACCAR Professor of Mechanical Engineering, University of Washington
Savas, Ömer	Professor of Mechanical Engineering, University of California at Berkeley
Shaffer, Franklin	Department of Energy National Energy Technology Laboratory
Wereley, Steve	Professor of Mechanical Engineering, Purdue University
Yapa, Poojitha	Professor of Civil and Environmental Engineering, Clarkson University

Turbulent Jets

Natural | Man made: Planned | Man Made: Accidental

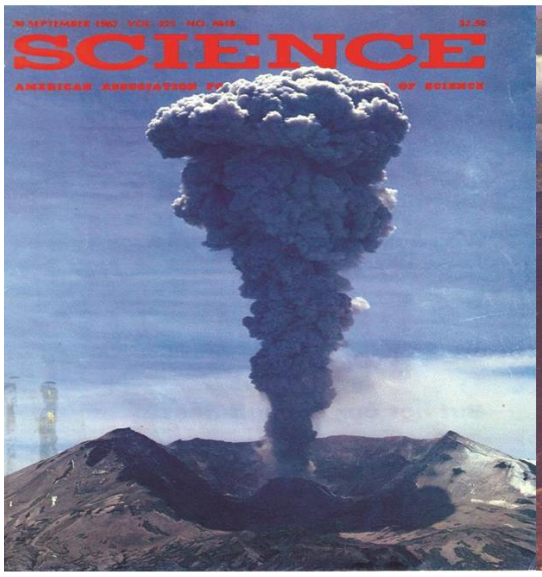

36 PHYSICS TODAY / AUGUST 1987

Turbulent Round Jet

Gross feature are inertia dominated at sufficiently high Reynolds numbers

Conservation of momentum :

$$J = \int \rho u^2 dA = constant$$

Similarity profiles:

$$u(r,x) \sim f(\tfrac{r}{x})/x$$

Uniform entrainment:

$$Q = \int u dA \sim (J/\rho)^{1/2} x$$

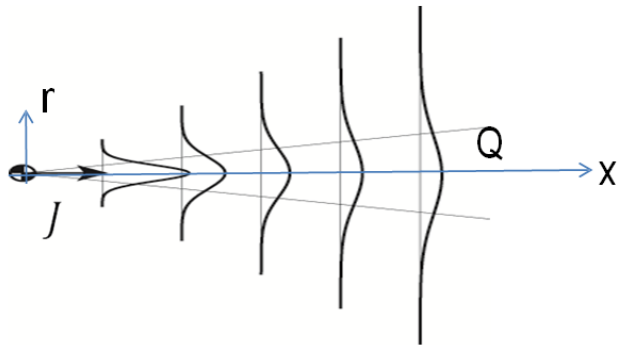

Short course in Turbulence

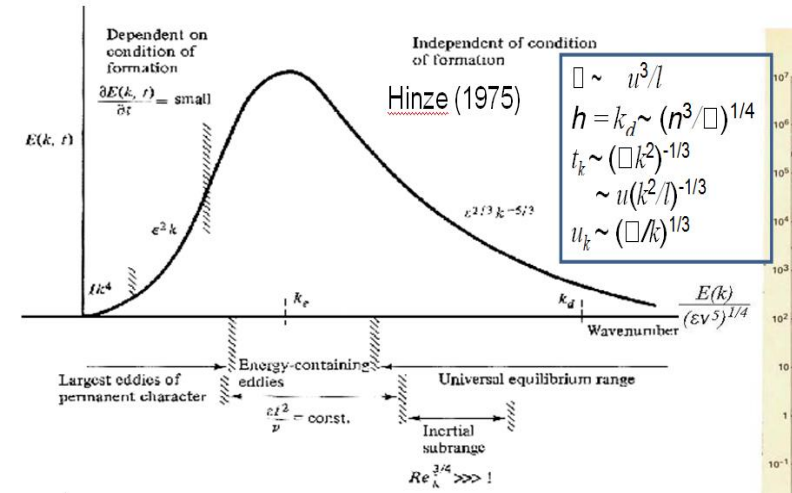

$\varepsilon \sim u^3/l$

$h = k_d \sim (n^3/\varepsilon)^{1/4}$

$t_k \sim (\varepsilon k^2)^{-1/3}$

$\sim u(k^2/l)^{-1/3}$

$u_k \sim (\varepsilon/k)^{1/3}$

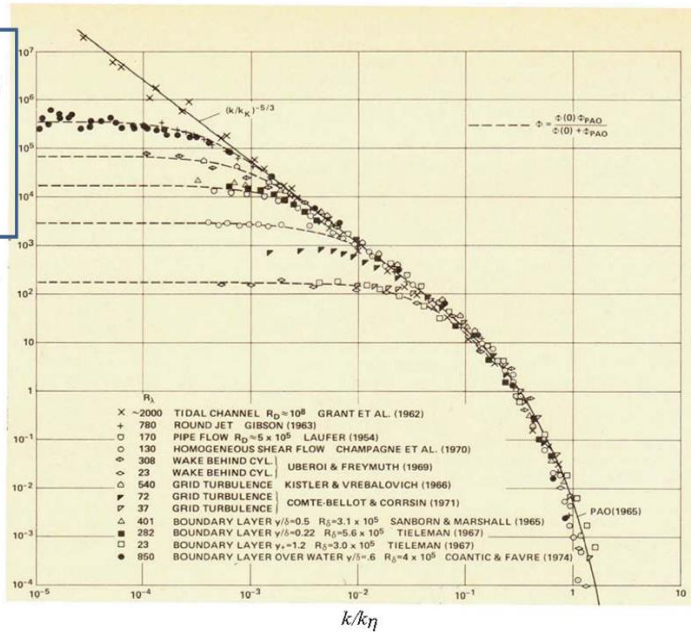

Chapman (1979)

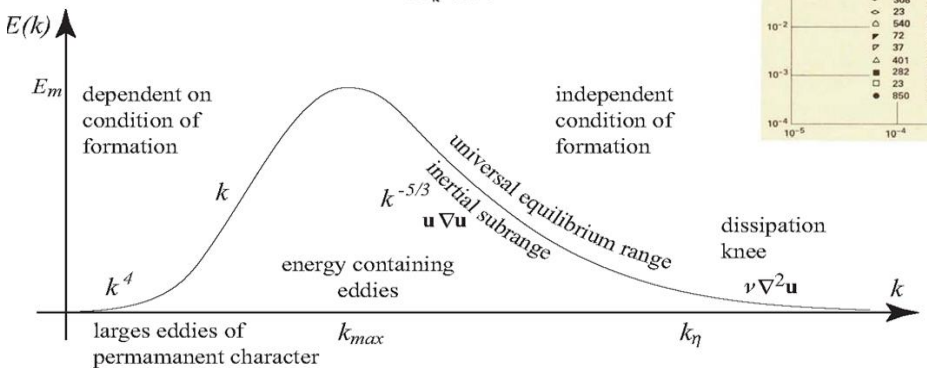

Jet Primer

Idealized jet

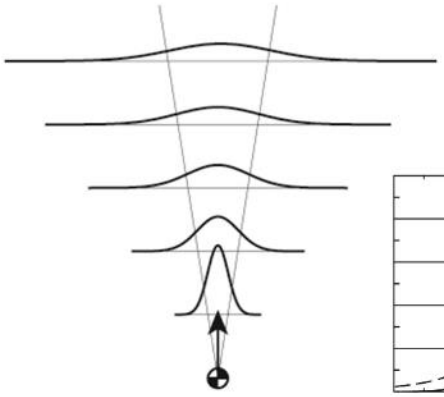

ρ, ν, J

$Re = \sqrt{J/\rho}\,/\nu$

profiles

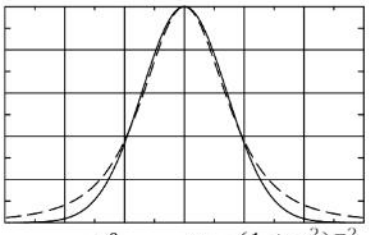

$u = e^{-r^2}$ $\quad u = (1+r^2)^{-2}$

Idealized real jet: near field

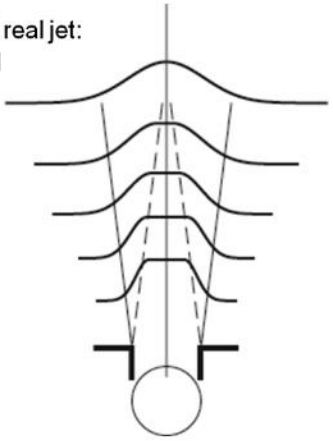

$\rho_1, \rho_2, \nu_1, \nu_2, D, J, Q$

&

upstream history!

Jet Primer: Near field

engineered reality

8.5 mm diameter nozzle after 47:1 smooth contraction, propane in air, (S&G 1986)

idealized real jet

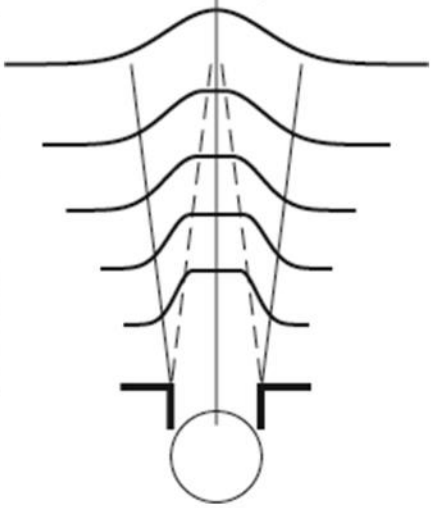

accidental reality

Severed DWH BOP, 50cm diameter (2010)

11

Small Tank Experiments at UC Berkeley

Flow setup

12

Fluid(@ 20°C)	Density (kg/m^3)	Viscosity (m^2/s)	Surface Tension (dynes/cm)	Flow
Water	998.2	$1.00x10^{-6}$	72.8	Water main
Silicone Oil 1	816.5	$1.00x10^{-6}$	17.4	Gear Pump
Silicone Oil 2	916.3	$5.02x10^{-6}$	19.7	Gear Pump

Green water soluble fluorescent dye
Red oil soluble fluorescent dye

Example of a dyed jet:

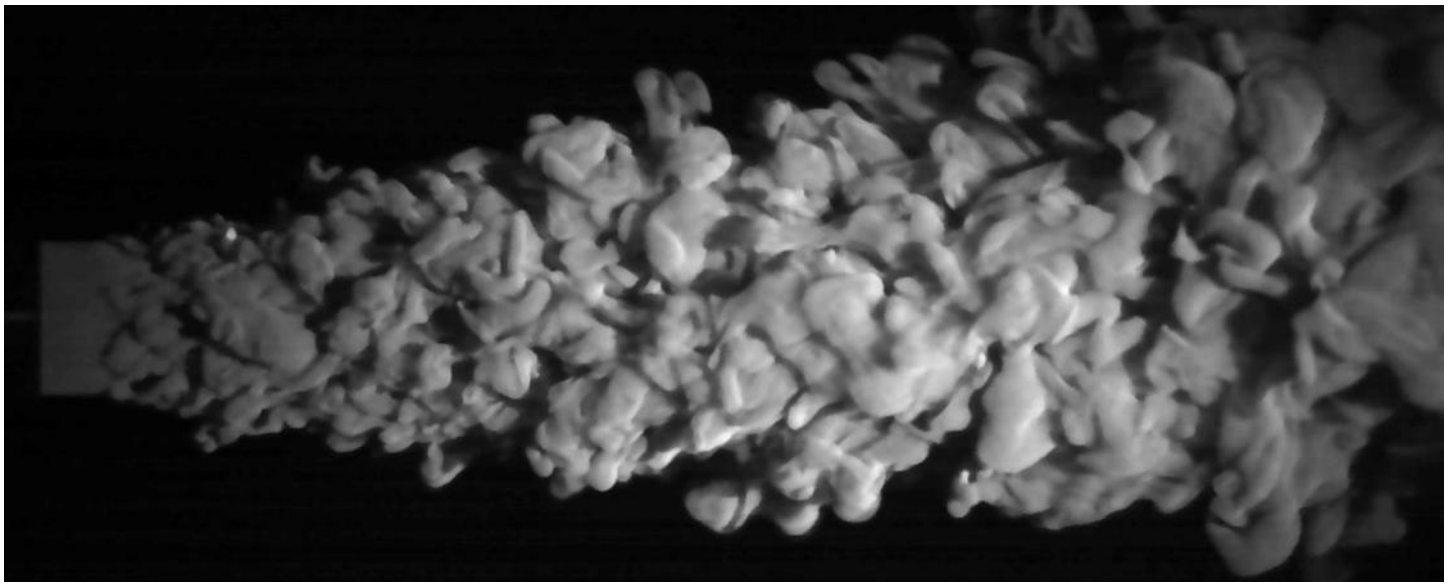

Flow rate estimation strategy

- Determine interface velocity
  - High speed imaging
  - Preprocessing
    - Canny filtering
      - smoothing
        - Sobel edge detection
      - PixTif
  - WALPT-Image Velocimetry

- Discharge rate estimation
  - extend to discharge fluid
    - Bernoulli's principle
    - assume a velocity profile:
      - Gaussian or algebraic
  - Integration within interface shell: Q

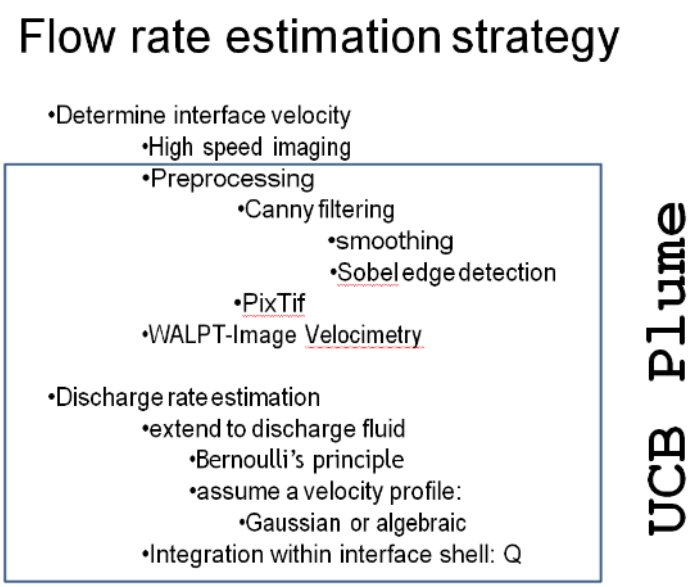

UCB Plume
Software - Flow Diagram

- Initialization
  - checks for all required files in directory
- User inputs flow parameters
- Autonomous process
  - First pass using edge detection to optimize PixTif parameters for second pass
  - Second pass using PixTif'ing, calculates celerity and radius of jet at near field, to estimate flow rate

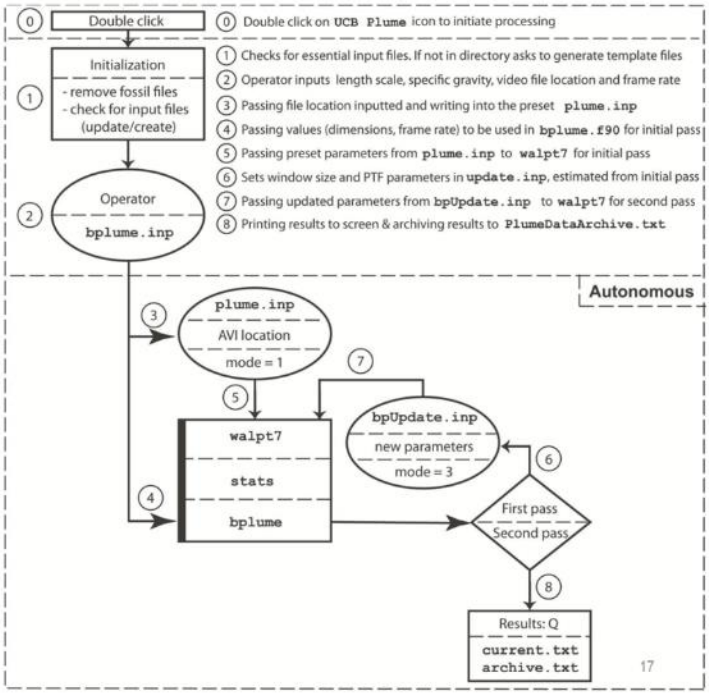

Assumptions

- Axially symmetric Gaussian profile
- Inertia dominated near field
- Celerity based on density difference[1]
- Entrainment negligible in the region of interest

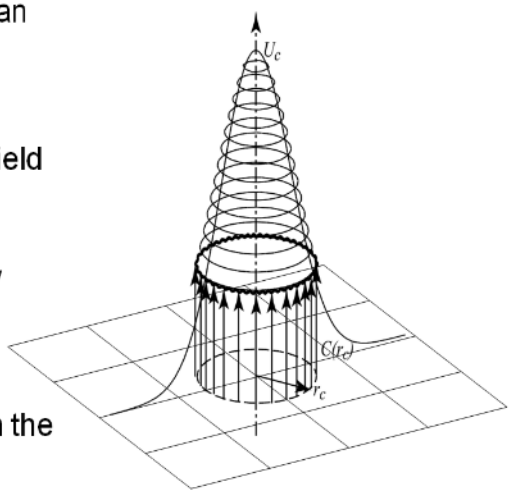

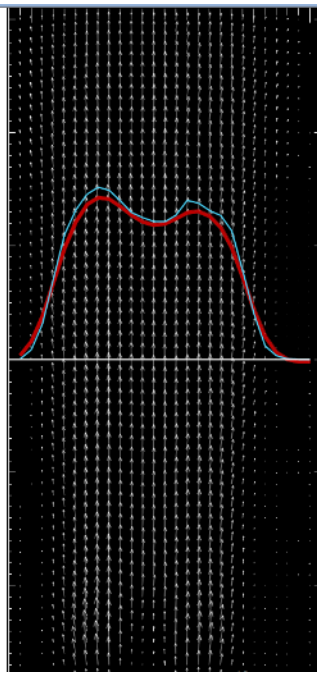

- *Gaussian Filter Application*
  - Blurs the image to mitigate noise induced false-edges
- Sobel Operator
  - Using both horizontal and vertical gradients to estimate edge location
- Thresholding to Extreme Values
  - Rounds-off values above and below a level of the intensity range in the image sequence, while preserving a span of mid range values

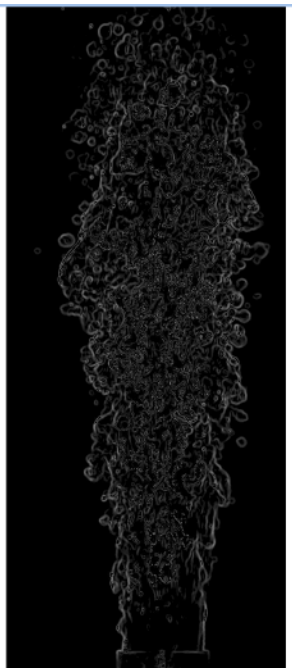

1cs Silicone Oil Jet
Re = 2.70×10^{4}
Frame rate = 1000 Hz
Exposure = 498 µs
Error $_{\text{flow rate}}$ = 9%

19

Pixelwise Time Filtering PixTif

- Features move at given speed
- Time history of intensity value at a given pixel is extracted
- Features with distinct speeds have distinct signatures in the fluctuation of the pixels intensity history
- Features of a speed can be efficiently filtered in Fourier space with a convolution
- Essentially a *3D (x,y,t)* Fourier transform and filtering

December 1, 2014

PIXTIF: Pixelwise Time Filtering

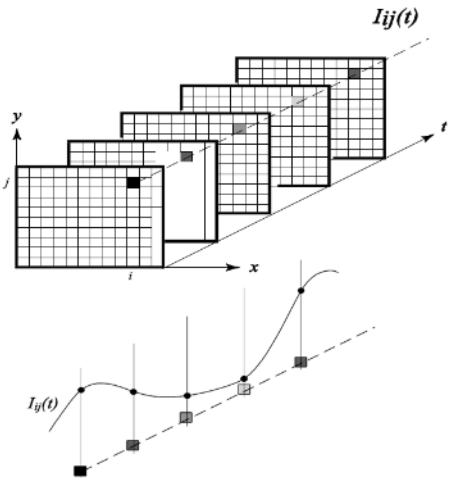

$$\tilde{I}_{ij}(t) = F^{-1}\{ F\{ I_{ij}(t) \} * G(\omega) \}$$

Fluorescent Waterjet

Raw Image

Edged Image

PixTif'ed Image

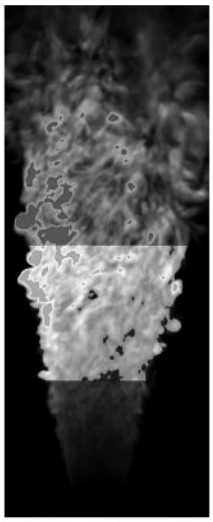

Integration Region

Re = 6.65×10^3
Frame rate = 500 Hz
Exposure = 998 µs
Error $_{\text{flow rate}}$ = 3%

Fluorescent Waterjet

Raw Image

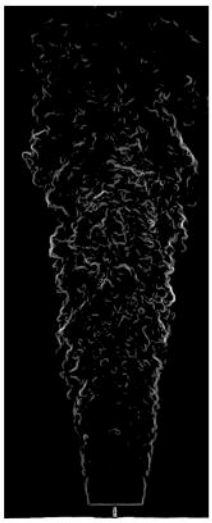

Edged Image

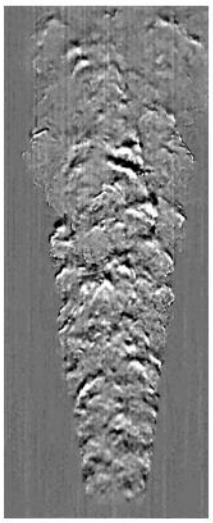

PixTif'ed Image

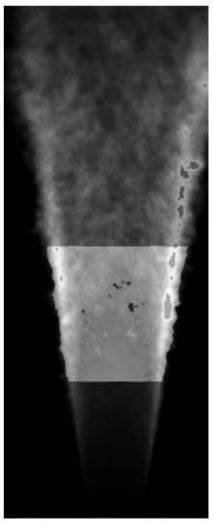

Integration Region

Re = 4.83×10^4
Frame rate = 500 Hz
Exposure = 998 µs
Error $_{\text{flow rate}}$ = 18%

1cs Silicone Oil Jet

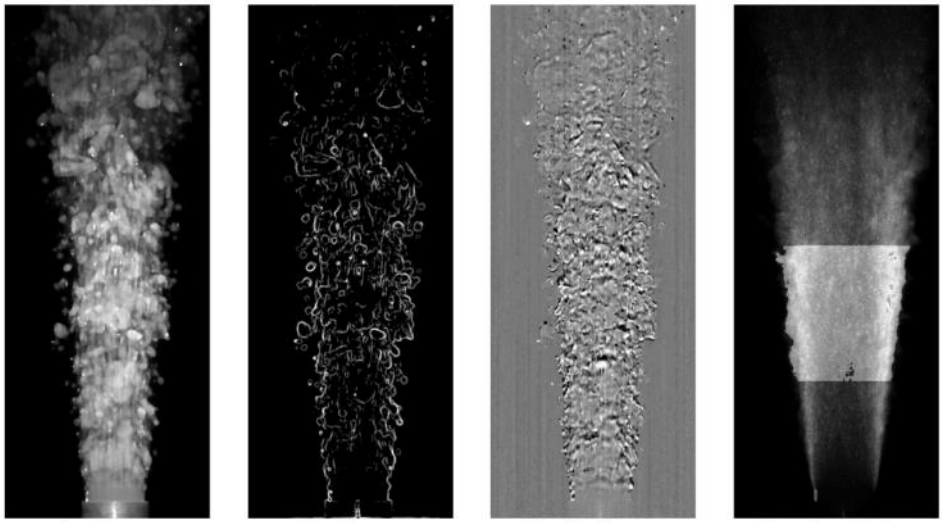

Raw Image | Edged Image | PixTif'ed Image | Integration Region

Re = 3.60×10^4
Frame rate = 1000 Hz
Exposure = 498 µs
Error $_{\text{flow rate}}$ = 7%

23

5cs Silicone Oil Jet

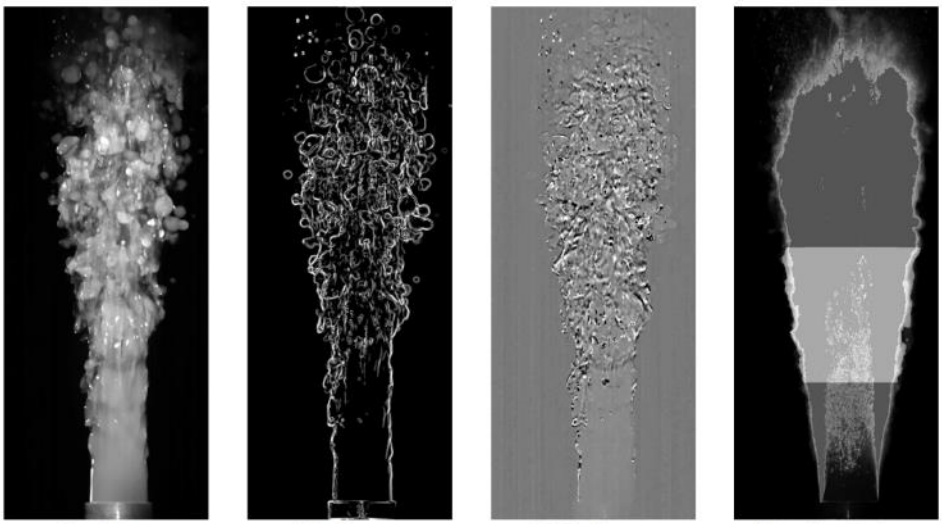

Raw Image | Edged Image | PixTif'ed Image | Integration Region

Re = 4.50×10^3
Frame rate = 1000 Hz
Exposure = 498 µs
Error $_{\text{flow rate}}$ = 11%

24

Summary of Our Experiments

Fluid	Frame Rate (fps)	Flow Rate (gpm)	Re	Error
Water	500	1.02	4.50×10^3	3%
Water	500	4.10	2.67×10^4	23%
Water	500	7.40	4.83×10^4	18%
1cs	1000	4.14	2.70×10^4	9%
1cs	1000	5.52	3.60×10^4	7%
5cs	1000	3.45	4.50×10^3	11%
5cs	1000	5.80	7.56×10^3	2%
5cs	1000	6.90	9.00×10^3	15%

Sample Data

Experiment	FR	Type/aviFolder#	Measure FR (GPM)	Mode,Passes	Edge	Filter Parameters	nxw.nyw	u	v	Calculated FR (GPM)	FlowR	v/u
FWJ -009	500	FV07	1.02	1.1	0	5.4.8	32.32	0.009	0.085	0.02	-0.98	9.4
FWJ -009	500	FV07	1.02	1.1	30	5.4.8	32.32	0.394	0.092	0.67	-0.34	0.2
FWJ -009	500	FV07	1.02	1.1	0	1.4.8	32.32	0.108	0.06	0.18	-0.82	0.6
FWJ -009	500	FV07	1.02	1.1	0	5.4.8	64.64	0.061	0.500	0.10	-0.90	8.2
FWJ -009	500	FV07	1.02	1.1	30	5.4.8	64.64	0.484	0.113	0.41	-0.60	0.2
FWJ -009	500	FV07	1.02	1.1	0	1.4.8	64.64	0.587	0.271	0.49	-0.51	0.5
FWJ -009	500	FV07	1.02	1.1	0	5.4.8	128.128	1.041	0.864	0.89	-0.11	0.8
FWJ -009	500	FV07	1.02	3.2	0	1.4.8	64.16	1.164	0.018	0.99	-0.03	0.0
FWJ -009	500	FV07	1.02	3.2	0	1.6.12	64.32	0.644	0.218	1.10	0.08	0.3
FWJ -009	500	FV07	1.02	3.2	0	1.8.16	64.32	0.851	0.204	0.72	-0.28	0.2
5CS -008	1000	FV18	3.45	1.1	0	5.4.8	32.32	0.181	0.053	0.26	-0.92	0.3
5CS -008	1000	FV18	3.45	1.1	30	5.4.8	32.32	1.223	0.053	1.65	-0.52	0.0
5CS -008	1000	FV18	3.45	1.1	0	1.4.8	32.32	0.308	0.056	0.42	-0.88	0.2
5CS -008	1000	FV18	3.45	1.1	0	5.4.8	64.64	0.924	0.292	1.25	-0.66	0.3
5CS -008	1000	FV18	3.45	1.1	30	5.4.8	64.64	2.706	0.044	3.65	0.06	0.0
5CS -008	1000	FV18	3.45	1.1	0	1.4.8	64.64	1.610	0.246	2.17	-0.17	0.2
5CS -008	1000	FV18	3.45	1.1	0	5.4.8	128.128	2.213	0.614	2.98	-0.14	0.3
5CS -008	1000	FV18	3.45	3.2	0	1.4.8	64.16	3.211	0.041	4.33	0.26	0.0
5CS -008	1000	FV18	3.45	3.2	0	1.6.12	64.32	3.674	0.215	4.95	0.43	0.1
5CS -008	1000	FV18	3.45	3.2	0	1.3.6	64.32	3.473	0.236	4.68	0.36	0.1
1CS -009	1000	FV17	4.14	1.1	0	5.4.8	32.32	0.191	0.054	0.2	-0.95	0.3
1CS -009	1000	FV17	4.14	1.1	30	5.4.8	32.32	1.440	0.063	1.54	-0.63	0.0
1CS -009	1000	FV17	4.14	1.1	0	1.4.8	32.32	0.283	0.039	0.3	-0.93	0.1
1CS -009	1000	FV17	4.14	1.1	0	5.4.8	64.64	0.998	0.313	1.07	-0.76	0.3
1CS -009	1000	FV17	4.14	1.1	30	5.4.8	64.64	2.516	0.032	2.69	-0.35	0.0
1CS -009	1000	FV17	4.14	1.1	0	1.4.8	64.64	1.499	0.169	1.6	-0.61	0.1
1CS -009	1000	FV17	4.14	1.1	0	5.4.8	128.128	2.145	0.66	2.29	-0.45	0.3
1CS -009	1000	FV17	4.14	3.2	0	1.4.8	64.16	3.108	0.047	3.32	-0.28	0.0
1CS -009	1000	FV17	4.14	3.2	0	1.5.10	64.32	3.526	0.164	3.77	-0.09	0.0
1CS -009	1000	FV17	4.14	3.2	0	1.7.14	64.32	3.523	0.162	3.77	-0.09	0.0
1CS -009	1000	FV17	4.14	3.2	0	1.8.16	64.32	3.486	0.144	3.73	-0.13	0.0

Closing Remarks

In lab we are able to estimate the flow rates within 20% at medium Reynolds numbers

- Windowing
  - Based on the inadequate sampling rate of the video be able to window out Fourier modes that may contaminate results with aliasing errors
- Ambient Noise Insensitivity
  - Mitigating the effect of particles in the foreground of the video have of the velocity field calculation
- Extensive Validation
  - Testing the software on a range flows varying:
    - High Reynolds numbers
    - Ambient lighting
    - Recording parameters

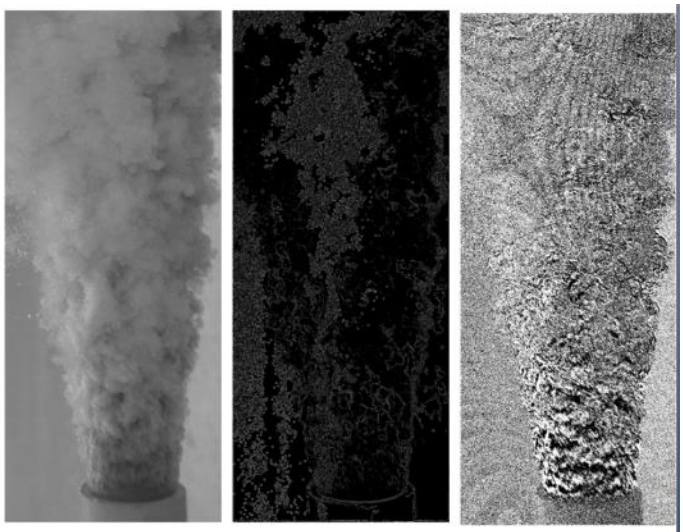

OHMSETT Experiments

Fluid = JP5 Fuel [3]
Re = 1.47×10^4
Frame rate = 1000 Hz
Exposure = 498 µs

Development of an ROV Video Analysis Tool for Rapid Measurement of Submerged Oil/Gas Leaks

Funded by

DOE NETL, Energy Policy Act: 2011-2014
> $750k

DOI-BSEE Project E13PS00032: 2013-2106
$728k

Development of a ROV Deployed Video Analysis Tool for Rapid Measurement of Submerged Oil/Gas Leaks

The Team

BSEE Managers: Paula Barksdale, Tim Steffek

NETL: Frank Shaffer, Mehrdad Shahnam, Pankaj Saha, Igor Haljasmaa

UC Berkeley: Ömer Savas, Eric Ibarra, Kenneth Lee, Giorgio deVera

OHMSETT Mar Inc: Dave DeVitis, et al.

Development of a ROV Deployed Video Analysis Tool for Rapid Measurement of Submerged Oil/Gas Leaks

Lead PI's

Frank Shaffer

- DOE R&D Lab for 30 years
- Specialize in high speed imaging of multiphase flows
- Project Manager, Policy Analyst

Professor Ömer Savas

- PhD in Aeronautics from Cal Tech, 1979
- Full Prof. at UC Berkeley Mechanical Engineering
- 40+ years studying turbulent flows, specializing in high speed imaging of turbulent flows

The Beginning: April 20, 2016

- Major oil leak at 5000 ft depth
- No proven technology to measure the discharge rate
- Level of response dictated by discharge rate

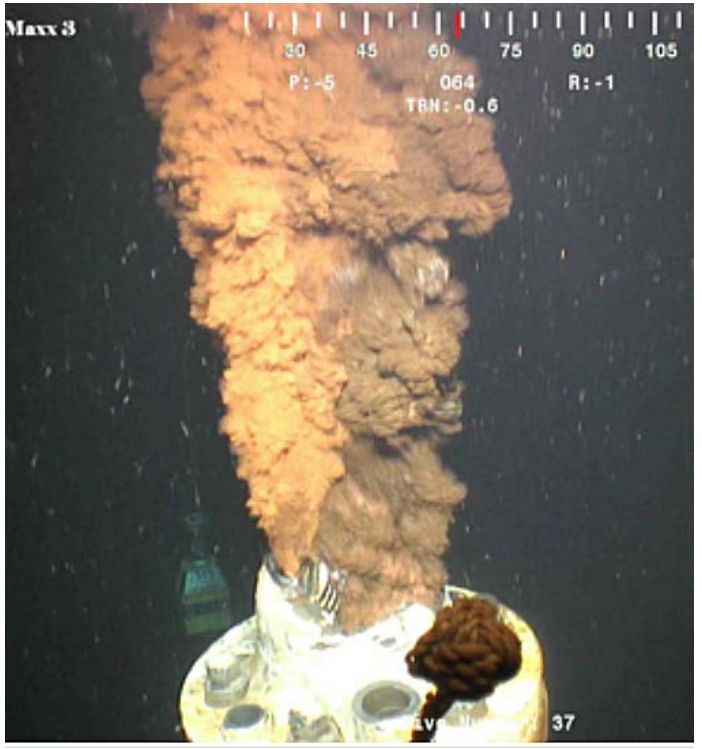

ROV Video

- One of the first responses to a submerged oil/gas leak will be to send a ROV down to view the leak

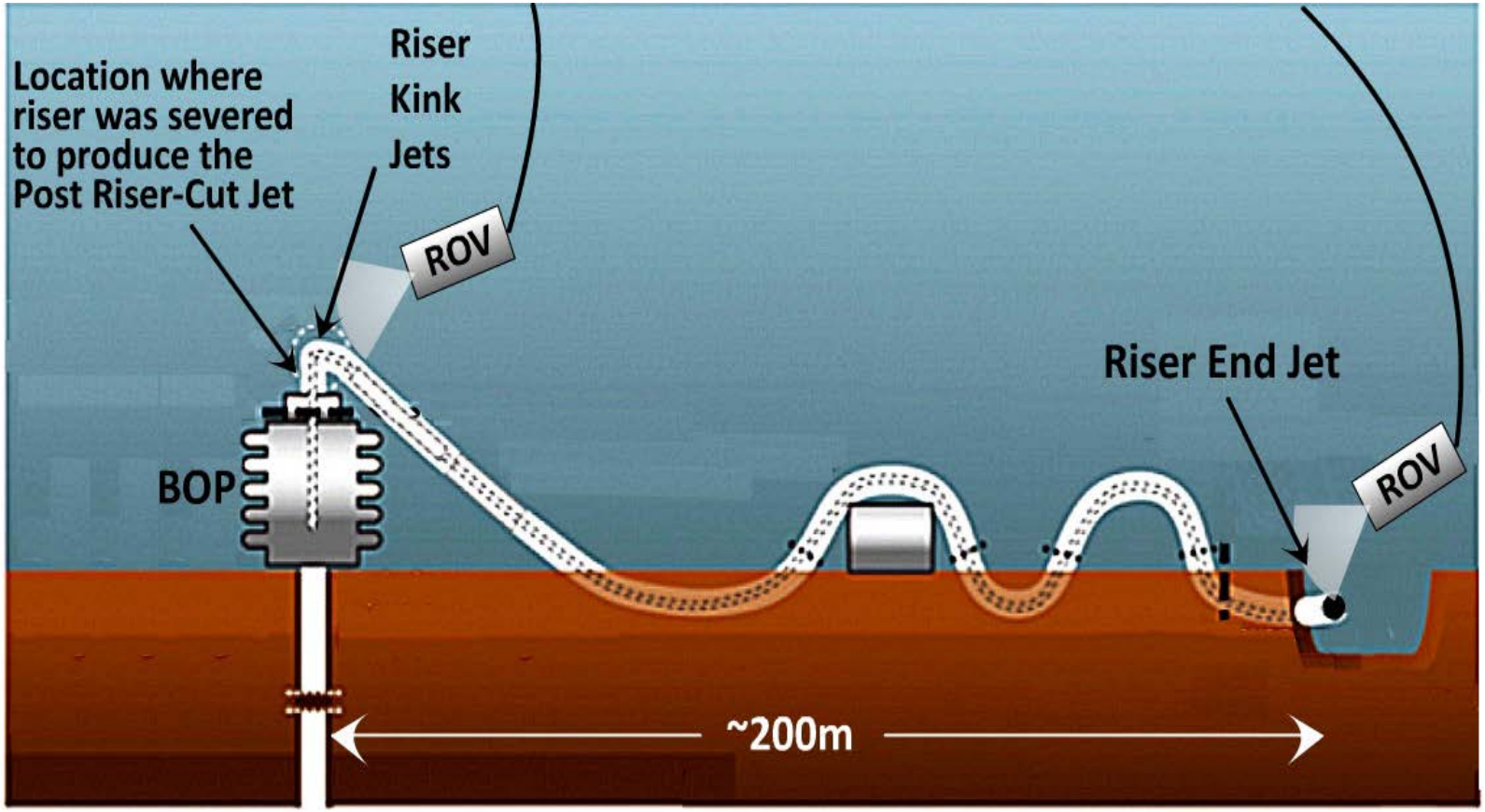

ROV locations during the DWH oil leak

Background: DWH Leak Estimates & FRTG Plume Team

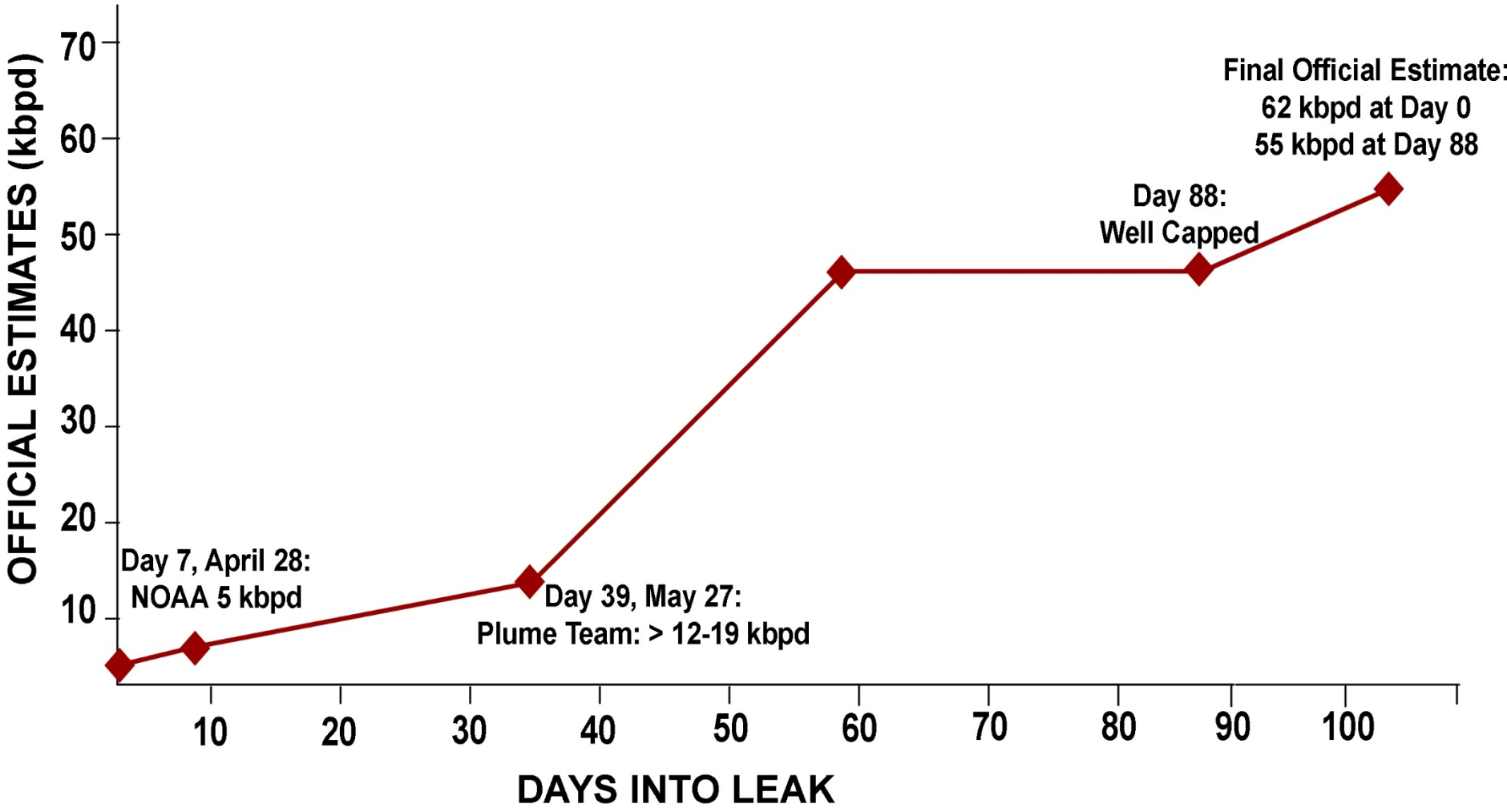

FRTG Plume Team

- Given ROV video of leaks
- Charged with quickly developing first estimates
- Leaks were in the form of turbulent jets.
- All significant leaks will be turbulent jets

FRTG Plume Team: Technical Approach

Turbulent jets have “visible features” propagating at the jet boundary

- Turbulent eddies
- Vortices
- Entrained particles

Frame 1 at t1

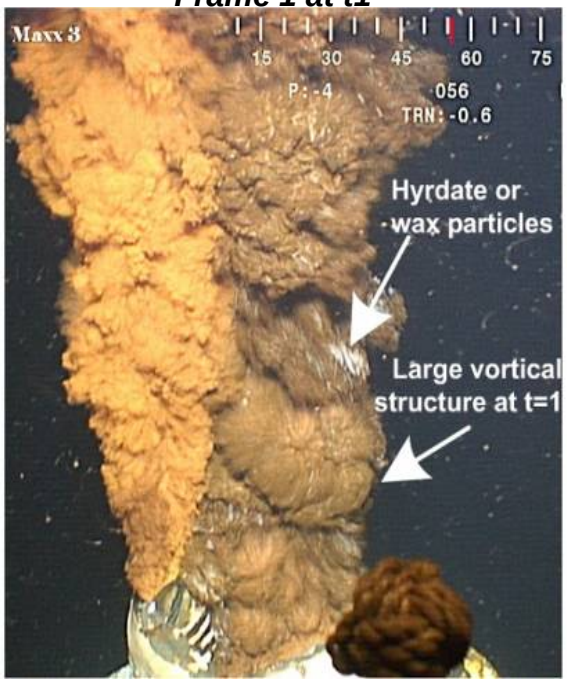

Frame 2 at t2

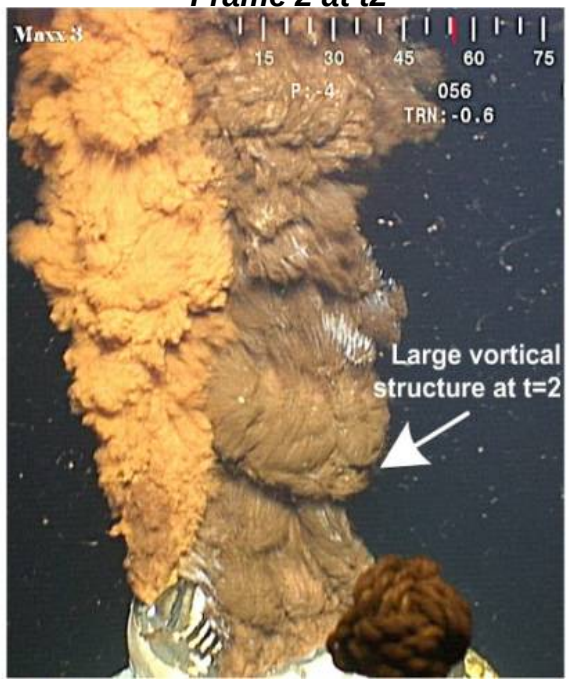

Frame 3 at t3

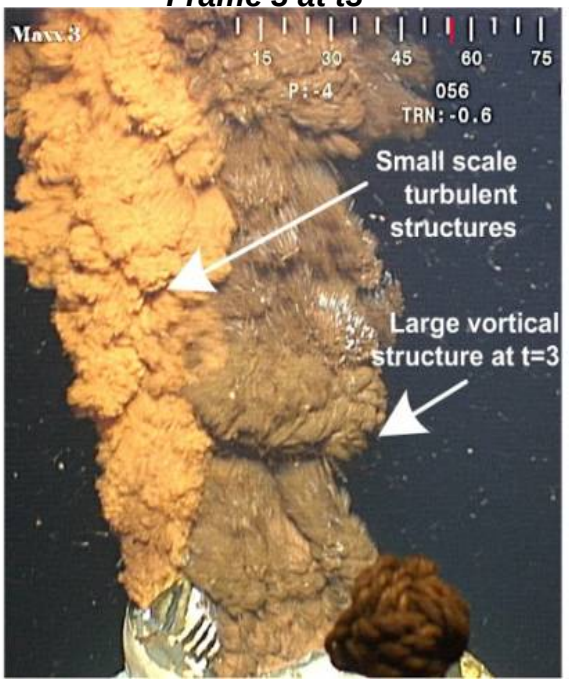

FRTG Plume Team

- Measured velocity of visible features at boundaries of leak jets
- *Two types of measurement:*
  - *Manual (by hand)*
  - *Automated using Particle Image Velocimetry (PIV) software*
- Velocity of visible features can be used to estimate the jet discharge rate

$$Q = \overline{V}_{jet} A = \overline{V}_{jet} \pi/4 D_{jet}$$

$\overline{V}_{jet} = f (V_{visible\ features})$ *Prof. Savas will explain this later.*

D_{jet} *from video*

FRTG Plume Team

- Plume Team Results
  - Manual measurements: 43, 55, 62.5 kbpd
  - Automated measurements: 34, 34, 35 kbpd

- *Difference in estimates*
  - PIV software: *first application, unproven*
  - $\bar{V}_{jet} = f\,(\,V_{visible\ features}\,)$ *: not well understood, unverified*

FRTG Plume Team

- Manual tracking of visible features on Macondo leak jets
- Manual tracking is easy, but somewhat subjective
- NIH ImageJ MTrackJ software used for tracking

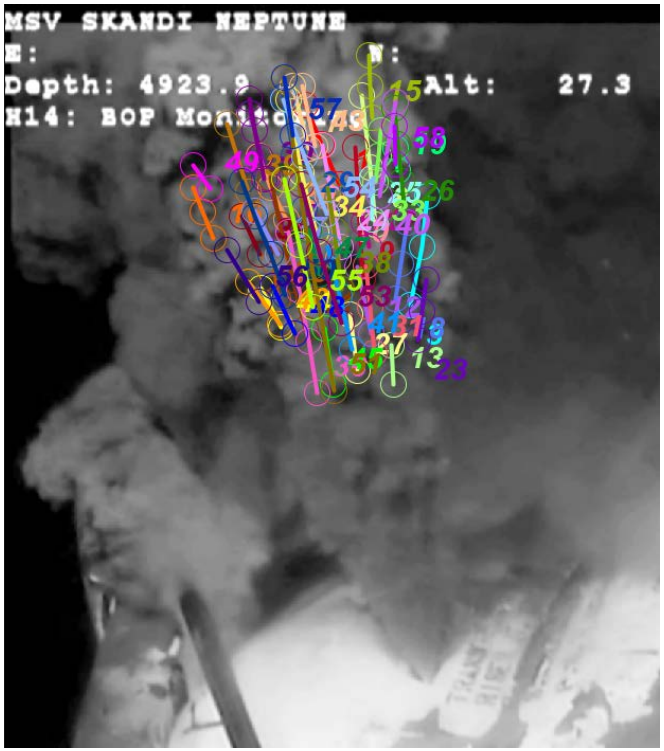

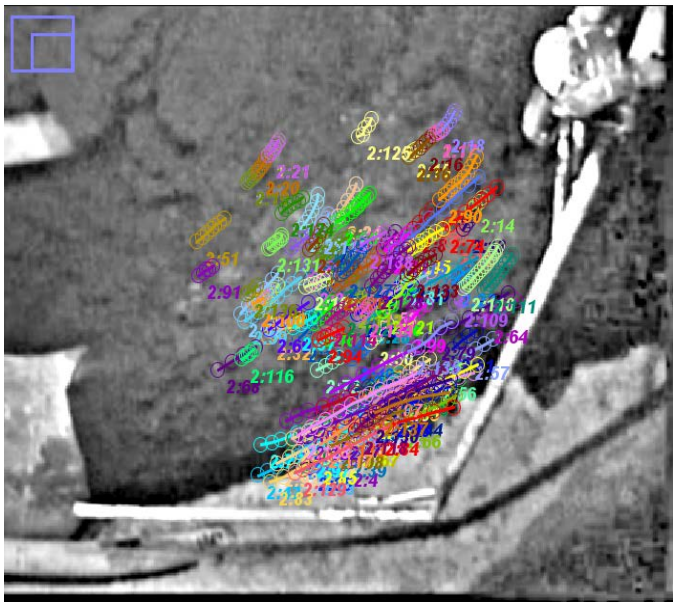

Post Plume Team Research
GOALS

1. Verify that visible features can be accurately measured

2. Understand the relationship between the velocity of visible features and internal velocity of a leak jet

$$\overline{V}_{jet} = f\left(V_{visible\ features} \right)$$

3. Develop and verify an automated video analysis tool

Post Plume Team Research
APPROACH

1. Water dye-jet experiments in UC Berkeley Tow Tank
2. Small scale oil jet experiments at UC Berkeley
3. Large scale oil jet experiments at OHMSETT
4. Computer simulations (Computational Fluid Dynamics, CFD) of OHMSETT jets
5. Test automated analysis tool on 1-4

Dye-Jet Experiments in UC Berkeley Tow Tank

- Started in 2011
- Created dye-colored water jets (4” and 8” dia) to simulate the DWH leak jets. Reached conditions (Re ~ 500,000) of the DWH leak jets
- The velocity of the jet was mapped with high speed video and Laser Doppler Anemometry (LDA)
- LDA is the gold standard for velocity measurements

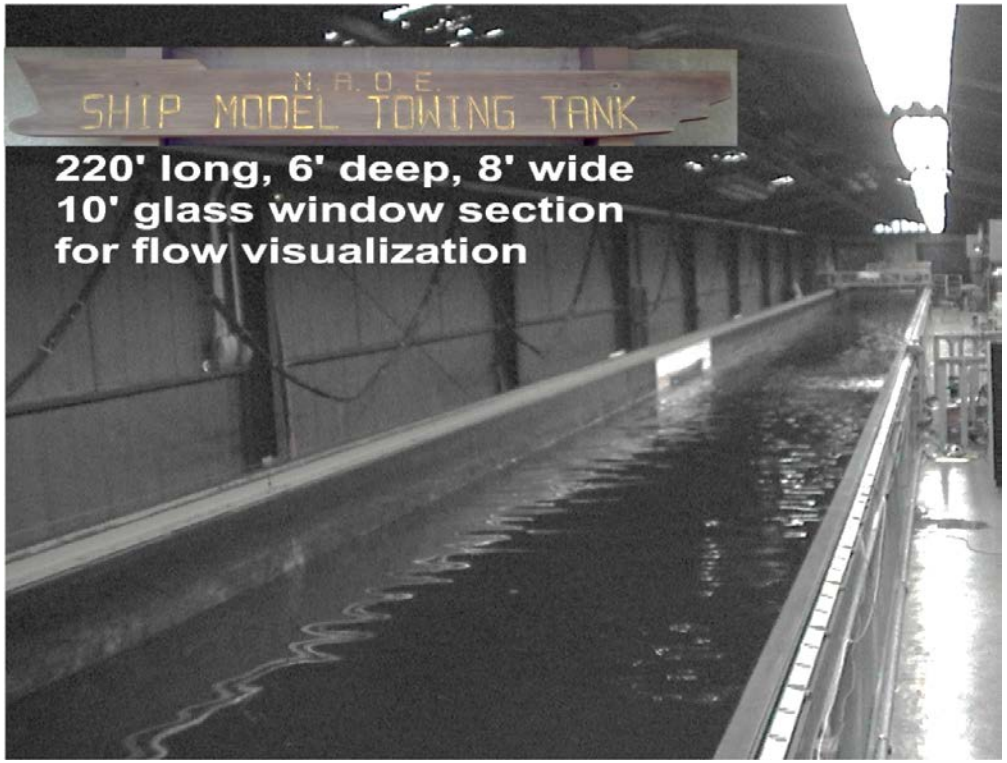

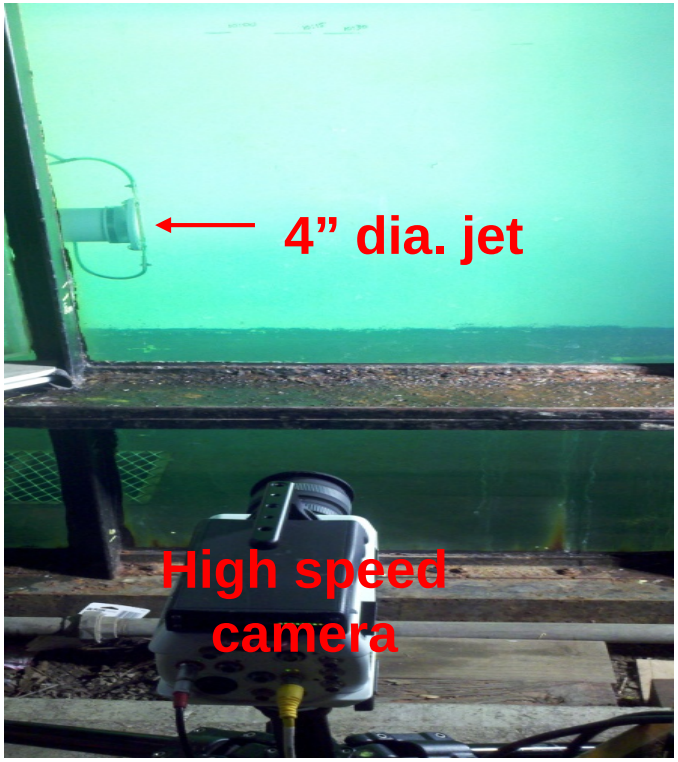

Dye Colored Water Jet Tests at UC Berkeley

Dye point injection and dye rake injection were used to visualize jet features with high speed video

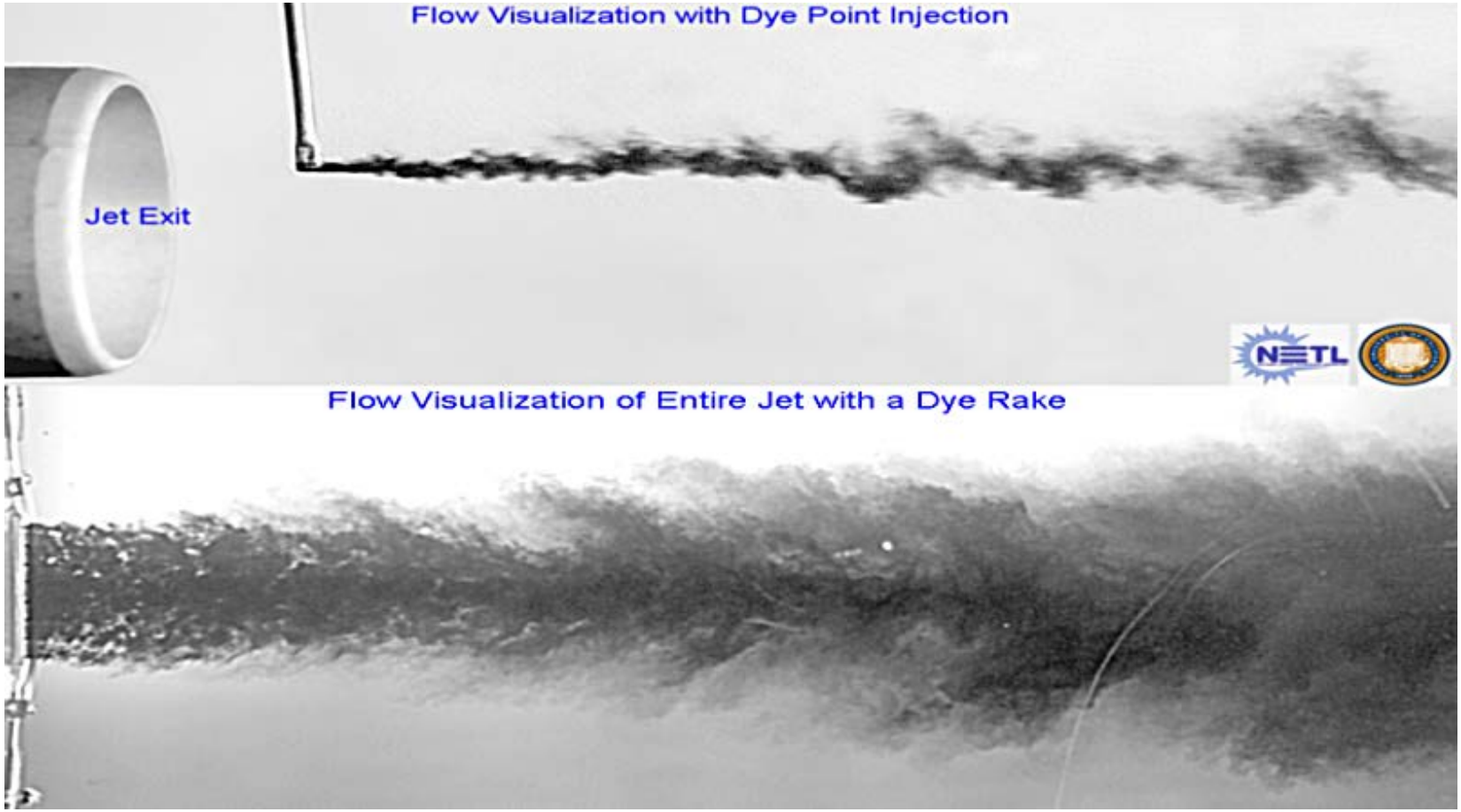

Dye Colored Water Jet Tests at UC Berkeley

- Automated measurement of visible features using Image Correlation Velocimetry

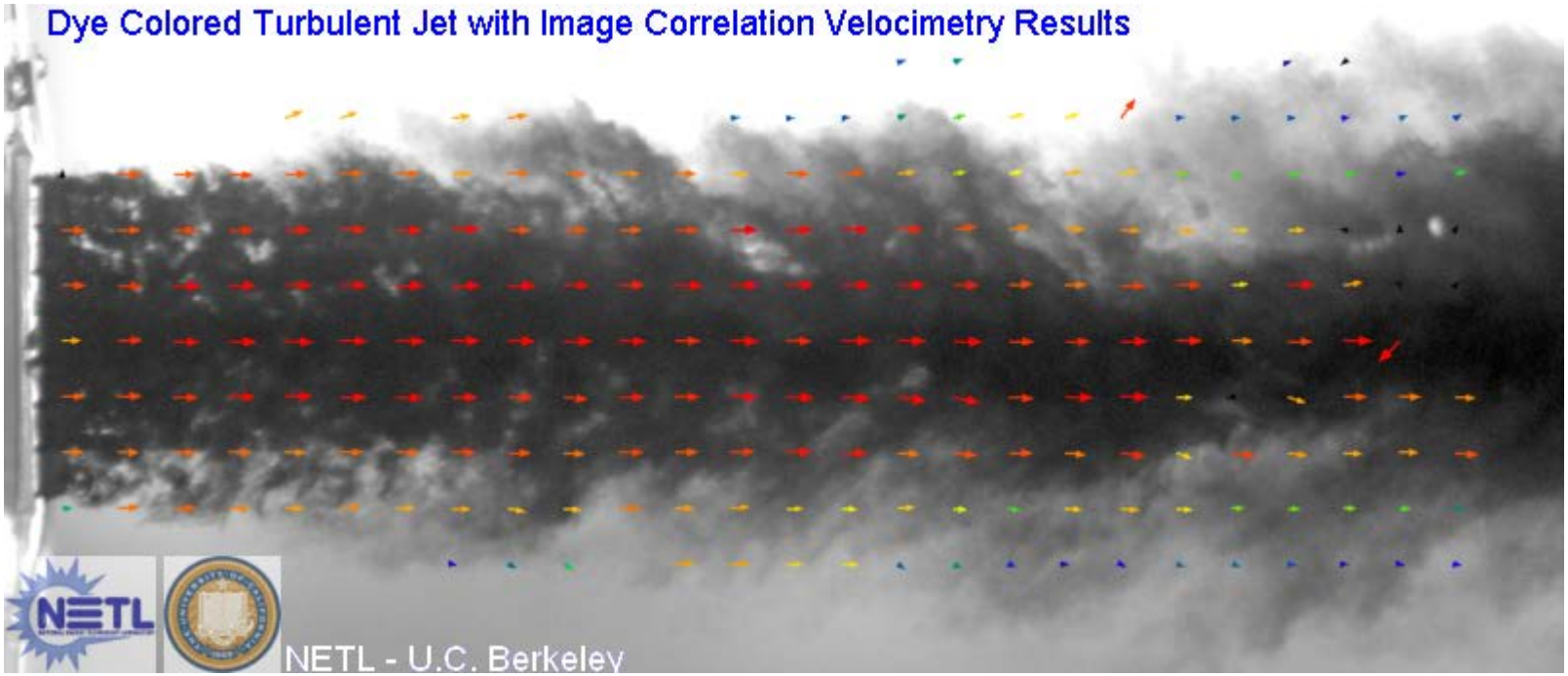

Computational Fluid Dynamics (CFD) Simulations of Submerged Oil Jets

Dr. Mehrdad Shahnam and Dr. Pankaj Saha of NETL

1. It is not impossible to make detailed velocity measurements inside an immiscible jet of an opaque fluid like crude oil
2. CFD allowing us to see the velocity field inside
3. Video animations can be created from CFD simulations. The video animations can be used to test automated measurement software.
4. CFD simulations run on NETL's supercomputer system. At >500 Teraflops, is one of the Top 100 supercomputers in the world.

Post Plume Team Research
Computational Fluid Dynamics (CFD)
Simulations of Submerged Oil Jets

Simulation of OHMSETT Test 26

LES of OHMSETT Test 26. Time between frames is 465 microsec. 115 pixels = 1"

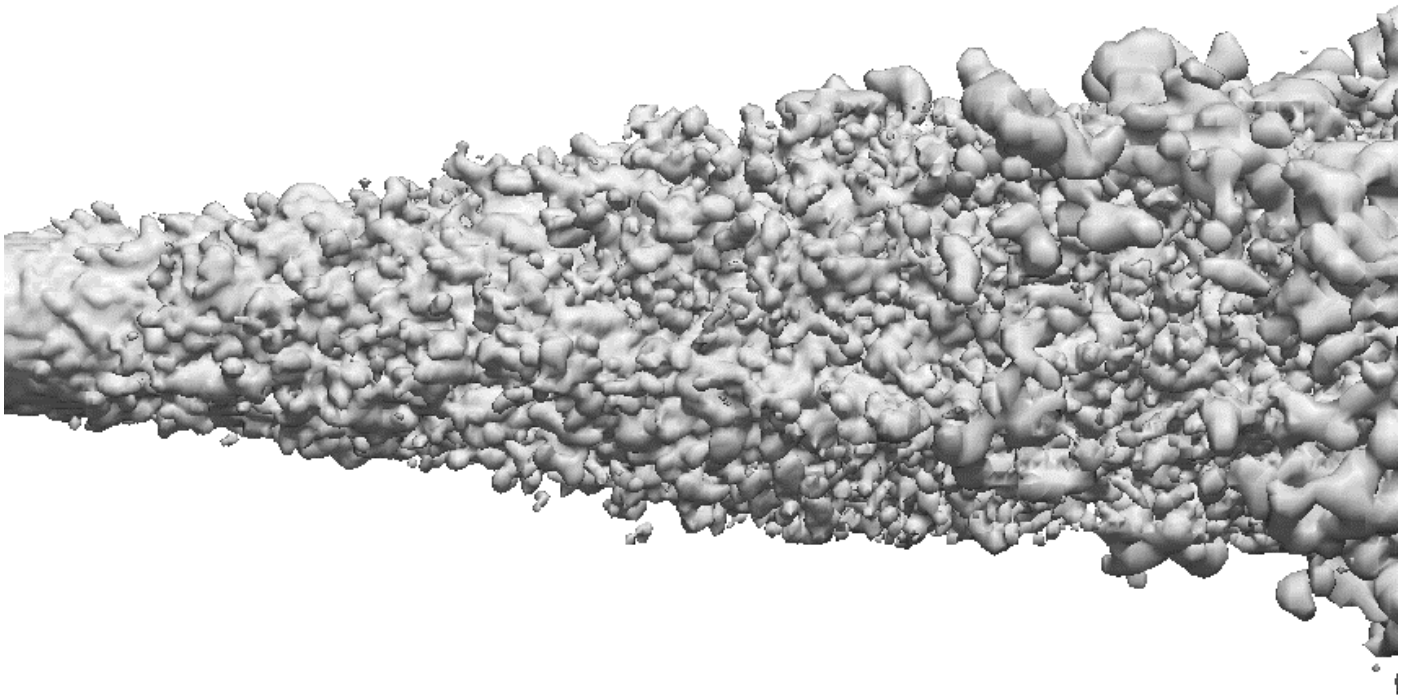

BSEE Project Task 3:
Large Scale Oil Jet Tests at OHMSETT

- Largest oil leak tests to date
- Rates up to ~30,000 bpd, but for short periods
- Shakedown tests were done in June
- 1” and 2” dia oil jets were created and recorded with high speed video and GoPro submerged cameras

SUMMARY

- Thank you for supporting this work!
- Completed water dye-jet and small scale oil jet experiments at UC Berkeley
- Completed large oil jet experiments at OHMSETT
- Completed CFD simulations of submerged oil jets
- Developed UCB Plume Analysis Tool
- Still testing UCB Plume Tool on OHMSETT jets

HOW TO RESPOND TO A SUBMERGED OIL LEAK?

1. Apply manual tracking and turbulent jet theory for quick estimate. "Quick" means hours or less.

2. Apply UCB Plume Analysis Tool
   - Seek Professor Savas' guidance

3. May be necessary to bring in ROV with higher frame rate camera to increase accuracy of estimates

4. Have an "independent" response team established and on call to apply 1-3

On near field structures of round jets

Eric Ibarra, Franklin Shaffer† and Ömer Savaş‡

Department of Mechanical Engineering,
University of California, Berkeley, CA, 94720-1740, USA

(Received xx; revised xx; accepted xx)

30 March 2017

An analysis of flow visualization using opaque fluorescent turbulent water and oil jet(at jet Reynolds number of $\mathcal{O}(10^4)$) is introduced. This analysis is based on a quantitative characterization of the surface features along the jet. In previous work, these features are tracked using a method that is, in essence, similar to PIV processing. but the cross correlation is performed on the visible features of the efflux. The near field interface of the turbulent water jet shows local isotropy, with feature size commensurate to the jet Reynolds number. At jet Reynolds number greater than $\mathcal{O}(10^3)$, the oil jets were observed to break up into a range of droplet sizes convecting at various speeds. The dynamics of these droplets − breakup, amalgamation, and transitional states − are discussed.

Key words: jets, shear layers, turbulence

1. Introduction

Figure 1 shows the near field images of three jet discharges. Frame (a) show a snapshot of the Deepwater Horizon (DWH)/Macondo Well oil spill in the Gulf of Mexico in April 2010 (Savas 2012). In this accidental discharge, the upstream conditions in the ducts are unknown. The discharging oil is opaque, hence, only the interface is visible. The Reynolds number is $\mathcal{O}(10^5)$. The visible features at the interface are signatures of the flow turbulence. Any quantitative statements regarding the discharge have to be based solely on the information that can be extracted from these features. In contrast, frame (b) shows hydrogen-bubble visualization of the near-field cross-sectional view of a well-controlled water jet egressing from a 5.1 cm diameter nozzle at $Re = 9000$ (Yule 1978). The flow at the discharge plane is uniform and free of turbulence. The unstable cylindrical shear layer develops into as series of vortex rings, the celerite of which can easily be determined from a sequence of images, whereby, the volume flux, for example, can be deduced. The vortex rings develop stream wise instabilities at higher Reynolds numbers (Savaş & Gollahalli 1986), but the overall ring structure dominates the near field, which is well understood. Frame (c) of figure 1, taken from below, is somewhat an intermediate state between the frames (a) and (b). The flow at the exit plane is the developed turbulent pipe flow profile. The discharge fluid is opaque, hence only the interface features are accessible. The Reynolds number is about 6000. The interface *shell* lacks the orderliness of frame (b), and at the same time is less disorderly than (a). In fact, the spatial statistical uniformity suggests that some features of the interface should be tractable to be able to

† Email address for correspondence: Franklin.Shaffer@netl.doe.gov
‡ Email address for correspondence: savas@berkeley.edu

make quantitative statements about the flow with some acceptable confidence level. It is this aspect of the flows that is the subject matter of this paper.

2. Experimental setup

2.1. *Flows*

Figure 2 shows the schematics of the experimental setup: the flow loop and the optical layout. The flow loop is shown in figure 2(a). Experiments are conducted in a $120^{\mathtt{w}} \times 240^{\mathtt{l}} \times 120^{\mathtt{h}}\mathrm{cm}^3$ glass water tank at a water level of about 105 cm. Jet fluids are discharged into the tank through a vertical smooth copper tube of inner diameter $D = 1.38$ cm, outer diameter of 15.9 mm and length of 42 cm, hence, a length to diameter ratio of 30 (1/2-inch L copper tubing). A 30-mesh screen is placed at the entrance to the tube to insure uniformity at the beginning and also trip the flow to promote transition. The tube is protrudes from the center of a 68-cm diameter ground plane. Water and two silicone oils of viscosities of 1-cs and 5-cs (Clearco Products Co.: PSF-1cSt Octamethyltrisiloxane and PSF-5cSt Dimethicone) are used as the discharge jet fluids. The properties of the liquids are given in Table 1. The water jet was coloured with fluorescein sodium salt injected upstream into the flow circuit from a dye reservoir (dye reservoir concentration: 1 g/l, 0.1% by weight). The oil jets are coloured with oil soluble fluorescent tracing dye (Kingscote Chemicals, # 506250-RF16, jet fluid concentration 0.07% by weight). The fluorescein used in water experiments was neutralized using chlorine bleach (Chlorox). The oils were almost completely recovered and stored away at the completion of the experiments.

2.2. *Flow drive systems*

During the flow visualization runs with water jets, the jet fluid is directly supplied from the laboratory supply line. The inherent lower temperature of the line water, usually few degrees Celsius lower than the ambient temperature, has been sufficient to provide high enough refractive index difference between the jet fluid and the stagnant water in the tank to facilitate schlieren photography. During the PIV runs, a centrifugal pump is employed to generate the water jets by recirculating the seeded water in the tank. For simultaneous PIV and schlieren photography, the line, made off copper, was wrapped with a heating pad (Walgreen Heating Pad Model CAT94C) to heat the jet fluid slightly to obtain sufficient refractive index difference for imaging. During all water jet runs, the flow rate was set by a ball valve and monitored by an industrial grade turbine flow meter of 1% accuracy (GPI Model No: G2S07N09GMA).

Oil jet experiments required special care. As opposed to the water jets which were operated manually and run *continuously*, the oil jets were run on extremely short intervals under computer control, typically 10 seconds long, to minimize the oil usage. The oil jets were driven by a calibrated gear pump (PENTAIR Model: SHURFLO BBV5) coupled to a microstepper motor (Compumotor). The runs consisted of ramp up, pre-acquisition steady state, image acquisition, and ramp down phases that are synchronized with the imaging system, all under computer control. The jet oil was contained by a pontoon at the free surface of the tank for quick recovery and recycling into the experiment.

2.3. *Optical layout*

The schematics of the optical layouts for schlieren/shadowgraph imaging, interface flow visualization, cross-sectional visualization, and PIV are all shown jointly in figure 2(b). Any two imaging schemes could be utilized simultaneously.

2.3.1. *Schlieren system*

The classical schlieren layout using two concave mirrors, of 400-cm focal length and 45-cm diameter, in the Z-configuration is employed here. Due to space constraints, the collimated middle section of the Z is folded using two large front surface mirrors that intercept the collimated beam nearly perpendicularly, arranged not to interfere with other imaging schemes. An LED light source is used for illumination (Leica KL 1500LED). The light beam is shaped using a matched achromatic doublet pair (Thorlabs MAO:103030-A), a pinhole, and a microscope objective. The system is used both with a single knife edge and simultaneously with two orthogonal knife edges after the light beam is split by a cubical beam splitter.

2.3.2. *PIV system*

For PIV, the tank is seeded with hallow silver coated hallow ceramic spheres of diameter 45μm (Potter Industries Inc., AG-SF-20, 0.8 g/cm^3). The illumination is done using a 10W CW argon-ion laser (American Laser Corporation). The PIV laser sheet is also used for cross sectional visualization of the water jets when the jet is dyed and the tank had no particles. The immiscibility of oils and water and their mismatched refractive indices precludes cross sectional viewing of the oil jets in water.

2.3.3. *Interface visualization*

The interface of the dyed jet fluid is recorded under oblique nearly collimated illumination from a 1000-lumen LED flash light placed downstream at an angle of about 35° as shown in figure 2(c).

2.3.4. *Imaging*

The flow fields are recorded using simultaneous schlieren and FV, IDT X3 and Y3 cameras. The cameras are operated in continuous mode. Imaging rates of 500, 1000 and 2000 Hz at exposure times of 998, 498 and 494 μs are employed for water jet runs. Imaging rate is 1000 Hz at the maximum exposure time of 498 μs to record oil jet runs. For simultaneous imaging, the cameras are operated in master-slave mode.

2.4. *Flow parameters and scales*

The primary flow parameter is the Reynolds number Re

$$Re = \frac{Q}{\nu_j D} \tag{2.1}$$

which is based on the viscosity of the jet fluid ν_j, discharge pipe diameter $D = 1.38$ cm and volumetric flow rate Q. The flow rate Q is measured with a high precision flow meter for the water jet runs and determined through a calibration chart for the positive displacement gear pump for the oil jet runs.

When the discharge flow is turbulent, the jet/ambient interface shows many scales of cascading turbulent eddies. The key parameter in description of the turbulence is the dissipation rate ϵ which is of order

$$\epsilon \sim \frac{u^3}{l} \sim \frac{Q^3}{D^7} \tag{2.2}$$

where u and l are the velocity and length scales of the energy carrying largest eddies in the flow, which are approximated as U and D when numerical values are needed. The turbulent kinetic energy is dissipated at viscous length scales η, the Kolmogorov scales,

$$\eta \sim \frac{1}{k_d} \sim (\nu^3/\epsilon)^{1/4} \tag{2.3}$$

where ν is the kinematic viscosity and k_d the wavenumber corresponding to η, $k_d \sim 1/\eta$. The ratio of the Kolmogorov scales to the largest eddy scale is

$$\frac{\eta}{l} \sim Re^{-3/4}. \tag{2.4}$$

In the intermediate range of eddy scales (η, l), the universal equilibrium range or the inertial subrange, the eddies of a given wave number have eddy turn over time of t_k and eddy turnover velocity of u_k scales that are independent of viscosity,

$$t_k \sim (\epsilon k^2)^{-1/3} \sim u^{-1}(k^2/l)^{-1/3} \tag{2.5}$$

$$u_k \sim (\epsilon/k)^{1/3} \tag{2.6}$$

The momentum *injection* rate $\rho_j M$ is based on the flow rate Q

$$M = QU = \frac{4}{\pi}\frac{Q^2}{D^2} \tag{2.7}$$

where U the average discharge velocity at the tube exit plane. Buoyancy flux B is written as

$$B = gQ\left(\frac{\Delta\rho}{\rho_w}\right) = gQ\left(\frac{\rho_w - \rho_j}{\rho_w}\right) \tag{2.8}$$

where g is the gravitational acceleration. Finally, the Morton length ℓ_M is determined as

$$\begin{aligned}\frac{\ell_M}{D} \equiv \frac{M^{3/4}}{B^{1/2}}\frac{1}{D} &= \left(\frac{4}{\pi}\right)^{3/4}\left(\frac{\rho_w}{\Delta\rho}\right)^{1/2}\frac{Q}{g^{1/2}D^{5/2}} \\ &= \left(\frac{4}{\pi}\right)^{3/4}\left(\frac{\rho_w}{\Delta\rho}\right)^{1/2}\frac{\nu_j Re}{g^{1/2}D^{3/2}}\end{aligned} \tag{2.9}$$

The ℓ_M is used to gage the effect of the buoyancy of the jets in the near field.

2.5. *On Video Frame Rate*

When estimating flow discharges rate from the videos of visible shell of discharging turbulent jets, the framing rate is a primary factor in deciding what approach should be taken. If the framing rate is too slow, typically 30 Hz, then the fine turbulent features on an image frame are independent of those in the adjacent frames, especially at higher Reynolds numbers. Then, one is left with the largest scales of the flow of size order D the flow, which are convected at speeds of order U, hence the framing rates of order $f \sim U/D$ is sufficient to track them where U is jet velocity and D is a measure of the jet diameter. Under such conditions, the processing is rather subjective, usually manual, therefore, very laborious. As an example, for the DWH spill (figure 1(a)) Q=0.1 m^3/s (53,000 bbl/day) through a 0.5 m diameter pipe end, sampling rate of several Hz is sufficient, e.g., typical video rate of 30 Hz was ample.

If turbulent eddies are to be utilized for flow rate estimation from videos, one must first decide the size of the eddies that will be employed. Turbulent eddies identified as markers of the flow for velocimetry must remain nearly frozen between successive images in the video stream in their turnover process so that they can act as passive markers of their carrier translational motion. Hence, the camera framing rate f must be sufficiently high so that the eddy does not rotate significantly between successive frames,

$$f \gg (\epsilon k_v^2)^{1/3}$$

where k_v is the desired eddy wavenumber for marking the fluid for velocimetry. The marker wavenumber k_v is selected based on the interrogation window size, typically $w \times w = 32 \times 32$ pixels, hence $1/k_v$ should be much smaller than the window size w

$$k_v \gg 1/w \tag{2.10}$$

an order of magnitude or more. Finally, we have

$$f \ggg (\epsilon/w^2)^{1/3}$$

In lieu of the double $\gg$ signs, we suggest a factor in the range of 10-100

$$f \sim 10(\epsilon/w^2)^{1/3}$$

Using the ostensible parameters

$$f \sim 10(Q/D^{7/3})w^{-2/3} \tag{2.11}$$

As an example, let's take a pixel size of 10^{-3} m ($\sim [1000 \times 1000]$ pixels camera looking at a 1m $\times$ 1m area), $Q = 0.1m^3/s$ (53,000 bbl/day, DWH Spill of 2010) and $D = 0.5$ m, $w = 32$ pixels

$$f \sim 10(Q/D^{7/3})w^{-2/3} \sim 50\ Hz$$

For a typical Berkeley experiment, let's take a pixel size of 10^{-4} m ($\sim [1000 \times 1000]$ pixels camera looking at a 0.1m $\times$ 0.1m area), $Q = 1 \times 10^{-4}m^3/s$ and $D = 0.013$ m, $w = 64$ pixel

$$f \sim 10(Q/D^{7/3})w^{-2/3} \sim 1000\ Hz$$

Filtering the video deck for k_v (Laplace filtering image frames) and

$$t_{k_v} = (\epsilon k_v^2)^{-1/3} \tag{2.12}$$

(PixTifing sequential pixels)

For manual tracking

For manual tracking of the largest eddies, with $w \sim D/4$, equation 2.11 suggests for DWH example video framing rate of

$$f \sim 20$$

which is nearly the common video frame rate.

3. Flow images

Table 2 lists the experiments carried out in this study. The table lists the Reynolds numbers as well the estimates of the Morton lengths and the Kolmogorov scales based on the jets' parameters. Imaging rates and exposure times are listed which are utilized in discussing the flow scales. Simultaneous imaging modes are also indicated in the table.

3.1. *Sample images*

Figure 3 shows sample flow images for water and the two silicone oil jets at comparable flow conditions. The Reynolds numbers are high enough that the tripped flows in the discharge tube are developed turbulent flows. That none of the flows show any orderly ring-like structure as those seen in figure 1(b) may be taken as confirmation of developed turbulent flows in the tube. The water jet in frame (a) shows the jet-ambient fluid interface clearly. The interface distorts immediately after the fluid leaves the tube and develops into an intricate topology. Shadows brought about due to the opacity of the dyed jet fluid makes the details of the interface clearly visible. Despite the very intricate shape of the interface, there is no indication that it is not contiguous. Frames (b) and (c) show the 1-cs 5-cs oil jets that have visually comparable scales to those in frame (a). Reflections off the convoluted interfaces and the surfaces of the detached oil bubbles make both pictures *starry*. As in (a), flow at the end of the discharge pipe have evidence of developed turbulent flow in the pipe. In stark contrast to the homogeneous jet in (a), the oil jets exhibit axial striations, or ligaments. Further, instead of the mushroom excursions into the ambient fluid visible in (a), we now see detached oil droplets in the ambient fluid. It is not clear if there are water droplets in the jet fluid, though. Another feature clearly visible, is the underlying large scale, arrowhead (chevron) structures in the oil jets which do not seem to have a counterpart in the water jet in (a). Unexpectedly, the lower Reynolds number flow of the 5-cs oil jet in frame (c) has finer scales that the 1-cs oil at at a higher Reynolds number in frame (b). *And we don't know why!*

3.2. *Water jets*

Edge visualization

Figure 4 shows sample flow images of water jets at three Reynolds numbers. The discharge flows at the tube exit are evidently turbulent as the interfaces deform well within one diameter of the exit plane. At the lowest Re in frame (a), the jet-ambient fluid interface is sharply defined; the camera resolution seems to be sufficient to capture all flow surface details. At the intermediate Re in frame (b) there is a stark decrease in the size of the interface features, as expected with increasing Reynolds number. At the highest Re in frame (c), the image has become blurred. There are two obvious reasons for this: the expected size of the turbulence is getting smaller, hence falling out of the spatial resolution of the camera and the exposure time of the camera is longer than the time scale of the interface features, hence smearing the images. A third reason is that

the turbulent dissipation time scale has become comparable to the species diffusion time scale, therefore no longer sharp interfaces as those in frames (a & b).

Figure 5 shows averages of 2048 images corresponding to about 4 seconds of the flows in figure 4. The length of the image sequence is not long enough to produce a smooth mean image at the lowest Reynolds number in frame (a), which is not unexpected. A study of the corresponding video sequence indicate that the outermost features of the jet fluid move very slowly compared to the features that seem to be deeper in the jet. In fact, some of the jet fluid parcels seem to be nearly stagnant when they are move deep into the ambient fluid. The length of the image sequence in frame (b) seems to be barely enough to generate a smooth average image. This aspect of the flow is discussed further below in connection with schlieren imaging. The average flow picture in frame (c), however, is smooth, indicating the four seconds of flow at this Reynolds number has been sufficiently long to capture a sufficient number of slow moving jet fluid parcels at the edge of the jet. The images, both instantaneous and average ones, suggest that jet edge is spreading at angle of about 6° (confirm and check against literature).

Schlieren viuslaization

Simultaneous flow visualization at the jet edge and schlieren visualization through the jet is available for water jet experiments (Table 2). The schlieren images corresponding to those in figure 4 are shown in figure 6, at a slightly lower magnification. As opposed to the shell visualization, the schlieren images give an integrated image of the jet along the light path, hence, it superimposes all scales of the jet. Frames (a) and (b) show much finer textures than the corresponding images in figure 4, as the result of projecting all flow details across the jet onto a plane. The details get finer as the Reynolds number increase four-fold from (a) to (b). A further increase of three-fold from (b) to (c) is expected to generate even fines details in the flow field in frame (c). However the imaging capability of the camera is not able capture these finer details. Hence only the largest slower moving features are recorded in the image.

(Carry out FFT analysis to quantify the scales in images for further discussion below. Also check for mixing transition a la Dimotakis, Bereidenthal.)

Thus, the schlieren video sequence show nearly stagnant jet fluid parcels at the edge as well a very fast moving flow features in the interior of the jet. Human eye is able to separate these features that are moving at disparate speeds. To some limited degree, features moving at high speed below the *canopy* of slow moving outer features can also be identified in the shell visualization video, but the opacity of the jet fluid limits visible depth at the jets edge. We propose a technique to separate these feature for their speeds: enter PixTif.

(Use edge detection, followed by PixTif'ing to separate fast moving features via WALPT. Then, use PIV data to calibrate the schlieren/edge results.)

3.3. *Oil jets: 1cs*

Edge visualization

Figure 8 shows sample flow images for 1-cs oil jet at three Reynolds numbers. The flow in the tube in frame (a) is expected to be transitional since the flow is intentionally tripped upstream by the screen mesh and the Reynolds number is about 4000, beyond its critical value. Also, the Morton length for the flow is rather short (Table 2), hence the flow is buoyancy dominated. The combined effects of the immiscibility of the jet and ambient liquids and buoyancy effects, compounded by the expected transitional nature

of the discharge flow results in large detached parcels of oil after a short distance of undulations. As the Reynolds number is increased by six-fold in frame (b), the discharge tube length becomes adequate the achieve turbulent flow at the exit of the tube. The flow leaving the tube now shows as streamwise features the wall signatures of the turbulent flow in the pipe. Further increase in the Reynolds number in frame (c) results in finer details as expected, both on the jet surface and in the size distribution of the droplets.

(Quantify droplet size and velocity distribution and shape oscillations. a very tall order.)

Figure 9 shows averages of 2048 images for 1-cs oil jet at three Reynolds numbers. The transitional nature of the jet results in an average contraction soon after discharge followed by a barrel formation in frame(b). The average picture at higher Reynolds numbers in frames (b) and (c) indicate a classical growth patter, at a slightly smaller cone angle in (b).

(Measure growth angles.)

Shadowgraphy

Figure 10 shows shadowgraph images corresponding to the snapshots in figure 8. Due to the large difference between the refractive indices of water and oils, the oils jet appear dark , nearly black, in the shadowgraph pictures. The shadowgraph images are taken at a noticeably lower magnification, hence the features in the visible images look smaller in the shadowgraph images. At the lowest Reynolds number in (a) the flow field is fragmented, seems to be a collection of large oil patches. The discharging jet shows a combination of sinuous and varicose instability. At the higher Reynolds numbers, the flows exhibit a less disorderly pattern, The detached oil packets are clearly visible as oil droplets of various sizes, mostly spherical. On examination of the corresponding video sequences, one can clearly identify oscillations of the shapes of largest droplets. At the highest Reynolds number in frame(c), the observed droplet size gets smaller.

(Construct droplet size histograms.)

(Identify and quantify droplet shape oscillations.)

Figure 11 shows average shadowgraph imaged corresponding to the average pictures in figure 9. The average picture at the lowest Reynolds number in frame (a) nearly duplicates its counter part in figure 9(a). The jet remains nearly of uniform width a hint of oscillation with wave length of about three diameters. The mean shadowgraph images in (b) and (c) nearly math the corresponding visible images in figure 9. The mean shapes of the jets are now better revealed. The highest Reynolds number jet spreads a slightly larger rate.

(Measure growth angles.)

3.4. *Oil jets: 5cs*

Edge visualization

Figure 12 shows sample flow images for 5-cs oil jet at three Reynolds numbers. The flow in the tube in frame (a) is expected to be nearly developed parabolic laminar since the Reynolds number is about 800, below its critical value in tube with $L/D \approx 32$, adequate for full laminar flow development. The jet fluid in water still maintains contiguity in the field of view despite large undulations. AS in the i cs jet fluid, the Morton length for the flow is short (Table 2), hence this flow is also buoyancy dominated. At the higher Reynolds numbers, the oils jets break up and droplets form at the edge of the jet. The average size of the droplets and the surface features get smaller as the Reynolds number increases from frame (b) to (c). An unexpected observation is that the 5cs oil jet at

$Re \approx 8000$ in figure 12(c) shows finer scales than the 1cs oil jet at $Re \approx 24,000$ in figure 8(b).

(Quantify scale difference.)

Figure 13 shows averages of 2048 images for 5-cs oil jet at three Reynolds numbers. At the lowest Reynolds number in frame(a), the jet shows almost no spread. As in the case on figure 9(a), there is a hint of undulations in the shape of the jet at the higher Reynolds numbers the jest are growing, at a slightly higher rate for the highest Reynolds number in frame(c).

Shadowgraphy

Figure 14 shows shadowgrpaph imaged corresponding to the snapshots in figure 12. As in the visible picture, the jet fluid at the lowest Reynolds numbers remain contiguous, with varicose instability at the discharge. At higher Reynolds number, the jet surface brakes up into droplets, with decreasing size and increasing number density at the highest Reynolds number, which corroborates the features seen in figure 12(b,c).

Figure 15 shows average shadowgraph images corresponding to the average pictures in figure 13. At the lowest Reynolds number flow, the jet discharges without much growth. Also, hints of the varicose instability are visible near the pipe exit plane. The average images in frames (b) and (c) are similar to those in figure 11(b, c) except for a slightly larger spreading angle.

*(Measure growth angles.)*2

(Construct droplet size histograms.)

(Identify and quantify droplet shape oscillations.)

4. Image processing for turbulent scales: PixTif'ing

A video deck is a discretized three dimensional object of intensity $I(x, y; t) \approx I_{ij,k}$. When preprocessing the deck for a particular wave number k_v for image velocimetry, the image deck is first spatially filtered at each image plane using an appropriate filter, e.g. Laplacian filter. The spatial filtering parameters are set using equation 2.10. Then the deck is filtered in time at each pixel for the time scale $t_v = (\epsilon k_v^2)^{-1/3}$.

Processing is done using Fast Fourier Transform algorithms. Discrete time functions $I_{ij}(t)$ are constructed by stacking the light intensity values at a given pixel in the video image deck (figure 16). The intensity functions $I_{ij}(t)$ are then filtered in the frequency domain following Fourier transform and transformed back into the time domain:

$$\tilde{I}_{ij}(t) = \mathcal{F}^{-1}\{\ \mathcal{F}\{I_{ij}(t)\} * G(\omega)\ \}. \tag{4.1}$$

The parameters for the filter kernel $G(\omega)$ are chosen with the help of equation 2.12, which are the same for the entire image deck.

5. Mean flow at the interface

Profiles

Quantitative conclusions

6. Turbulence at the interface

Size distribution

Velocity distribution

Interface flow model / Generalization

7. Droplet dynamics at the interface

Size distribution

Velocity distribution

Shape oscillations

Breakup and amalgamation

Interface droplet model / Generalization

8. Closing remarks

Novel observations

Quantitative conclusions

Implications & Generalizations

Acknowledgements

BSEE contract

REFERENCES

Bhatti, M. S. & Shah, R. K. 1987 Turbulent and transition flow convective heat transfer in ducts. Editors: S. Kakaç, R. K. Shah, & W. Aung. New York. Wiley Interscience.

Bogusławski, L. & Popiel, Cz.O. 1979 Flow structure of the free round turbulent jet in the initial region. *J. Fluid Mech.*, **90** (3), 531–539. DOI: 10.1017/S0022112079002378

Brown, G. & Roshko, A. 1974 On density effects and large structure in turbulent mixing layers. *J. Fluid Mech.*, **64** (4), 775–816. DOI: 10.1017/S002211207400190X

Catrakis, H.J. & Dimotakis, P.E. 1996 Mixing in turbulent jets: scalar measures and isosurface geometry. *J. Fluid Mech.*, **317**, 317–406. DOI: 10.1017/S002211209600078X

Chen, A.L., Jacob, J.D. & Savaş, Ö. 1999 Dynamics of corotating vortex pairs in the wakes of flapped airfoils. *J. Fluid Mech.*, **382**, 155-193. DOI: http://dx.doi.org/10.1017/S0022112098003814

Coles, D. 1981 Prospects for useful research on coherent structure in turbulent shear flow. *Proc. Indian Acad. Sci. (Eng. Sci.)* **4**, 111 –127 .

Coles, D. 1985 The uses of coherent structure (Dryden Lecture). 1-13. *AIAA Paper 85-0506.* http://dx.doi.org/10.2514/6.1985-506

Dimotakis, P.E. 2000 The mixing transition in turbulent flows. *J. Fluid Mech.*, **409**, 69–98. DOI: 10.1017/S0022112099007946

Eastwood, C.D., Armi, L. & Lasheras, J.C. 2004 The breakup of immiscible fluids in turbulent flows. *J. Fluid Mech.*, **502**, 309–333. DOI: 10.1017/S0022112003007730

Hinze, J.O. 1955 Fundamentals of the hydrodynamics mechanisms of splitting in dispersion processes. *AIChE J.* **1**, 289-295. DOI: 10.1002/aic.690010303

Hinze, J.O. 1975 Turbulence, McGraw-Hill Inc., New York, NY.

Hu, H., Saga, T., Kobayashi, N. & Taniguchi, N. 2003 Analysis of a turbulent jet mixing flow by PIV-PLIF combined system. *J. Visualization*, **7**(1), 33 – 42.

Kolmogorov, A.N. 1949 On the breakage of drops in a turbulent flow. *Dokl. Akad. Nauk. SSSR*, **66**, 825 - 828. English translation in *Selected Works of A. N. Kolmogorov*, Vol. 1. Ed. V. M. Tikhomirtov, pp. 339–343, Springer.

Laufer, J. 1954 The structure of turbulence in fully developed pipe flow. *NACA- TR 1174.*

Lawn, C. J. 1971 The determination of the rate of dissipation in turbulent pipe flow. *J. Fluid Mech.*, **488**(3), 477 - 505.

Mathew, J. & Basu, A.J. 2002 Some characteristics of entrainment at a cylindrical turbulence boundary. *Physics of Fluids*, **14** (7), 2065–2072. DOI: 10.1063/1.1480831

McNutt, M.K., Camilli, R., Crone, T.J., Guthrie, G.D., Hsieh, P.A., Ryerson, T.B., Savaş, Ö. & Shaffer, F. 2011 Review of flow rate estimates of the Deepwater Horizon oil spill. *PNAS.* doi: 10.1073/pnas.1112139108

Morton, B.R. 1959 Forced plumes. *J. Fluid Mech.*, **5**(1), 151–163.

Nikuradse, J. 1932 Gesetzmäsigkeiten der turbulenten Stromung in glaten Rohren. Translated as 'Laws of turbulent flow in smooth pipes', NASA TT F-10, 359 (1966).

Nikuradse, J. 1933 Strömungsgesetze in rauhen Rohren. *VDI-Forschungsheft no.* 356. Translated as 'Laws of Flow in Rough Pipes', NACA-TM 1292 (1950).

Ortega, J.M., Bristol, R.L. & Savaş, Ö. 2003 Experimental study of the instability of unequal strength counter-rotating vortex pairs. *J. Fluid Mech.*, **474**, 35–84. DOI: 10.1017/S0022112002002446

Popiel, C.O. & Trass, O. 1991 Visualization of a free and impinging round jet. *Experimental Thermal and Fluid Science*, **4** (3), 253–264. doi:10.1016/0894-1777(91)90043-Q

Savaş, Ö. & Gollahalli, S.R. 1986 Flow structure in near-nozzle region of gas jet flames. *AIAA J.* **24** (7), 1137–1140. http://dx.doi.org/10.2514/3.9404

Savaş, Ö. 2012 A visual study in the near field of turbulent jets and implications for estimating accidental discharges. *Experiments in Fluids* **53**(5), 1501–1514. doi:10.1007/s00348-012-1372-7

Schlichting, H. 1979 *Boundary-Layer Theory, 7th ed.*, McGraw-Hill.

Sholl, M. & Savaş, Ö. 1997 A fast Lagrangian PIV method for study of general high gradient flows. *AIAA Paper 97-0493.* http://dx.doi.org/10.2514/6.1997-493

Sobel, I. & Feldman, G. 1968 A 3×3 isotropic gradient operator for image processing. Presented at a talk at the Stanford Artificial Project. (Indirect reference.)

Taylor, G.I. 1934 The formation emulsions in definable fields of flow. *Phil. Trans. R. Soc. A* **146**, 501–523. DOI: 10.1098/rspa.1934.0169

Turner, J.S. 1979 Buoyancy effects in fluids, Cambridge University Press, Cambridge

Westerweel, J., Fukushima, C., Pedersen, J.M. & Hunt, J.C.R. 2005 Mechanics of the turbulent-nonturbulent interface of a jet. *Physical Review Letters* **95**.(17). DOI: 10.1103/PhysRevLett.95.174501

Westerweel, J., Petracci, A., Delfos, R. & Hunt, J.C.R. 2011 Characteristics of the turbulent/non-turbulent interface of a non-isothermal jet. *Phil. Trans. R. Soc. A* **369**, 723–737. DOI: 10.1098/rsta.2010.0308

Wygnanski, I. J. & Champagne, F. H. 1973 On transition in a pipe. Part 1. The origin of puffs and slugs and the flow in a turbulent slug. *J. Fluid Mech.*, **59**, 281 – 335.

Yule, A.J. 1978 Large-scale structure in the mixing layer of a round jet. *J. Fluid Mech.*, **89** (3), 413–432. DOI: http://dx.doi.org/10.1017/S0022112078002670

liquid	$\rho\ [kg/m^3]$	$\nu\ [m^2/s]$	$\sigma\ [N/m]$	n
water	998.2	1×10^{-6}	7.28×10^{-2}	1.330
1cs silicon oil	816.5	1×10^{-6}	1.74×10^{-2}	1.383
5cs silicon oil	916.3	5×10^{-6}	1.97×10^{-2}	1.397

TABLE 1. Jet fluid properties at $20^{\circ}C$.

flow #	**jet fluid**	Re	ℓ_M/D	η [μm]	**fps exp.** [μsec]	**imaging**	**remarks**
1		0.59	∞	20.4		ScV/FV	"FWJ-T.10-1.02gpm"
2		1.20	-	12.0	500	ScV/FV	"FWJ-T.08-2.06gpm"
3		2.39	-	7.2		ScV/FV	"FWJ-T.11-4.10gpm"
4		4.31	-	4.6	998	ScV/FV	"FWJ-T.07-7.40gpm"
5		6.29	-	3.5		ScV/FV	"FWJ-T.12-10.8gpm"
6		7.22	-	3.1		ScV/FV	"FWJ-T.10-12.4gpm"
7		0.58	-	20.9		ScV/ScH	"great finds"
8		1.20	-	12.0		ScV/ScH	"great finds"
9		2.49	-	7.0	1000	ScV/ScH	"great finds"
10	water	3.58	$\times 10^4$ -	5.3		ScV/ScH	"great finds"
11		4.65	-	4.3	995	ScV/ScH	"great finds"
12		5.97	-	3.6		ScV/ScH	"great finds"
13		7.29	-	3.1		ScV/ScH	"great finds"
14		0.59	-	20.4		ScV/PIV	"great finds"
15		1.16	-	12.3	2000	ScV/PIV	"great finds"
16		2.32	-	7.3		ScV/PIV	"great finds"
17		4.60	-	4.4	494	ScV/PIV	"great finds"
18		5.33	-	3.9		ScV/PIV	"great finds"
19		0.40	1.8	27.4		Shd/FV	"1cs-T.10-1rps"
20		0.80	3.5	16.3	1000	Shd/FV	"1cs-T.11-2rps"
21	1cs oil	2.41	$\times 10^4$ 10.5	7.1		Shd/FV	"1cs-T.09-6rps"
22		3.21	14.0	5.8	498	Shd/FV	"1cs-T.07-8rps"
23		4.02	17.5	4.9		Shd/FV	"1cs-T.08-10rps"
24		0.80	2.6	91.5		Shd/FV	"5cs-T.10-1rps"
25		3.21	10.4	32.3	1000	Shd/FV	"5cs-T.02-4rps"
26		4.02	13.0	27.4		Shd/FV	"5cs-T.08-5rps"
27	5cs oil	4.82	$\times 10^3$ 15.6	23.9	498	Shd/FV	"5cs-T.03-6rps"
28		6.43	20.8	19.2		Shd/FV	"5cs-T.04-8rps"
29		8.03	26.0	16.3		Shd/FV	"5cs-T.07-10rps"

TABLE 2. Scope of the experiments. Flow numbers are used for identification in the discussion. Simultaneous imaging modes are indicated as pairs of FV-flow visualization, ScH-schlieren with horizontal knife edge, ScV-schlieren with vertical knife edge, Shd-shadowgraph, and PIV-particle image velocimetry.

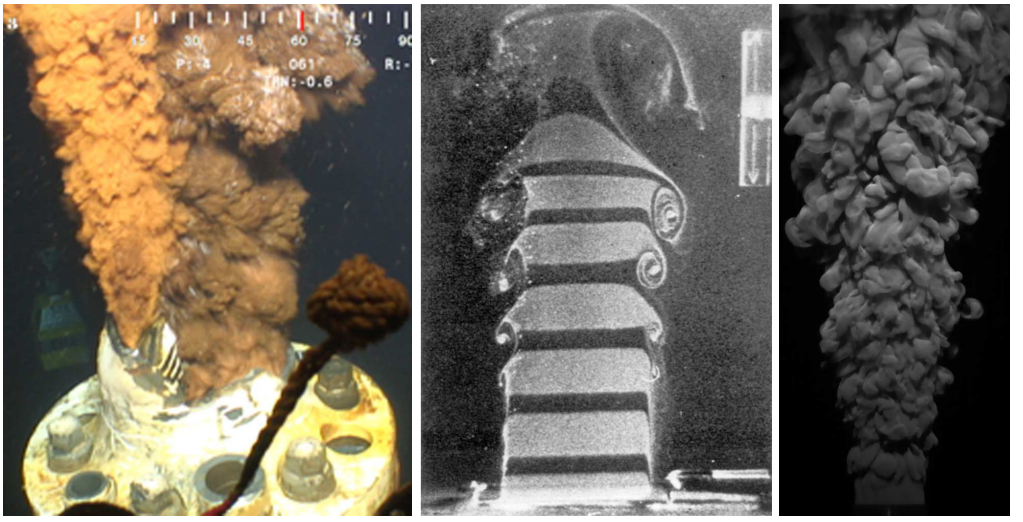

(a) (b) (c)

FIGURE 1. Motivation: near fields of jets: (a) accidental discharge from a 50-cm diameter severed pipe at a submarine oil field well head where the flow conditions unknown, (b) a well engineered water jet from a 5.1 cm diameter nozzle where all conditions are known (Yule 1978), and (c) our water jet of discharging developed turbulent pipe flow in a 1.38 cm diameter pipe.

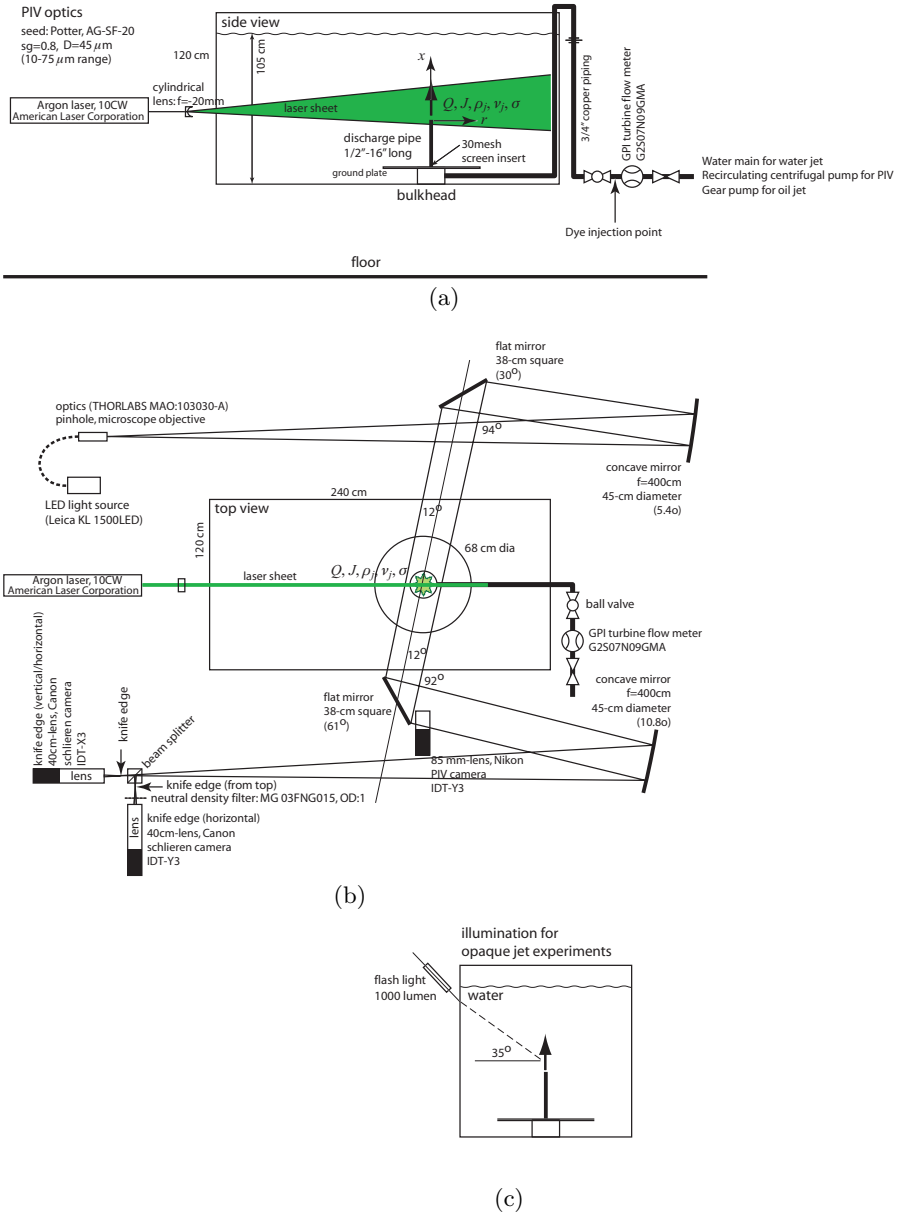

FIGURE 2. Experimental setup: (a) flow geometry, cross-sectional illumination, and (r, x) coordinate system (side view) (b) schlieren system and camera positions (top view), and (c) illumination for interface visualization (end view). The optical path between the schlieren light source and the cameras is about 15 meters.

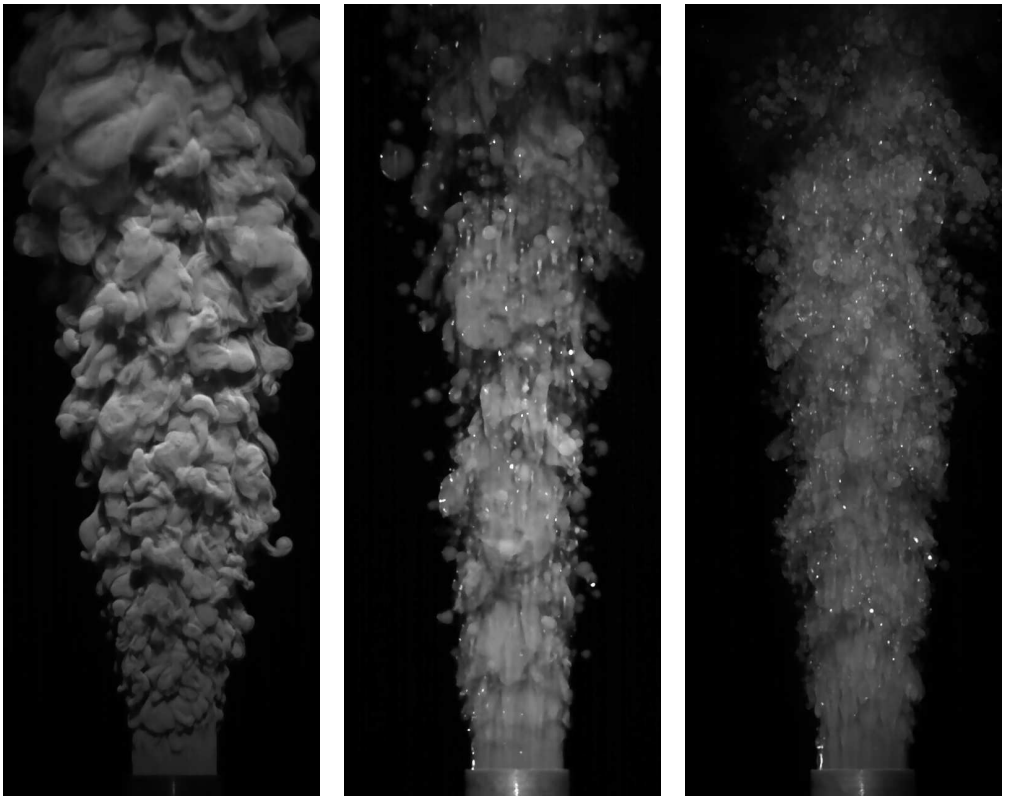

(a) (b) (c)

FIGURE 3. Sample images three jets: (a) Water jet: Re $= 0.59 \times 10^4$, (b) 1 cs oil jet: Re $= 2.41 \times 10^4$, and (c) 5 cs oil jet: Re $= 0.80 \times 10^4$. Flows 1, 21 & 24.

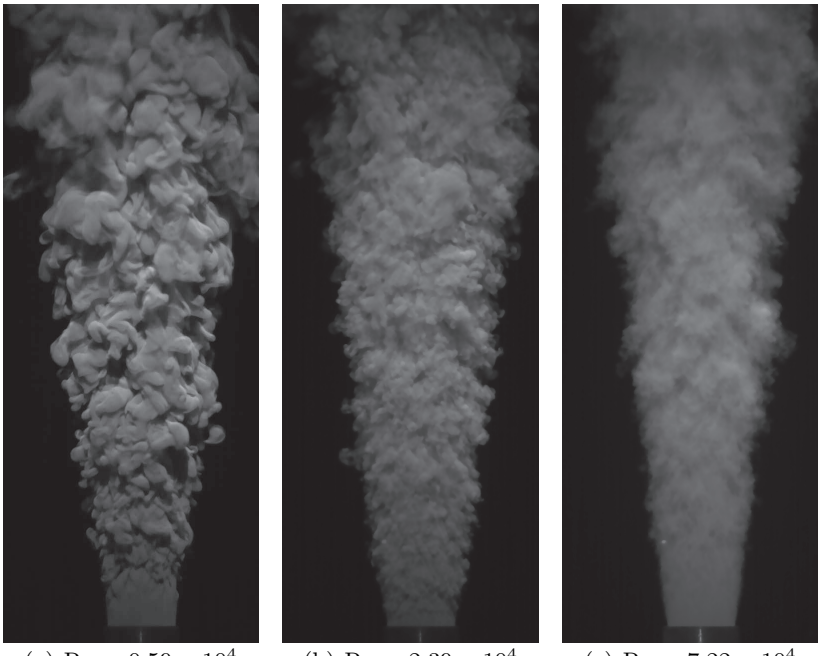

(a) $\mathrm{Re} = 0.59 \times 10^4$ (b) $\mathrm{Re} = 2.39 \times 10^4$ (c) $\mathrm{Re} = 7.22 \times 10^4$

FIGURE 4. Fluorescent water jet experiments: Flows 1, 3 & 6.

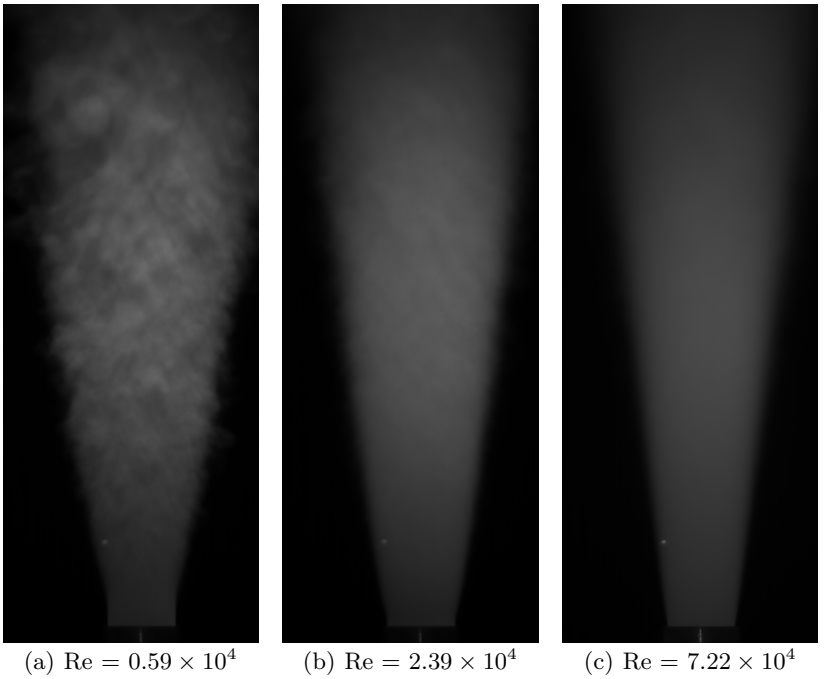

(a) $\mathrm{Re} = 0.59 \times 10^4$ (b) $\mathrm{Re} = 2.39 \times 10^4$ (c) $\mathrm{Re} = 7.22 \times 10^4$

FIGURE 5. Fluorescent water jet experiments: intensity average 2048 images: Flows 1, 3 & 6.

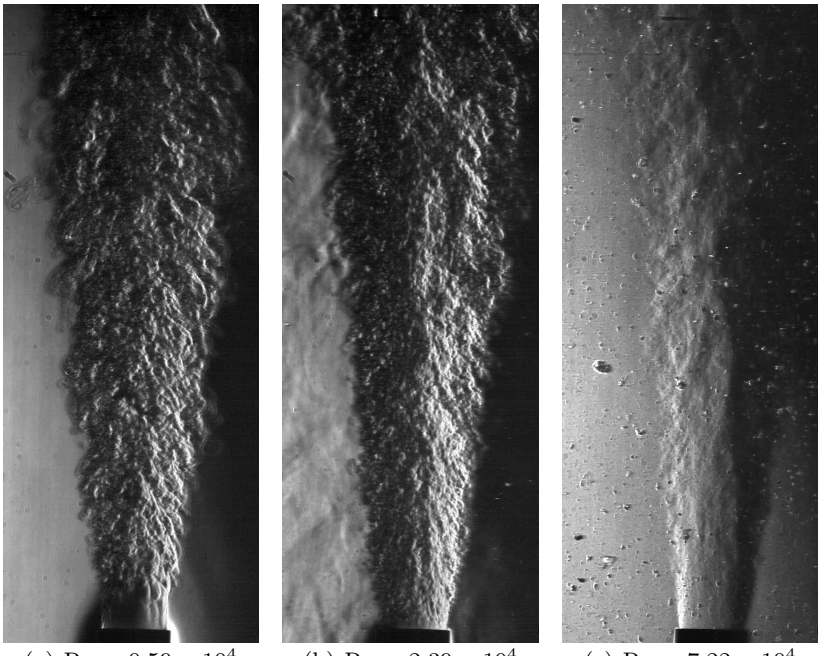

(a) $\mathrm{Re} = 0.59 \times 10^4$ (b) $\mathrm{Re} = 2.39 \times 10^4$ (c) $\mathrm{Re} = 7.22 \times 10^4$

FIGURE 6. Fluorescent water jet experiments: Schlieren images corresponding to the frames in 4; Flows 1, 3 & 6.

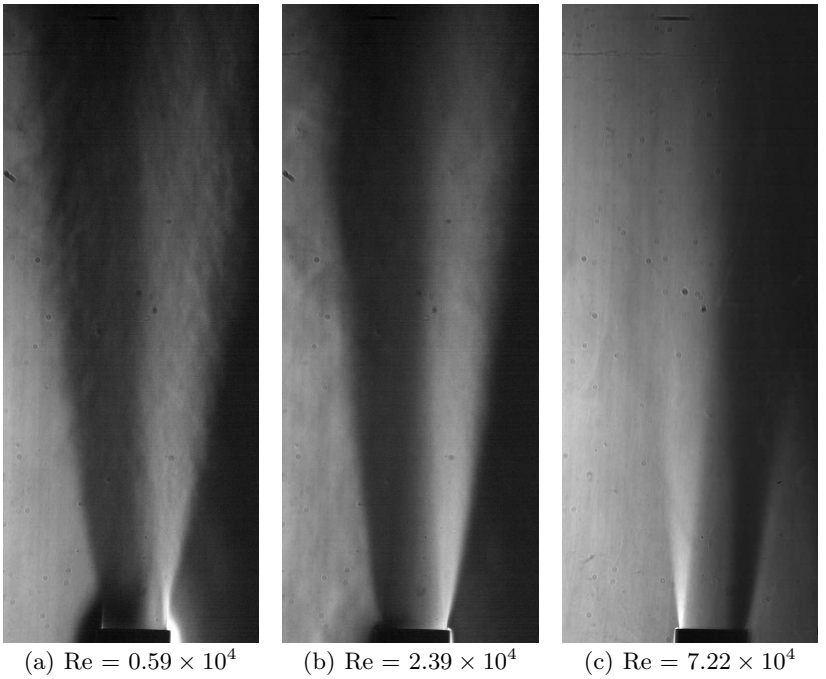

(a) $\mathrm{Re} = 0.59 \times 10^4$ (b) $\mathrm{Re} = 2.39 \times 10^4$ (c) $\mathrm{Re} = 7.22 \times 10^4$

FIGURE 7. Schlieren of fluorescent water jet experiments: intensity average 2048 images: Flows 1, 3 & 6.

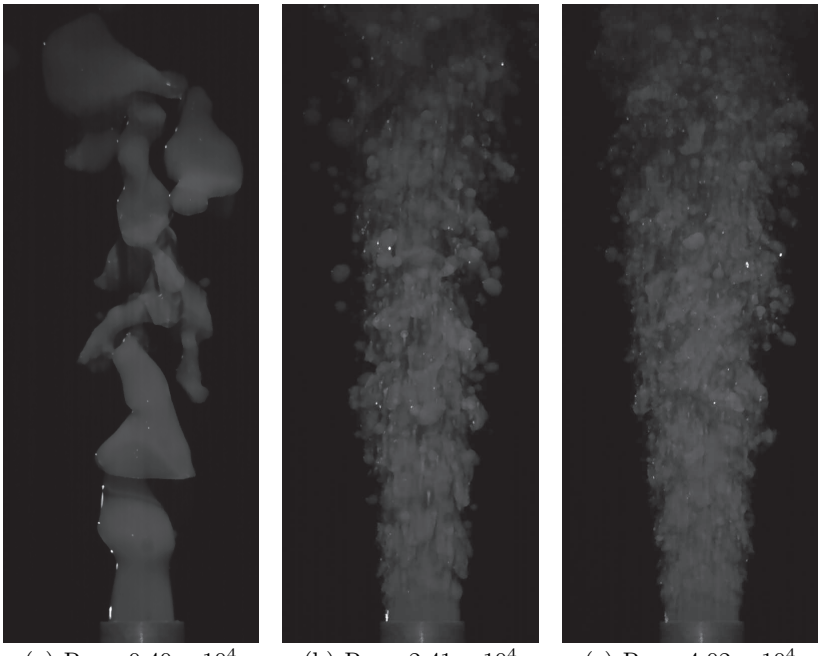

(a) $\mathrm{Re} = 0.40 \times 10^4$ (b) $\mathrm{Re} = 2.41 \times 10^4$ (c) $\mathrm{Re} = 4.02 \times 10^4$

FIGURE 8. 1cs silicon oil jet experiments: Flows 19, 21 & 23.

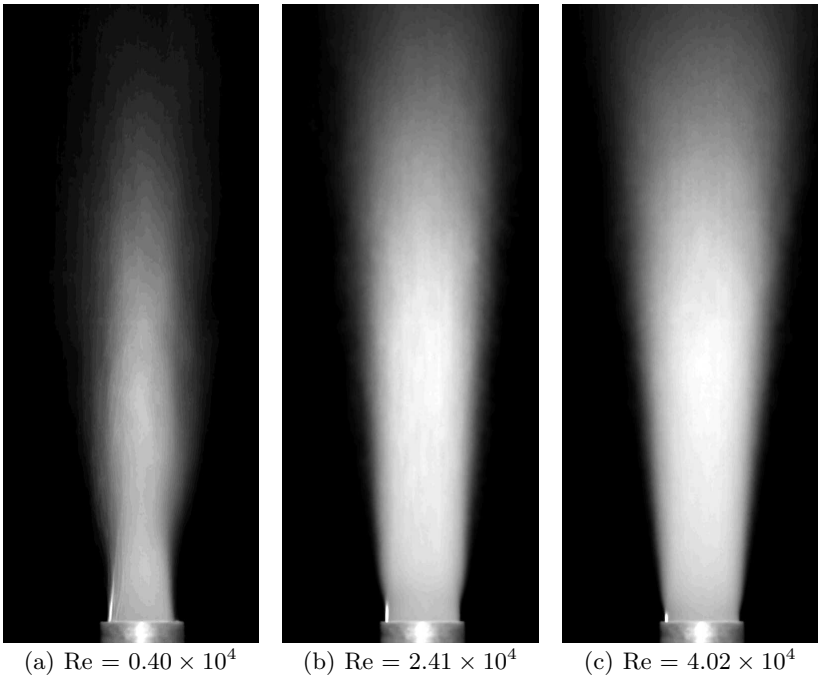

(a) $\mathrm{Re} = 0.40 \times 10^4$ (b) $\mathrm{Re} = 2.41 \times 10^4$ (c) $\mathrm{Re} = 4.02 \times 10^4$

FIGURE 9. 1cs silicon oil jet experiments: intensity average 2048 images: Flows 19, 21 & 23.

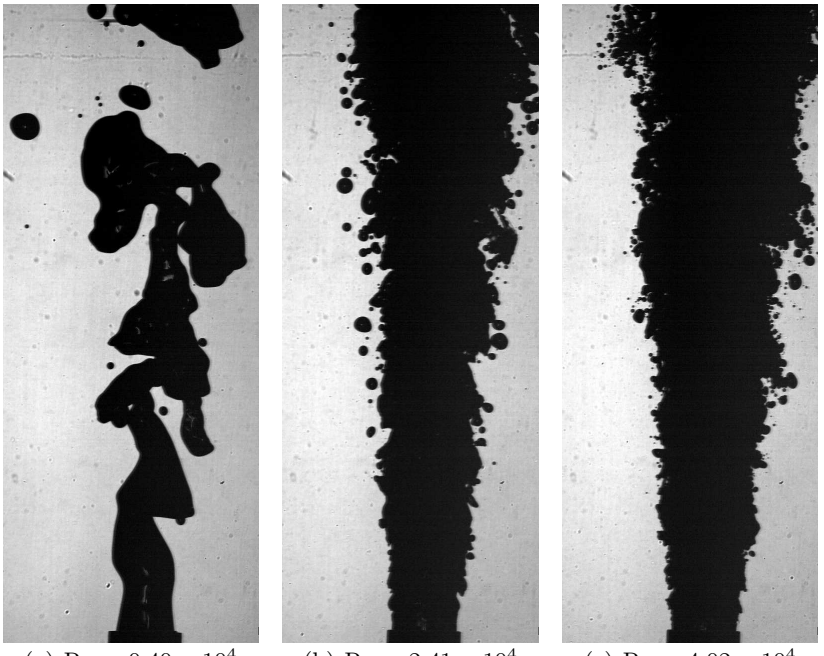

(a) $\mathrm{Re} = 0.40 \times 10^4$ (b) $\mathrm{Re} = 2.41 \times 10^4$ (c) $\mathrm{Re} = 4.02 \times 10^4$

FIGURE 10. Shadowgraph of 1cs silicon oil jet experiments: Flows 19, 21 & 23.

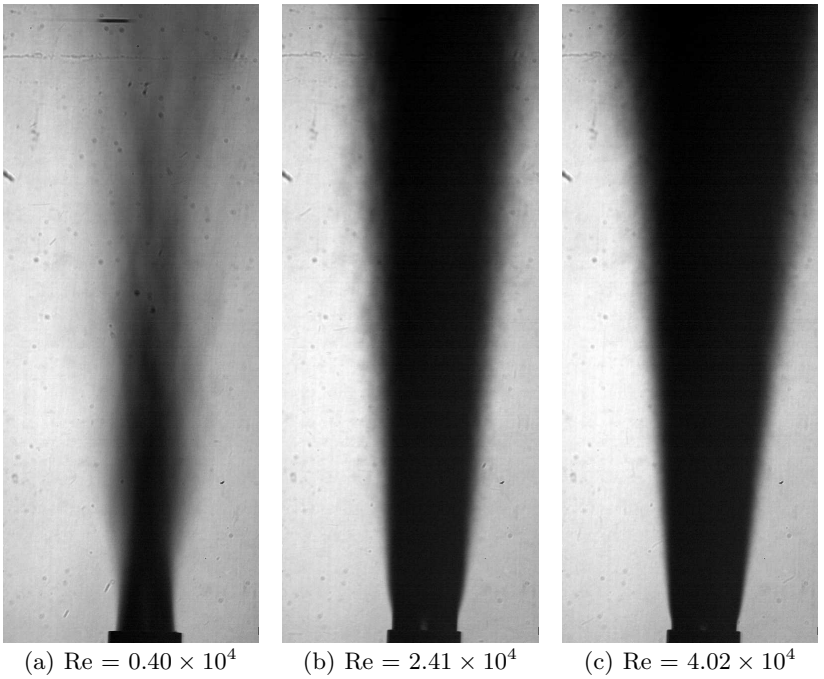

(a) $\mathrm{Re} = 0.40 \times 10^4$ (b) $\mathrm{Re} = 2.41 \times 10^4$ (c) $\mathrm{Re} = 4.02 \times 10^4$

FIGURE 11. Shadowgraph of 1cs silicon oil jet experiments: intensity average 2048 images: Flows 19, 21 & 23.

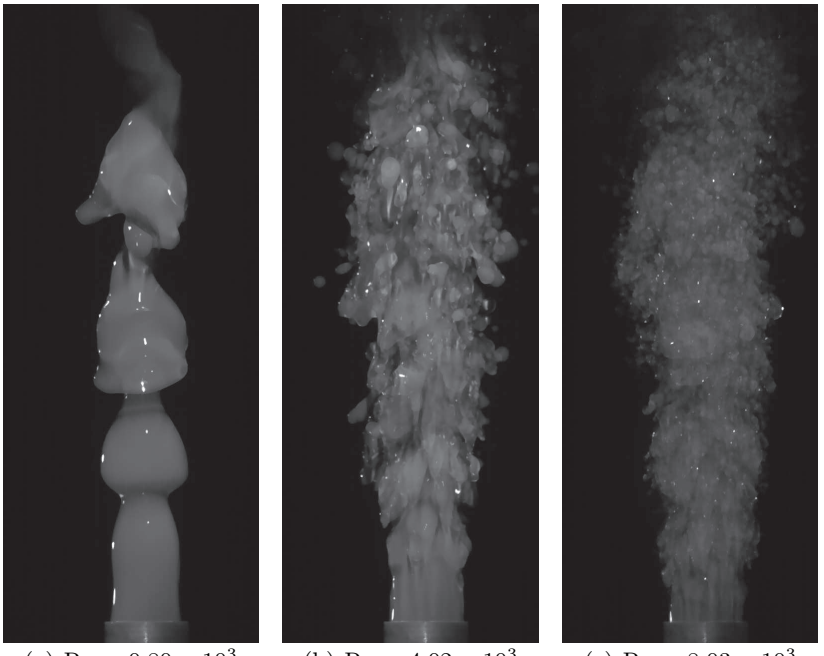

(a) $\mathrm{Re} = 0.80 \times 10^3$ (b) $\mathrm{Re} = 4.02 \times 10^3$ (c) $\mathrm{Re} = 8.03 \times 10^3$

FIGURE 12. 5cs silicon oil jet experiments: Flows 24, 26 & 29.

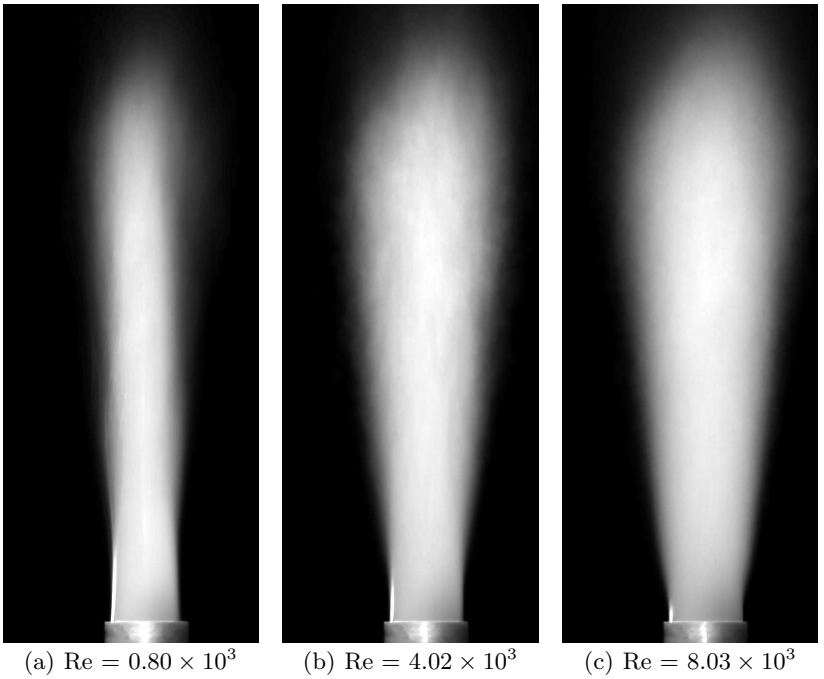

(a) $\mathrm{Re} = 0.80 \times 10^3$ (b) $\mathrm{Re} = 4.02 \times 10^3$ (c) $\mathrm{Re} = 8.03 \times 10^3$

FIGURE 13. 5cs silicon oil jet experiments: intensity average 2048 images: Flows 24, 26 & 29.

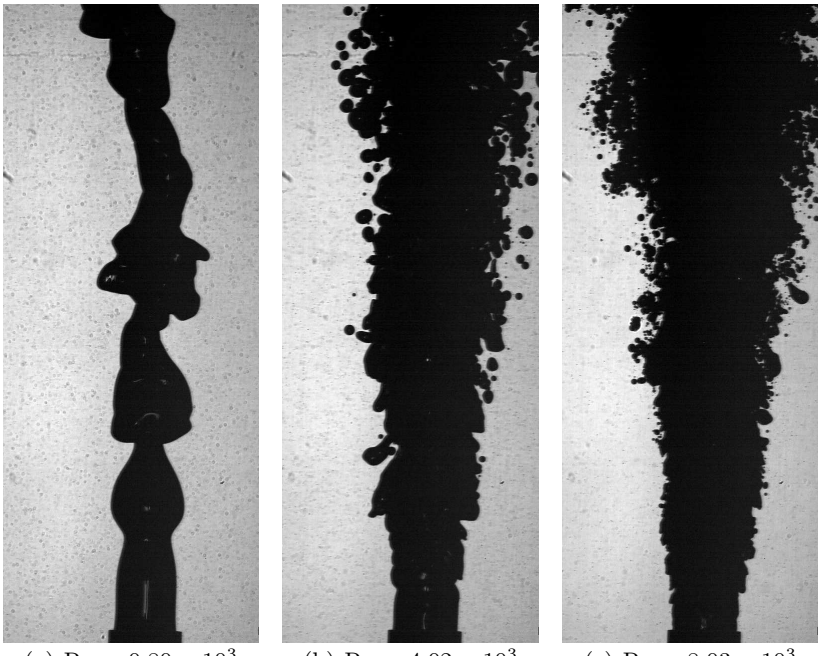

(a) $\mathrm{Re} = 0.80 \times 10^3$ (b) $\mathrm{Re} = 4.02 \times 10^3$ (c) $\mathrm{Re} = 8.03 \times 10^3$

FIGURE 14. Shadowgraph of 5cs silicon oil jet experiments: Flows 24, 26 & 29.

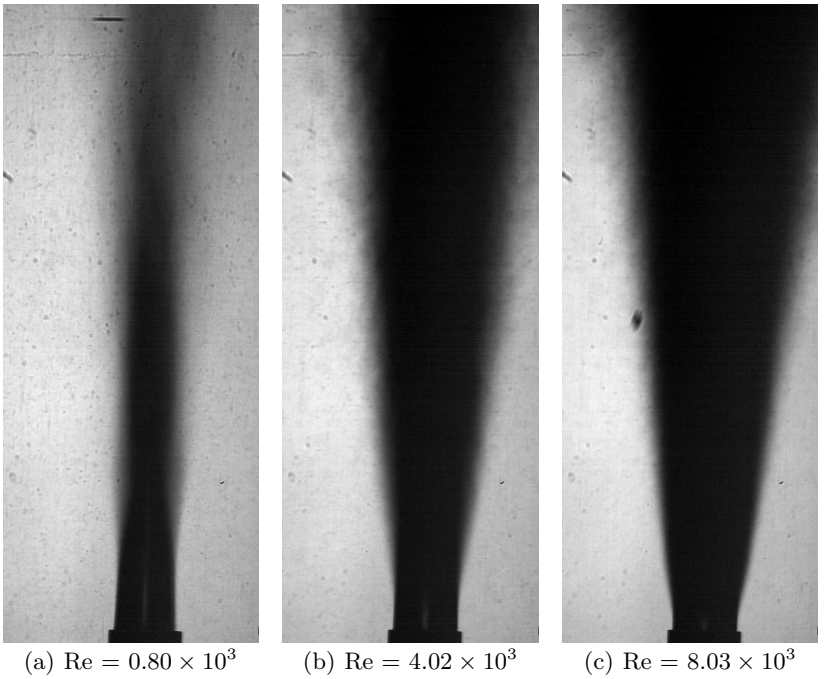

(a) $\mathrm{Re} = 0.80 \times 10^3$ (b) $\mathrm{Re} = 4.02 \times 10^3$ (c) $\mathrm{Re} = 8.03 \times 10^3$

FIGURE 15. Shadowgraph of 5cs silicon oil jet experiments: intensity average 2048 images: Flows 24, 26 & 29.

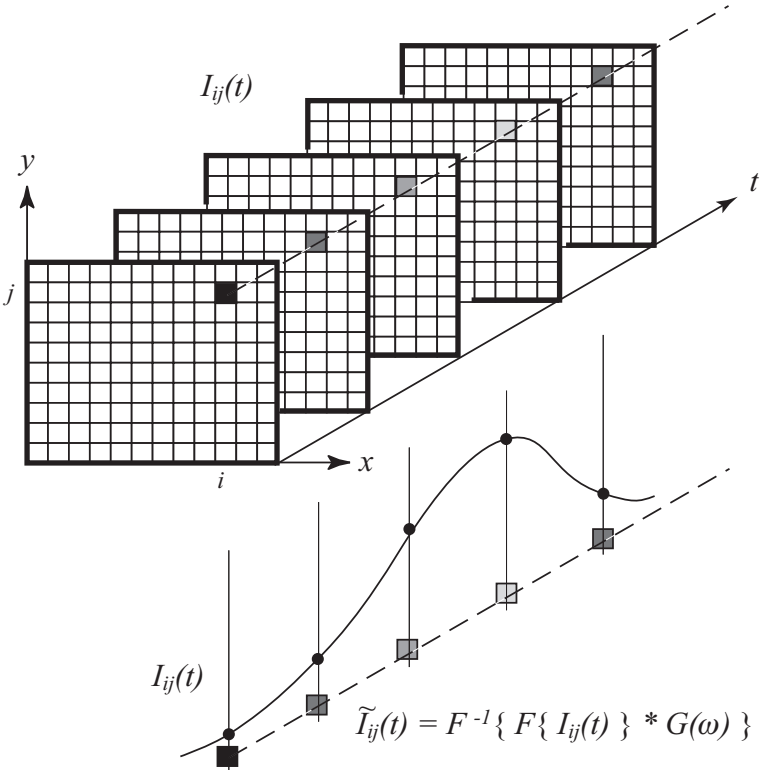

FIGURE 16. PixTif illustration. Discrete time functions $I_{ij}(t)$ are constructed by stacking the light intensity values at a given pixel in the video image deck. The intensity functions $I_{ij}(t)$ are then filtered in the frequency domain following Fourier transform and transformed back into the time domain: $\tilde{I}_{ij}(t) = \mathcal{F}^{-1}\{\ \mathcal{F}\{I_{ij}(t)\} * G(\omega)\ \}$. The parameters for the filter kernel $G(\omega)$ are chosen with the help of equation 2.12, which are the same for the entire image deck.

FIGURE 17. Steps in image processing for velocimetry at the jet interface. (a) a raw image of the flow (b) Gaussian blur (c) edge filter (d) PixTif (e) WALPT result.

FIGURE 18. Velocity profiles at the interface.